Novel MRI techniques in the diagnosis of Musculoskeletal infection in children

Dr Afshin Alavi, MD (Cologne University), FRCR

Consultant for Adult and Interventional Radiology

Consultant for Paediatric Radiology

Section of Paediatrics

Division of Infectious Diseases

Department of Medicine

Imperial College London

Submitted in fulfilment of a Doctor of Medicine (Res.) Degree

May 2021

Declaration of Originality:

I declare that the content of this thesis is all my own work and based on my research project, except where I have referenced or acknowledged the work of other fellows.

Copyright Declaration :

Abstract

Introduction:

Musculoskeletal infections in children are common and if not adequately treated can result in poor prognoses. Early diagnosis and rapid treatment are crucial. The clinical and laboratory results are often non-conclusive or misleading. Radiology has always played a part in the diagnosis of Paediatric musculoskeletal infections. MRI is the most sophisticated MSK imaging tool and advanced MRI protocols with tailored techniques can improve the diagnostic yield of MRI in Paediatric MSK infection.

Methods:

99 children with acute MSK pain and signs of infection were prospectively recruited. Each patient had a MRI scan on the first day of admission. A tailored MRI protocol was utilised, consisting of structural and biodynamic (DWI & SCE) sequences. Two consultant MSK radiologists independently analysed the scans and completed evaluation forms consisting of qualitative and semi-quantitative questions. The quantitative data from DWI and SCE sequences were separately analysed.

Results:

103 MRI scans were performed. 3 scans were excluded due to incomplete protocols. 5 quantitative DWI and 3 SCE analyses were excluded due to irregularities of the values. The most common clinical diagnosis was infection. The feasibility of the protocol was excellent. The accuracy of the MRI protocol was good-excellent. The most accurate sequence was SCE. The diagnostic accuracy of the readers was good compared to an agreed gold standard. The most valued sequence by the readers for the diagnostic process was SCE. There were no relevant statistical thresholds for ADC and most of permeability values except for one regarding MSK infection.

Conclusion:

The tailored MRI protocol of the study is a feasible diagnostic tool with high level of diagnostic accuracy for paediatric MSK infections. The advanced MRI techniques in this study are the strengths of the protocol, which have demonstrated high accuracy and subjective diagnostic confidence. The quantitative values of the biodynamic sequences are promising parameters which need further evaluation in future studies.

Table of content

Declaration of originality……..2

Copyright declaration……2

Abstract……3

Table of content……..4

List of tables……...13

List of figures……16

Abbreviation……...18

Chapter 1: Introduction……21

1-1 Background……...21

1-2 Musculoskeletal infection……..21

1-3 Epidemiology and incidents……22

1-4 Aetiology……23

1-5 Pathogeneses and transmission……26

1-5-1 Cartilage evolution……..26

1-5-2 Vascular evolution……..27

1-5-3 Bone marrow conversion and reconversion……...27

1-6 Risk factors……28

1-7 Diagnosis……...29

1-7-1 Clinical features and presentation……29

1-7-2 Differential diagnosis……..29

1-7-3 Laboratory and microbiology investigations……...31

1-7-4 Imaging diagnostic……31

1-7-4-1 Radiography……..32

1-7-4-2 Ultrasonography……32
1-7-4-3 Scintigraphy……...33
1-7-4-4 Computed tomography……34
1-7-4-5 Magnetic resonance imaging……..35
1-7-4-6 Comparison of the imaging modalities……..36
1-7-5 Ideal imaging tool……38
1-7-6 Advanced magnetic resonance imaging……38
1-7-7 Introduction to diffusion weighted imaging……40
1-7-7-1 Diffusion phenomenon of water molecules (Brownian motion)……40
1-7-7-2 Diffusion weighted imaging, basics and principles……..42
1-7-7-3 Diffusion weighted imaging techniques……46
1-7-8 Diffusion weighted imaging in paediatric skeleton……49
1-7-8-1 Specific diffusion characteristics of immature skeleton……..49
1-7-8-2 Clinical applications of DWI in paediatric musculoskeletal system……..52
1-7-9 Introduction to contrast enhanced semiquantitative and quantitative MRI……53
1-7-9-1 Serial and dynamic contrast enhanced magnetic resonance imaging……54
1-7-9-2 Signal intensity or time intensity curves……55
1-7-9-3 MR modelling……55
1-7-9-4 Pharmacokinetic modelling……56
1-7-9-5 Image analysis and pharmacokinetic fit……58
1-7-9-6 A compromise model……59
1-7-9-7 MRI sequence and image acquisition technique……60
1-7-9-8 Contrast agent and administration……61
1-7-10 SCE and DCE imaging in paediatric MSK system…….....62
1-7-10-1 DCE and SCE characteristics of immature skeleton…….....62
1-7-10-2 Clinical application of DCE imaging in paediatric MSK……63
1-7-11 Available research for MRI of acute paediatric MSK infection……..64

1-8 Treatment……..65

1-9 Complications and prognosis……..66

Chapter 2: Study aim and hypotheses……67

2-1 Study aim……..67

2-2 Hypotheses……67

Chapter 3: Context, material and methods……69

3-1 Study context……69

3-1-1 Introduction……..69

3-1-2 Background of the study……69

3-1-3 Pilot data and estimated cohort size……70

3-1-4 Ethics approval……73

3-1-5 Data management……..74

3-2 Material and methods……74

3-2-1 Study structure……74

3-2-2 Cohort……...74

3-2-3 Inclusion and exclusion criteria……75

3-2-4 Recruitment……... ……75

3-2-5 Information, consent and assent forms ……76

3-2-6 Magnetic resonance imaging……77

3-2-6-1 Imaging site……77

3-2-6-2 Radiography team……77

3-2-6-3 Patient preparation and immobilisation, Scanning method……77

3-2-6-4 MR scanners and coils……78

3-2-6-5 MRI protocol development……..78

3-2-6-5-1 Sequence selection……79

3-2-6-5-2 Sequence optimisation……80

3-2-6-5-3 Study protocol…..……..88

3-2-6-5-4 Contrast agent……...89

3-2-7 MRI criteria……..89

3-2-8 Gold standard……..91

3-2-9 Readers……92

3-2-10 Evaluation form……93

3-2-11 Reading process……..94

3-2-12 Quantitative data measurements……...95

3-2-12-1 ADC value measurement……..95

3-2-12-2 Permeability (semiquantitative) measurements and curves……97

3-2-13 Data preparation ……..98

3-2-14 Statistical analysis……99

3-2-14-1 Inter and Intraobserver agreements……..100

3-2-14-2 Statistical analysis of the main data (qualitative & quantitative)……...102

3-2-14-2-1 Feasibility……...102

3-2-14-2-2 Diagnostic accuracy of the MRI protocol (evaluation form's qualitative data)…103

3-2-14-2-3 Statistical analysis of the numerical data of the evaluation forms to evaluate the diagnostic value of single sequences (readers' preferences)……...104

3-2-14-2-4 Statistical analysis of the permeability and ADC values…….105

Chapter 4: Diffusion Weighted Imaging……108

4-1 Introduction……108

4-2 Altered diffusivity in musculoskeletal infection in children……..109

4-3 Material and methods……..109

4-3-1 Objective……109

4-3-2 Ethic approval……...110
4-3-3 Study structure……..110
4-3-4 Demographic of the study population……110
4-3-5 Magnetic resonance imaging and the imaging protocol……111
4-3-6 Quantitative image analysis……111
4-3-7 Qualitative and semiquantitative analysis……112
4-3-8 Data preparation……...113
4-3-9 Data analysis and statistics……114
4-3-9-1 Inter and intraobserver data analysis……..114
4-3-9-2 Main data analysis……..114
4-4 Results……..116
4-4-1 Cohort……116
4-4-2 Feasibility of DWI……117
4-4-3 Inter and Intraobserver agreement tests……..117
4-4-4 ROI measurements' consistency analyses for ADC values……..119
4-4-5 Diagnostic accuracy of DWI……..119
4-4-6 Readers preferences or subjective ranking of the study's sequences……122
4-4-6-1 Ranking based on image conspicuity……..123
4-4-6-2 Ranking based on diagnostic confidence……...127
4-4-7 Quantitative statistic and quantitative diagnostic thresholds……131
4-4-7-1 Main data ADC value analysis……131
4-5 Discussion……...140
4-6 Limitations……...145
4-7 Conclusion……..146

Chapter 5: Serial contrast enhanced imaging…….....148
5-1 Introduction……148

5-1-1 Permeability contrast enhanced imaging in paediatric MSK system……...148

5-1-2 Altered permeability in musculoskeletal infection in children……149

5-1-3 Challenges of pharmacokinetic modelling and quantitative assessment of permeability contrast enhanced MRI……...149

5-2 Material and methods……....150

5-2-1 Objective……151

5-2-2 Ethical approval……151

5-2-3 Study structure……151

5-2-4 Study cohort and demographic……..151

5-2-5 Inclusion and exclusion criteria……..152

5-2-6 Information, consent and assent forms……152

5-2-7 Recruitment……...152

5-2-8 Magnetic resonance imaging, scanners and coils……..……152

5-2-9 MRI protocol and serial contrast enhanced (permeability) sequences……...153

5-2-10 Contrast agent……153

5-2-11 Analytic software for permeability analysis……154

5-2-12 Serial contrast enhanced image acquisition……..154

5-2-13 Semiquantitative image analysis……155

5-2-14 Qualitative image analysis……156

5-2-14-1 Readers……156

5-2-14-2 Evaluation form……156

5-2-14-3 Reading process and gold standard……157

5-2-15 Data preparation……157

5-2-16 Data analysis……..157

5-2-16-1 Inter and intraobserver agreement test……157

5-2-16-2 Main data analysis……..157

5-2-16-3 Statistical analysis of the semiquantitative permeability values……157

5-3 Results……..158

5-3-1 Cohort……158

5-3-2 Feasibility of permeability imaging (SCE)……159

5-3-3 Inter and intraobserver agreement tests……..159

5-3-4 ROI measurements' consistency analyses for permeability values……161

5-3-5 Diagnostic accuracy of the SCE sequences……162

5-3-6 Diagnostic value of the SCE sequences and their ranking…….....165

5-3-6-1 Correlation based on Image conspicuity……165

5-3-6-2 Correlation based on diagnostic confidence……...168

5-3-7 Time intensity curves (qualitative & semiquantitative) analysis……170

5-3-8 Main data permeability value analysis……..171

5-3-8-1 Quantitative statistic and quantitative diagnostic thresholds (ROC test)……...171

5-4 Discussion……...179

5-5 Limitation……187

5-6 Conclusion……..189

Chapter 6: Tailored magnetic resonance imaging protocol for MSK infection in children……191

6-1 Introduction……191

6-1-1 Musculoskeletal infection in children……191

6-1-2 Diagnosis of musculoskeletal infection in children……..191

6-1-3 Imaging diagnosis of musculoskeletal infection in children……...192

6-2 Material and methods……...192

6-2-1 Objective……192

6-2-2 Ethic approval……...193

6-2-3 Study population……...193

6-2-4 Magnetic resonance imaging……193

6-2-5 Magnetic resonance imaging protocol……..193

6-2-6 Readers……194

6-2-7 Evaluation form……194

6-2-8 Reading process……..194

6-2-9 Data preparation……...194

6-2-10 Data analysis and statistics……..195

6-2-10-1 Inter and intraobserver data analysis……195

6-2-10-2 Main data analysis……195

6-3 Results……..195

6-3-1 Cohort……195

6-3-2 Feasibility of the MRI protocol……197

6-3-3 Inter and Intraobserver agreement tests..……198

6-3-4 ROI measurements' consistency analysis for ADC values……199

6-3-5 ROI measurements' consistency analysis for Permeability values ……199

6-3-6 Accuracy test of the study protocol and the single sequences……199

6-3-7 Diagnostic value of the study's sequences and their ranking……...203

6-3-7-1 Correlation based on Image conspicuity……203

6-3-7-2 Correlation based on diagnostic confidence……..206

6-3-8 Quantitative statistic and quantitative diagnostic thresholds……209

6-3-8-1 Main data ADC value analysis……209

6-3-8-2 Main data permeability value analysis……209

6-4 Discussion……...210

6-5 Limitations……...218

6-6 Conclusion……..219

Chapter 7: What has been learned and future development……...220

Bibliography……222

Appendix……240

Appendix 1- Ethical approval……240

Appendix 2- Patient information sheet……...246

Appendix 3- Consent and Assent forms……256

Appendix 4- Evaluation form……263

List of Tables

Table 1: The most common paediatric microorganism……...24

Table 2: Differential diagnoses of paediatric musculoskeletal infections…….30

Table 3: Sensitivity and specificity of different imaging modalities…..…….36

Table 4: Advantages and imaging findings of different imaging modalities…….37

Table 5: Demographic of study's participants & anatomical incidence (pilot data)…71

Table 6: Number of scans and participants of the main pathologies (pilot data)……71

Table 7: Accuracy test of the whole protocol of the pilot retrospective study…….72

Table 8: Cohen's kappa agreement between the readers of the pilot study……..72

Table 9: Details of the studies sequences……88

Table 10: Signal changes of the study's sequences during an infection…….90

Table 11: Combination of the clinical findings of the Gold standard……92

Table 12: The incident of the affected anatomical locations……110

Table 13: Number of the excluded patients and scans for DWI……..117

Table 14: ICC test for inter & intraobserver agreement tests of the DWI sequence118

Table 15: ICC test for intraobserver agreement of manual ADC measurements….119

Table 16: Correlation between DWI & clinical diagnoses (8 diagnostic categories)120

Table 17: Correlation between DWI & clinical diagnoses (2 diagnostic categories)120

Table 18a: Accuracy test of single sequences for the first reader (2 categories)…121

Table 18b: Accuracy of single sequences for the second reader (2 categories)….122

Table 19: Descriptive statistics of the conspicuity scores (first reader)…….124

Table 20: Descriptive statistics of the conspicuity scores (second reader)……...124

Table 21: Friedman ANOVA test results of the conspicuity scores (both readers)..125

Table 22: Paired sample sign test for conspicuity scores of the first reader…….126

Table 23: Paired sample sign test for conspicuity scores of the second reader…..126
Table 24: Descriptive statistics of the diagnostic confidence scores (first reader)..128
Table 25: Descriptive statistics of the diagnostic confidence scores (sec. reader)..128
Table 26: Friedman ANOVA test of diagnostic confidence scores (both readers)..129
Table 27: Paired ample sign test of diagnostic confidence score (first reader)……130
Table 28: Paired ample sign test of diagnostic confidence score (second reader).130
Table 29: Statistic details of ROC test for ADC values and number of infections…132
Table 30: Mean ADC values of participants with and without infection…….137
Table 31: Kruskall-wallis mean ranking of the ADC values of the main diagnoses.139
Table 32: Mann-whitney U significant test for the mean ADC value differences….139
Table 33: Demographic of the study participants regarding SCE sequences……..152
Table 34: Consort table with the number of excluded patients & scans for SCE …158
Table 35: ICC test for inter and intraobserver agreement for SCE sequences.....160
Table 36: ICC test for consistency of manual permeability ROI measurements…..161
Table 37: Cohen's kappa accuracy tests of SCE sequences with 8 diagnoses…...163
Table 38: Cohen's kappa accuracy tests of SCE sequences with 2 diagnoses…...163
Table 39: Accuracy tests for single sequences for the first reader (2 diag.)…….....164
Table 40: Accuracy tests for single sequences for the second reader (2 diag.)…..164
Table 41: Sign test for conspicuity scores of SCE sequences of the first reader....166
Table 42: Sign test for conspicuity scores of SCE sequences of second reader….167
Table 43: Sign test of diagnostic confidence scores for SCE of the first reader…..169
Table 44: Sign test of diagnostic confidence scores for SCE of the second reader169
Table 45: Excluded SCE studies for ROC analysis of the permeability values……171
Table 46: Descriptive statistic results of the ROC tests for AUC……....173
Table 47: Descriptive statistic results of the ROC tests for TME……173
Table 48: Number of scans and participants for the main pathologies……..196

Table 49: ICC tests for inter & intraobserver agreements of the single sequences.198
Table 50: Accuracy tests of final readers diagnoses (2&8 diagnostic categories)...200
Table 51: Accuracy tests of first readers' single sequence diagnoses (8 diag.).....201
Table 52: Accuracy tests of second readers' single sequence diagnoses (8 diag.)202
Table 53: Sign tests of conspicuity scores of all sequences for the first reader.....204
Table 54: Sign tests of conspicuity scores of all sequences for the second reader205
Table 55: Sign tests of diag. confidence scores of all sequences (first reader).....207
Table 56: Sign tests of diag. confidence scores of all sequences (second reader).208

List of Figures

Figure 1: Schematic of Brownian motion as described by Robert Brown……41

Figure 2: Schematic of spin dephasing and rephasing by Diffusion gradients……...43

Figure 3: Most common DWI pulse sequences……...48

Figure 4: Chronological changes of T2 fat sat sequences of immature skeleton…...50

Figure 5: Chronological appearances of T1 sequences of immature skeleton……...51

Figure 6: Schematic of ADC analysis (Olea Sphere)……..…84

Figure 7a-7c: Schematic of permeability value analysis (Olea Sphere)…….....86-87

Figure 8: Readers preference based on conspicuity scores (Column graph)……..125

Figure 9: Readers preference based on diag. confidence scores (Column graph).129

Figure 10: ROC curve of the ADC values in osseous lesions……133

Figure 11: ROC curve of the ADC values in muscular lesions……134

Figure 12: ROC curve of the ADC values in fluid collections……..134

Figure 13: ROC curve of the ADC values in joint effusion……...135

Figure 14: ROC curve of the ADC values in soft tissue lesions……..135

Figure 15: ROC curve of the ADC values in synovial lesions……136

Figure 16: ROC curve of the ADC values of bone marrow infection versus normal137

Figure 17: Box plot graph of the ADC values of the main diagnoses groups……...138

Figure 18: TME ROC curve of hyperaemic osseous lesions..……...174

Figure 19: TME ROC curve of hyperaemic muscle and soft tissue lesions…..…...175

Figure 20: AUC ROC curve of hyperaemic osseous lesions..……...176

Figure 21: AUC ROC curve of hyperaemic muscle and soft tissue lesions…..…...177

Figure 22: AUC ROC curve of hyperaemic synovium.…….....178

Figure 23: AUC ROC curve bone infarction...……...179

Figure 24: Permeability curve of a poly articular juvenile idiopathic arthritis…….185

Figure 25: Permeability curve of a septic arthritis……186

Figure 26: Cake diagram of the main pathologies (8 categories)……...197

Figure 27: Cohen’s kappa values of the accuracy tests of the single sequences…202

Abbreviations:

2D 2 dimensional

3D 3 dimensional

AIF Arterial input function

AUC Area under the curve

B1 Main magnetic field

Cp Plasma concentration

CT Computer tomography

DCE Dynamic contrast enhanced imaging

DCI Dynamic contrast imaging

DSC Dynamic susceptibility contrast

DWI Diffusion weighted imaging

Dyn. Dynamic

FA Flip angle

FSE Fast spine echo

Gd Gadolinium

GRE Gradient echo

Hct Haematocrit

ICC Interclass correlation coefficient

K_{ep} Endothelial reflux rate or rate constant

K^{trans} Endothelial transfer constant

Kg Kilogram

LAVA Liver acquisition with volume aquisition

Mg Milligram

MRI Magnetic resonance imaging

MSK Musculoskeletal

PD Proton density (sequence)

PET Positron emission tomography

r1 Tissue relaxivity

ROC Receiver operating characteristics

ROI Region of interest

Sat Saturated (fat saturated)

SCE Serial contrast enhanced imaging

SE Spine echo

SNR Signal to noise ratio

SS-EPI Single shot echo planar imaging

SS-FP Steady state free precession (imaging)

T1 T1 weighted MRI sequence

T2 T2 weighted MRI sequence

T10 Tissue native T1 value before Gd administration

$T10_{blood}$ Blood native T1 value before Gd administration

t_onset Time of contrast agent administration

TB Tuberculosis

TE Time of Echo

TME Time to maximum enhancement (permeability value)

TR Time of repetition

TSE Turbo spine echo

V_e Fractional extravascular extracellular space volume

V_p Fractional plasma volume

CHAPTER 1: Introduction

1-1 Background:

Bacterial infections in paediatric population are widely disseminated and involve different organ systems, however the majority of these either remain subclinical, or if they are symptomatic, the diagnosis and the treatment are usually unremarkable with good prognosis (1,2). Unfortunately infections of the skeletal system do not follow the same rules since these infections can have nonspecific signs and symptoms mimicking traumatic injuries or other possible benign or malignant aetiologies (1,2). Musculoskeletal infections often fail to be recognised early in the course of the disease and the subsequent treatment is in many cases suboptimal potentially leaving children with long term disabilities and significant morbidities (1,2).

1-2 Musculoskeletal infection in children:

Musculoskeletal infection is an inflammation of the musculoskeletal system, usually with a bacterial agent, which can include one or multiple compartments of the musculoskeletal system (1). Musculoskeletal infections can be divided into three main compartmental subgroups including infections of soft tissue, bone and joints (1) and can be further divided into 7 clinical diagnoses:

1- Osteomyelitis
2- Septic arthritis
3- Myositis
4- Cellulitis
5- Fasciitis
6- Spine infections including discitis and spondylodiscitis

7- Deep neck infections

The course of infection can be:

1- Acute if the duration of the symptoms is less than 2 weeks
2- Subacute (2 weeks< symptom's duration <4 weeks)
3- Chronic if symptoms persist over a month (3,4).

Musculoskeletal infections in children differ in many ways from adult musculoskeletal infections including the following:

1- The usual infectious agents
2- The pathogeneses
3- The musculoskeletal components
4- The compositions and vascularity of the affected tissue
5- The course of infections and how the immature immune system reacts

The above are a few of many aspects which vary between paediatric and adult populations. There are even significant differences between neonatal, early and later childhood infections due to complex anatomical, physiological and pathophysiological changes of the growing skeleton in the first eighteen years of life.

The course of soft tissue infections is usually mild in children, whereas infections of bones (osteomyelitis) and joints or synovial membrane of the joints (septic arthritis) in children are usually serious infections with complex diagnostic problems and difficult or prolonged treatment implications. The aetiology, pathogenesis, presentation and immune response to osteomyelitis or septic arthritis in children differ substantially from adults due to profound differences in their musculoskeletal and immune systems. These differences will be explained in the following sections. The diagnosis of osteomyelitis and septic arthritis in children continues to be challenging and does not follow the conventional recognised adult route.

1-3 Epidemiology and incidents:

The annual incidence of paediatric MSK infection varies slightly in different Western populations; the estimated incidence for acute septic osteoarthritis (osteomyelitis + septic arthritis) in children is 5-12 per 100,000(5). The reported annual incidence of childhood osteomyelitis including acute and sub-acute infections is 3-20 per 100,000 (6). Acute osteomyelitis has a lower incidence in developed countries (8–10 per 100,000) in comparison to the developing countries which may have an incidence up to 80 per 100,000 (7–10). The incidence of septic arthritis is about half the rate of osteomyelitis (10).

The incidence varies between different age groups and gender and is higher in children below three years of age, with a maximum incidence in children below the age of one (6). Children under the age of 5 account for more than half of all musculoskeletal infections (7,10,11). The incidence of acute osteomyelitis is higher in boys, with an estimated male-female ratio of 1.9 to 1.0 (6,11–15). The majority of musculoskeletal infections are focal and predominantly involve the long bones, especially the tibia and femur however multifocal involvement is present in up to 6.8% in infants and even up to 22% in neonates has been reported (6).

There is a significant increasing incidence worldwide of MSK infections, particularly osteomyelitis (16).

1-4 Aetiology:

There are a wide range of microorganisms implicated in Paediatric MSK infection (5). Interestingly the aetiology of the acute haematogenous infection has changed substantially since the introduction of haemophilus influenza vaccine. In north west Europe staphylococcus aureus is now the leading pathogen (44-80%, mainly MSSA) replacing haemophilus influenza, closely followed by Kingela kingae (14-50%, increased <36 months) and group B streptococcus in neonates (5,17,18). Many microorganisms are much more common in particular age groups, or cause joint or bone infections more frequently. There are also certain predisposing diseases

associated with particular microorganisms in children with chronic conditions such as sickle cell disease, Beta thalassaemia or immunosuppressed children (congenital, post chemotherapy or bone marrow transplant treatment).

Appropriate knowledge of these details is important for further differentiation of possible pathogens once the diagnosis of infection is stablished.

Faust et al (5) categorised the main paediatric pathogens in different subgroups according to their frequency and age related predisposition shown in **table 1**(5 p. 2 table 1).

Organism frequency	**Age Specification**
Common	
Staphylococcus aureus(MSSA), 44–80%	All age groups
Kingella kingae, 14–50%	< 5 Years (increased <36 months)
Rare	
Methicillin-resistant *S aureus*, 40–50% in USA, rare in UK	
PVL MSSA	2-18 Years
GAS	2-5 Years
GBS	Neonates
Non-typeable *Haemophilus* spp. (incidence unknown)	1 Month – 5 Years
Haemophilus influenzae type b (non-immunised or immune deficient)	1 Month – 5 Years

Escherichia coli (neonates)	Neonates
Streptococcus pneumoniae	1 Month – 5 Years
Coagulase negative staphylococcus (subacute)	2-5 Years
Very rare at any age (increased in immunodeficiency and where specific risk factors occur)	
Pseudomonas aeruginosa	Usually inoculation injuries hence >1 year old, mostly 2-5 years
Neisseria gonorrhoeae	
Neisseria menigitidis	Neonate, adolescent
Mycobacterium tuberculosis	Older children as OAI develops 2 years from primary infection
Salmonella spp. (sickle cell disease)	
Non-tuberculous mycobacteria (associated with defects of IFNg/IL pathway)	
Klebsiella spp.	
Bartonella henselae	
Fusobacterium (often multifocal)	
Aspergillus (immune suppressed)	
Candida albicans (immune suppressed, damaged bone)	Neonates

Table1,[Faust et al (5 p.2 table 1)**].**The Microbiological aetiologies of musculoskeletal infections in children in the UK**.** Group A streptococci (GAS); Group

B streptococci (GBS); Methicillin sensitive *Staphylococcus aureus* (MSSA); Osteoarticular infections (OAI); Panton-Valentine leucocidin (PVL).

1-5 Transmission and pathogenesis:

The main transmission routs of musculoskeletal infections in children are:

1- Haematogenous which is the most common route in neonates and younger children
2- Local spread from a nearby infection
3- Direct inoculation which is most often seen in older children(4,6).

The pathogen after entering the host induces a cascade of immune reactions which include hyperaemia of the affected organ, local hyper perfusion, endothelial permeability dysregulation, extravascular diffusion and cell migration, local tissue destruction and finally recovery with possible scar tissue or tissue defects. These are different phases of an infectious process or respectively the immune reaction.

The pathogenesis of musculoskeletal infection varies significantly between the mature and the growing skeleton, due to fundamental differences in anatomical components, parenchymal compositions, physiological activity and pathophysiological reactions. These differences are responsible for varying susceptibilities, differing immune reactions and differing responses to treatments with a resultant wide variation in outcomes. The most important differences which affect the diagnostic pathway, in particular the imaging diagnostic are summarised below.

1-5-1 Cartilage evolution:

The growing skeleton is initially completely cartilaginous, which over many years during the growing period, step by step, transforms into the final mature bony skeleton through the process of chondral ossification (primary and secondary). Therefore the composition of cartilage and bone is permanently changing during the skeletal growth process (19 PP.2545-2555). The metaphyseal and epiphyseal

cartilages initially communicate with each other however, with progressive ossification the ossified metaphysis will be separated from the gradually ossifying epiphysis through the growth plate cartilage (19 pp.2545-2555).

Children have two different types of cartilage in their skeleton, the epiphyseal fibrocartilage and the growth plate or articular hyaline cartilage; this is in contrast to adults who have only articular hyaline cartilage. The glucosamine glycan matrix substance of the hyaline cartilage in children contains more water in comparison to adult hyaline cartilage but there is a less pronounced difference between the fibre rich fibro cartilage and the water rich articular and growth plate hyaline cartilage (19 pp.2545-2555).

1-5-2 Vascular evolution:

Vascular evolution is most profound in the metaphyseal and epiphyseal ends of the bones in the first few years of life. In neonates the central diaphysis vessels extend to the metaphysis where they create a vast number of slow flow small vessels and extend directly through the cartilaginous growth plate into the mostly cartilaginous epiphysis, and the cartilage is generally more vascular in comparison to the mature skeleton, hence osteomyelitis and parallel septic arthritis are very common in this age group (19 pp. 2883-2912). There are other characteristics encouraging this scenario in neonates including larger joint capsules and looser attachments of the periosteum to the bone in the first years of life (4). Later during the second year of life the changing growth plates stop blood vessels from crossing the physis and from then until the skeletal maturity, the growth plate acts as a barrier between the metaphysis and the epiphysis, which now have separate feeding vessels. This phenomenon explains the higher number of metaphyseal infections from the age of two to three (4,19 pp.2883-2912,20).

1-5-3 Bone marrow conversion and reconversion:

Bone marrow composition is another part of the musculoskeletal system that undergoes rapid change during childhood. The marrow changes from cellular red marrow (haematopoietic marrow) to less cellular yellow (fatty) marrow, which contains large fat cells follows a rigid pattern which is from the centre of the

diaphysis towards the metaphysis or the periphery of the bone (19 pp.2970-2976). The conversion of bone marrow accelerates in the first two decades of life (19 pp.2970-2996). The bone marrow in new-borns is nearly 100% haematopoietic marrow which then rapidly reduces to 75% by the age of fifteen, 60% in early adulthood and estimated 5% in later years when nearly 95% of cells are adipocytes (19 pp.2970-2996). Red marrow is the active haematopoietic marrow, which produces red and white blood cells and is immensely vascular; this in combination with the centrifugal pattern of marrow conversion explains the metaphyseal predisposition of musculoskeletal infections in children (19 pp.2970-2976).

Furthermore there have been significant changes in the presentation of acute haematogenous osteoarthritis in children over the past decades. The emergence of multi-resistance staphylococcus aureus variants and Panton-Valentine leucocidin gene positive strains which have transformed the virulence of the most common pathogen are the cause of many of these changes (10,21). Musculoskeletal infection in children is now more common, more destructive, and more likely to be associated with complications outside the bony structures (10).

1-6 Risk factors:

There are many proposed predisposing factors for musculoskeletal infections described in multiple publications (4,17,18,22–25) with varying effects including congenital and acquired conditions, which are listed here:

1- Immune deficiencies (primary or secondary which are divided to immune or drug related)
2- History of skin or soft tissue infection
3- History of close contact with people with skin or soft tissue infection
4- Traumatic injuries of the musculoskeletal system, including mild injuries
5- Routine participation in contact sport
6- Preceding Respiratory or urinary tract infection

7- Sickle cell disease or similar haematological disorders (haemophilia, Beta thalassaemia…)
8- Pre-existing joint or skeletal abnormalities
9- Recent history of medical interventions including insertion of central venous lines
10- Ethnicity
11- Socioeconomic factors, including income, living standard…
12- Recent travel (4,17,18,22–25).

1-7 Diagnosis:

The diagnosis of musculoskeletal infections in children has been historically challenging (3,4,26,27). The main clinical symptoms are non-specific, and the laboratory and microbiology results are not sensitive or specific enough for a reliable diagnosis (27–29). It has become apparent that early diagnosis and tailored comprehensive treatment will lead to faster recovery and better prognosis, therefore prompt and adequate diagnosis is vital(7,10,11). While the diagnosis should have a multidisciplinary approach including clinical findings, laboratory, and microbiology tests, as well as diagnostic imaging, the desire for a more comprehensive more specific diagnostic tool however remains.

1-7-1 Clinical features and presentation:

The clinical signs and symptoms of painful musculoskeletal events including high temperature, soft tissue swelling, localised or multifocal pain, erythema and local lymph node enlargement, are not specific for infection as they can be caused by other conditions (30,31) and are not sensitive enough, particularly in subacute and chronic cases, or in neonates when the immune responses are still immature (3,27).

1-7-2 Differential diagnosis:

There are many diseases and conditions which mimic musculoskeletal infections. The varying age-related presentation, the immature immune response in the early years and the lack of adequate communication in neonates and small children make the differentiation even more difficult. The possible differential diagnoses are listed in table 2 [references (3,4,26,27)], which highlights that the main clinical signs and symptoms are not sufficient discriminatory findings to differentiate infection from other potential aetiologies emphasising the need for further specific diagnostic tools.

Differential Diagnosis	Main Symptoms			
	acute pain	soft tissue/ joint swelling	Temperature	multifocal pain
Non accidental injury, Trauma	(+)	(+)	(+)/(-)	(+)/(-)
Transient synovitis	(+)	(+)/(-)	(+)/(-)	(+)/(-)
Reactive arthritis	(+)/(-)	(+)/(-)	(+)/(-)	(+)/(-)
Infarction	(+)	(+)	(+)/(-)	(+)/(-)
Rhabdomyolysis (viral, trauma or drug related)	(+)/(-)	(+)/(-)	(+)/(-)	(+)/(-)
Musculoskeletal benign and malignant Tumours	(+)/(-)	(+)/(-)	(+)/(-)	(+)/(-)
Caffey Disease (Type I collagen mutation)	(+)/(-)	(+)	(+)	(+)/(-)
Chronic relapsing multifocal osteomyelitis	(+)	(+)	(+)/(-)	(+)

Table2. Differential diagnoses and the common symptoms(3,4,26,27)**.**

1-7-3 Laboratory and microbiological investigations:

Many laboratory parameters are unreliable, and the diagnostic yield is in many cases suboptimal(10,32). The white blood cell count can remain normal (5,29) or non-specific as can the ESR or CRP (5,33). The microbiological samples from joint fluid, periosteal pus or bone biopsy are positive in only a maximum of 40-50% of cases and blood cultures may only be positive in 9-22%(28,29) of cases. Tissue samples are more likely to be positive, but they frequently require invasive procedures under general anaesthesia or at least local anaesthesia (5,29). Blood cultures and tissue samples should be taken ideally, prior to starting antibiotic therapy for possible microorganism identification (34) and this ideal is often difficult to accomplish.

There are advanced new molecular techniques with higher sensitivities including PCR and broad range 16s rDNA PCR for rapid diagnosis however, these techniques also have their limitations (5,35,36). The limitations of PCR and broad range 16s rDNA PCR are availability, prolonged examination time, high sensitivity of the routine PCR for only one pathogen/strain whilst missing many other potential pathogen, the lower sensitivity and specificity of broad range 16s rDNA PCR if intended to cover multiple pathogens and finally the detection of bacterial DNA does not mean that the relevant bacterium has a pathogenic role as many children are colonised with different bacteria without being infected (5,35,36). When the clinical and laboratory tests are unable to differentiate MSK infection from other causes of musculoskeletal pain, imaging is the diagnostic tool which can lead to a specific diagnosis (27).

1-7-4 Imaging diagnostic:

Imaging has always played a pivotal role in the diagnosis of musculoskeletal infection in children and can be used to detect infection, guide intervention and monitor therapy (6). Imaging is the main diagnostic tool whenever the clinical symptoms, laboratory and microbiology results prove to be non-conclusive however the conventional approach including radiography, ultrasound and scintigraphy or in cases of slow treatment response magnetic resonance imaging (20,37) is no longer acceptable as early diagnosis in acute clinical setting is the most important factor

which influences the prognosis (3). There are multiple imaging modalities which can be used to detect MSK infections in children; the following is a brief description of these modalities including their advantages and shortcomings.

1-7-4-1 Radiography:

Radiography is a useful tool to visualise and evaluate structural and traumatic bony deformities. Radiography is suitable for detection of infection-related osseous abnormalities and occasionally soft tissue changes including soft tissue swelling or joint space expansion due to joint effusion. The bony changes in an infectious process, however, are not radiographically evident in the first 7-10 days and even after ten days the detection rate is suboptimal (20,38,39). The sensitivity of radiography is only 20% after 10 and up to 75% after 14 days and the specificity is reported to be 75-83% after 14 days (4,6,12,30,40–44). Radiography is suitable for excluding the possibility of other bony pathologies such as fractures, detecting subacute osseous changes and prognostic long term follow-ups, but is not a reliable acute phase diagnostic tool. Radiography involves low level radiation which is not significant in acute diagnostic situations but the possibility of adverse cumulative doses should be considered when multiple follow-ups are required and thus radiation exposure is one of radiography's handicaps.

There are no specific radiographic osseous changes which are characteristic for infection and there is a large overlap in osseous changes between bony infection, infarction and multiple benign and malignant tumours which can be a source of false positive or negative results.

Radiography is still commonly used however as the first line diagnostic tool as it is fast, uncomplicated, available and is a relatively simple monitoring tool in cases of osseous change(30,43).

1-7-4-2 Ultrasonography:

Ultrasonography is a non-invasive, affordable and broadly available modality which can detect soft tissue changes in the acute phase, including soft tissue oedema, sub periosteal collection, and joint effusion as early as 48 hours after onset of infection

(4,45). Although ultrasound is extremely useful in the detection of soft tissue abnormalities, fluid collections and guidance of interventions, the findings are usually nonspecific and the bony changes remain undiagnosed with ultrasound. The invisibility of intraosseous changes especially in the early phases of an osteomyelitis and the operator dependency are the main disadvantage of ultrasound (6). Other limitations of ultrasound are inability to sufficiently cover large areas of interest or detect multifocal processes. The sensitivity and specificity of ultrasound in acute MSK infection is 55% and 47% respectively(46).

Ultrasound is mainly used as a complementary tool in the diagnosis of MSK infections, to detect joint effusion or soft tissue collection. A negative ultrasound scan does not exclude an infection.

1-7-4-3 Scintigraphy (nuclear medicine):

The principle of Nuclear medicine examinations' is based on intravenous administration of a radionuclide, which emits radiation that is then detected by a camera sensitive to ionising radiation (31). Abnormal uptake, perfusion or metabolism of a radionuclide, due to a pathological process, for example, an infection can be detected. Scintigraphy is more sensitive in the detection of osteoarticular infections when compared to radiography. The signal intensity can be raised within 24 to 72 hours of symptom onset (4,20), although the sensitivity is impaired in the first 48 hours(31,43). There are different nuclear medicine's studies for diagnosing osteomyelitis in children, including the ^{18}F-fluorodeoxyglucose positron emission tomography (FDG-PET), triple-phase ^{99m}Tc-methylene diphosphonate (the most common type of scan when referred to as scintigraphy), gallium and indium-111 white cell scans (6,31,47). The two later type of scans do not show bony details and cannot differentiate between bone and soft tissue infections (44). The highest sensitivity and specificity in the diagnosis of osteomyelitis in adults has been postulated to FDG-PET(sensitivity of 94-99% and specificity of 75-99%), however the use of PET is limited in children due to its significant radiation burden, poor availability and lack of evidence, based on large paediatric studies (6,47).

The main strength of scintigraphy is its high sensitivity when the field of view is large, which enables it to detect multifocal processes. The sensitivity and specificity of bone scintigraphy with large field of view are 80-88% and 82-85% respectively(30,43).

Scintigraphy has gradually been replaced over the last decades by MRI, due to scintigraphy's suboptimal resolution, the lower specificity in comparison to MRI, the inability to differentiate between overlapping tissue structures or organs and the high radiation burden(4,20,30,48), which is more than 10 mGy (organ dose) in average for bone marrow for scintigraphy (10). Availability and high cost are other limiting factors for nuclear medicine scans. Bone scintigraphy is still useful when the infection is close to a metallic prosthesis, which can cause significant artefacts in CT and MRI.

1-7-4-4 Computed tomography:

Computed tomography (CT) is a cross-sectional imaging tool with high osseous resolution which has been used in the past as a diagnostic tool to detect and characterize bony and to a lesser degree soft tissue changes in children with musculoskeletal infection. CT can reveal structural changes of the bones in an infectious process such as bony defects or sinus tracks, although structural changes of the bones are not part of the findings in the acute phase and are normally apparent much later in the course of infection as part of subacute or chronic changes.

The cross-sectional nature, the higher resolution, the improved sensitivity and the ability to cover larger areas in comparison to radiography promoted computed tomography to be included in the list of imaging modalities utilised traditionally to diagnose Osteomyelitis. The sensitivity and specificity of CT in diagnosis of MSK infection are respectively 67% and 55%(43,49).

The emergence of MRI and its establishment in MSK imaging has transformed the role of CT in the diagnosis of osteomyelitis. The lower sensitivity, specificity and tissue differentiation of CT in comparison to MRI, the inability to detect soft tissue or bone marrow oedema and its high radiation burden are the main factors limiting its

widespread use in this context. The lower sensitivity, specificity and soft tissue differentiation are the sources of potential false negative or positive results. CT is still a valuable tool when patients are unable to undergo MRI examination (43).

1-7-4-5 Magnetic resonance imaging:

MRI has transformed musculoskeletal imaging since its emergence more than 30 years ago and has become the most utilised imaging tool for musculoskeletal diseases of all types. MRI has the advantage of excellent soft tissue characterization and differentiation with detailed bone marrow and soft tissue resolution (26), which enables it to detect and distinguish between bone marrow oedema, osseous lesions, bony infiltration and different bone marrow compositions. MRI can depict the early signs of a musculoskeletal infection within the first 24 to 48 hours (20,26) and can differentiate between acute, subacute and chronic changes, making it the most desirable imaging tool in the diagnosis of childhood MSK infection. Furthermore contrast enhanced MRI has the potential to improve the diagnostic yield of MRI in the detection of musculoskeletal infections and although some studies have suggested that the diagnostic benefit of contrast agent is not relevant (26,50), more recent studies have shown the advantages of contrast enhanced MRI and proven the contrary (30,51).

MRI is particularly useful in children (4) considering the cartilage content of paediatric skeleton and the presence of growth plates together with the changing bone marrow composition and different types of vascular supply in children when compared to adults (38). The sensitivity and specificity of MRI vary in different paediatric and adult studies 82-100% and 75-99% respectively although most of the studies are based on small and/or mixed (paediatric & adult) populations and mixed levels of evidence (level 3 and 4 evidence)(6,13,47,52,53).

MRI allows whole-body imaging which is crucial in multifocal infections or chronic recurrent multifocal osteomyelitis. The lack of ionising radiation is another significant benefit of MRI in paediatric imaging. The main disadvantage of MRI in younger children is the duration of the examination which can affect their compliance(6). There are many approaches to reduce the scanning time such as faster sequences

or to improve the compliance of young children including sedation, general anaesthesia, and the use of dedicated paediatric play specialists which will be explained in material and methods section. Other disadvantages of MRI are the relative high cost and in some places poor availability (43).The presence of some electronic device such as cardiac pace maker can pose a contraindication for the use of MRI due to the risk of malfunction(43).

MRI has the potential to detect and differentiate musculoskeletal infection, alter clinical management and create a road map for surgical or minimally invasive radiological interventions(26,54).

1-7-4-6 Comparison of the imaging modalities:

The sensitivity and specificity of imaging modalities in the differential diagnosis of acute musculoskeletal infection are presented below in table 3(4,6,12,13,30,40-49,52,53).

Imaging modality	Sensitivity	Specificity
Radiography	20% (after 10 days)-75% (after 14 days)	75%-83% (after 14 days)
Ultrasonography	55%	47%
Scintigraphy	80-88%	82-85%
Computed tomography	67%	55%
Magnetic resonance imaging	82-100%	75-99%

Table3. Sensitivity and specificity of different imagining modalities in the diagnosis of acute musculoskeletal infection according to literature(4,6,12,13,30,40-49,52,53).

Table 4 below is a modification of table 2 of Pineda et.al (44) comparing different imaging modalities in the differential diagnosis of acute musculoskeletal infection in children.

Imaging modality	Advantages	Disadvantages	Findings
Radiography	Inexpensive, Available, Reproducible	Late diagnosis, Radiation exposure	Lytic lesions, periosteal elevation or thickening, loss of trabecular architecture, new bone building
Sonography	Available, Inexpensive	Operator dependent, Small FOV, Inability to detect bony changes	Fluid collection, Periosteal elevation
Scintigraphy	Sensitive, Early detection	Low specificity, High-radiation exposure, Often equivocal results, Long examination, cost, lack of differentiation of overlapping tissue	Focal hyperaemia/ Hyperperfusion, Focal bone uptake
Computed tomography	Good spatial resolution	Radiation exposure, Cost, possible poor availability	Soft tissue density changes, Bony irregularities, Periosteal elevation, Increased density of fatty marrow
Magnetic resonance imaging	Excellent resolution and tissue differentiation, Early detection, high sensitivity and specificity	Cost, possible poor availability, Long examination, Contraindication in presence of some medical implants (pace maker,..)	Signal intensity changes in bone and soft tissue, Periosteal elevation, Exclusion of collections and oedema, contrast enhancement

Table4. Advantages, disadvantages and imaging findings of different imaging modalities in the diagnosis of acute musculoskeletal infection in children Pineda et.al (44).

1-7-5 Ideal imaging tool:

Musculoskeletal infection in children is a rapidly changing dynamic process caused by a pathogen, the immune response is equally a dynamic process with multiple phases including, hyperaemia, permeability changes, oedema, proliferation and compositional changes of the bone marrow.

Early diagnosis is crucial as it can potentially determine the prognosis; however the majority of the early changes are subtle without apparent macroscopic irregularities, but with rapid changes at a molecular level. The molecular and cellular reorganisation of the extracellular architecture due to permeability changes of the vessels and migration of immune system cells are the early changes which are invisible to most imaging modalities.

The role of imaging is to visualise the immune response in the affected tissue. Hence the ideal imaging tool should be a dynamic and modifiable tool which can detect the early immune reaction and identify the rapid parenchymal changes.

The desire for a more comprehensive and accurate diagnostic tool was the motivation for this work and its potential will be addressed in the following chapters.

1-7-6 Advanced Magnetic resonance imaging:

MRI is the most versatile imaging modality available to us with endless modifiable parameters and the capability to capture early changes of a dynamic process such as musculoskeletal infection in children.

The magnetic relaxation of different tissue in a magnetic field varies based on the tissue structural compositions. The magnetic relaxation of a magnetised tissue in a magnetic field is mainly based on energy transfer to the environment (T1 relaxation)

or between the magnetised elements (T2 relaxation) which can neutralise each other(55).

The structural or conventional MRI sequences are primarily qualitative imaging tools, which mainly rely on qualitative interpretation of varying magnetic relaxation (longitudinal=T1 and transversal=T2) properties of different tissue in order to distinguish between normal and pathologic tissue(56).

There are however more advanced MRI techniques which utilise functional or biodynamic tissue properties, to not only qualitatively visualise but also semi quantitatively or quantitatively differentiate between various types of tissue such as diffusion weighted imaging (DWI) and serial or dynamic contrast enhanced imaging (SCE/DCE).

Diffusion weighted imaging, translates the unique pattern of Brownian motion of water molecules in different tissue environments into a qualitative map based on tissue specific diffusion coefficients which can be quantified. DWI provides qualitative imaging information and quantitative values which can characterise the microscopic architecture of the tissue(55,57)

Dynamic or serial enhanced imaging is based on rapid and repetitive acquisition of images from the area of interest (the same slice = dynamic or multiple consecutive slices = serial) before, during and after contrast agent administration. The acquired images are valuable qualitative information concerning mainly contrast enhancement processes. There are mathematical models that can calculate qualitative and quantitative curves based on contrast exchange rates at the level of vascular barriers in the tissue and thus reveal the dynamic of the perfusion and permeability characteristics of the tissue. Dynamic or serial enhanced imaging delivers detailed qualitative images and semi-quantitative or quantitative values concerning the trans-endothelial contrast agent transfer(58,59).

Whilst routine qualitative MRI sequences can capture macroscopic irregularities of an infectious process; the early microscopic changes can be depicted by advanced qualitative, semi-quantitative and quantitative MRI techniques, such as diffusion weighted imaging (DWI) and dynamic or serial contrast enhanced imaging. These

characteristics of advanced MRI techniques suggest that they may be the most suitable diagnostic tools available in the rapid diagnosis of musculoskeletal infection in children.

1-7-7 Introduction to Diffusion weighted imaging:

Diffusion-weighted magnetic resonance imaging (DWI) is a recent addition to paediatric musculoskeletal MR sequences (57). The signal intensity of DWI relies on the stochastic Brownian motion, or self-diffusion, of water molecules in all three dimensions at a microscopic level within tissues (57).

DWI is one of the few MRI sequences which can offer qualitative and quantitative information.

The most important factors of diffusion weighted sequences are the diffusion sensitising impulse or signal combinations (gradients) of the sequence and the sensitivity for diffusion effects created by the given impulse combination, which is called B value.

The higher the B value the stronger are the diffusion effects.

ADC values are the quantification of diffusion properties of the scanned tissue, and the ADC maps represent the cross-sectional mapping of the ADC values.

ADC values are the most established magnetic resonance quantitative measures and reflect the cellularity and water molecule motion restriction in tissue (57).
DWI sequences are suitable for whole-body imaging and can improve conspicuity and sensitivity in a multifocal process(57,60).

The diffusion properties of water molecules in Vivo and their role in MRI are explored in the following sections.

1-7-7-1 Diffusion phenomenon of water molecules (Brownian motion):

Robert Brown, a Scottish botanist noticed in 1827, that tiny pollen grains suspended in still water, moved in different directions in complex paths (61). This phenomenon (illustrated in Fig. 1) can be observed for any small particles in a low viscosity fluid

and is caused by the random thermal motions of fluid molecules colliding with particles in the fluid, this is called **Brownian motion** (61).

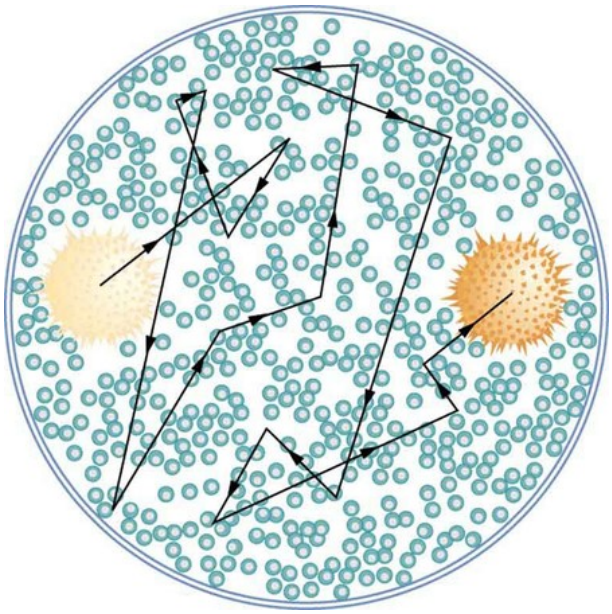

Fig. 1 (51fig. 2.1.1)- The position of a pollen grain in water, measured every few seconds under a microscope, exhibits Brownian motion

The stochastic Brownian motion or the self-diffusion of water molecules is unimpaired in pure water at room temperature; however, the architecture of organic tissues is more complex and restricts the free diffusion of water molecules to different degrees in comparison to pure water.

The stochastic Brownian motion of water molecules or small particles in different fluids can reveal detailed information about the tortuosity of their environment and even the size of the surrounding molecules and atoms.

Brownian motion has been a topic of research for many researchers since its emergence in early 19^{th} century including Albert Einstein who published multiple papers that explained how Brownian motion could be used to measure the size of atoms and molecules (61,62).

Erwin Hahn was one of the pioneering researchers who performed experiments in the 1940s and 1950s in the field of magnetic resonance imaging, using Brownian molecular motion of spins in a magnetic field (63).

The diffusion phenomenon of water molecules has been employed in recent years in the field of magnetic resonance imaging to create more sensitive and robust imaging tools and improve the diagnostic yield of MRI.

1-7-7-2 Diffusion weighted imaging, basics and principles:

Diffusion weighted imaging is a magnetic resonance technique which relies on self-diffusion of water molecules in tissue (63,64).

The basic principle of the diffusion-weighted sequences is based on sensitising spin echoes to Brownian motion of water molecules in tissue and visualising it as signal attenuation (63,65,66).

Erwin Hahn described in his paper “Spin echoes” in 1950 that the employment of a magnetic field gradient during a spin echo experiment can influence the signal due to the diffusive properties of the spins (63,67).

Stejskal and Tanner developed the Hahn model, and in order to improve the quantification of the diffusion effect responsible for signal decay in their model, they employed two equal gradients on both sides of the 180 degree pulse following the initial 90 degree pulse of a spin echo sequence, the so called Stejskal-Tanner diffusion gradients (63,68).

This finding was published in 1965 in their paper “Spin Diffusion Measurements: Spin Echoes in the Presence of a Time Dependent Field Gradient”. It was the first successful attempt to quantify the diffusion properties of molecules in a liquid using a gradient couple (63).

The function of the equal unidirectional diffusion couple is to dephase and rephase the magnetising vectors of the spins, and consequently attenuation of the received MR signal, which varies based on the diffusion of different molecules (63,68). Following the first diffusion gradient, the spins are dephased, however the phase angles of the spins vary slightly based on their spatial location and the inhomogeneity of the magnetic field (63,68). If the spins are stationary the second diffusion gradient neutralises the phase angle of the spins, and the spins after the second gradient will return to the same magnetisation configuration before the

implementation of the first diffusion gradient without measurable signal attenuation (63,68). If the spins are not stationary and are moving randomly then they will have varying spatial locations and experience unequal magnetic fields by the time of the second diffusion gradient, hence the second gradient is not able to neutralise the effect of the first gradient and revert the phase angle, consequently a varying random phase difference between the spins will remain (63).

The consecutive unequal distribution of the phase angles provokes a visible signal attenuation(63) which depends on the strength of the gradients, the time interval between the gradients, spatial inhomogeneity and the extent of molecular diffusion.

The visualisation of the signal attenuation based on the implementation of diffusion gradients and the stochastic motion of the spins are the basic principles of diffusion weighted imaging.

The effects of the diffusion gradients on stationary and mobile spins are illustrated in Fig. 2 which was published by Dietrich et al. in 2009(63 p.2 fig.1).

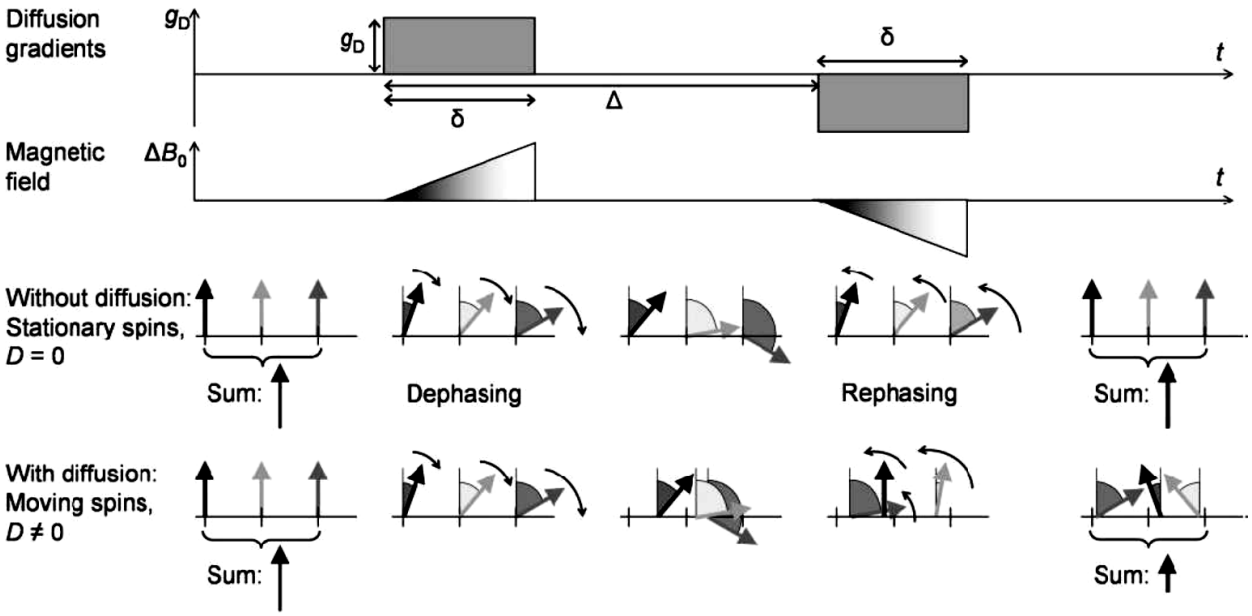

Fig.2(63 p.2 fig.1)- The influence of diffusion gradients in case of stationary or diffusing spins and the consecutive varying effect is demonstrated for stationary and moving spins. B_0= Magnetic field, g_D= Diffusion gradient amplitude, δ= Duration of the diffusion gradient, ∆= Interval between the onset of the diffusion gradients.

The magnitude of molecular diffusion is quantitatively determined by the diffusion coefficient (D) which is generally direction dependent and is measured in mm^2/s (55 p.77). It describes the mean displacement (d) of water molecules per time unit (63).

The main characteristics of the diffusion gradients are their strength or magnitude, the duration of the diffusion gradients and the time interval between the two diffusion gradients which is represented by diffusion weighting or b-value of the gradient impulse pair (57).

The unit of b-value is s/mm2 and can be calculated using the characteristic parameters of the employed gradient impulse pair and the gyromagnetic ratio of the involved spins(63):

$$b = (\gamma \cdot g_D \cdot \delta)^2 \cdot (\Delta - \delta/3)$$

g_D = Diffusion gradient amplitude

δ = Duration of the gradients

Δ = Interval between the gradients onsets

γ = Gyromagnetic ratio (the ratio of the magnetic moment to the angular moment of a particle)(60)

The range of the most commonly used b-values is between 0 and 2000 s/mm2. There is no diffusion effect when b-value is 0, and the signal is purely related to the specific characteristics of the spin echo sequence which is T2 weighted the majority of the time.

The role of b-value in a DWI pulse sequence is the same as the role of echo time in a T2 weighted sequence, hence higher b-value (increased diffusion effect) means more contrast and higher conspicuity, but at the cost of reduced signal intensity (63). In addition, higher diffusion weightings require longer echo times due to the long diffusion gradient pulses, thus the signal to noise ratio (SNR) of the high diffusion-weighted images is further decreased (63). In diffusion weighted sequences with low b-values the diffusion contrast is less pronounced, and the signal reflects the fluid

content and perfusion effects of the tissue much more. In contrast increasing b-values improves the diffusion sensitivity of the sequence and shifts the contrast from perfusion to diffusion effects, hence finding the balance between diffusion contrast and reduced background noise on the one hand and perfusion contrast and increased signal to noise ratio, on the other hand, can be challenging (63).

Generally increasing b-value is accompanied by signal intensity decay in tissue with a bi-exponential pattern, where the initial exponent is due to signal loses caused by blood flow and perfusion while the second exponent is mainly due to extravascular extracellular water motion (57).

Water molecules are the most important diffusing molecules in diffusion weighted imaging, they travel approximately 30 micrometres per 50 ms at 37 degrees Celsius if there are no barriers to limit their motion (57). However the diffusion of water molecules in the human body is neither free nor random as there are many cells, cell membranes, cell organelles, macromolecules, fibres and other obstacles which prevent the free water molecule diffusion in vivo, hence the diffusion phenomenon of water molecules in the human body is restricted and determined by its microscopic cellular structure and surrounding architectural tortuosity (57).

The diffusion coefficient decreases in vivo in comparison to free water owing to relatively restricted diffusion (63). The measured diffusion coefficient in vivo is called “apparent diffusion coefficient” (ADC), the word apparent reflects other factors besides diffusion that contribute to signal loss including cell membranes, large macromolecules and fat cells to name a few (56).

Apparent diffusion coefficient or ADC total consists of multiple fractions; the main fractions are ADC slow and ADC fast. The fast fraction reflects mainly the perfusion aspect of the total tissue diffusivity and is apparent when calculating the ADC for low b-values, while the slow fraction mainly reflects the diffusion aspect of the tissue diffusivity and is calculated using high b-values (57). However, in most cases it is only ADC total or simply ADC reported, which encompasses both fractions depending on the used b-values.

The mathematical definition of ADC value is the gradient of the logarithmic decrease in signal intensity between two or more b values (56).

ADC maps are the cross-sectional calculations of ADC values; their grey scale signal intensity values represent the mean ADC in the imaged voxels (55). The signal intensity of ADC maps correlate directly with the diffusivity in the imaged tissue, hence increased diffusivity means increased signal and restricted diffusivity means decreased signal (the opposite of DW images). There are minimum, maximum and mean ADC values for a particular region of interest, as the ADC values are calculated on a pixel by pixel basis for each voxel and presented in mm2/s (56).

Diffusion weighted imaging reveals the molecular structure, the cellular architecture and the spatial tortuosity of organic tissues by exploiting the Brownian motion or diffusion of water molecules in extravascular spaces.

1-7-7-3 Diffusion weighted imaging techniques:

Many sequences can be utilised for diffusion weighted imaging. The addition of diffusion sensitising gradients following the initial radio frequency is usually the first step. There are many problems to overcome when using diffusion sensitised sequences including the inherently low spatial resolution or significant degrading artefacts caused by motion or eddy currents.

The first sequences which were employed for diffusion weighted imaging were stimulated-echo and simple spin echo pulse sequences (69–71). These early approaches suffered significantly under long acquisition times with the consecutive significant motion artefacts. These sequences are not applied anymore in routine clinical work(63).

Single shot spin echo echo-planar (SS-EPI) sequences are the most broadly used DWI sequences. The echoes in echo planar sequences are produced by rapid activating and deactivating of frequency gradients which can have a repetition of 128

per single shot in 50-70ms (16-20 images per second). However this means that the matrix is limited to a multiple factor of 128 (55).

The echo planar sequences are very fast due to their rapid acquisition time and offer relatively good SNR. There are however a few major inherent limitations of DWI echo-planar sequences including susceptibility artefacts at tissue or implants interfaces, low resolution which is due to limited matrix size, eddy current effects and ghosting artefacts due to poor fat suppression.

There have been many positive developments in the recent years to address the described limitations including improved gradient system with reduced eddy currents effects, more enhanced fat saturation techniques which reduce ghosting artefacts and application of new parallel imaging techniques with the consecutive reduction of geometric distortion and at the same time an improvement of the spatial resolution (63).

Multi-shot echo planar acquisition is another approach to reduce the artefacts and increase the resolution of SS-EPI sequences through dividing the echo planar acquisition (echo train) of a single impulse between multiple impulses with shorter echo trains, however, this approach increases the total scanning time.

Single shot fast spin echo or turbo spin echo sequences are another type of fast diffusion weighted sequences with spin echo train acquisitions similar to echo planar sequences. These sequences are better known as “rapid acquisition with relaxation enhancement” (RARE) or “half Fourier-acquisition single-shot turbo-spin-echo” (HASTE) sequences(63).

The sequences are relatively insensitive to motion and susceptibility artefacts, but are limited in their spatial resolution and are affected by other artefacts causing image blurring in the direction of phase gradients. There are solutions to improve some of the described artefacts including parallel imaging for better spatial resolution and acquisition of multiple averages to increase the SNR (63).

A more promising approach to rectify the limitations of SS-FSE or TSE sequences is utilising diffusion-weighted PROPELLER (periodically rotated overlapping parallel lines with enhanced reconstruction) sequences (63). In a PROPELLER type sequence k-space is covered repetitively with rotating rectangular strips which leads to consecutive oversampling of the centre of k-space and improves the resolution and the motion robustness of the sequence but at the cost of longer sequences.

A completely different type of diffusion weighted sequence is the steady-state free precession (SSFP) sequence. The diffusion-weighted version of SSFP sequence is called CE-FAST or contrast-enhanced Fourier acquired steady-state technique(63,72,73). SSFP sequences are gradient echo sequences with only one diffusion gradient in each repetition time and variable rephasing gradient intervals; hence accurate b- value registration and ADC measurement (quantitative information) are not possible(63). The SSFP sequences deliver valuable qualitative information and are fast, thus insensitive to motion.

The diffusion weighted sequences used in this study are spin-echo echo-planar sequences.

Dietrich et al.(63 p.4 fig.2) summarised the SS-SE-EPI pulse sequence in their paper ‘Diffusion weighted imaging in bone marrow, in the following diagram:

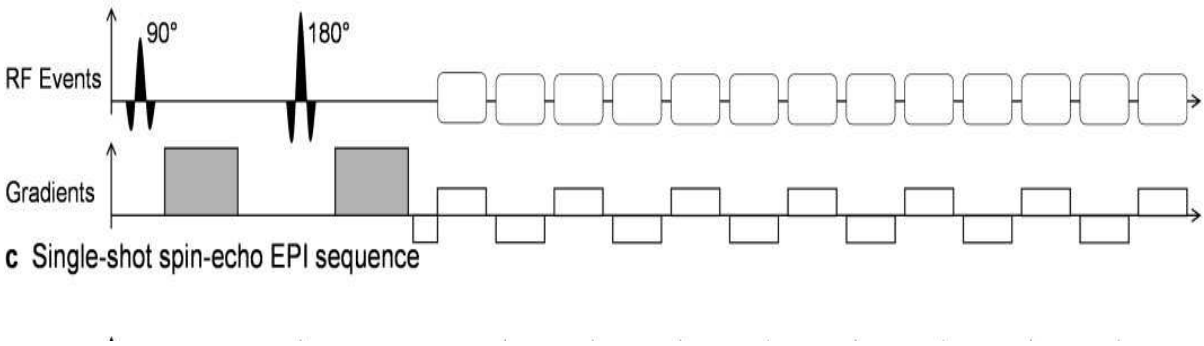

Fig.3(63 p.4 fig.2)- SS-SE-EPI pulse sequence is simplified here by demonstrating the diffusion gradients as grey boxes and imaging gradients in read out direction as white boxes. The radio frequency impulses (with their amplitudes) are displayed

parallel, to demonstrate the order of events and image acquisition. Echo train (multiple repetitions) structure of SS-SE-EPI sequence.

1-7-8 Diffusion weighted imaging in paediatric skeleton:

1-7-8-1 Specific diffusion characteristics of immature skeleton:

Diffusion weighted imaging in the paediatric musculoskeletal system is a functional imaging technique with increasing popularity outside of oncological diagnostic imaging.

Diffusion weighted imaging reveals the molecular architecture of the tissue and delivers quantitative functional biomarkers concerning tissue pathologies.

The paediatric skeleton is particularly affected by alterations in diffusion of water molecules, therefore it is better suited to diffusion weighted imaging than mature skeleton(74). The diffusion weighted images are contrast richer in the paediatric skeleton in comparison to adult skeleton.

There are a range of disparities between the growing and the mature skeleton which can explain its suitability for diffusion weighted imaging:

-Paediatric skeleton contains more water, and therefore the diffusivity and ADC values are increased(74).

-Paediatric skeleton is more vascular with increased perfusion which means elevated ADC fast components of ADC total(57,74).

-Paediatric skeleton contains significantly more cartilage (more water) and less calcific bone with reduced bony interfaces, hence susceptibility artefacts at the level of joints are reduced(74).

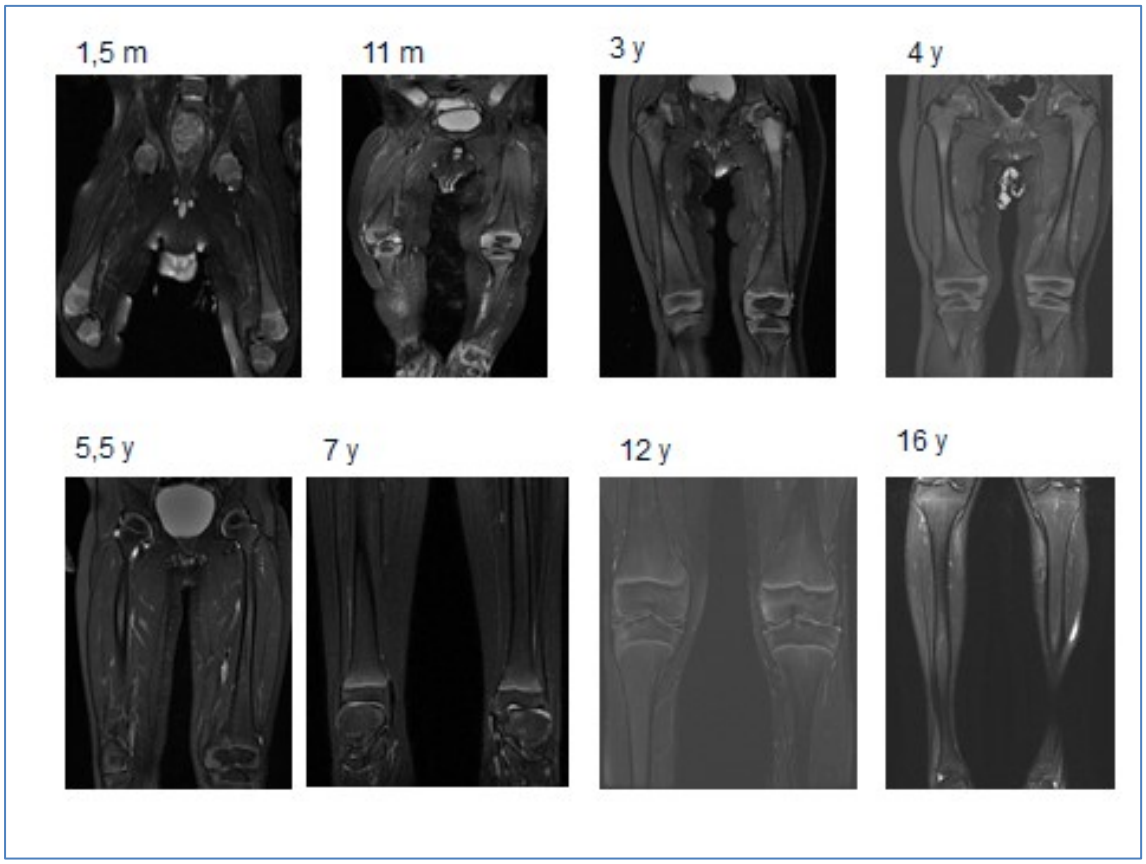

Fig.4- Chronological appearances (changes) of T2 weighted fat saturated images, comparing bone and cartilage content of lower limbs of 8 paediatric patients, age 1,5-192 months. The purpose of this chronological image series is to highlight the high content of cartilage in paediatric skeleton and its chronological change (reduction) over the years. Paediatric skeleton contains more cartilage and water but less fat in comparison to adult skeleton. Please see the text here and 1-5-1 to 1-5-3.

-Paediatric bone marrow contains significantly more red marrow with smaller cells than fat marrow with large hydrophobic cells. The ADC value is continuously falling during normal skeletal maturation, mostly due to normal bone marrow conversion.

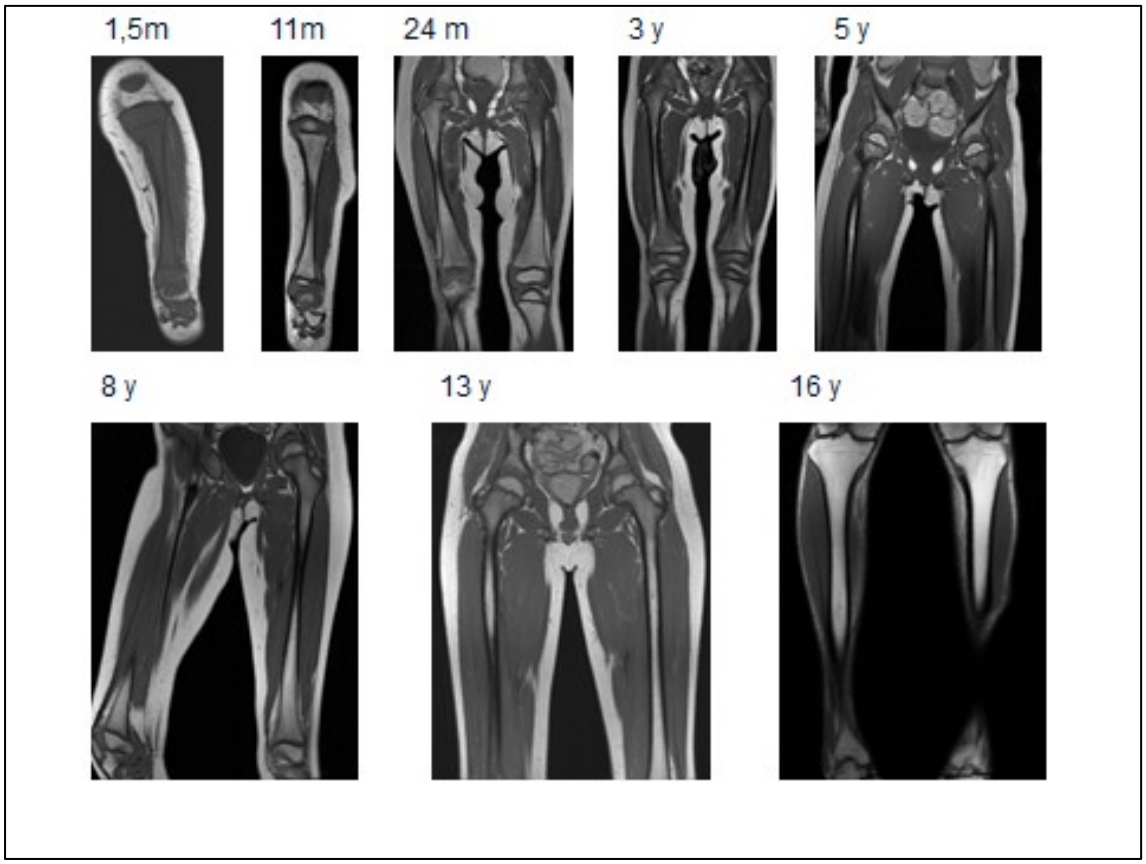

Fig.5- Chronological appearances (changes) of T1 weighted signal of paediatric lower limbs, age 1,5-192 months. The purpose of this chronological image series is to highlight that paediatric skeleton contains more red marrow (less fatty marrow) in comparison to adults and is subjected to a gradual bone marrow conversion following a centrifugal pattern during the skeletal maturity.

-Paediatric skeleton is less trabeculated (higher paucity) and the trabecular structure is less organised. This is another potential reason for higher ADC values due to less restricted diffusivity(74,75).

Diffusion weighted imaging is therefore highly applicable to the paediatric skeleton with promising results according to many recent publications (64,76–78).

There are, however remaining challenges in diffusion weighted imaging of the paediatric musculoskeletal system because the above-listed characteristics of the

paediatric skeleton are permanently changing during skeletal maturation with changing relative composition of red and yellow marrow and changes in the relative composition of cartilage and bony elements with a reduction and change in the pattern of vascularity.

The diffusion in paediatric skeletons decreases throughout the period of skeletal maturity with reduction of ADC values, which are not only age-related, but also related to the anatomical location and gender, as bone marrow conversion and vascular devolution follow a rigid pattern and are accelerated in girls(74). As an example, the ADC value is lower in the diaphysis than in the metaphysis. These details are important considerations in qualitative and quantitative diffusion weighted imaging of immature skeleton (74,79).

1-7-8-2 Clinical applications of DWI in paediatric musculoskeletal system:

Diffusion weighted imaging has the capability to provide qualitative and quantitative information concerning permeability, fluid content, vascularity (perfusion) and cellularity of tissue in paediatric musculoskeletal system, thus pathologies which can cause changes or destructions in the intercellular and extracellular architecture should be detectable with DWI.

Diffusion weighted imaging has been proposed to be useful in a variety of clinical pathologies including, avascular necrosis (74,80,81), trauma (66,82), rheumatoid diseases (64,78), benign and malignant lesions (74,77) and whole body imaging in oncology(57,83).

It has been shown that ischaemia and inflammatory changes in the paediatric musculoskeletal system including hyperaemia, increased perfusion, necrosis extracellular leak and the consecutive oedema can cause signal alterations in DWI(66,74,80–82), however the diagnostic performance of DWI has not been evaluated in paediatric musculoskeletal infection.

There is paucity in the literature concerning the utility of DWI in musculoskeletal infection in children. There are only a small number of publications available which have briefly addressed diffusion weighted imaging and described its usefulness and its potentials in diagnosis of paediatric musculoskeletal infection (64,74,76,78).

There are more publications concerning the application of DWI in the adult musculoskeletal system including subacute and vertebral infections(57,63,83–87), which provide useful general principles of DWI and predict possible outcomes in paediatric population, however direct comparison or extrapolation of their findings for paediatric population is not possible, in view of the significant differences between adult and paediatric MSK systems and infections (see chapter 1 section 1-1 to 1-6).

1-7-9 Introduction to contrast enhancement based semi-quantitative and quantitative MRI:

MRI has predominantly been utilised in the past as a qualitative imaging tool in clinical practice. Semi-quantitative and quantitative magnetic resonance imaging have been recognised as advanced ways to analyse, differentiate and possibly characterise tissue biology (58,88).

Quantification in magnetic resonance imaging represents a paradigm shift, a modern approach of utilising imaging (58,89) to asses disease in a quantified manner. The scanner is utilised as a highly sophisticated camera in qualitative studies, while in quantitative or semi-quantitative studies, the scanner is used as an advanced measuring tool, a scientific device capable of measuring many properties of each tissue voxel (e.g. T1, T2, ADC value, magnetisation transfer, metabolite concentration, AUC, TME, K^{trans}, K_{ep})(58).

MRI has been shown to be valuable as a non-invasive and nonionizing modality for obtaining vascular information (90–92). There are multiple magnetic resonance techniques, which are designed to visualise microvascular architecture of lesions and quantify the biodynamic processes at the capillary and molecular level. These methods are divided in two main approaches; the first is the application of an exogenous intravascular contrast agent based on gadolinium, including dynamic

susceptibility contrast MRI (DSC-MRI), serial or multiphase contrast-enhanced MRI (SCE) and dynamic contrast-enhanced MRI (DCE-MRI). The second is application of an endogenous contrast agent using magnetically labelled arterial blood or blood oxygenation differences, including arterial spin labelling (ASL) and blood oxygenation level dependent (BOLD) imaging (90,92).

ASL and Bold imaging provide only semi-quantitative perfusion information with relative low SNR (90,92–96). DSC-MRI provides information about relative (semi-quantitative) perfusion, blood volume and mean transit time, using the first pass bolus tracking of contrast agent (90,97–99). SCE-MRI delivers qualitative maps or signal intensity curves and semi-quantitative parameters concerning perfusion and permeability characteristics of the tissue with relatively high SNR and a good balance between spatial and temporal resolutions. DCE-MRI provides the ability to analyse tissue's microvasculature from a different perspective in comparison to other techniques by allowing accurate quantitative assessment of biodynamic of the microvascular permeability (92).

1-7-9-1 Serial and dynamic contrast enhanced magnetic resonance imaging:

The common principle of serial and dynamic contrast-enhanced MRI is based on rapid sequential magnetic resonance image acquisition over an uninterrupted period of time, before, during and after administration of exogenous low molecular weight MR contrast agent(92). The sequences are usually gradient echo T1 weighted and the contrast agent is gadolinium-based.

The serial contrast enhanced or multiphase contrast enhanced MRI is based on rapid serial image acquisition through the whole volume, consisting of multiple consecutive relatively thin slices in the field of view. Dynamic contrast enhanced MRI is based on repetitive rapid (dynamic) image acquisition of the same slice (a relatively thick slice/slab) in the field of view. The spatial resolution and SNR are higher in the SCE whilst the temporal resolution and the dynamic properties are higher in DCE. SCE can deliver qualitative diagnostic contrast enhanced images, time intensity curves and semi-quantitative tissue enhancement values, whilst DCE

can provide time intensity curves, semi-quantitative values and quantitative measures concerning the permeability status of the tissue.

Conventional contrast-enhanced MRI reveals contrast enhancement at a single point in time, whilst SCE and DCE MRI display a whole range of fluent contrast kinetics in tissue before, during and after contrast agent circulation, and thus facilitates insight into parenchymal microvascular properties (92).

The dynamic contrast agent perfusion in tissue, reduces the T1 value and changes the signal rapidly (58). The consecutive signal intensity time curve, derived from the rapid signal changes, represents a surrogate of tissue perfusion, vascular permeability and extravascular leakage volume(100–102).

1-7-9-2 Signal intensity or Time intensity curves:

The signal intensity curves are based on dynamic changes of the signal intensity before, during and after contrast agent transit through biologic tissues. The time intensity curves are the graphic demonstration of signal intensity (on Y axis) against time (on X axis) as a measure for duration of contrast agent application. Signal intensity time curves can provide semi-quantitative values, including area under the curve (AUC), time to maximum enhancement (TME), wash in, wash out and pick enhancement, but for real quantification of tissue permeability and perfusion, the signal intensity curves have to be transformed to contrast agent concentration time curves (58,92). The shape of the time intensity curve and their semi-quantitative measures are valuable tools for detection, differentiation and determination of the activity of pathological processes as they can vary between different pathological conditions which otherwise have similar imaging characteristics(103,104). There are furthermore recent publications which have postulated a strong correlation between semi-quantitative parameters (derived from time intensity curves) and quantitative parameters of permeability contrast enhanced MRI in malignancies such as lower GI malignancies(105).

1-7-9-3 MR modelling:

The function of the MRI model, is to extract contrast agent concentration from the MRI signal (58). Once the contrast agent concentration as a function of time is established, appropriate pharmacokinetic analyses can reveal contrast agent distribution in body based on different biological characteristics (58,102).

The MRI model consists of the following two components:

1- The T_1 value is reduced after the contrast agent is applied based on the following equation: $1/T_1 = 1/T_{10} + r_1C$, T_1 is reduced from its native value T_{10} by the presence of a concentration C of Gd and r_1 is the relaxivity which is the constant of proportionality between Gd concentration and increase in relaxation rate $R1 = 1/T_1$ (58).
2- The signal increases with T_1 reduction following a model which is specific to each sequence type according to the following equation: $S = S_0 \frac{(1-e^{-TR/T1}) \sin\theta}{(1-e^{-TR/T1}) \cos\theta}$

Where S_0 is the relaxed signal ($TR>>T1$, $\theta=90^o$), and θ is the flip angle (FA). S_0 can be found from the measured pre-Gd signal(58).

There is a clear relationship between signal and contrast agent concentration based on the bi-componential model described above, which necessitates the values of r_1, T_{10} and flip angle (58,102).

1-7-9-4 Pharmacokinetic modelling:

The Pharmacokinetic model determines how the contrast agent distributes in different compartments of the body based on varying biodynamics (58). The modelling is independent of the imaging conditions and is in principle independent of imaging modality (58,100).

Different pharmacokinetic models have been proposed and most of these are based on a compartmental model, the three main models are by Tofts and Kermode(102), Larsson *et al* (106) and Brix *et al* (101).

The pharmacokinetic model attempts to extract multiple physiological parameters from the concentration-time curves by analysing the transport of contrast agent between the blood plasma and extravascular extracellular space and vice versa (90).

The most commonly used pharmacokinetic model is based on the standard two compartmental model comprising plasma and extravascular extracellular space, known as Tofts model(107). The model estimates the main parameters of trans-endothelial volume transfer K^{trans}, K_{ep}, V_p and V_e (90). K^{trans} is the volume transfer constant between blood plasma and extravascular extracellular space, whilst K_{ep} is the rate constant between extravascular extracellular space and blood plasma, and the volume of extravascular extracellular space per unit volume of tissue is V_e (V_e x K_{ep}= K^{trans})(90). V_p is the plasma concentration volume fraction per unit volume of tissue which is however, less commonly used. The relationships between the main parameters of trans-endothelial volume transfer are as follows:

$\{K^{trans} = V_e \times K_{ep}\}$, $\{K_{ep} = \frac{1}{\text{TTP tissue} - \text{TTP Plasma}}\}$,

$\{V_e = x = \frac{\text{C gdtissue}}{\text{C gdplasma}}\}$

TTP=time to reach the peak intensity value,

C gd= gadolinium concentration(107)

The Toft pharmacokinetic model is summarised in the following formulae:

$$C_t(t) = K^{trans} \int_0^t C_p(\tau) e^{-k_{ep}(t-\tau)} d\tau + v_p C_p(t)$$

There are different parameters in the above formulae including fixed parameters such as FA, TR, Hct, T_{10}, $T_{10blood}$ and r_1 which have fixed values and are required before fitting can start, free parameters such as K^{trans}, V_e, K_{ep}, V_p and t_onset (the onset time of the contrast bolus) which are estimated as part of the fitting process and contrast agent concentration parameters such as C_p (plasma concentration) and C_t (tissue concentration) which are used temporarily as part of the process of modelling the signal(58,59).

The pharmacokinetic model above translates permeability and perfusion phenomenon at the capillary level into quantitative measures. The trans-endothelial leakage determines the proportion of perfusion or permeability information which is provided by K^{trans} (58). Sophisticated models are able to separately describe perfusion and permeability information (58,108,109).

1-7-9-5 Image analysis and pharmacokinetic fit:

The preparation for image analysis begins with calculation of the tissue native T_1 value (T_{10}), alternatively a standard value can be utilised(58). This step is necessary for both semi-quantitative and quantitative calculations(58,102,110). There are different methods for calculating the native T1 value (T_{10}), which are usually time consuming. The most common way of native T1 calculation is collecting the pre-contrast values of a spoiled T1 weighted gradient echo sequence with different flip angels for each voxel and creating a pre-contrast map(110). Many industrial software providers use standard native T1 values for different type of tissue.

The next step is image acquisition before during and after contrast agent application. The signal intensity and blood / plasma concentration can be calculated with the help of the following equations: $^{1}/_{T1} = {}^{1}/_{T10} + r1c$, $C_p = C_b / (1-Hct)$, C_p is plasma and C_b is blood concentration. This step is important for calculation of time intensity and time concentration curves, with their semi-quantitative values, and the pharmacokinetic modelling.

The final step is calculation of arterial input function or AIF from blood signal, failing this a population related average for different temporal resolutions can be employed (58,102). This step is necessary for pharmacokinetic modelling and quantitative measurements(110).

Once the AIF value is available the mathematical fitting of the model values to the measured data can proceed, according to Toft model in 1-7-9-4 as follows:

1- Calculation of the model signal for the free parameters (K^{trans}, K_{ep}, V_e, V_p,..)
2- Calculation of the difference between the model signal value at each time point and the measured data

3- The calculated differences are then squared and summed up across each time point to create a total difference
4- The total difference will be minimised through adjustment of the free parameters

Using the above procedures the model is fitted to the data obtained in each case(58).

The Image analysis and implementation of the fitted model can proceed on an individual ROI basis, which represents the easier method, or on a pixel by pixel basis to produce a map for the whole organ, which is the more complex mathematical approach (58,90).

The generated final free parameters are the permeability quantitative information, which in combination with the obtained qualitative information from the qualitative images and semi-quantitative data from the time intensity curves create a powerful tool to visualise, characterise and quantify tissue pathologies.

1-7-9-6 A Pragmatic model:

Historically blood vessel trans-endothelial transfer alterations were assessed by static imaging of contrast agent transit through the examined tissue in a time frame following contrast agent administration. In contrast DCE imaging visualises and differentiates different phases of contrast agent transit and provides quantitative biodynamic information concerning the tissue properties at a microvascular level (90,92,111,112). The spatial resolution and SNR of DCE sequences are inferior to static post contrast (conventional) sequences and the DCE sequences examine one segment (a slab) of the entire volume; hence there is a trade-off when tissue permeability alterations are examined with DCE sequences.

Amarnath *et al.* have observed in a study evaluating the quantitative pharmacokinetic parameter of DCE sequences in breast lesions that a significant number of sub centimetre lesions were only identified on subtracted images of high spatial resolution series and not on the high temporal resolution series (107). They have concluded that the reliability for detection and perhaps characterisation of sub

centimetre lesions in dynamic analysis with inherent poor spatial resolution remains questionable (107). An alternative approach would be to perform static pre and post contrast imaging additionally to routine DCE imaging, in order to improve the detectability and characterisation; however this model would be extremely long and not acceptable for paediatric population in an acute clinical setting.

Utilising SCE (or multiphase contrast enhanced) sequences with thinner slices throughout the whole field of view, higher spatial resolution and SNR, but with reduced number of pre and post contrast frames and moderately reduced temporal resolution may represent a pragmatic model to detect and characterise the pathology within the time constrains of an acute paediatric setting. SCE sequences are able to deliver qualitative and semi-quantitative information. The most common semi-quantitative information derived from SCE sequences are time to maximum enhancement (TME) and area under the signal intensity curve (AUC) which have been utilised in this study and reflect tissue contrast enhancement charateristics.

1-7-9-7 MRI sequence and image acquisition technique:

Permeability contrast-enhanced imaging (T1 weighted) is rapid sequential imaging of the same field of view before and after contrast agent injection for several frames and over a period of time (58,102). The pre-contrast T1 value is usually measured prior to the contrast enhanced sequence, or a standard T1 value can be utilised (58,102).

The most commonly used sequences for serial and dynamic contrast-enhanced imaging are 3D T1 weighted spoiled gradient-recalled echo sequences such as FSPGR sequence from GE, Milwaukee USA (92). The sequence parameters need to be well balanced in order to achieve a suitable compromise between coverage, temporal and spatial resolution (58).

The accuracy, reproducibility as well as the optimal value of the flip angle, is very important for MRI modelling, accurate calculation of K^{trans}, the estimation of arterial input function (AIF) and balancing between contrast agent sensitivity and dynamic range (58). The magnetic field homogeneity (B1) is equally crucial as it influences the flip angle homogeneity (58). Transmit and receive surface or phase array coils

usually do not provide a homogenous magnetic field and consequently suboptimal flip angles and thus the body transmit coils should be prioritised, as they provide better magnetic field homogeneity (58). 3D sequences are preferred, as they offer more advanced FA homogeneity and higher SNR. However there is a trade-off as the temporal resolution may be lower for 3D sequences for the same amount of spatial coverage (92).

There are other factors which can improve the SNR and resolution, including faster gradients and multiphase array receiver coils.

The ideal geometric plane for DCE or SCE sequences for appendicular as well as axial skeleton, is the coronal or a modified coronal plain, as the main arteries can be sampled along their lengths, removing wash in effects and respiratory artefact is in plane and hence easier to correct (58).

The length of the DCE sequences should be well estimated, in order to sample the enhancement plateau and cover the slope of the tissue concentration curve as K^{trans} represents the slope, K_{ep} represents the shape and V_e represents the maximum height of the concentration curve (58).

Respiratory motion is much less relevant in MRI of the appendicular skeleton, but it causes serious artefacts in the axial skeleton, and thus needs to be addressed, in consideration of the age range (0-18) and the level of compliance (58). Free breathing technique and minimising diaphragm movement by having one or both hands above the head, breath hold technique for short sequences, free breathing with respiratory monitoring and guided free breathing are possible solutions based on the level of compliance (58). Motion correction and spatial registration software can reduce motion artefacts and should be employed if available, as it may improve the pharmacokinetic fit (58).

1-7-9-8 Contrast agent and administration:

The size of contrast agent molecules influences the level of permeability and consequently K^{trans} values, furthermore linear configured gadolinium (Gd) based contrast agents are associated with parenchymal accumulation and nephrogenic

systemic fibrosis, thus smaller molecules with cyclic configurations are preferred(58). There is a variety of cyclic/macrocyclic gadolinium based agents including Gadovist, Dotarem and ProHance. Prohance is the smallest macrocyclic gadolinium based product available at the moment at 559 Daltons. Pump injection with a rate of 2-3 ml/s followed by a saline injection of minimum 5-10 ml has been suggested for adults and teenagers as the best practice due to better reliability and consistency, however hand injection is also possible if required (92).

1-7-10 Serial and dynamic contrast enhanced imaging in paediatric musculoskeletal system:

Dynamic or serial contrast enhancement based imaging of the musculoskeletal system is not widely utilised in the clinical setting in children. The serial and dynamic contrast enhanced imaging has the potential to detect and differentiate similar pathologies based on the specific characteristics of tissue trans-endothelial leakage under different circumstances(103,104,113). The advantageous characteristics of paediatric musculoskeletal system for serial and dynamic contrast enhanced imaging and the relevant clinical applications are discussed in the following sections.

1-7-10-1 Tissue perfusion and permeability characteristics of immature skeleton:

The Paediatric skeleton differs significantly from the adult skeleton, not only in anatomical compartments and parenchymal compositions, but in elemental structures such as different types of cartilage(19). The disparities between immature and mature skeletons are not static, but permanently evolving over the period of maturation, based on rapid development of the growing skeleton.

The paediatric musculoskeletal system is more subjected to altered perfusion and permeability at microvascular level based on a range of differences from the mature skeleton. The paediatric musculoskeletal system is therefore better suited for serial and dynamic contrast enhanced imaging.

The fundamental differences between the growing and the mature skeleton are responsible for greater perfusion and possibly permeability in the paediatric skeleton and are as follows:

-The paediatric skeleton contains substantially more cartilage, which follows a strict pattern (centrifugal) of gradual ossification(19). Paediatric cartilage contains more water and is more vascular (see Fig. 4 in 1-7-8-1), hence there is higher perfusion and possible more active permeability (26,74).

-Paediatric bone marrow is significantly richer in active red marrow, predominantly in the metaphysis (see Fig. 5 in 1-7-8-1) and the red marrow is immensely more vascular(19). There is increased perfusion and permeability in the red marrow rich compartments of the paediatric skeleton.

-The paediatric skeleton is significantly more vascular in comparison to the adult skeleton with a rapidly changing pattern in early childhood(19). The paediatric vascular evolution is most profound in the metaphyseal and epiphyseal ends of the bones. The hyper vascularity and larger network of sluggish capillaries are significant contributory factors for higher perfusion and permeability(10,19).

-The immaturity of vascular endothelium and immune response in early childhood are additional contributory factures, which can influence the trans-endothelial permeability.

Serial or dynamic contrast enhanced imaging is therefore much more applicable to paediatric skeletons based on the above listed characteristics of the immature skeleton.

There are, however, challenges in serial and dynamic contrast enhanced imaging of the paediatric musculoskeletal system as the characteristics of the paediatric skeleton are permanently evolving during skeletal maturation with changes in the relative composition of cartilage and bony elements, changing relative composition of red and yellow marrow and changing pattern of vascularity.

The alterations of permeability characteristics based on evolutional changes of the immature skeleton are not only age related, but also depend on anatomical location and gender, as the evolution starts in appendicular skeleton before axial skeleton, follows a centrifugal pattern in the bones and is particularly accelerated in girls.

1-7-10-2 Clinical applications of serial and dynamic contrast enhanced imaging in paediatric musculoskeletal system:

Dynamic contrast enhanced imaging has been utilised since early 1990s in the diagnosis of breast cancer and brain tumours in adults to improve the diagnostic yield(90,107,114). Dynamic contrast enhanced MRI utilisation was established early on in non-oncological diagnosis, including adult rheumatology (115–117), and soon after was introduced in paediatric oncology(113,118), especially in the assessment of musculoskeletal tumours(118,119).

There have been many studies in recent years which have employed the benefits of fast and repetitive contrast passage over multiple frames to improve MR angiography(120) or functional MR urography (121–124).

The advantages of sequential or rapid dynamic enhanced imaging of synovial membrane, cartilage or articular inflammatory processes (JIA) have been evaluated over the last decade by a few research groups(104,125,126) with relatively promising outcomes. Serial or dynamic contrast-enhanced imaging has not been evaluated systematically in musculoskeletal infection in children whilst the positive diagnostic value of contrast enhancement or even permeability imaging has been suggested in some adult and paediatric studies(10,20,47,103,104).

1-7-11 Available research for magnetic resonance imaging of acute paediatric Musculoskeletal infection:

The utility of MRI in the diagnosis of musculoskeletal infection in children has been evaluated in multiple retrospective studies in recent years, with extremely positive results which support the previous assumption that MRI is the most sophisticated imaging tool in the diagnosis of musculoskeletal infections (3,10,20,37).

The value of diffusion weighted imaging in paediatric musculoskeletal disorders has been previously discussed in a few retrospective studies (74,77,80) and there are even a small number of prospective small studies that have analysed the feasibility and validity of diffusion weighted imaging in the diagnosis of juvenile idiopathic arthritis and chronic recurrent multifocal osteomyelitis (76,78,127). Most of these studies have shown positive results.

The role of contrast enhanced MRI in the diagnosis of paediatric musculoskeletal infection has been controversial in the past, based on a few retrospective studies (26,51). However, more recent studies have revealed the beneficial aspects of contrast enhanced MRI (3,51,128). The benefits of dynamic or serial contrast enhanced imaging and the retrieved qualitative information have also been discussed in a few small studies (103).

This study is the first prospective and exclusively paediatric study which evaluates the diagnostic impact of MRI in the diagnosis of musculoskeletal infection in a larger study group. Furthermore, this is the first study which compares the structural MRI sequences with diffusion weighted and serial contrast enhanced MRI sequences in a paediatric population with the differential diagnosis of acute musculoskeletal infection.

1-8 Treatment:

The majority of musculoskeletal soft tissue infections in children with sufficient immunity have simple courses and are self-limiting or only require a short course of oral antibiotic treatment without significant complications.

In more significant musculoskeletal infections, such as septic arthritis or osteomyelitis, intravenous antibiotic therapy and radiological or surgical interventions are the foundation of therapy (3,34). Intravenous antibiotic treatment should start immediately, as soon as the clinical diagnosis has been made as delaying therapy increases the risk of complications (34). If rapid surgical or radiological interventions are indicated to drain intraosseous, soft tissue or articular collections, a widespread pragmatic approach has been to delay the antibiotic therapy to accommodate the intervention, but for no longer than four hours (3,34). The duration of antibiotic treatment has been controversially discussed in the literature(17,18,129,130), however the recommendation of the paediatric infection disease department here in

Imperial College NHS Trust is 2 to 3 weeks for septic arthritis and 4 to 6 weeks for osteomyelitis.

1-9 Complications and prognosis:

Musculoskeletal infections in children are responsible for a large number of devastating complications with relatively high morbidity and mortality. In a retrospective study carried out by Cunnington et al (2009), from eight patients with PVL positive osteoarticular infections, one died and five were likely to have significant long-term morbidity related to orthopaedic complications (17). Below is a list of complications which can accompany paediatric musculoskeletal infections(3,4,17,26).

1- Recurrence or developing delayed new sites of infection
2- Joint destruction, arthrodesis
3- Bone destruction and bone deformities
4- Growth plate damage with premature growth plate closure causing limb length discrepancies, axial skeleton deformities and scoliosis
5- Pathological fractures, pseudoarthrosis
6- Avascular necrosis
7- Sepsis and multi organ failure
8- Deep vein thrombosis
9- Joint dislocation
10- Vertebra magna or block vertebra (3,4,17,26).

The vast majority of complications are due to delayed diagnosis or inadequate treatment, thus early diagnosis is crucial in the acute clinical setting (3,17,20,26,131). The focus of my thesis is on the imaging diagnosis of acute musculoskeletal infection in children, thus the chronic or late imaging features of paediatric MSK infection including follow up imaging which are partially listed above are not part of the scope of this research project.

CHAPTER 2: STUDY AIM AND HYPOTHESES

2-1 Study aim:

1. To evaluate the feasibility of MRI as a diagnostic tool for detection of MSK infection in children.

2. To evaluate the accuracy of MRI as a diagnostic tool for diagnosis of paediatric MSK infection.

3. To compare Diffusion weighted and serial contrast enhanced imaging with the structural MRI sequences for the diagnosis of musculoskeletal infection.

4. To explore the value of ADC and semiquantitative permeability parameters as diagnostic thresholds for paediatric musculoskeletal infection.

2-2 Hypotheses:

Hypothesis 1:

Diffusion weighted imaging is a feasible magnetic resonance diagnostic tool which can deliver qualitative and quantitative information. DWI can detect musculoskeletal changes and accurately diagnose infections of the paediatric skeleton. The hyperaemia and oedema in MSK infection in children can lead to elevated ADC values which could deliver diagnostic thresholds for paediatric musculoskeletal infection (will be discussed in chapter 4).

Hypothesis 2:

Serial contrast-enhanced imaging is a feasible MRI tool which has qualitative and semiquantitative properties. SCE sequences improve the conspicuity of the lesions and

increase the diagnostic confidence of the readers in comparison to structural sequences whilst delivering good or excellent level of diagnostic accuracy in paediatric musculoskeletal infection. The endothelial leak, perfusion and permeability disturbances in MSK infection in children can lead to characteristic changes of semiquantitaitve permeability values (AUC and TME) with diagnostic thresholds for paediatric musculoskeletal infection (will be discussed in chapter 5).

Hypothesis 3:

The proposed, advanced MRI protocol in this study is feasible for paediatric population and delivers a variety of qualitative, quantitative and semiquantitative information. The proposed MRI protocol can diagnose musculoskeletal infection in children with high level of accuracy (will be discussed in chapter 6).

Chapter 3: Context, Material and Methods

3-1 study context:

3-1-1 Introduction:

The significance of MSK infection in children, the problems of making an early diagnosis in the acute clinical setting, the large number of potential complications and in complex cases the poor prognosis, have all been described in the Introduction (chapter 1). Radiology has always played an eminent role in the diagnosis of MSK infection in children and MRI has now taken centre stage in this diagnostic assessment. In this chapter, I will explain the development of the initial idea and describe the structure and methods of the study.

3-1-2 Background of the study:

The driving motivation for this study was the continuing problematic struggle experienced in the diagnosis of MSK infection in children and the lack of sophisticated early detection tools. MRI has been the leading modality in MSK diagnostic in adults but has failed to take the lead in paediatric musculoskeletal infection diagnostic, despite its excellent MSK tissue resolution and lack of radiation.

London is one of the largest and the most populated capital cities in Europe and well known for its multi-ethnicity. One of the inevitable challenges of such a densely populated environment is, having to frequently deal with complex and life threatening infectious diseases. The medical department of Imperial College London is particularly known for its expertise in infectious disease, and this is especially true of the paediatric Infectious disease team which has acquired an international reputation in this field alongside world class medical facilities, treating a huge number of complex patients with infective diseases on a regular basis.

I have experimented with a number of approaches in magnetic resonance imaging in the past, and have attempted to construct a modern, robust, feasible and accurate MRI tool, tailored for MSK infection in children, using sophisticated imaging approaches in MRI. This work aims to replace the complex diagnosis of musculoskeletal infection in children with an accurate single imaging examination. The basic structure of the study was adopted from a previous retrospective study which is described in the following section.

3-1-3 Pilot data and estimated cohort size:

Unpublished pilot data from one of my retrospective studies concerning magnetic resonance imaging of musculoskeletal infection in children has provided the basis of the plan for this prospective study.

The MRI protocol of the current prospective study (see section 3-2-6-5-3) was designed in 2010 and has been in use since then. The MRI scans of all paediatric patients who were acutely admitted to Imperil college NHS trust's St Marys hospital with the clinical differential diagnosis of Musculoskeletal infection between December 2010 and April 2012 and had a MRI scan, using the same protocol as in the current prospective study, were retrospectively reviewed by two experienced MSK radiologists independently. The final diagnoses of the reading radiologists were then compared with the final clinical diagnoses based on the clinical discharge notes, which were made available to me, in order to evaluate the diagnostic accuracy of the protocol.

The reading radiologists had both more than 5 years experience in MSK radiology and the discharge clinical details included the therapeutic course and all laboratory, microbiology, radiology and surgical results. The evaluation form was similar to the evaluation form used in the current prospective study. The ADC and permeability values were not included in the study. 63 patients with 63 MRI scans were retrospectively included in the pilot study, the following tables summarise the details of the cohort and the clinical diagnoses.

	Number of participants	Mean age in months	Incidence of pelvis & lower limbs	Incidence of shoulder & arms	Incidence of neck, thorax and spine	Number of MRI scans
Boys	31	76	24	2	5	31
Girls	32	61	21	3	8	32
Total	63	69	45	5	13	63

Table5. Demographics of study participants and the incidence of affected anatomical locations. The most common anatomical locations were pelvis and lower limbs.

	Total	Excluded	Infection	Infarction	Inflammation	Other pathology	Normal
MRI exams	63	6	36	6	4	6	5
Patients	63	6	36	6	4	6	5
Male	31	4	16	3	1	4	3
Female	32	2	20	3	3	2	2

Table6. Number of scans and study participants for the main pathologies

The final diagnoses of the readers were compared with the final clinical diagnose by means of Cohen kappa test in order to assess the accuracy of the MRI protocol retrospectively. The final diagnoses of the readers were also compared with each other to assess the readers' agreement.

There were 63 patients included in the retrospective pilot study over a period of sixteen months and 6 were excluded (90% = recruitment rate) due to suboptimal scan quality. The following tables are summarising the Cohen's Kappa results as a measure of accuracy of the MRI protocol.

Whole MR protocol versus clinical diagnoses	Measure of agreement Kappa value	Sensitivity	Specificity	P value	95% interval lower-upper bound
First reader diagnoses ~ Clinical diagnoses	0.647	82%	84%	<0.001	0.000-0.051
Second reader diagnoses ~ Clinical diagnoses	0.684	81.3%	88%	<0.001	0.000-0.051

Table7. Correlation between final readers' diagnoses and final clinical diagnoses with 2 diagnostic categories (Infection, non-infection), Kappa value is the rate of agreement.

Whole MR protocol agreement	Measure of agreement Kappa value	Sensitivity	Specificity	P value	95% interval lower-upper bound
First reader diagnoses ~ Second reader diagnoses	0.719	86.2%	85.7%	<0.001	0.000-0.051

Table8. Kappa agreement between the readers (Interobserver agreement)

The positive results of the pilot data were encouraging enough to support a prospectively designed MRI focused study.

The sample size of the pilot study was the basis for my prospective study to estimate the possible size of a cohort, over a period of two years given the nature of the study and the inclusion criteria (see section 3-2-3). I estimated that 100 patients could be

recruited over a period of 2 years based on the pilot data and the fact that all of the patients would be admitted to hospital.

It has been acknowledged that the sample size calculation based on the sample size and the study duration of the retrospective pilot study was a pragmatic and clinical approach rather than a prospective statistical calculation, hence a retrospective statistical sample size calculation was performed by one of the biomedical statisticians of the University College London based on the input data of the pilot study including sample size, prevalence of musculoskeletal infection and the specificity and sensitivity. The utilised software was Epitools FreeCalc for sample size calculation analysis and the calculation method was modified hypergeometric exact, which is the preferred method for small samples. The method used by the above software was described by Cameron and Baldock in 1998(132). The calculated output data revealed a minimum required sample size of 21 by a population level sensitivity of 0.962 and a population level specificity of 0.956, which means a type I error of 0.038 and a type II error of 0.044. The calculation was repeated using the simple binomial method (preferred method for large population) which has revealed the same minimum sample size. If the calculation would have been performed using the input data of the main study (current study) the minimum sample size would have been 48 with very similar sensitivity and specificity. The retrospective sample size calculation was reassuring and supporting the clinically calculated studies sample size.

3-1-4 Ethics approval:

The research is compliant with the national and international research governance framework guidelines.

The approval of the radiology research committee was granted in August 2013 and the approval of the imperial college joint research committee was granted in October 2013. The National ethics committee approved the study proposal after two corrections and the second review in May 2014 (Rec reference: 14/SW/0086, IRAS project ID: 139300). The study officially started in September 2014. However, the recruitment and the actual study data collection started in October 2014. The annual

compliance form of the national ethics committee was completed and sent for annual approval up until the end of the recruitment phase in May 2017. The Study was compliant with the national ethics committee guidelines and no incidents were recorded during the study. All ethic approval related documents are included in the appendix (appendix 1).

3-1-5 Data management:

All Study documents including the consent and assent forms were stored in a locked drawer in a locked office accessible only by security smart card in St Mary's Hospital (Imperial College NHS Trust). The final data set was entered into excel files and stored in external storage in the same setting as the study documents.

3-2 Material and Methods:

3-2-1 Study structure:

This is a single site prospective study which aims to evaluate the feasibility of the tailored study's MRI protocol designed to diagnose musculoskeletal infection exclusively in children, and further to determine the accuracy of the protocol against a defined gold standard. The gold standard was the final diagnosis of an experienced paediatric infectious disease consultant based on clinical presentation, physical examination, laboratory/microbiology/histopathology results, symptom resolution following adequate treatment and the inclusion of the clinical and genetic phenotypes (see section 3-2-8 gold standard). The inter and intra-observer agreements have been assessed prior to the study due to the prospective structure of the study, using a subset of data from the pilot study.

3-2-2 Cohort:

The estimated Cohort size based on the pilot data from my retrospective study between December 2010 and April 2012 was 100 cases. The study was initially

planned over a period of two years, however in order to meet the target and recruit 99 patients the study period was prolonged by 6 months.

3-2-3 Inclusion and exclusion criteria:

This is an exclusive paediatric study, which evaluates the value of MRI and advanced MRI sequences in MSK infection.

Inclusion criteria are as follows:

1- Age <18 years
2- Acute admission
3- Acute musculoskeletal pain/symptoms
4- General and clinical sign and symptoms which could be in keeping with an infection (clinical differential diagnose of MSK infection)
5- First scan

Consequently the exclusion criteria are as follows:

1- Age > 18 years
2- Routine admission or scan
3- No or longstanding chronic musculoskeletal symptoms
4- No sign and symptoms of an infection (the differential diagnosis doesn't include MSK infection)
5- Follow up scans
6- Refusal to take part in the study

3-2-4 Recruitment:

The recruitment pathway started in all of the cases in the paediatric A&E department or paediatric infectious disease ward in St Mary's hospital (imperial college NHS trust London), to which all patients were acutely admitted or transferred. The radiology department, the relevant radiographers (See section 3-2-6-2) and ultimately the principal investigator were in most cases immediately informed and the patients and their parents were then approached on the paediatric ward or in the imaging department by the principal investigator where they were invited to participate in the

project following a detailed explanation and discussion of the information sheet of the study and reassurance that the participation is voluntary. The paediatricians in the A&E department and on the wards were aware of this project and as the principal investigator was the main paediatric MSK radiologist in the trust, he was always immediately approached by the paediatric team as part of the rapid diagnostic pathway. MRI imaging was performed in most cases as part of the acute diagnosis workup in the first 24 hours of admission before any surgical interventions. The acute MRI scans were performed within the first week from symptom onset.

3-2-5 Information, Consent and Assent forms:

The primary structure of the information, consent and assent forms of this study were gathered according to the recommendations of the joint research committee of Imperial College. The formats and the document contents adhered to the information, consent and assent forms presented in a recent study of the paediatric infectious disease department of Imperial College (A study to improve the diagnosis and treatment of childhood infection, inflammation and allergy, Principal investigator Prof. Mike Levin) in October & November 2013. The forms were then reformatted and improved based on Imperial colleges research committee recommendations (in December 2013) and after the first review of the national ethics committee, subsequently amended and finalised in early 2014.

Patients' information forms were divided into four groups and adjusted for different age groups and for parents or guardians to cover all aspects of the projects. The four information form groups are included in the appendix 2 and are as follows:

1- Age under 10
2- Age between 10 and 15
3- Age between 15 and 18
4- Parents or guardians

The Consent and Assent forms were designed in three categories and adjusted to reflect the age of the patients and for parents or guardians to confirm that they have understood the context of the study and that they are voluntarily participating to

support the research project. The three groups are included in the appendix 3 and are as follows:

1- Assent form for children under the age of 16 (voluntary form)
2- Consent form for children aged between 16 and 18
3- Consent form for parents or guardians

The patients and their parents were asked to sign two copies, one copy for the research team and the second copy with the information forms for the participants and parents or guardians.

3-2-6 Magnetic resonance imaging:

3-2-6-1 MR Imaging site:

This is a single site study, and all of the scans were performed at St Mary's Hospital Imperial college NHS trust London.

3-2-6-2 Radiography team:

Two senior MR radiographers from the existing St Mary's Hospital radiography team, with experience in the selected magnetic resonance techniques, which were utilised in this study, and were involved in the pilot study were recruited. The radiographers were trained to perform the entire scanning process, implement the complete post processing functions (DWI reformatting and ADC maps calculation and multiphase subtractions of the pre and post contrast sequences) and to support the patients and their parents.

3-2-6-3 Patient preparation and immobilisation, scanning method:

Patients were initially assessed by the paediatric team and the paediatric play specialist team, in order to establish if they were able to tolerate the MRI environment.

Patients, who could not tolerate the MRI environment or were too young, were scanned under general anaesthesia, sedation or with the help of paediatric play

specialist team with preparation prior to the examination. The scanning methods for different age groups were classified in five groups including the following:

1- Age 0-2 months with feed and wrap
2- Age 2-8 months with oral sedation
3- From 8 months till 4 years with general anaesthesia (this group includes children with severe autism)
4- From the age of 5 with the help of Paediatric play specialist
5- Older children and teenagers were scanned routinely

3-2-6-4 MR Scanners and Coils:

Three magnets from the available four magnets in St Mary's hospital were utilised in this study including two 1.5 Tesla (Signa HDX model, GE medical system Milwaukee) and one 3 Tesla scanners (Discovery 750 model, GE medical system Milwaukee).

The different coils used in this study were multichannel superficial phased array coils, with different sizes and number of channels, which were dependent on the required field of view, including superficial joint and extremity coils, head and neck coils and for larger fields of view, cardiac or superficial body coils.

3-2-6-5 MRI protocol development:

The Idea of developing a tailored magnetic resonance approach to detect MSK infection in children emerged through a longstanding struggle with unsatisfactory, static and one-dimensional diagnostic tools, which are commonly utilised.

The imaging pathway usually begins with plain X-ray and ultrasound with MRI reserved as the last option in the course of infection, and the routine MRI protocols which were conventionally used outside of this study are usually identical to the protocols used in traumatic MSK injuries in adults.

The problems with the original approach are the use of less sensitive modalities and protocols which focus on late-stage changes with a usual delay of 7-14 days.

The ability to differentiate between possible pathologies is another handicap of the previous routine protocols.

It has been described in the introduction, that MSK infection in children is a dynamic process and hence a suitable MRI tool should be equally dynamic and ideally capable of revealing different phases (see section 1-5) of the infectious process.

The main advantages of routine MRI sequences in musculoskeletal imaging are excellent tissue characterisation and differentiation with detailed resolution (26). These properties of MRI have established its position as the most suitable tool for imaging musculoskeletal pathologies over the past decades.

The original idea of this study was to tailor MRI sequences according to different phases of paediatric musculoskeletal infection in order to improve early detection, and utilise the quantitative, semi-quantitative and qualitative properties of DWI and serial contrast enhanced imaging to create a comprehensive diagnostic tool.

The parameters of the routine sequences frequently used in MSK imaging including TR (repetition time), TE (echo time) and flip angle were adjusted to address the specific characteristics of paediatric population and growing skeleton and to try to depict earlier the host immune reaction in MSK infection.

The functional MRI techniques (DWI and SCE) were included in the study to improve on the existing qualitative properties of the imaging protocol and to enhance the diagnostic capability of the imaging tool through introduction of quantitative and semi-quantitative properties.

Quantification in MRI represents a new way of thinking about imaging, recognised in recent years as an important approach to characterise tissue biology(58).

The study protocol and the selection of specific sequences are discussed in the following sections.

3-2-6-5-1 Sequence selection:

The sequences used in this study were specifically chosen to visualise the rapid changes in the paediatric musculoskeletal system during an infectious process (see section 1-5) and based on the study's MRI criteria (see section 3-2-7).

The T1 sequence was chosen in order to best depict the bone marrow composition changes and disturbances of the fatty conversion of the bone marrow during an infection, to confirm bone marrow oedema, to detect infiltrative processes which can mimic an infection and to filter subtle fractures such as stress fractures which otherwise might not be visible with other sequences.

The T2 sequence with fat saturation was included in the study protocol to detect tissue hyperaemia and focal oedema, to exclude fat containing lesions, to delineate solid pathologies with different signal characteristics to the fat and native tissue and to detect fluid collections or joint effusions.

The DWI sequence was part of the novel approach of this study to enhance the qualitative information of the routine sequences through additional qualitative and quantitative information based on molecular diffusivity at a cellular level (see 1-7-7, 1-7-8). The idea was to use the diffusion characteristics of the tissue and the variation of diffusivity due to pathophysiological changes to detect the early changes in an infectious process such as hyperaemia, vascular permeability disturbances, focal oedema and the consecutive changes of the extravascular molecular diffusion.

The T1 fat sat serial pre and post contrast sequences (permeability or perfusion imaging) are the second original addition to the conventional paediatric MSK infection protocol. These sequences can depict increased blood flow in an infectious process and improve the capability of the protocol in not only detection but also differentiation from some differential diagnoses such as infarction. These sequences were however not added to the protocol purely to improve the qualitative information of the protocol in diagnosis of MSK infection but their addition was also an attempt to utilise the semi-quantitative and possibly the quantitative information of vascular and tissue permeability dysregulations during an infectious process.

3-2-6-5-2 Sequence optimisation:

T1 spine echo sequences (SE) are known for excellent image quality and spatial resolution, due to insensitivity of the SE sequences against static field inhomogeneity(55), however after discussion with my supervisor, the GE application specialist and study radiographer team the decision was made to use fast spine echo (FSE) sequences in order to shorten the scanning time which is crucial for paediatric patients. The following modifications are part of the effort to optimise the study's T1 sequence for paediatric population / MSK infection:

-The TR of the sequence is relatively short to reduce the scanning time and optimise the T1 weighting or T1 contrast(55)

-The TE of the sequence is short which improves the SNR(55)

-The choice of slice thickness and inter-slice spacing has been carefully balanced to achieve optimal spatial resolution with good SNR and without prolonging the scanning time

The same decision was made for the study's T2 sequence, to use FSE sequences as they are fast and robust. Equally the TR and TE are relatively short to address the scanning time and SNR. The choice of slice thickness and inter-slice spacing ratio of the T2 sequence also adhered to the T1 sequence. Fat saturation has been additionally included for T2 sequences in order to improve the contrast of the sequence and the conspicuity of the lesions.

DWI sequence in this study is a spin echo, echo-planar (EPI) sequence with inversion recovery fat suppression (57,74,80).

EPI sequences are fast and less sensitive to motion artefacts and FSE-EPI sequences are even faster with higher resolution and contrast as the signal decay is based on T2 and not T2* properties(55), hence they are more suitable for children and are the most commonly used DWI sequences(57,74,78,127). The speed and the relative resilience of FSE-EPI sequence against motion artefacts were the main reasons to choose this sequence for this study. The fat suppression technique utilised in this study is STIR, as STIR technique offers the most homogenous fat suppression independent from field strength and are relatively insensitive to

magnetic field inhomogeneity. STIR technique is the default fat saturation technique for DWI sequences on St Mary's hospital scanners and was recommended by GE application specialist.

The chosen B values for this study were B0 and B500, which are widely suggested B values for musculoskeletal system according to many publications (57,64,74,77,80). Optimal B values for paediatric musculoskeletal system were not objectively evaluated in this study, as the choice of B values (B0 and B500) was based on recommendation in the literature (57,64,74,77,80). It would have been beneficial to use multiple B values with lower and higher B values, for more accurate calculation of ADC values, and for potential identification of optimal B values. The lower b values are representing more the initial perfusion aspect of the diffusion process whilst the higher B values representing more the real (later) diffusion, hence multiple B values consisting from lower and higher B values would have been beneficial but at the cost of much longer examination in an acute clinical setting.

The motion artefacts were mainly prevented through the rigid preparation and immobilisation protocol of the study (see section 3-2-6-3) although spine echo- EPI sequences are relatively insensitive to motion.

The main limitations of the EPI sequences are susceptibility artefacts, low image signal to noise ratio, eddy current effects with consecutive geometric distortion and ghosting artefacts due to poor fat suppression.

I have improved these limitations in this study by implementing the following modifications and reconstructions:

<u>1-Susceptibility artefacts:</u>

1- Spine echo (FSE) sequences added to EPI pulse sequences minimise susceptibility artefacts in comparison to routine gradient echo EPI sequences(74).
2- The susceptibility artefacts are minimised in the axial plane(64) and the magnetic field is more homogenous in axial plane(74), hence the DWI

sequences in this study were performed in axial plane. The susceptibility artefacts are reduced in appendicular skeleton.

3- The axial sequences were then reconstructed into the coronal plane using a 2 to1 slice thickness increment, to improve the spatial resolution.
4- The final reconstructed series were then inverted to increase the hot spot conspicuity.

2-Low image signal to noise ratio:

1- The low signal to noise ratio is mainly due to field inhomogeneity and signal decay based on T2* properties of the EPI sequence gradients. Using spin echo or FSE-EPI sequences replace T2* based signal decay with T2 based signal decay and replaces echoes produced by on and off rotating gradients with those which are created by 180 degree impulses and therefore SE (FSE)-EPI sequences have higher signal to noise ratio and resolution.

3-Eddy current artefacts:

1- Fast on and off switching of gradients and magnetic field inhomogeneity are the main sources of the currents and the consecutive signal decline, known as eddy current effect. Utilising SE (FSE)-EPI sequences improve the field homogeneity and reduces significantly the on and off turning of gradients, which will improve the eddy current artefacts.
2- The magnetic field is less homogenous in coronal or sagittal plane, hence the DWI sequences in this study were performed in axial plane.

4-Ghosting artefact due to poor fat suppression:

1- Ghosting artefact is usually an issue of sequences which utilise chemical shift (Dixon technique) or frequency selective fat suppression. Optimal field homogeneity and shimming and ideally reduced number of interacting gradients in the main sequence are important for these sequences as any inhomogeneity can cause suboptimal or inhomogeneous fat saturation, especially in periphery of the field of view which in combination with parallel imaging or motion can cause ghosting artefacts. Hence I have decided to use

inversion recovery technique for fat suppression which is the most robust fat suppression technique.

2- Improved field inhomogeneity was achieved by using spine echo (FSE)-EPI sequences to reduce the number of on and off rotating gradients.

Figure 6 demonstrates an example of DWI sequence, ADC map and calculation.

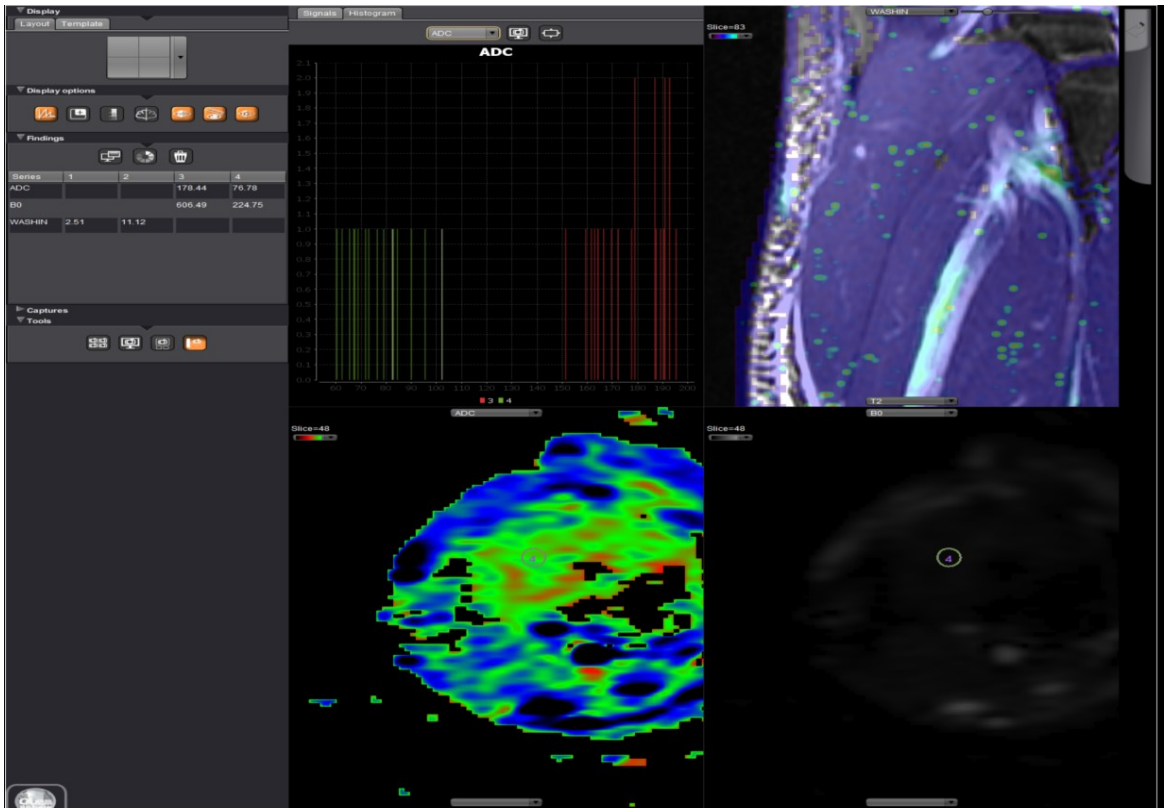

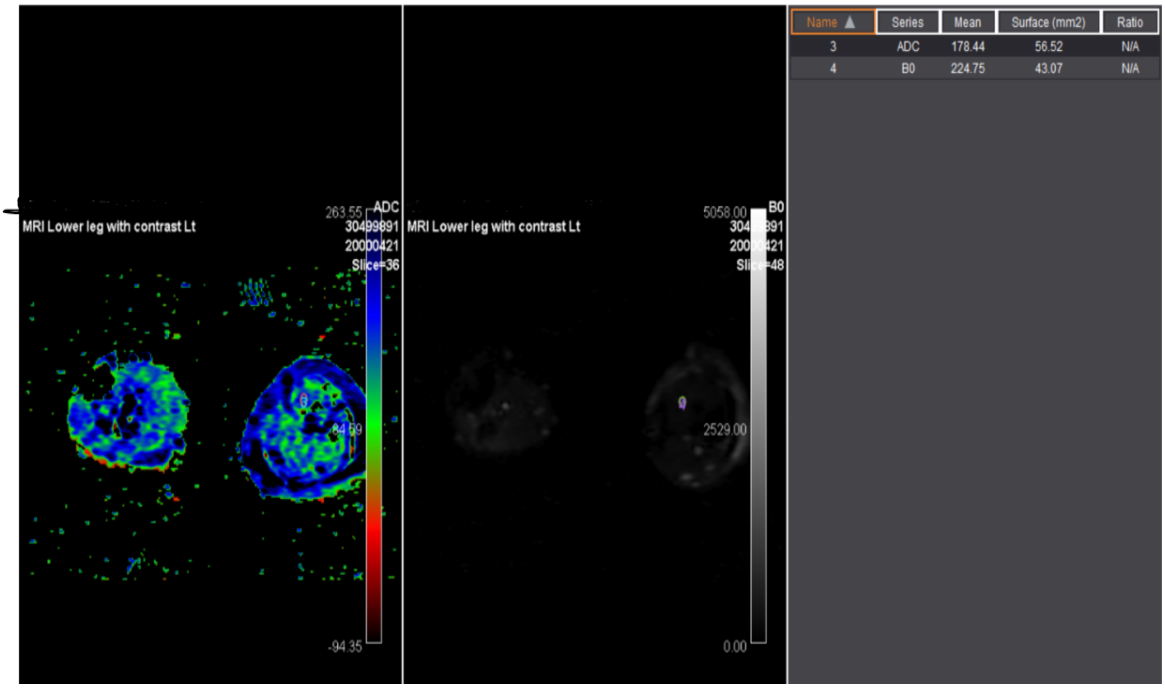

Fig. 6- DWI sequence and ADC analysis: The ADC analysis includes the quantitative values of tissue diffusivity and diffusion restriction (ADC values) with the relevant curves and the cross sectional mapping of the ADC values (ADC maps)

The Study's SCE sequences are Fat saturated LAVA (Liver acquisition with volume acquisition) sequences which are 3D spoiled Fat saturated T1 weighted gradient echo sequences. Although as the name states they are designed for Liver imaging, they have excellent paediatric musculoskeletal properties which were utilised in this study. These sequences allow 3D acquisition, thinner slices and inter-slice spacing and were part of the sequence modification introduced for this study. The Lava sequences are very fast with high contrast, spatial resolution and high signal to noise ratios. These characteristics are very important for an acute paediatric protocol and made additional optimisation unnecessary. The temporal resolution of the SCE sequences in this study (27 second) is low-moderate as the acquisition is serial through the whole volume of the field of view over multiple frames with very thin slices (see section 1-7-9-6). Pharmacokinetic modelling could not be usefully applied to these sequences as they were fat saturated which affect the signal steady state and the sequences were not long enough to sample the entire plateau phase of the signal intensity / concentration time curves which is crucial for calculation of K_{ep} and K^{trans}. The relative low temporal resolution and the use of a standard native T1

relaxation time were still acceptable for the software that I have used according to the manufacturer but not ideal for a meaningful pharmacokinetic modelling, hence the term serial contrast enhance or multiphase contrast enhanced was used.

Serial contrast enhanced sequences improve the diagnostic properties of the study protocol in two separate ways:

1- Qualitative analysis (image analysis)
2- Semi-quantitative analysis (intensity curve analysis)

Figure 7 (a-c) demonstrate a summary of analysis, measurements, parameters and curves extracted from the studies SCE (fat sat LAVA) sequences.

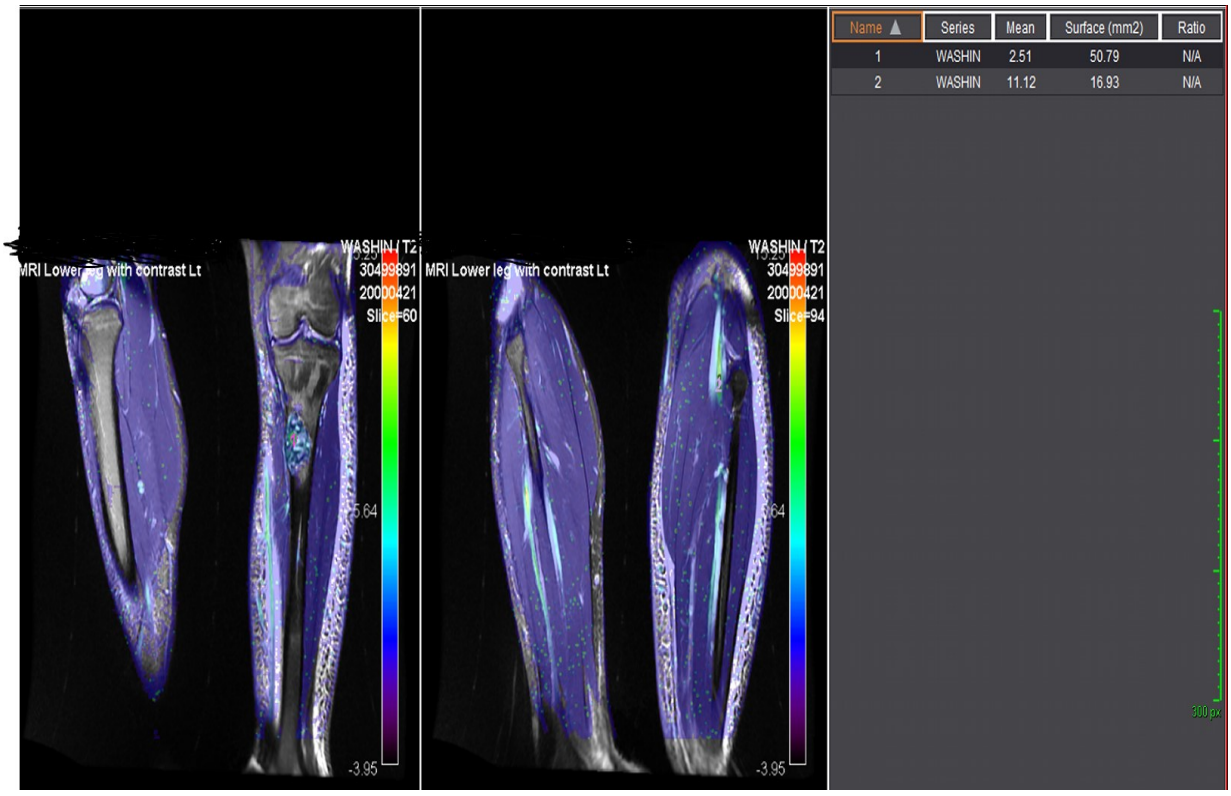

Fig. 7a- Permeability measurement

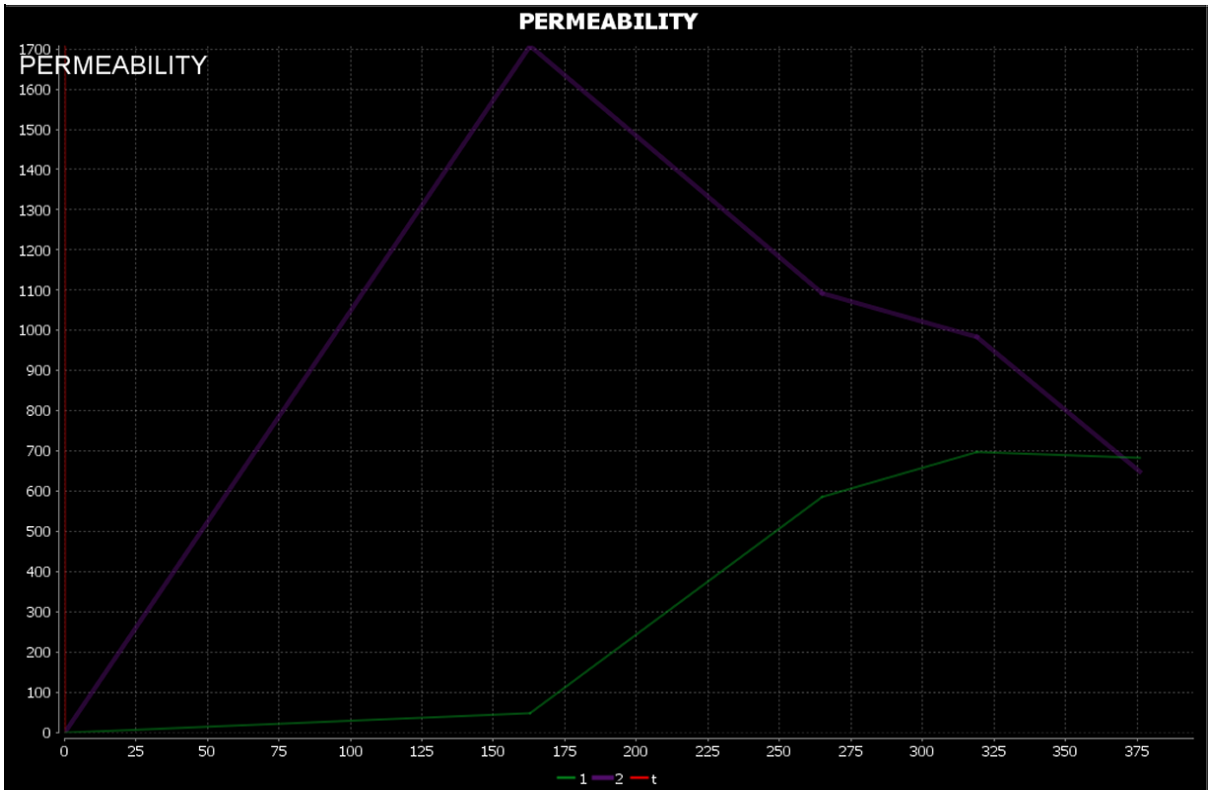

Fig. 7b- Permeability curves

Name	Series	Mean	Min	Max	Sd	Surface (mm2)	Count	Ratio
1	KEP	0.17	-0.00	0.41	0.13	50.79	18	N/A
1	WASHOUT	0.32	-0.05	1.84	0.54	50.79	18	N/A
1	PEAK	629.07	273.31	870.96	186.73	50.79	18	N/A
1	VE	0.44	-0.00	1.23	0.32	50.79	18	N/A
1	WASHIN	2.51	1.67	3.33	0.46	50.79	18	N/A
1	TME	283.79	269.09	293.37	7.74	50.79	18	N/A
1	KTRANS	0.11	0.03	0.17	0.05	50.79	18	N/A
1	AUC	74074.83	37876.28	145880.71	23830.65	50.79	18	N/A
1	CHI2	28437.91	648.54	165036.40	46887.98	50.79	18	N/A
1	VP	-0.00	-0.00	0.00	0.00	50.79	18	N/A
2	KEP	2.30	0.03	8.38	2.84	16.93	6	N/A
2	WASHOUT	5.55	4.84	7.62	0.95	16.93	6	N/A
2	PEAK	2127.53	1917.95	3020.89	400.34	16.93	6	N/A
2	VE	0.08	0.02	0.25	0.08	16.93	6	N/A
2	WASHIN	11.12	10.12	15.19	1.83	16.93	6	N/A
2	TME	196.14	193.99	200.45	2.14	16.93	6	N/A
2	KTRANS	0.18	0.01	0.82	0.29	16.93	6	N/A
2	AUC	457298.87	415177.70	642827.03	83082.48	16.93	6	N/A
2	CHI2	108283.45	13564.73	544302.69	195027.43	16.93	6	N/A
2	VP	0.50	0.44	0.54	0.03	16.93	6	N/A
3	ADC	178.44	151.15	195.58	13.05	56.52	21	N/A
3	B0	606.49	264.03	883.02	180.21	56.52	21	N/A
4	ADC	76.78	60.09	102.44	11.78	43.07	16	N/A
4	B0	224.75	212.01	243.97	8.67	43.07	16	N/A

Fig. 7c- Permeability values:

Pre and Post contrast multiphase subtraction was an addition to contrast enhanced sequences in this study, to improve contrast and conspicuity and ease the differentiation between hyperaemia and abnormal permeability. The subtracted images are excellent road maps for interventional and surgical procedures if required.

3-2-6-5-3 Study protocol:

The study protocol is a combination of sequences which offer qualitative, semi-quantitative and quantitative information and is as follows:

-T2 fat sat spine echo sequence in two planes (coronal & axial, eve. sagittal)

-T1 spine echo sequence in coronal plane (eve. axial or sagittal)

-Diffusion weighted sequence (spine echo-echo-planar sequence) in axial plane with coronal reconstruction and inversion, ADC map calculation

-T1 fat sat pre and serial post contrast sequence (LAVA) in coronal plane (eve. sagittal or axial) with post processing multiphase subtractions and semiquantitative analyses including permeability curves and values

- T2 fat sat (coronal plane) and DWI (axial plane) whole body sequences with coronal reconstruction and inversion (in case of DWI sequences) are initially performed when the process is multifocal

Table 9 summarises the details of the study protocol.

	T2 fat sat	T1	DWI	T1 fat sat SCE
Plane	Coronal and axial	Coronal	Axial	Coronal
Slice thickness/ mm	2-5	2-5	2-5	1-4
Sequence type	Spine echo/ FSE	Spine echo/ FSE	Spine echo/ EPI	Gradient echo/ Lava
Acquisition type	2D	2D	2D	3D

TR	3080 - 8720	464 - 840	7625 - 8000	4.72 - 6.29
TE	62.56 - 72.26	7.35 - 11.5	69.3 - 82.7	2.08 – 3.13
Number of averages	1 - 2	1	2 - 8	0.7
Spacing between slices	3 - 4	3 - 4	4 - 6	1
Echo train length	8 - 18	3 - 4	1 - 1	1 – 2
Pixel bandwidth	88.8 – 122.07	122.07 – 162.77	781 - 1953	244 – 1302
Flip angle	90 - 111	90 - 111	90	12
Acquisition matrix	384 x 224	448 x 224	128 x 96	320 x 192
Inversion time	-	-	180 - 220	7 - 23

Table9. Details of the study's sequences

3-2-6-5-4 Contrast agent:

The most suitable contrast agents for permeability contrast enhanced imaging are those with smaller molecules and cyclic configuration (please also see 1-7-9-8). The MRI contrast agent used in this study was ProHance (gadoteridol) which is the smallest cyclic configured gadolinium based contrast agent on the market. The used contrast agent dose was 0.2 mg per KG body weight following by 5 ml saline.

3-2-7 MRI criteria:

The MRI criteria for septic osteoarthritis are as follow:

1- Low signal intensity on T1 sequences including abscesses
2- High signal intensity on Fat saturated water sensitive sequences including in abscesses (T2 fat sat)
3- Contrast enhancement in Fat saturated T1 SCE sequences in the infectious area and rim enhancement in abscesses. SCE sequences can not only

differentiate between infection and infarction but also differentiate between hyperaemia and abnormal permeability or leak

4- Brodie abscess is a common manifestation of Subacute osteomyelitis in children with relatively characteristic MRI findings including a central non contrast enhancing fluid filled cavity, an enhancing high signal intensity granulation tissue ring on T1 weighted post contrast sequences, a sclerotic low signal intensity outer ring, and peripheral bone marrow oedema (3,4,26,133)
5- Infection shows increased signal in DWI sequences with or without real restriction (decreased signal on ADC maps) which depends on the level of oedema, cell necrosis, the extravascular extracellular macromolecules and blood cells
6- Abscesses may reveal real restriction on ADC maps which depends on the protein concentration of the abscess fluid
7- In chronic osteomyelitis, imaging may show an involucrum, sequestrum, or cloaca(3,26,133).

The combination of signal changes demonstrated in table 10 for each sequence was used in this study to diagnose MSK infection in children.

Sequences	MSK infection related signal changes
T2 fat sat	Hyper-intense signal in the infectious tissue, Hyper-intense signal in fluid collection in the infectious tissue or joint
T1	Hypo-intense signal in the infectious tissue $_1$, Hypo-intense signal in fluid collection in the infectious tissue or joint
DWI	Hyper-intense signal in the infectious tissue, Hyper-intense signal in fluid collection in the infectious tissue or joint (with or without signal loss in ADC maps)
T1 fat sat pre/post contrast	Possible signal reduction in the infectious tissue or fluid collection in the pre-contrast phase, increased signal in the infectious tissue or the rim of infectious fluid collection (abscess) or synovial membrane in case of joint involvement in the post contrast phase, significant signal contrast in affected tissue in subtracted images

Table10. The combination of signal changes of the study's sequences which were used to diagnose MSK infection in children. **(1) Not compulsory as subtle infections might not cause enough signal reduction in T1 sequences.**

This study evaluates the merit of ADC values and permeability parameters as possible quantitative and semi-quantitative diagnostic tools in the diagnosis of musculoskeletal infection (Chapters 4 and 5).

3-2-8 The Gold standard:

The first Gold standard set out in this study, was based on the final clinical information including:

1- Physical examination,
2- Laboratory and microbiology results,
3- Histopathological and intraoperative findings
4- Resolution of the disease following adequate treatment.

This was evaluated in the early stage assessment and subsequently; the gold standard was amended to include the clinical and genetic phenotypes of those patients who were also included in EUCLIDS study (see below in the brackets).

Finally, an experienced paediatric infectious disease consultant with more than 10 years' experience reviewed the combined information and summarised the ultimate diagnosis (Gold standard).

The final gold standard for this study was therefore the **ultimate diagnosis made by the paediatric infectious disease consultant** which was based on a combination of information described above. Table eleven demonstrates the breakdown of cases with positive clinical results which have helped in some cases alone, and in some cases in combination to conclude the final clinical diagnoses (gold standard).

Clinical parameters used for the gold standard	Number of (+/-) confirmations which have influenced the final clinical diagnosis (gold standard)
Physical examination	14
Laboratory and microbiology results	49
Histopathology and intraoperative findings	26
Resolution of the symptoms following adequate treatment	41
Euclid study results	27

Table11. Clinical findings which have influenced (alone or in combination) the Gold standard and their breakdown.

The chosen paediatric infectious disease consultant was recommended by the paediatric infectious disease team (Imperial College).

[EUCLIDS study is a multi-centre European paediatric infectious disease study and the first attempt to map the clinical and genetic information of the recruited patients and the infectious agent to create clinical and genetic phenotypes].

3-2-9 Readers:

Two experienced musculoskeletal radiologists with substantial experience in paediatric MRI imaging were chosen from the imperial college NHS trust radiology team for the study to act as blinded readers. The first reader has been consultant musculoskeletal radiologist for adult and children for 14 years and the second reader has been consultant musculoskeletal radiologist for adult and children for 7 years at the time of reading. The readers were familiar with the study protocol but did not know the individual patients or their scan results.

3-2-10 Evaluation form (available in appendix 4):

The basic structure of the study's evaluation form was chosen from the evaluation form of the pilot study (Dec. 2010-Apr. 2012), which focused on detection, diagnosis and conspicuity of abnormalities. However, the pilot study's evaluation form was not comprehensive enough to offer sufficient data to support sufficiently the study's hypothesis. The evaluation form was amended to cover different aspects of the single sequences and provide numerical and categorical (non-numerical) data and was modified following discussions with my supervisors and selected readers.

The initial evaluation form that was used for the inter and intraobserver agreement analyses with only ten patients did not feature diagnostic confidence score. The diagnostic confidence score section was subsequently included in the evaluation form as part of the addendum.

The final version of the evaluation form (see appendix 4) was a comprehensive model covering most features of single MRI sequences with categorical, dichotomous and numerical data to enable categorical and numerical statistical comparative tests.

The different aspects of the single sequences and the study protocol were addressed in the final evaluation form, which are as follows:

1- Detectability of the abnormality (YES / NO, Yes means an abnormality is visible and No means an abnormality is not visible)
2- Conspicuity score (1-5, 1 means no conspicuity, and 5 means excellent conspicuity)
3- Diagnosis capability, or is a diagnosis possible, was also a yes / No type question and was based on findings of a single sequence, a combination of sequences or whole protocol
4- Diagnostic confidence score (1-5, 1 means no confidence, and 5 means very confident)
5- Most useful sequence (The sequence with the highest confidence score, based on which a diagnosis could be made or is deemed most useful)

The only patient details included in the evaluation form were patient age and study ID number. The evaluation form is available in Appendix 4.

3-2-11 Reading process:

The studies were anonymised and all recognisable details were removed prior to the reading process.

The readers were unaware of individual patient diagnoses, and they reviewed the scans independently without access to patient's clinical details.

The reading process was strictly structured, with scoring guidelines and clear diagnostic MRI criteria, which were explained to the trained readers in order to minimise the chance effect and the investigator or readers bias in the statistical analysis.

The MRI protocol was divided in to two sets of sequences prior to the reading process:

- T1, T2 fat sat and DWI sequences with reconstructions and ADC maps
- T1,T2 fat sat and SCE sequences with reconstructions and subtractions

Subsequently, the readers reviewed the two sections separately on two separate occasions and randomly.

The readers reviewed 10 cases in each reading session which were chosen randomly from 10 different patients with different sets of sequences (each scan was divided in two sets of sequences), each sequence was reviewed based on its own merit and the questions of the evaluation form (appendix 4) for each sequence were answered separately, and each scan was evaluated in two different reading sessions for the two sets of sequences of the scan, which means three sequences of each scan in one reading session and in different random order.

The initial plan was to ask the readers to review the sequences (T1, T2 fat sat, DWI, SCE) of each scan separately in four different sessions (1 session for each sequence type), in order to avoid any reader's bias and enable a meaningful and objective comparison of the conspicuity and confidence scores of the DWI and SCE

sequences, with the anatomical (T1 & T2 fat sat) sequences. The current reading set up might influence the scores of the last sequences (in a set of 3 sequences per case) based on the values of the first viewed sequences and thus the final comparison might not be completely independent, however due to significantly limited availability of the readers in an acute university clinic, I have decided with my supervisors to reduce the reading sessions by half, hence dividing the protocol in two sets of scans including conventional and DWI sequences and conventional and serial contrast enhanced sequences. Once the readers have reviewed both sections of each scan they were permitted to evaluate the whole protocol (at the end of the reading of the second session). The readers did not have homogenous reading sessions with only one type of sequence combination. In this way, each scan which was divided into two sections was reviewed on two separate random occasions.

The reading sessions were not on consecutive days or weeks but separated over weeks or months. The reading sessions of the readers were on different days.

The readers initially reviewed each a set of ten cases in 4 sessions from a previous pilot study with the same sequence combination to produce enough data for statistical interobserver and intraobserver agreement tests.

3-2-12 Quantitative data and measurements:

The sequence combination of the study offers an array of qualitative semi-quantitative and quantitative information, the qualitative information was captured in the evaluation form and categorised into nominal or ordinal (numerical) data ready for statistical analysis, but the semi-quantitative and quantitative information of the study had to be first measured, prepared and classified prior to statistical analysis.

3-2-12-1 ADC value measurement:

GE health care advantage workstations (ADW, Volume share 5, HP 2800 workstation 2011, GE medical system Waukesha, Milwaukee USA) and GE software (HP 2800 with angio viz, 2011) for DWI and ADC measurement were used for the quantitative measurement of the ADC values.

DWI sequences provide qualitative and quantitative information about the scanned tissue however the quantitative maps (ADC maps) and the ADC values need to be calculated.

The first step is to calculate the ADC map. The ADC map calculation was done automatically by the GE scanner workstations as part of the scan process.

The ADC values in this study were measured in 2D and in axial plain and once the region of interest was identified on the ADC map, a circular ROI from DWI software tool box was placed in the middle of the lesion to measure the ADC value of the region in millimetre square per second. A reference measurement was performed for each measurement in an area with the same size ROI (mm2) in an equivalent portion of healthy tissue on the same or contralateral side. The ROI sizes were in a range of 30 – 105 mm2. This method of ADC measurement is the most common way of ADC measurement in the literature(64,76–78,134).

If the pathological process was expanding over different types of tissue, including multiple compartments or comprised of different components (cystic, solid), then multiple measurements in the lesion's different tissue types or compartments and equally multiple reference measurements in equivalent healthy tissue or compartment were performed to capture different characteristics of the lesion.

The measured values from different tissue were separately compared and statistical tests and curves (ROC test) were created separately for different tissue types and compartments for example ROC test for bony lesions, or for muscular lesions...

If the process was multifocal or bilateral similarly multiple measurements with multiple reference measurements were performed to represent different locations or possibly different pathologies.

The ADC measurements were exclusively performed by the principal investigator. The ADC assessment in this study produced an array of measured ADC values from different anatomical locations, different types of tissue and different parenchymal compartments.

In ten random cases the ADC values and the reference ADC values were measured twice, one and half months apart for the intraobserver agreement test of the ADC value measurements.

It has been described in the literature that scanning on different scanners (even with different field strength) from the same manufacturer does not show significant differences in mean ADC values(64,77,80,134). There have been no significant differences between the measured reference ADC values, in reference healthy tissue in different subjects between the three scanners in this study in keeping with the literature.

3-2-12-2 Signal intensity and contrast intensity curves and semi-quantitative serial contrast enhanced measurements:

Serial contrast enhanced or multiphase enhanced contrast imaging (section 1-7-9, 1-7-9-6) is the second nonconventional approach in this study which provides qualitative and semi-quantitative information concerning the scanned structure.

Serial contrast enhanced semi-quantitative measurements in this study were performed using the Olea advance software (Olea version 2.2 Vitrea / Vital medical system Minneapolis US) of Carestream Pacs package.

The principle of the measurement process is similar to ADC value assessment; once the pre and post contrast serial sequences are available the software can create the intensity curves and calculate the semi-quantitative values including AUC and TME.

The semi-quantitative parameters were calculated in 2D, but in different planes (sagittal, coronal and axial), as the software is more accommodating in comparison to the software used for ADC value measurement, and the sequences are three-dimensional acquired sequences with nearly equal resolution in all three planes.

Once the region of interest was identified on the sample SCE image a hand-drawn circular ROI was placed in the middle of the lesion to measure the semiquantitative parameters and create the time signal intensity curves. Healthy reference measurements are more important in SCE semi-quantitative measurements, as the values are relative and reference measurements in normal contrast enhancing

equivalent healthy tissue can reveal the significance of the contrast enhancement interference. The ROI sizes should ideally be equal.

If the pathological process expanded over multiple compartments including different types of tissue or if the process was a multifocal process, then multiple measurements in the lesions and equally multiple reference measurements were performed. The measured values from different tissue were separately compared and statistical tests and curves (ROC test, Curve) were created separately for different tissue types and compartments for example ROC test for bony pathologies, or for muscular pathologies.

In ten random cases the semi-quantitative values and the reference healthy values were measured twice, one and half months apart to assess the intraobserver agreement for the ROI measurements of the semi-quantitative values. There was no significant difference between the measured reference values in healthy tissue in different subjects between the three scanners in this study.

The measurements were exclusively performed by the principal investigator.

3-2-13 Data preparation, modification and reformatting:

The complete record of the data produced by the readers was reformatted and transferred to an excel spread sheet with the study ID, age and gender of the patient together with the information from different sections of the evaluation form including the nominal and ordinal (numerical) data. Subsequently, the final diagnoses of the readers, the reporting clinical radiologist and the gold standard were added to the excel spread sheet. The free text diagnoses were reclassified into eight groups with generic names and allocated to a number between one and eight. The eight categories are as follows: Infection, Infarction, Benign lesion, malignant lesion, Inflammation, Fracture, Muscle injury, Normal. The numbers of the cases of the different diagnoses has been presented in the result section of chapter 4 and 5.

Separate excel sheets were created for the quantitative measurements including the ADC values and semi-quantitative values including SCE semiquantitative parameters (AUC and TME). The measured values were then divided into different

groups representing the different original tissues (bone, muscle...). The added free text diagnoses were also reclassified into eight groups with allocated numbers between one and eight. The quantitative values are paired values including the value for the pathology and the reference equivalent healthy value.

3-2-14 Statistical analysis:

The statistical work of the study is divided into two sections:

- Preliminary statistical tests (section 3-2-14-1): Statistical analysis of a pre-set of data including categorical and numerical data of 10 random patients from the pilot study to assess inter and intraobserver agreements. Cohen's kappa test was used for the categorical data and Interclass correlation coefficient (ICC) test was used for the numerical data

- Statistical tests of the study's (prospective) data (section 3-2-14-2): Statistical analysis of the main study data to assess feasibility and accuracy of the MRI protocol, to rank the MRI protocol's sequences and to calculate possible cut off values for the quantitative and semi-quantitative data (ADC, TME and AUC values). The intraobserver agreement or reproducibility of the quantitative and semi-quantitative data measurements was assessed with ICC test. Descriptive statistic was used for the feasibility assessment. Cohen's kappa test was used for accuracy tests of the categorical data. Friedman's ANOVA and paired sample sign tests were used for the ranking of the sequences (numerical data). Receiver operating characteristic curve/ test was used for the numerical data to calculate possible cut off values.

SPSS statistics program version 25 (IBM Company Chicago Illinois) was used for all statistical analysis in this study. The statistical software was provided by Imperial College London.

The chosen p value as a threshold for statistical significance was 0.05 for all tests.

The statistical tests utilised in each individual area of application were those recommended by Imperial college London biostatistics department.

3-2-14-1 Inter and intraobserver agreements:

The MRI scans of 10 random patients from the pilot study, using the same MRI protocol as in the main study were independently reviewed and scored twice with an interval of one and half months by the selected readers, following the same pathway described in 3-2-11.

The goal of this section was to evaluate the level of agreement between the readers and the level of consistency of the readers using the new MRI tool prior to the main study (prospective study). The data was a combination of numerical (scores) and categorical data (diagnoses), which was harvested from the evaluation form (see Appendix 4). ICC test was used for the numerical data and Cohen's Kappa test for the categorical data.

-Numerical data: The numerical part of the data included the conspicuity scores of the MRI protocol's sequences, and the intention was to determine the readers' inter and intraobserver agreements. The objective of the statistical analysis was inter and intraobserver agreements and the data was numerical with paired groups, therefore the most suitable test was the Interclass correlation coefficient (ICC) test. The readers were chosen (fixed), but the subjects were random and the test should reveal the homogeneity or agreement, therefore the two-way mixed effect model of type A interclass correlation coefficient was chosen for the numerical data. The ICC test was repeated four times for the main four different sequences of the study (T2 fat sat, T1, T1 fat sat serial contrast enhanced and DWI) for the interobserver agreement test and eight times for the intraobserver agreements (four tests for the four sequences for each reader).The most important values in this test which represent the level of agreement are statistical significance (p value) and the average measure. The ideal p value is <0.05 and regarding the ideal average measure there are different interpretations, the most common sited rules for Interclass correlation coefficient measures are propagated by:

Cicchetti (1994)(138):

- Less than 0.40—poor.
- Between 0.40 and 0.59—fair.

- Between 0.60 and 0.74—good.
- Between 0.75 and 1.00—excellent.

Koo and Li (2016)(139):

- below 0.50: poor
- between 0.50 and 0.75: moderate
- between 0.75 and 0.90: good
- above 0.90: excellent

12 ICC tests for inter and intraobserver agreement were in total performed.

-Categorical data: The categorical part of the data included readers' diagnoses and the clinical gold standard diagnoses. Correlation of interobserver and intraobserver categorical data could significantly strengthen the Inter and Intraobserver agreement (reliability and consistency) results of the ICC tests as most of the relevant agreement tests for categorical data have higher statistical strength than ICC test. The different values of the categorical data (free text diagnoses) were transformed into nominal variables, and the variables were labelled in SPSS program with numbers to simplify the analyses. The design of the test was pair observation, and the data was categorical with exclusive, but the same number of categories for each variable. I selected Cohen's kappa test to evaluate interobserver agreement by comparing the second reviews of the readers (one test) and intraobserver agreement by comparing the first and second review of each reader (two tests). A total of 3 Cohen's kappa tests were performed to analyse the agreement of the categorical data. Cohen's kappa test is a stronger agreement measure than the ICC test owing to its strong statistical value and it presents the real agreement without the expected agreement by chance.

There are many guidelines for the calculated kappa value in published literature, including Landis & Koch and Fleiss, however all of these provide arbitrary guidelines. In summary they follow nearly the same thresholds as the ICC values (poor < 0.4 < Moderate < 0.6 < Substantial < 0.8 < Excellent).

3-2-14-2 Statistical analysis of the main data including quantitative and qualitative data:

The main study data consists of categorical and numerical data. The categorical data includes the readers' diagnoses and the gold standard diagnoses and the numerical data includes the conspicuity and confidence scores and the measured permeability and ADC values.

The addition of diagnostic confidence scores to the final evaluation form used for the main study has doubled the volume of the numerical data of the evaluation form, as the initial form included only conspicuity score.

3-2-14-2-1 Feasibility:

The most common definition of feasibility in imaging studies is: the probability of successfully performing a study independent from the final results(140). I have utilised this definition for my study and introduced the following set criteria: patient numbers ~100, patient recruitment time =2 - 2,5 years and enrolment rate 90%<(140).

The patient numbers and recruitment time were estimated based on the results of the pilot study which was conducted over a period of 16 months with 63 patients. The enrolment rate was adhered to suggested rate from literature (140)for clinical studies. Simple descriptive statistic including percentages was suggested for the feasibility results by Imperial college biomedical statistic team as the study was a single site study with a moderate sample size(140).

The definition of feasibility and its practical translation in this study was adhered to recent radiology literature, however during the thesis review the narrowness of the definition and the relative limitation of its practical implementation was acknowledged. The term ''successful performing,, was not in detail defined and the exclusion process was not independently performed by the readers. This shortcoming however did not have any impact on the data and the data analysis.

3-2-14-2-2 Diagnostic accuracy tests of the MRI protocol based on the evaluation form's qualitative data (categorical tests):

The categorical data which were used for the diagnostic accuracy tests included the gold standard and the readers' diagnoses based on single sequences and the combined sequences (study protocol).

The free texts of the diagnoses were classified into eight representative groups and subsequently the eight groups were numerically relabelled (1 to 8) as follows:

1- Infection
2- Infarction
3- Benign tumour
4- Malignant tumour
5- Fracture
6- Inflammation
7- Normal
8- Muscular injury

The categorical paired data was produced by the two fixed readers who reviewed the scans independently. The eight relabelled groups or categories are independent and exclusive and their paired cross tables are square shaped (the same number of columns and rows), therefore similar to the inter and intraobserver agreement tests. Cohen's kappa test was used to determine the level of agreement or correlation between the final diagnoses of the readers which represents interobserver agreement based on the prospective data, and between the final diagnoses of the readers and the gold standard which represents diagnostic accuracy (2 x Cohen's kappa tests) of the study's MRI protocol. Similarly Cohen's kappa analyses were performed between the diagnoses based on the single sequences and the gold standard (8 tests) to evaluate the accuracy of the single sequences. The sensitivity and specificity were calculated in each Cohen's kappa analysis with (Monte Carlo significance exact test) 95% interval lower and upper bounds on SPSS. This is the standard way of presentation of Cohen's kappa test results in SPSS program.

There are many guidelines for the calculated kappa value in published literature, including Landis & Koch and Fleiss, however all of these follow nearly the same thresholds as the Cicchetti method for the ICC values (see in section 3-2-14-1).

3-2-14-2-3 Statistical analysis of the numerical data of the evaluation form (readers scores) to evaluate the subjective diagnostic value of single sequences or the readers' preferences:

The numerical data of the study concerning the readers' preferences and subjective priority of different sequences, which was derived from conspicuity and confidence scores, was extensive and provided an opportunity to correlate the different sequences with each other and determine which sequence or sequences are more subjectively useful and preferred by the readers.

The variables, which included conspicuity and confidence scores (numerical data), were paired samples that came from the same participants and the scoring system was a numerical system from 1 to 5, with 5 being excellent and 1 being poor.

The conspicuity and confidence scores were derived from the evaluation of the 4 different sequences of the study protocol, which means there are 4 groups for comparison and the data was non parametric, hence a multiple group comparison test for non-parametric numerical data should be employed which in the event of a significant difference should be followed by post-hoc comparison tests. Friedman's ANOVA test was chosen for the initial multiple groups testing for each scoring system as it can address all above mentioned requirements. There were two scoring systems for each of the two readers, which mean four Friedman's ANOVA tests. The p value was 0.05.

The conspicuity or confidence scores were derived from independent paired observations. The numerical data was non-parametric and the distribution of differences between the scores was not symmetrical hence Paired sample sign test or Sign test (two tailed in order to capture both ends of the area under the curve) was the most suitable test for post-hoc multiple testing in the event of significant differences of the Friedman's ANOVA tests. Multiple (repeated) comparisons testing between multiple, two groups, combinations is per definition prone to type one error,

thus Bonferroni adjustment was applied to the paired sample sign tests to control the risk of type one error. The Bonferroni adjustment is fulfilled when the initial p value (<0.05) is divided by the number of comparisons between the groups or with other words the number of comparison's hypotheses.

There were six comparison possibilities between the four main study sequences (T1 versus T2 fat sat, T1 versus DWI, T2 fat sat versus DWI,...) for each reader, hence twelve sign test analyses for each reader to cover both confidence and conspicuity scores. In total twenty four tests should have been performed for both readers in order to evaluate the readers preferences in the event of significant difference based on the Friedman ANOVA tests. The conspicuity and diagnostic confidence scores were separately for each reader analysed and were separately interpreted for each reader. There were six comparison possibilities between the four sequences of the study for the paired sample sign tests which means the p value, after Bonferroni adjustment would be <0.0167 (0.05/6 = 0.0167) for the paired sample sign tests.

The above statistical tests were recommended for the study data by the Imperial college London biomedical statistic unit.

3-2-14-2-4 Statistical analysis of the calculated permeability and ADC values:

At first the ADC and permeability values were measured twice on ten random cases from the main study data in the pathologic and healthy reference tissues, with an interval of 1.5 months, and subsequently, the intraobserver agreement or consistency of the measurement processes was calculated using a two-tailed ICC statistic test.

The quantitative and semiquantitative values produced by ADC and permeability value measurements were separately analysed and compared with the final diagnoses in order to determine possible correlations and tendencies or useful thresholds.

The numerical data derived from measured quantitative values of DWI and semiquantitative values of SCE sequences were divided based on where (location) they were measured into different tissue groups / compartments including:

1- Bone
2- Muscle
3- Extra-muscular soft tissue (subcutaneous fat...)
4- Cartilage
5- Synovial membrane
6- Joint fluid
7- Extra-articular fluid

The concept of the diagnostic tool in this study based on magnetic resonance imaging was partially to find statistical valid quantitative values or thresholds, which can enhance the diagnostic power of the gathered qualitative information from the imaging protocol, thus providing quantitative and objective diagnostic information.

Receiver operating characteristic test or ROC was chosen as it reveals the correlation between the measured values and the final diagnoses, and possibly offers a cut-off value with predictive potential based on the highest statistical sensitivity and specificity.

The receiver operating characteristics and curves of the measured ADC values in the different musculoskeletal compartments (bone, muscle, synovial membrane,…see above) were calculated considering the main four diagnoses (infection, infarction, benign and malignant processes) of the study. It means the ADC values of different musculoskeletal compartments are the variables and the main diagnoses are the categories.

The same process was followed for the two most relevant semi-quantitative permeability parameters (TME=Time to max. enhancement and AUC= Area under the curve) in order to create useful threshold values, where the TME and AUC values of different musculoskeletal compartments are the variables and the main diagnoses are the categories. The permeability values were however divided into four main tissue compartments including bone, cartilage, muscle / soft tissue and synovial membrane.

There are many ways to interpret the ROC test results and curves and the most representative value for interpretation is the decimal value of the area under the

curve. The interpretation of the categories is usually similar in most published ROC interpretations and can be summarised as follows,

1- 0.9 < Excellent
2- 0.8 < Good < 0.9
3- 0.7 < Fair < 0.8
4- Poor < 0.7

Chapter 4: Diffusion Weighted Imaging

4-1 Introduction:

Magnetic resonance imaging has established its position as the most powerful imaging tool for musculoskeletal pathologies. MRI offers superior resolution and characterisation of different musculoskeletal pathologies, particularly in demonstrating their composition, extent, compartmental involvement, and proximity to the neighbouring organs and neurovascular structure(56,141).

The advanced quality of the imaging that MR can provide together with the lack of ionising radiation has promoted MRI as the modality of choice for regional and whole body imaging in paediatric patients with musculoskeletal disorders (64).

Diffusion weighted imaging (DWI) is a newer functional imaging technique and a recent addition to the magnetic resonance sequences conventionally employed for diagnosis of paediatric pathologies (57,64). Diffusion weighted imaging provides qualitative and quantitative information about the microscopic architecture of tissue at a cellular level (57). The observed signal attenuation in diffusion weighted imaging is based on self-diffusion of water molecules in the intracellular and extravascular extracellular spaces(63).

The diffusion phenomenon of water molecules, the basic and principles of MRI imaging based on diffusion phenomenon and different types of diffusion weighted imaging techniques have been extensively explained in section 1-7-7 of chapter 1. Specific diffusion characteristics of immature skeleton and clinical applications of diffusion weighted imaging in paediatric musculoskeletal system with relevant literature have been presented in section 1-7-8 of chapter 1. The relevance of

diffusion weighted imaging in musculoskeletal infection in children will be explored in the following section.

4-2 Altered diffusivity in musculoskeletal infection in children:

The dynamic changes in the musculoskeletal system during an infection significantly alter the tissue diffusivity through hyperaemia, increased permeability, increased extracellular fluid and cells, replacement and destruction of fat cells and trabecular structure. These changes have been proposed (64,66,74,76,78) to explain diffusion changes initially with increased ADC values and a potential delayed decrease of diffusion and ADC values.

4-3 Material and methods:

4-3-1 Objective:

In this chapter of the study I will evaluate the feasibility and the diagnostic accuracy of diffusion weighted imaging in the diagnosis of musculoskeletal infection in children and compare with SCE and structural sequences. Furthermore I will compare the subjective conspicuity and diagnostic confidence of the DWI sequences based on readers scoring with the other sequences of the study's protocol and finally I will assess the measured ADC values in my study cohort to evaluate the diagnostic performance or differential diagnostic capability of ADC values and see if there are statistically significant ADC value thresholds for the differential diagnosis of musculoskeletal infection in children.

4-3-2 Ethic approval:

Institutional, local and national ethical approval was sought and obtained (see appendix 1).

4-3-3 Study structure:

The Study structure has been discussed in chapter 3, section 3-2-1.

4-3-4 Demographic of the study population:

99 paediatric patients were prospectively recruited over a period of two and a half years, between November 2014 and May 2017. The number of patients was estimated based on my retrospective pilot data.

There were 44 girls and 55 boys included in this study. The age of the subjects ranged between 1 and 216 months (18 years) with a mean age of 101 months (8 years). Table 12 below, summarises the demographics of the participants and the incidence of the affected anatomical locations.

	Number of participants	Mean age in months	Incidence of pelvis & lower limbs	Incidence of shoulder & arms	Incidence of neck, thorax and spine	Number of MRI scans
Boys	55	95	40	13	3	56
Girls	44	107	36	9	2	47
Total	99	101	76	22	5	103

Table12. Demographics of study participants and the incidence of affected anatomical locations. The most common anatomical locations were pelvis and lower limbs.

The inclusion / exclusion criteria and recruitment including the information, consent and assent forms have been presented in chapter 3 (section 3-2-3, 3-2-4 & 3-2-5).

4-3-5 Magnetic resonance imaging and the imaging protocol:

The information about imaging site, number and field strength of scanners, coils and imaging team has been presented in chapter 3, section 3-2-6 (3-2-6-1 till 3-2-6-6). Varying field strength was not expected to create relevant alterations in ADC value analysis in accordance with the literature (64,77,80,134), beyond minor possible increased susceptibility at higher field strength (80). However multiple reference ADC values per subject from reference anatomical locations (mid diaphysis...) were compared between the different field strengths to exclude possible relevant differences in ADC values.
The chosen diffusion weighted sequence for the study protocol was spin-echo echo planar sequence with two b-values (b=0 and b=500).

The sequences were acquired in axial plain in order to minimise the susceptibility artefacts (slice thickness=3-5 mm) with subsequent coronal reconstruction (reconstruction algorithm of 0.5 and slice thickness of 1.2-2.5 mm) and inversion of the images grey scales to improve the conspicuity of the lesions.

The ADC maps were automatically calculated by the scanner software and displayed in the axial plain. All of the series including the raw data, the reconstructed and inverted images were analysed.

The additional tailored MRI sequences of the study protocol have been presented in chapter3, section 3-2-6-5.

4-3-6 Quantitative image analysis (also see section 3-2-12-1):

The quantitative tissue diffusion properties were analysed by means of ADC measurement on axial ADC maps. GE health care advantage workstations (ADW, Volume share 5, HP 2800 workstation 2011, GE medical system Waukesha, Milwaukee USA) and GE software (HP 2800 with angio viz, 2011) for ADC measurement were used for the quantitative measurement of ADC values.

ADC values were obtained by drawing a region of interest in the main area of concern (the equivalent area with the maximum signal intensity on DW images).

The ADC measurements were conducted each time in one tissue compartment and at least 3 mm away from the tissue interfaces to avoid partial volume effect (80). The measurements were performed separately in different compartments in case of multi-compartmental lesions. Multiple ADC measurements were performed in case of multiple pathologies.

One set of ADC values including mean ADC and standard deviation were documented for each lesion and each compartment. The sizes of the ROIs were between 30 and 105 mm2.

Each ADC measurement was followed by a reference measurement in a similar location in healthy tissue. Separate reference ADC measurements in reference healthy anatomical locations, were performed to assess the possible ADC alterations in healthy standard tissue between different magnet field strength in different patients.

The measurements were conducted by an experienced paediatric radiologist with more than 10 years' experience in paediatric musculoskeletal imaging.

All ADC measurements (in pathological and healthy reference tissues) in 10 random cases were repeated 1.5 months later in order to assess the intraobserver agreement or consistency of the manual measurement's process.

4-3-7 Qualitative and semi-quantitative analyses:

The qualitative and semi quantitative analyses were conducted independently by two experienced musculoskeletal radiologists with paediatric experience (see section 3-2-9 for Readers), using a specifically designed evaluation form (see section 3-2-10 for evaluation form and appendix 4).

The evaluation form is a multi-parametric tool, which covers all subjective aspects of the study MRI sequences including the lesion detectability (yes/no), image conspicuity (scoring system, 1 to 5), diagnostic capability (yes/no), diagnostic

confidence (scoring system, 1 to 5) and final diagnoses based on single sequences (DWI sequences for this chapter) and the combined whole protocol.

The reading process (see section 3-2-11), was strictly structured with scoring guidelines and clear diagnostic MRI criteria (see section 3-2-7 for MRI criteria). The reading process was extensively explained to the readers in order to minimise the chance effect and the investigator or readers bias in the statistical analysis.

The lesion detectability and diagnostic capability were simple yes or no type (dichotomous) questions, whilst Image conspicuity and diagnostic confidence were analysed using a scoring system (numerical data), in order to produce more clear values. The image conspicuity and diagnostic confidence scores were used to compare different sequences with each other and will be presented in result section of this chapter (section 4-4-6).

The diagnoses of the readers based on single sequences including DWI sequence were compared with the Gold standard (see section 3-2-8 for Gold standard) in order to evaluate the diagnostic accuracy of DWI sequence.

4-3-8 Data preparation (see section 3-2-13 for more details):

Separate excel spreadsheets were populated for each reader with the qualitative and semi-quantitative data of the evaluation forms. The free text diagnoses were reclassified into eight groups with generic names and allocated to a number between one and eight.

Subsequently, the numerically transformed readers' diagnoses and the final clinical diagnoses (gold standard) were added to the excel sheets.

The quantitative data including the ADC values were populated separately in excel format. The measured values were then divided into different groups representing the different original tissue compartments (bone, cartilage, muscle, fat tissue, synovial membrane, intra and extra articular fluid) considering only the main four diagnoses (infection, infarction, benign and malignant processes). The quantitative values are paired values including the value for the pathology and the reference equivalent healthy value.

4-3-9 Data analysis and statistics:

SPSS statistics program version 25 (IBM Company Chicago Illinois) was used to conduct statistical analysis in this study. A p value of less than 0.05 was considered to be statistically significant.

4-3-9-1 Inter and intraobserver data analysis (see section 3-2-14-1 for more details):

The inter and intraobserver agreements were initially assessed. The readers evaluated independently 10 random cases from the pilot study with the help of the above described multi-parametric evaluation form. The numerical and categorical data were separated. The numerical data (quantitative information) includes conspicuity scores of the single sequences and the categorical data (qualitative information) includes readers' diagnoses based on single sequences and whole combined protocol.

The two-way mixed effect model of interclass correlation coefficient (ICC) test type A (with absolute agreement) was employed for the numerical data concerning the inter-observer and intraobserver agreements.

Cohen's kappa test was utilised for the categorical data concerning the inter-observer and intraobserver agreements. The statistical tests were recommended by Imperial college London biomedical statistic unit.

4-3-9-2 Main data analysis:

The feasibility (please see chapter 3, section 3-2-14-2-1) in this study was defined as successfully completing the scan with the study protocol. I have introduced the following set of criteria for the study's feasibility: patient numbers (~100), patient recruitment time (2 - 2.5 years) and enrolment rate (90%<)(140). The patient numbers and recruitment time were estimated based on the pilot study (chapter 3) and the enrolment rate adhered to the suggested rate from literature (140). Simple descriptive statistics including percentages was suggested for the feasibility results by Imperial college statistic team as the study was a single side study with a moderate sample size(140).

The data from the evaluation forms was divided into numerical and categorical data. The numerical data consisted of conspicuity and diagnostic confidence scores which are per definition semi-quantitative information and the categorical data consisted of readers diagnoses based on single sequences and whole MRI protocol, which are qualitative information.

Cohen's kappa test was performed to compare the readers' diagnoses (see chapter 3, section 3-2-14-2-2) based on single sequences including DWI with the clinical gold standard and assess the diagnostic accuracy of the single sequences and reveal the diagnostic accuracy value of DWI and other sequences of the protocol.

The numerical data of the study concerning the readers' preferences and subjective priority of different sequences including the conspicuity and diagnostic confidence scores was analysed to compare the different sequences with each other and determine which sequence or sequences are superior or preferred by the readers. The statistical tests used for this section of the chapter have already been explained in section 3-2-14-2-3, chapter 3.

The quantitative information extracted from the ADC maps are ADC values which were separately analysed (see chapter 3, section 3-2-14-2-4). At first two sets of ADC values of ten random cases from the main study cohort were measured twice, in the same 10 scans, in pathologic and healthy reference tissues with an interval of 1.5 months and the data was analysed using two tailed interclass correlation coefficient statistical tests to prove the intraobserver agreement of the quantitative (hand drawn) measurement.

Subsequently the ADC values of the entire cohort (all scans) were divided into seven main tissue groups including bone, cartilage, muscle, fat tissue, synovial membrane, intra and extra articular fluid.

Receiver operating curve or ROC statistical tests were performed for the ADC values of the seven different tissue compartments separately to reveal the order or relationship between the measured ADC values in each tissue compartment separately considering the main four diagnoses(infection, infarction, benign and malignant processes), to assess the potential of the ADC values in differentiating

MSK infection in children from other possible differential diagnosis by delivering cut-off values based on the highest statistically possible sensitivity and specificity to improve the diagnostic process.

It has been postulated in the literature(76,142,143) that the average ADC value in the bone marrow is increased in an infectious process in comparison to the normal bone marrow and other bony pathologies. I have compared the average ADC values of the infectious bony pathologies with the average ADC values of the non-infectious bony pathologies and the reference normal bone to evaluate the above finding in the literature. Kruskall-Wallis H test was performed, as the data was numerical and non-parametric to determine any significant differences between the multiple diagnosis groups (Infection, Non-infection, Normal) and subsequently, in the event of a significant difference, post hoc Mann-Whitney U test with Bonferroni correction was applied to find out where the significant difference lies.

The chosen p value for statistical significance for all statistical tests was 0.05.

The above statistical tests were recommended for the study data by the Imperial college London biomedical statistic unit.

4-4 Results:

4-4-1 Cohort:

Ninety nine children with acute musculoskeletal pain and suspected clinical diagnosis of musculoskeletal infection were prospectively recruited for this study.

One hundred and three MRI scans were performed on different admissions; using the same novel MRI protocol including diffusion weighted sequences and ADC maps. Below is a cohort table with the breakdown of the patients and scans.

Cohort	Number of cases
Approached candidates who have fulfilled the incl./excl. categories	99
Recruited patients	99
Patients/scans excluded due to incomplete scans (Hardware malfunction = HM or personal error of the operator = PE)	3 (HM=2, PE=1)
Scans performed(on 99 patients, including on multiple admissions)	103
ADC values excluded due to suboptimal ADC maps (based on inadequate scanning plane & susceptibility artefacts)	5

Table13. Cohort table with the number of excluded patients and scans for the DWI section of the study.

4-4-2 Feasibility of DWI:

All of the patients, except those who had their scans under general anaesthesia or sedation, tolerated the entire examination well including the average 5-6 min for DWI sequence. Only three patients (3%) had to be excluded due to incomplete scans and in all three cases personal error or equipment malfunction was the reason for incomplete data acquisition and not the patient cooperation. Hence the enrolment rate of the study was above the pre-set 90% and the feasibility was excellent. For more information please see section 3-2-14-2-1 in chapter 3.

4-4-3 Inter and Intraobserver agreement tests:

The readers initially reviewed 10 random cases independently from the pilot study with the same MRI protocol and a nearly identical evaluation form. The readers repeated the independent review of the same cases 1.5 months later.

The produced numerical (semi quantitative) data, which was derived from the scoring system of the evaluation form, was analysed with a two tailed ICC test and the categorical (qualitative) data was analysed with Cohen's kappa test (see section 4-3-9-1).

Table 14 illustrates Interclass correlation coefficient results of inter and intraobserver reliability tests of the semi quantitative results of the DWI sequences.

There was an excellent correlation (according to Koo & Li) of the semi quantitative data (conspicuity scores) concerning the DWI sequences between the readers (p value= 0.002).

The intraobserver agreement of semi quantitative data concerning the DWI conspicuity scores was excellent for the first reader (p value=0.001), and moderate-good for the second reader (p value= 0.006).

	Interclass correlation average[a] measures	%95 confidence interval lower - upper bound	Significance = p value
Intra-observer agreement test of reader 1	0.895	0.433 – 0.948 0.604 – 0.974	0.001
Intra-observer agreement test of reader 2	0.723	-0.072 – 0.875 -0.155 – 0.933	0.006
Inter-observer agreement test between the readers	0.883	0.377 – 0.943 0.548 – 0.971	0.002

Table14. Interclass correlation coefficient test for inter and intraobserver agreement, p value is significant < 0.05.
a. This estimate is computed assuming the interaction effect is absent, because it is not estimable otherwise.

The categorical data extracted from the evaluation form, consisting of the readers' diagnoses was analysed with Cohen's kappa test. The kappa measure of agreement between the readers was 0.756 and the p value was 0.001 (sensitivity= %87.5 and specificity > %90), in keeping with good agreement. The intraobserver agreements based on Cohen's kappa test were good-excellent (kappa value = 0.756 & 1, p value = 0.001).

The inter and intraobserver agreement is good-excellent, considering the categorical and numerical data from the evaluation form.

4-4-4 Intraobserver agreement of the hand drawn ROI measurements' of the ADC values:

The manual ROI measurement of ADC values was repeated in ten random cases in the lesion as well as in the healthy reference tissue one and a half month later.

The data was analysed using two tailed interclass correlation coefficient (ICC) test with absolute agreement to assess the intraobserver agreement of the measurements.

The agreement was excellent for both, pathological (ICC= 0.945, p= 0.000) and reference (ICC= 0.893, p= 0.000) tissues as shown in Table 15.

	Interclass correlation	%95 confidence interval, lower and upper bound	Significance= P value
Intraobserver agreement of pathological single measures[a]	0.945	0.806 - 0.986	<0.001
Intraobserver agreement of pathological average measures[b]	0.972	0.893 – 0.993	<0.001
Intraobserver agreement of reference single measures[a]	0.893	0.632 – 0.972	<0.001
Intraobserver agreement of reference average measures[b]	0.943	0.775 – 0.986	<0.001

Table15. Interclass correlation coefficient test for manual ADC measurements intraobserver agreement, p value is significant < 0.05.
a. The estimator is the same, whether the interaction effect is present or not.
b. This estimate is computed assuming the interaction effect is absent, because it is not estimable otherwise.

4-4-5 Diagnostic accuracy of DWI (see section 3-2-14-2-2):

The categorical data derived from readers diagnoses based on DWI sequences was compared with the clinical gold standard using a categorical comparison test (Cohen's kappa test) to determine the diagnostic accuracy of diffusion weighted imaging.

Cohen's kappa test was performed twice, as there were two readers, to assess the level of agreement between the DWI diagnoses of the readers with the final clinical diagnoses (gold standard). Cohen's kappa tests results are summarised in the following tables, table 16 includes the complete 8 categories of diagnoses (see section 3-2-14-2-2, chapter 3) and table 17 includes only 2 diagnostic categories (infection versus not infection).

DWI based diagnoses of the readers versus Gold standard	Measure of agreement Kappa value	Sensitivity	Specificity	Sig. = p value
DWI Reader 1~ Clinical diag.	0.647	76%	90.3%	<0.001
DWI Reader 2~ Clinical diag.	0.672	78.4%	92%	<0.001

Table16. Level of agreement between DWI diagnoses and clinical gold standard with 8 diagnostic categories. The kappa value is the rate of agreement between DWI diagnoses (experimental diagnostic tool) and the clinical gold standard (standard diagnostic tool). The sensitivity and specificity relate to DWI as the diagnostic tool for MSK infection in comparison with the clinical gold standard, p value is significant < 0.05.

DWI based diagnoses of the readers versus Gold standard	Measure of agreement Kappa value	Sensitivity	Specificity	Sig. = p value
DWI Reader 1~ Clinical diag.	0.671	76%	90.3%	<0.001
DWI Reader 2~ Clinical diag.	0.715	78.4%	92%	<0.001

Table17. Level of agreement between DWI diagnoses and clinical gold standard with 2 diagnostic categories (infection versus non infection). The kappa value is the rate of agreement. The sensitivity and specificity relate to DWI as the diagnostic tool for MSK infection in comparison with the clinical gold standard p value is significant < 0.05. The lower and upper bounds of the 95% confidence interval were 0.000 – 0.029 for DWI sequences of both readers.

The kappa value of the first reader is moderate-good and the kappa value of the second reader is good. The kappa value improves slightly when running the test with 2 diagnostic categories whilst the sensitivity and specificity for infection is unchanged. The results of the Cohen's kappa tests are promising and reflect the relative high diagnostic accuracy of DWI sequence with good sensitivity and excellent specificity.

The diagnostic accuracies of the study's sequences were calculated independently and presented as demonstrated in SPSS statistic program with kappa value, significance level (p-value), sensitivity, specificity and 95% confidence interval lower-upper bound.

The results of the diagnostic accuracy tests (Cohen's kappa) for the remaining sequences of the protocol are demonstrated in Table 18a (first reader) and 18b (second reader).

Diagnoses based on single sequences versus Gold standard, first reader	Kappa value	Sensitivity	Specificity	Sig.= p value
T1 diagnoses ~ clinical diagnosis	0.631	62.2%	96.8%	<0.001
T2 fat sat diagnoses ~ clinical diagnosis	0.732	75.7%	95.2%	<0.001
T1 fat sat serial contrast diagnoses ~ clinical diagnosis	0.755	78.4%	95.1%	<0.001

Table18a. Diagnostic accuracy test results for single sequences' versus the gold standard (2 diagnostic categories) for the first reader. The 95%

confidence interval lower-upper bound was 0.000-0.029 for all three sequences (SPSS statistics).

Diagnoses based on single sequences versus Gold standard, second reader	Kappa value	Sensitivity	Specificity	Sig.= p value
T1 diagnoses ~ clinical diagnosis	0.441	40.5%	98%	<0.001
T2 fat sat diagnoses ~ clinical diagnosis	0.760	81.1%	93.7%	<0.001
T1 fat sat serial contrast diagnoses ~ clinical diagnosis	0.892	91.9%	96.8%	<0.001

Table18b. Diagnostic accuracy test results for single sequences' versus the gold standard (2 diagnostic categories) for the second reader. The 95% confidence interval lower-upper bound was 0.000-0.029 for all three sequences (SPSS statistics).

The highest kappa value of the single sequences was from SCE sequences, in keeping with good – excellent diagnostic accuracy (see section 3-2-14-2-2 for classification) and the lowest was from T1 sequences, in keeping with poor – moderate diagnostic accuracy. The kappa values of DWI and T2 sequences were intermediate in keeping with moderate or good accuracy. Equally the highest sensitivity was from SCE sequences and the lowest from T1 sequences whilst the sensitivity values of DWI and T2 fat sat sequences were intermediate. The specificity of all sequences was excellent and above 90%.

While the accuracy of diffusion weighted sequences is moderate or good the accuracy of the SCE sequences is good or excellent. The results of the whole protocol in comparison to the clinical gold standard and the positive complimentary effect of different sequences of the protocol will be discussed in chapter 6.

4-4-6 Readers preference or subjective ranking of the study sequences (see section 3-2-14-2-3 for methodology):

The diagnostic accuracy of diffusion weighted sequences were assessed with Cohen's kappa test (section 4-4-5), however to determine the subjective value of the qualitative information of the DWI sequences in comparison to other sequences in the study protocol or the readers preference, the readers were asked to score the conspicuity and diagnostic confidence of different sequences for each case in order to produce a semi-quantitative or semi-objective data.

The conspicuity and diagnostic confidence scores of DWI sequences were compared with the scores of T1, T2 fat sat, and serial contrast enhanced sequences for each reader to determine any differences in the observations based on different quality of information, which each sequence can deliver and to establish a preference order in case of consistent differences between the sequences.

The data, which was derived from the conspicuity and diagnostic confidence scoring of the study sequences, was initially analysed with a multiple comparison test (Friedman ANOVA) to establish significant differences between the groups. The Friedman ANOVA tests demonstrated significant differences for both readers' scoring groups and thus post-hoc multiple group comparison tests were performed.

The scoring data of the 4 study sequences (T1, T2 fat sat, DWI and SCE) was subsequently divided to six paired groups (DWI versus T1, DWI versus SCE, T1 versus SCE, DWI versus T2 fat sat,…), for each type of score (x2 scoring system) and each reader (x2 readers) which means 24 pairs in total. As the data was non parametric and the distribution of the paired values' differences was asymmetric, the paired sample sign test or simply sign test with Bonferroni adjustment (see section 3-2-14-2-3) was considered to be the most suitable test to evaluate and reveal the differences between the paired groups and determine the subjective value of DWI sequences or readers preference.

4-4-6-1 Ranking based on image conspicuity:

Table 19 - 23 demonstrate the results of the Friedman ANOVA and paired sample sign tests for conspicuity scores of diffusion weighted sequences in comparison to the structural and serial contrast enhanced sequences. Tables 19 and 20 show the initial descriptive statistics.

	Mean	Std. deviation	*25th per. Median	*50th per. Median	*75thper. Median	Mean rank
DWI	4.36	1.064	4	5	5	2.66
T1	3.59	1.385	3	4	5	1.96
T2 fat sat	4.19	1.140	4	5	5	2.52
T1 fat sat serial contrast	4.55	0.860	4	5	5	2.87

Table19. Descriptive statistics of the conspicuity scores of the first reader including the mean values of the conspicuity scores for comparison.

*(25th-75th percentiles of Median)

	Mean	Std. deviation	*25th per. Median	*50th per. Median	*75th per. Median	Mean rank
DWI	4.11	1.138	3	4	5	2.44
T1	3.54	1.338	3	4	5	1.90
T2 fat sat	4.21	1.207	4	5	5	2.66
T1 fat sat serial contrast	4.62	0.671	4	5	5	3.00

Table20. Descriptive statistics of the conspicuity scores of the second reader including the mean values of the conspicuity scores for comparison.

*(25th-75th percentiles of Median)

The descriptive statistic tables above display a relative ranking or preference by the readers.

The following graph summarises the mean values of the scores.

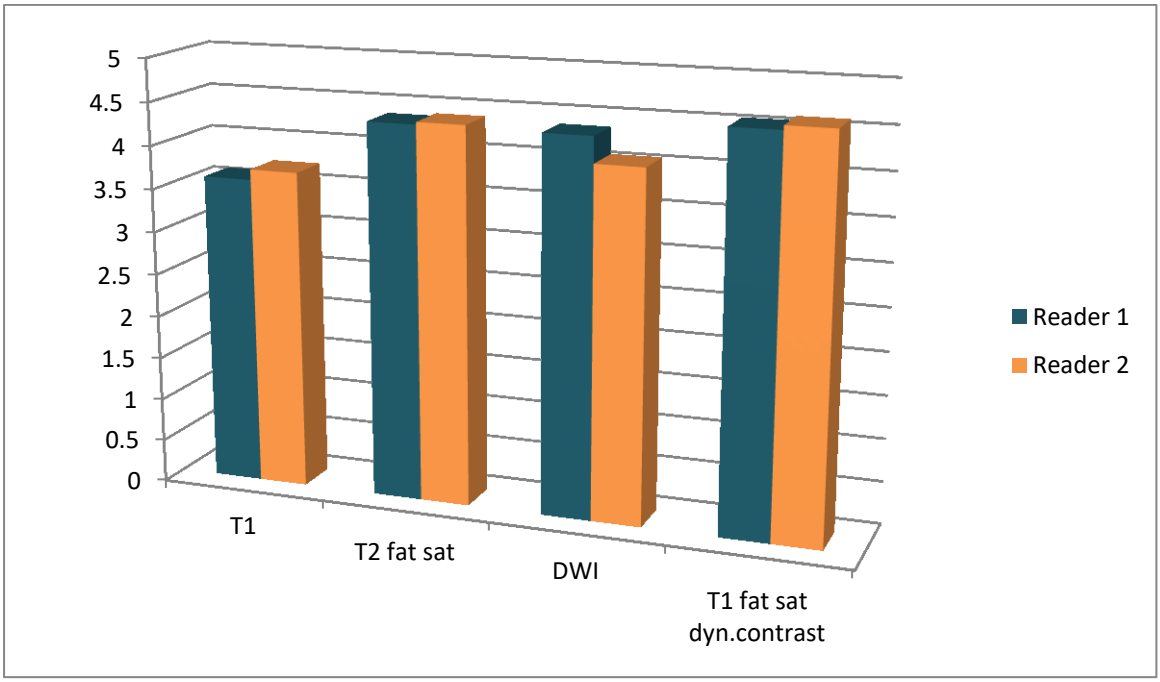

Fig. 8- The above clustered column graph compares the mean values of the conspicuity scores of the study sequences and simplifies the readers' preferences based on conspicuity scores.

The final results of the Friedman ANOVA multiple comparison tests for the conspicuity scores of both readers are summarised in table 21.

Friedman ANOVA	Friedman test (Chi-square) Value	p Value (Asymp. Sig.)
First reader	44.668	0.001
Second reader	59.298	0.001

Table21. Friedman ANOVA test results of the conspicuity scores for both readers.

The Friedman tests demonstrated significant differences for both readers regarding the conspicuity scores of the studies sequences. The Friedman test results necessitated post-hoc multiple group comparison tests to be performed in order to find out where the significant differences lie.

Tables 22 and 23 demonstrate the paired sample sign test results for the conspicuity scores. The p value has been adjusted using Bonferroni correction.

Paired groups	Sig. Sign test (2-tailed) = p value	Z score	Frequencies of the scores excluding the ties
DWI ~ T1	<0.001	-4.002	DWI>T1 by 34 cases
DWI ~ T2 fat sat	0.480	-0.707	DWI>T2 fat sat by 6 cases
DWI ~ T1 fat sat serial contrast enhanced	0.243	-1.167	T1 fat sat serial contrast> DWI by 9 cases

Table22. Paired sample Sign test results of the conspicuity scores with p values (Sig. Sign test) and frequency differences after exclusion of ties for the first reader which shows by how many cases one sequence was preferred to the other sequence after exclusion of ties (Z score is the calculated statistical Magnitude of this difference). P value is <0.0167.

Paired groups	Sig. Sign test (2-tailed) = p value	Z score	Frequencies of the scores excluding the ties
DWI ~ T1	0.008	-2.634	DWI>T1 by 25 cases
DWI ~ T2 fat sat	0.176	-1.354	T2 fat sat>DWI by 12 cases
DWI ~ T1 fat sat serial contrast enhanced	0.001	-3.283	T1 fat sat serial contrast> DWI by 26 cases

Table23. Paired sample Sign test results of the conspicuity scores with p values (Sig. Sign test) and frequency differences after exclusion of ties for the second reader which shows by how many cases one sequence was preferred to the other sequence after exclusion of ties (Z score is the calculated statistical Magnitude of this difference). P value is <0.0167.

The results of the sign tests verify the tendency outcomes of the initial descriptive part of the statistics.

The paired sample sign test results of the first reader ranked DWI sequences ahead of T2 fat sat and T1 sequences but behind T1 fat sat serial contrast enhanced sequences, however the only significant p value was between DWI and T1 and the relationships between DWI and T2 fat sat or T1 fat sat serial contrast enhanced sequences were more in form of tendencies or relative ranking rather than statistically significant differences.

The paired sample sign test results of the second reader were statistically clearer, but the ranking's order was relatively similar to the first reader, demonstrating T1 fat sat serial contrast enhanced sequence ahead of DWI sequence and DWI ahead of T1 sequence but the second reader ranked T2 fat sat sequence better than DWI sequence.

The ranking of the second reader was statistically significant for 2 tests including DWI versus T1 and SCE versus DWI with p- values < 0.0167. The difference between DWI and T2 fat sat sequences is not statistically significant and the relationship was more in form of a relative ranking similar to the first reader.

The sign test results of the conspicuity scores reveal the readers preference of the study sequences when detecting pathologies.

4-4-6-2 Ranking based on diagnostic confidence:

Table 24 - 28 demonstrate the results of the Friedman ANOVA and paired sample sign tests for diagnostic confidence scores of diffusion weighted sequences in comparison to the structural and serial contrast sequences. Tables 24 and 25 show the initial descriptive statistics.

	Mean	Std. deviation	*25th per. Median	*50th per. Median	*75th per. Median	Mean rank

DWI	4.25	1.043	4	5	5	2.52
T1	3.71	1.289	3	4	5	1.98
T2	4.38	0.877	4	5	5	2.55
T1 fat sat serial contrast	4.61	0.793	4	4	5	2.95

Table24. Descriptive statistics of the diagnostic confidence scores of the first reader including the mean values for comparison.

*(25^{th}-75^{th} percentiles of Median)

	Mean	Std. deviation	*25^{th} per. Median	*50^{th} per. Median	*75^{th} per. Median	Mean rank
DWI	3.83	1.198	3	4	5	2.37
T1	3.33	1.326	3	3	5	1.88
T2	4.15	0.947	4	4	5	2.60
T1 fat sat serial contrast	4.55	0.687	4	5	5	3.16

Table25. Descriptive statistics of the diagnostic confidence scores of the second reader including the mean values for comparison.

*(25^{th}-75^{th} percentiles of Median)

There is a clear tendency similar to conspicuity scores. The following graph illustrates the observed tendency in the means.

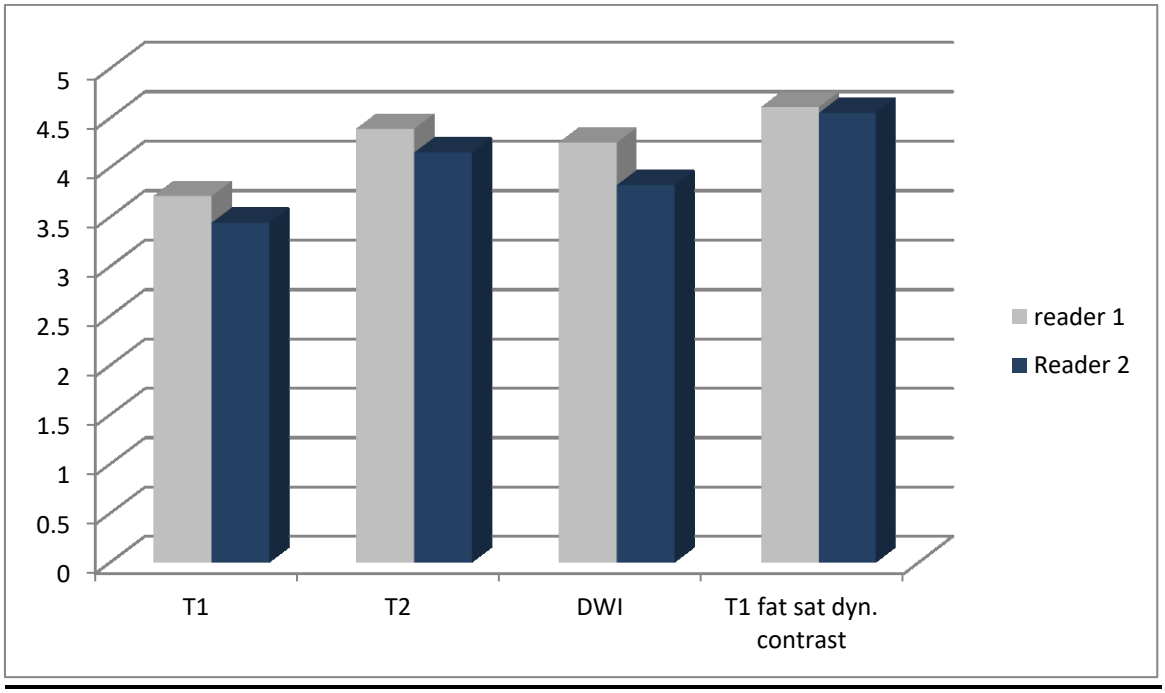

Fig. 9- The above clustered column graph compares the mean values of the diagnostic confidence scores of the study sequences and simplifies the readers' preferences based on diagnostic confidence scores.

The final results of the Friedman ANOVA multiple comparison tests for the diagnostic confidence scores of both readers are summarised in table 26.

Friedman ANOVA	Friedman test (Chi-square) Value	p Value (Asymp. Sig.)
First reader	48.169	0.001
Second reader	70.021	0.001

Table26. Friedman ANOVA test results of the diagnostic confidence scores for both readers.

The Friedman tests of the diagnostic confidence scores demonstrated significant differences for both readers and necessitated additional post-hoc multiple group comparison tests to demonstrate the significant differences.

The sign tests of the diagnostic confidence scores were more conclusive than the conspicuity scores with significant p-values (< 0.0167, after Bonferroni adjustment) for all tests, except in one test (DWI versus T2 fat sat). Tables 27 and 28 demonstrate the paired sample sign test results for the diagnostic confidence scores.

	Sig. Sign test (2-tailed) = p value	Z score	Frequencies of the scores excluding the ties
DWI ~ T1	0.001	-3.323	DWI>T1 by 28 cases
DWI ~ T2 fat sat	0.779	-0.280	T2 fat sat>DWI by 3 cases
DWI ~ T1 fat sat serial contrast enhanced	0.002	-3.031	T1 fat sat serial contrast> DWI by 22 cases

Table27. Paired sample Sign test results of the diagnostic confidence scores with p values (Sig. Sign test) and frequency differences after exclusion of ties for the first reader which shows by how many cases one sequence was preferred to the other sequence after exclusion of ties (Z score is the calculated statistical Magnitude of this difference). P value < 0.0167

	Sig. Sign test (2-tailed) = p value	Z score	Frequencies of the scores excluding the ties
DWI ~ T1	0.007	-2.700	DWI>T1 by 25 cases
DWI ~ T2 fat sat	0.160	-1.404	T2 fat sat>DWI by 13 cases
DWI ~ T1 fat sat serial contrast enhanced	0.000	-4.642	T1 fat sat serial contrast> DWI by 39 cases

Table28. Paired sample Sign test results of the diagnostic confidence score with p values (Sig. Sign test) and frequency differences after exclusion of ties for the second reader which shows by how many cases one sequence was

preferred to the other sequence after exclusion of ties (Z score is the calculated statistical Magnitude of this difference). P value < 0.0167

The results of the paired sample sign tests above follow the trend of the descriptive part of the statistics and are similar to the results of the conspicuity scores; however the margins were different, indicating how much one sequence was preferred to the other.

Both readers rated T1 fat sat serial contrast enhanced sequence ahead of DWI sequence and DWI sequence ahead of T1 sequence, whilst DWI and T2 fat sat sequences were rated similarly. The p-values were all significant, except the the p value of DWI-T2 fat sat paired sample sign test. The DWI and T2 fat sat sequences were very close, with similar results and without statistically significant differences.

The DWI sequence related ranking, based on diagnostic confidence scores, is identical to conspicuity score ranking.

The diagnostic confidence scores' sign tests not only exhibit the preferences of the readers when making a diagnosis based on a sequence, but also reveal the degree of reader's experience (level of confidence) concerning the study sequences.

4-4-7 Quantitative statistic and quantitative diagnostic thresholds (for methodology see section 3-2-14-2-4):

One hundred and three MRI scans, including diffusion weighted sequences on ninety-nine children were performed. In total, eight scans were excluded for quantitative ADC measurement, ninety-five DWI sequences were analysed for ADC measurements. 3 cases were excluded for qualitative and quantitative analyses due to incomplete or inappropriate DWI sequences and 5 cases were excluded only for the quantitative ADC analysis as the ADC maps were suboptimal for ADC value measurement, mainly due to susceptibility artefacts and inappropriate scanning plane.

4-4-7-1 Main data ADC value analysis:

900 ADC value measurements in total were performed on 95 DWI sequences in pathological and healthy reference targets. The measurements were not equally split between the cases as it was dependent on the extent of the lesion and the different compartments it involved, for example some cases had 10 or 12 (5 or 6 pairs) ADC values and some only 2 (1 pair) ADC values.

Subsequently, the data was divided into seven groups based on seven different tissue compartments (section 4-3-9-2). There were eight coded clinical diagnoses (gold standard) and four main diagnoses with sufficient number of cases.

Multiple Receiver operating characteristic (ROC) analyses were separately performed and ROC curves were created, based on different tissue compartment and different clinical diagnoses, however, some ROC analyses were not relevant as the number of pathological cases were too low. The most relevant ROC tests are demonstrated below. The ROC tests were completely separately performed and interpreted.

The statistic details of the area under the curve of the ROC tests of the measured ADC values for infectious lesions are presented in table 29.

	Area under the curve	Sig. p value	95% confidence interval lower-upper bound	Patients with infection	Patients without infection
Bone Infection	0.520	0.787	0.376 – 0.664	22	47
Muscle infection	0.679	0.219	0.398 – 0.961	13	6
Synovial infection	0.325	0.322	0.025 – 0.625	10	4
Soft tissue infection	0.550	0.661	0.326 – 0.774	15	12
Joint effusion infection	0.604	0.405	0.366 – 0.842	18	8
Fluid collection infection	0.603	0.483	0.347 – 0.858	13	6

Table29. Area under the curve statistics and the number of positive and negative cases

The best results in table 26 are from Muscular infections, however the results are between poor and fair and closer to 0.5 value (random effect) and the p-values are all more than 0.05, therefore the values are not statistically significant and the test is not able to determine a threshold for infection.

The best statistical result between all different diagnoses was from ROC analyses of the ADC values of cases with Bone marrow infarction (p-value = 0.134), which however is still not statistically significant.

The following ROC curves demonstrate the relationship of infections' curves, with the diagonal reference line, which is produced by ties and represents random effect without any statistical relevance.

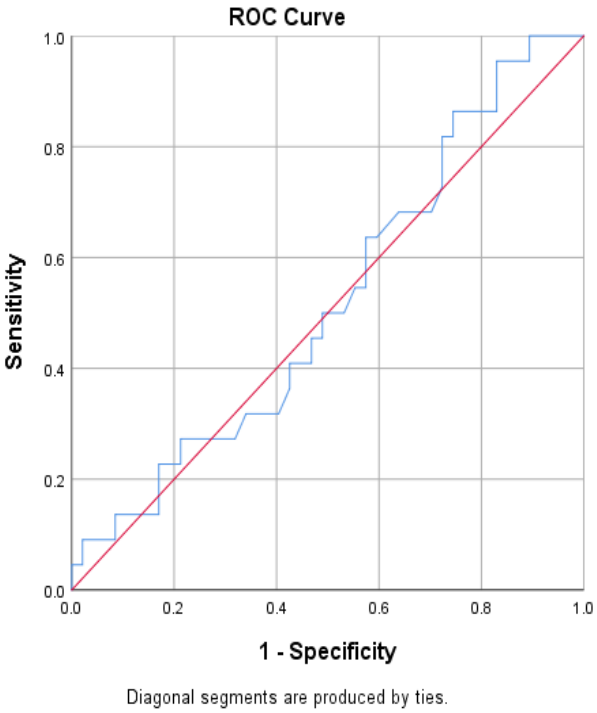

Fig. 10- Bone

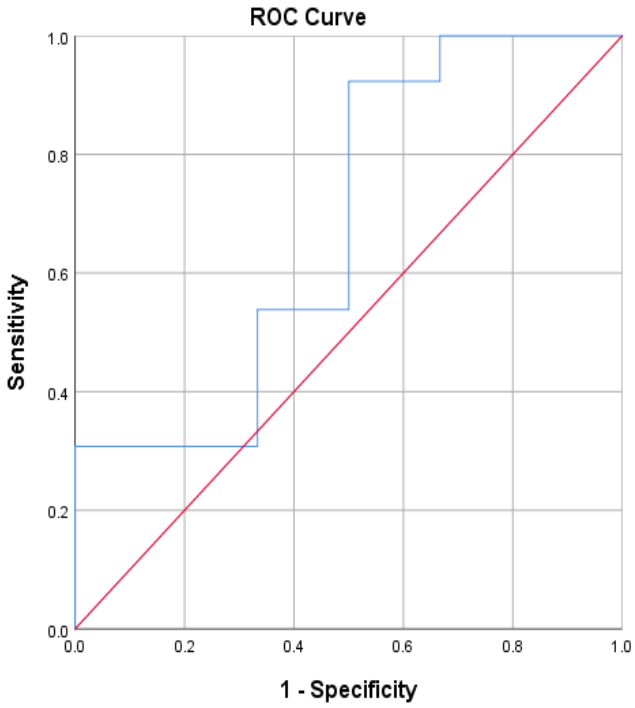

Fig. 11- Muscle

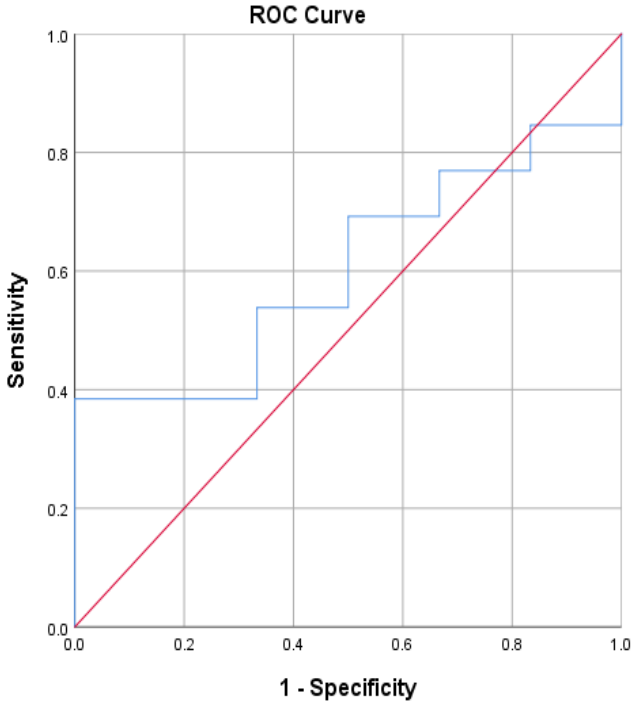

Fig. 12- Fluid collection

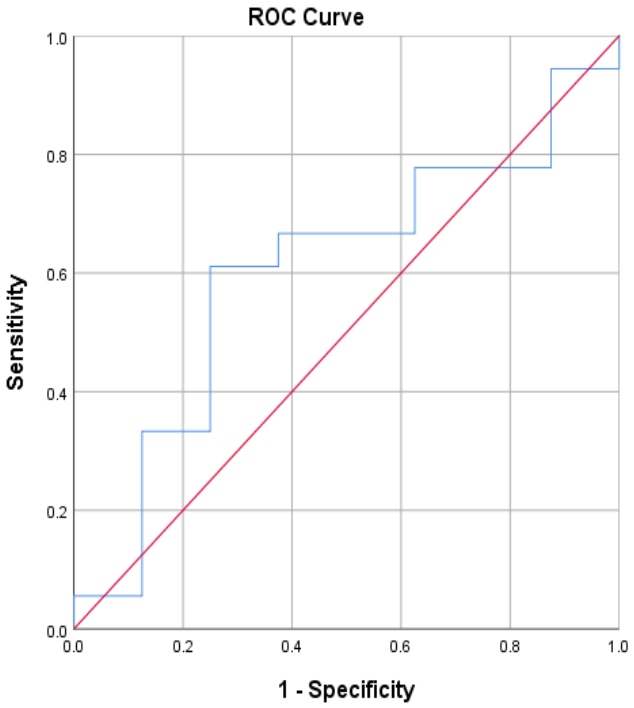

Fig. 13- Joint effusion

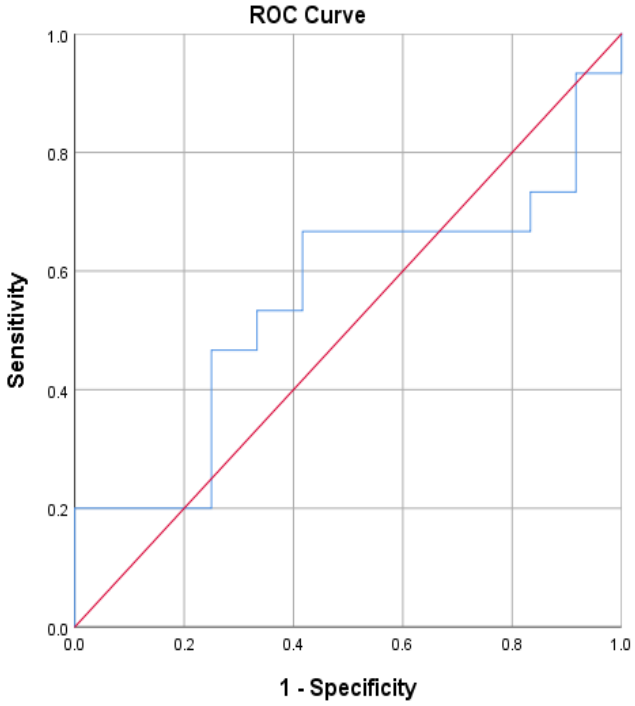

Fig. 14- Soft tissue

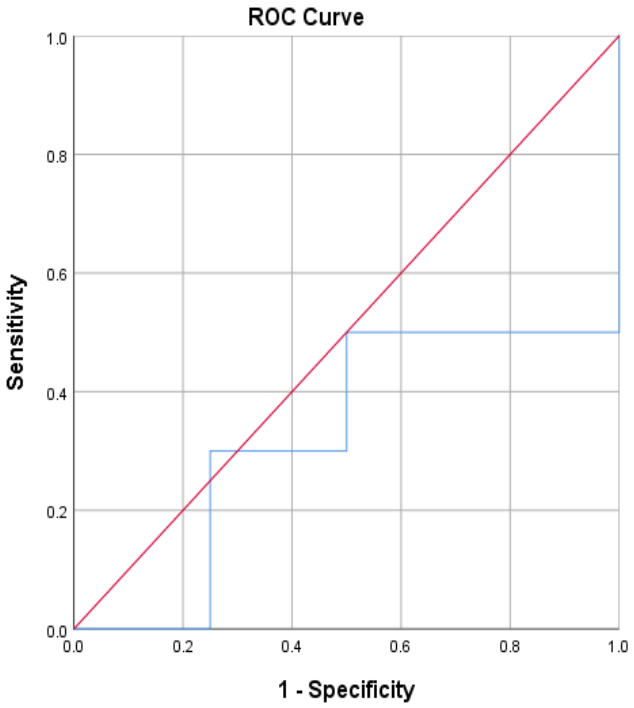

Fig. 15- Synovium

The median value of the area under the curve of the above ROC curves is 0.547 and the min and max values are 0.325 and 0.679, these results are too close to 0.5 value of the diagonal reference line, hence diagnostic differentiation of MSK infections in children based on ADC threshold values is not possible.

There were 22 patients with musculoskeletal infection involving bones. The ADC values of the affected bony regions were higher than the reference healthy regions except in 2 cases.

Figure 16 reveals the area under the curve of the ROC analysis for bone marrow infection in comparison to normal bone marrow. The area under the curve has improved in figure 16 in comparison to figure 10 based on deductions of other pathologies.

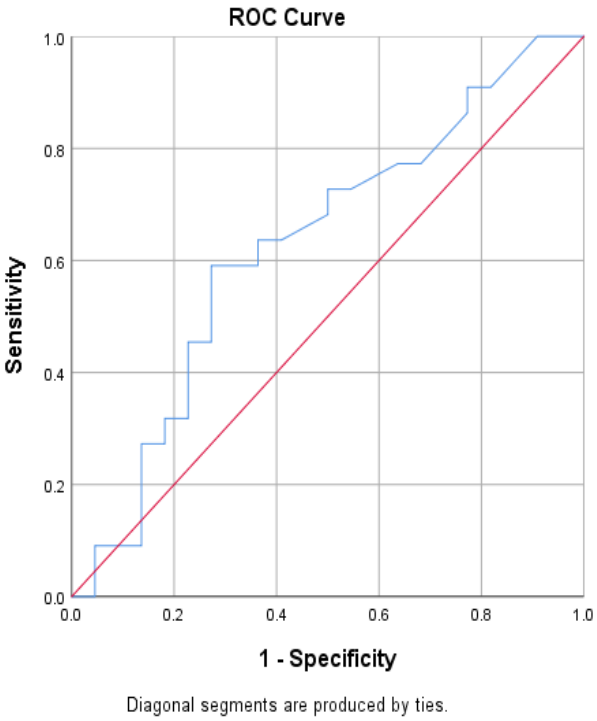

Fig. 16- Bone marrow infection and normal bone marrow (excluding the other pathologies)

There is a descriptive presentation of ADC values measured in the bones in table 30 to elicit the potential of ADC values.

	Bone infections	Non-infectious bone pathologies	Normal bones
Mean ADC values mm^2/s, (Standard deviation)	140.6 x 10^{-5} (55.6)	132.3 x 10^{-5} (50.7)	99.7 x 10^{-5} (45.7)

Table30. Mean apparent diffusion coefficient values among patients with bony infection, non-infectious pathologies and normal reference bone

The average ADC values of bone infection are slightly higher than the average ADC values of the non-infectious bony changes and the average ADC values of the reference normal bone.

The distribution of mean apparent diffusion coefficient values of bony lesions in the study group is displayed in the boxplot graph (fig. 17) below to demonstrate the relationship of the ADC values of the following three clinical groups:

1- Infection group
2- Non- infection group
3- Normal group

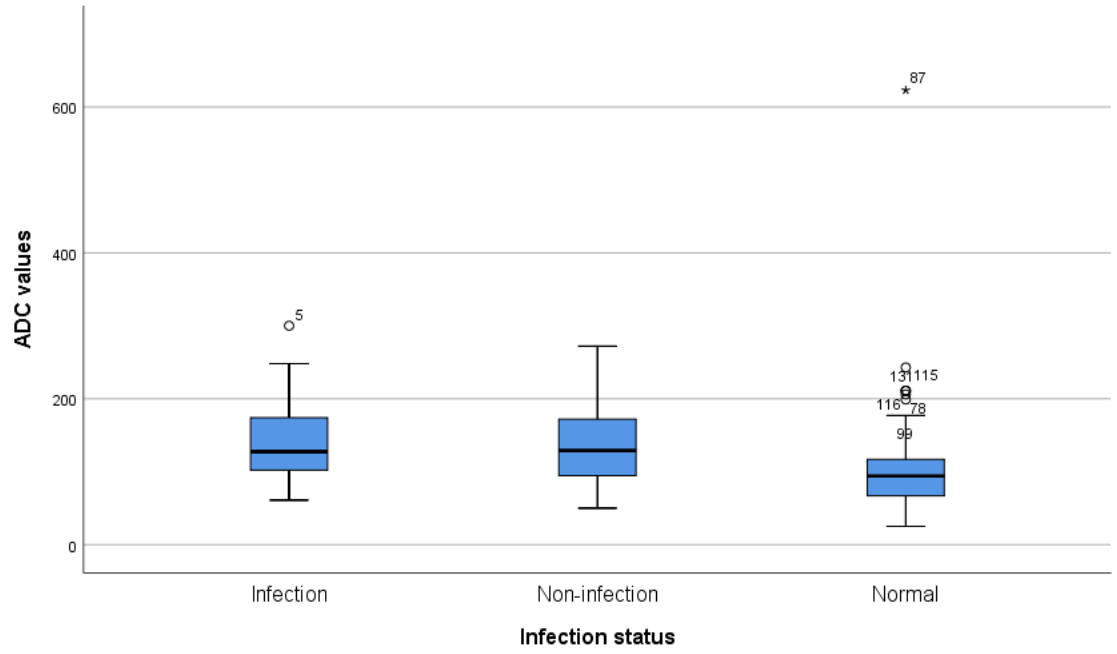

Fig. 17- ADC values of the bone lesions of the main clinical groups (infection, non-infection pathology, normal). ADC [mm^2/sec]

The ADC values of the above three groups were compared in order to determine possible significant differences. The numerical data was non-parametric, not paired and including more than 2 groups or independent variables (infection, non-infection pathology and normal) hence Kruskall-Wallis H test was chosen for the statistical comparison.

The Kruskall-Wallis H value was 22.598 and the p value (Asymp. Sig.) 0.001. Table 31 demonstrates the mean ranks of the average ADC values of the above three diagnosis groups based on Kruskall-Wallis H test.

Kruskall-Wallis test	ADC normal group	ADC non-infection	ADC infection
Mean rank	47.13	76.96	80.80

Table31. Kruskall-Wallis H test mean ranking of the ADC values for the three main diagnostic groups.

As the test result showed significant difference based on the p value, post hoc multiple group comparison tests were applied to determine where the significant difference lies. The Mann-Whitney U test was utilised, as the data was non-parametric, for multiple group comparison and Bonferroni correction was applied to adjust for type one error that can be caused by multiple group comparison testing. The Bonferroni adjustment is fulfilled when the initial p value is divided by the number of comparisons (multiple comparison tests) or with other words the number of hypotheses, which in this case means 0.05 divided by 3 or 0.0167. The following table demonstrates the Mann-Whitney U test results.

Diagnostic groups/ Test results	Mann-Whitney U	Wilcoxon W	Z score	p value
Infection-Normal	289.000	2000.000	-3.761	0.001
Non infection-Normal	733.500	2444.500	-4/057	0.001
Infection-Non infection	496.500	1624.500	-0.264	0.792

Table32. Mann-Whitney U test results (Post –hoc multiple group comparison)

The results show no statistically significant difference between the two main diagnosis groups (Infection versus Non infection). This finding correlates with the

results of the ROC analyses. The significant p values are between normal and pathologic bone groups.

The distribution of the mean ADC values of other tissue compartments (muscle, synovium, cartilage...) follow the same pattern as reflected in the ROC curves.

4-5 Discussion:

Diffusion weighted imaging is a molecular imaging tool and a novel approach in paediatric MSK radiology which can reveal the biologic tissue characteristics and structural changes of parenchymal microarchitecture at a molecular level(57,76).

The growing skeleton in children is particularly suited for diffusion imaging and offers more diffusion related signal due to a variety of specific characteristics of immature skeleton(74) which have been explained in chapter 1 section 1-7-8-1.

There is increased awareness of utility of diffusion weighted imaging in paediatric musculoskeletal diagnostic with promising results based on multiple publications (64,76–78,81,127,144).There have been a number of prospective studies, evaluating aspects of diffusion weighted imaging in particular, non-oncological musculoskeletal diseases in children with limited number of patients (76,78).

This is the first prospective and exclusively paediatric study evaluating the utility of DWI in musculoskeletal infection, in comparison to conventional and serial contrast enhanced imaging sequences.

The clinical potential of diffusion weighted imaging in paediatric populations with suspected MSK infection, is to visualise the pathology, detect multifocal lesions and characterise biological specifications of the investigated tissue (76). DWI is a valuable tool to differentiate benign MSK conditions from malignant lesions (76,84).

The excellent feasibility results of this study (90%<), confirm the outcomes of the few prospective studies performed in children(76,78). All of the patients in this study

tolerated the extra scan time of approximately 5 min for DWI sequence very well except those very young children who required a general anaesthetic. There were only a small number of cases excluded (nearly 3%) (see sections 4-4-1 and 4-4-2).

There are minor differences between different field strengths including slight varying signal to noise ratio (SNR), susceptibility artefacts and fat saturation levels, however these are usually without statistically relevant effects in ADC values(64,77,80,134). The reference ADC measurements in reference tissue in this study between different subjects did not significantly vary between different scanners and magnetic fields, in accordance with many previous studies (64,77,80,134,145,146).

The reading process in this study was independent and as such inter and intraobserver agreements were initially assessed. The results of inter and intraobserver agreement tests were good-excellent.

The measurement ROIs for ADC values in this study were hand drawn (30-105 mm2). It has been postulated that hand-drawn ROIs might be a source of potential error (80), however our intraobserver agreement (ICC) test results of study's hand-drawn ADC measurements were excellent and did not support the postulated concerns.

DWI sequences are usually water sensitive T2 based sequences with Fat saturation, which are sensitive to diffusion effects due to additional diffusion gradients, hence different aspects of tissue can be evaluated with DWI and different information can be produced including the following:

1- Subjective, qualitative information (DWI sequences and ADC maps)
2- Objective, quantitative information (ADC maps and ADC values)

Local infectious processes start with hyperaemia and go through different phases, including increased permeability, extravasation of inflammatory cells, accumulation of extracellular inflammatory cells and proteinaceous agents and destruction of extracellular matrix. It has been suggested in recent literature that different stages of an MSK infection could potentially be detected and possibly differentiated through different properties of DWI sequences(64,74,83,147,148).

DWI has demonstrated its usefulness in visualising and further characterising inflammatory and infectious bone marrow lesions based on cellularity and water content, according to recent literature(76).

Increasing extravascular fluid and inflammatory cells during an infectious process, returns increasingly higher signal intensities in DWI sequences and higher ADC values(75,76,142,149). My study results have verified the slightly higher mean ADC value, in a musculoskeletal infection (see table 30 and fig. 17), however the signal intensity in ADC maps can vary from high to low signal intensity based on a number of factors including the concentration of extravascular inflammatory cells, particles and content of the extravascular fluid (proteinaceous fluid,..).

Proteinaceous fluid as in abscesses shows restricted diffusion and low ADC values. This phenomenon in abscesses is due to high cellular and protein content of the abscess cavity, however as with tumours their imaging features change over time (83). As time progresses, the centre of an abscess begins to liquefy, which reflects in increased diffusion, T2 shine through and ADC values (83,147,148).

The readers' diagnoses based on DWI sequences demonstrated good level of agreement with the final clinical diagnoses with moderate or good kappa values (sensitivity of 76%-78.4%, specificities of 90.3%-92%) in keeping with good diagnostic accuracy for DWI sequences.

The specificity of DWI is superior to all other imaging modalities (see section 1-7-4-6 and table 3) which are used in diagnosis of acute MSK infection in children, whilst the sensitivity of DWI is superior to all other modalities but scintigraphy which has a slightly higher sensitivity at a cost of significant radiation and involves the need for cannulation and injection. The good sensitivity and excellent specificity combined with lack of radiation and cannulation are the winning points for DWI in comparison to other imaging modalities for detection and differentiation of acute MSK infection in children.

This study's results showed that the diagnostic accuracy of DWI based on only qualitative information derived from DWI sequences is superior to T1 sequences, equal to T2 sequences and slightly inferior to serial contrasted enhanced sequences

(see section 4-4-5, tables 16, 17 and 18). It has to be considered, however that the additional quantitative information derived from ADC maps (ADC values) were not presented to the readers and was not included in their decision making, as in this study the diagnostic accuracy of different sequences was calculated and compared based on the qualitative information derived from the sequences in order to separately evaluate the true value of the quantitative information of the DWI. Cannulation of children has always been challenging and injection of contrast agents has been accompanied with possible risks. The lack of cannulation and possible contrast agent related risks and the additional quantitative information derived from ADC values should be included in the evaluation of DWI merit in diagnosis of paediatric MSK infection which then most likely will improve the diagnostic value of DWI in comparison to other sequences and should be investigated in a future study.

The results of the Friedman and paired sample sign tests that compared the conspicuity scores of the study's sequences revealed that the conspicuity of DWI sequences is superior to T1 sequences and nearly equal to T2 fat saturated sequences and whilst the results of the paired sample sign test of the second reader placed T1 fat sat serial contrast enhanced sequence ahead of DWI with a p value of 0.001, the paired sample sign test of the first reader did not show a statistically significant difference between the two sequences (p value = 0.243).

The signal intensity is increased in infectious lesions of the musculoskeletal system in DWI sequences as in the fat saturated sequences, however the possibly better conspicuity of DWI sequences was postulated in some previous studies to be due to lower resolution of the background bone marrow and surrounding tissue(64,76) and to a degree due to additional diffusion properties. This phenomenon was observed in multiple cases in this study, where DWI conspicuity was advanced in comparison to T2 fat sat and serial enhanced T1 fat sat sequences, nevertheless the mean conspicuity score differences were not statistically significant.

The Friedman and paired sample sign tests of the diagnostic confidence scores in this study demonstrated a clearer picture concerning readers' preferences in comparison to conspicuity scores with more statistically significant differences. While the diagnostic confidence scores of DWI sequences were clearly better than T1

sequences (p value < 0.0167), there was no statistical significant difference between DWI and T2 fat sat sequences. The readers' ranked serial enhanced T1 fat sat sequences superior to DWI based on the diagnostic confidence scores.

The ADC values are the quantitative measures of the ADC maps derived from DWI sequences. The ADC values of this study were evaluated with descriptive statistics and ROC tests.

Typical ADC value of normal fatty bone marrow is relatively low, between 0.0002-0.0005 mm2/s(63), which is most likely due to the size and lipophilic characteristics of the fat cells. Therefore pathological marrow has higher ADC values and increased diffusivity; due to replacement of large fat cells with smaller cells, destructions of the cells and tissue structures(63,74).

It has been postulated in previous studies, that ADC values during an infectious process, usually increase due to increased diffusivity in contrast to malignant lesions, which typically exhibit reduced diffusivity with reduced ADC values (76,142,143).

These findings also apply to the paediatric skeleton, however diffusivity of the immature bone marrow is more complex and is highly dependent on water, cellular, cartilage and fat volume of the bone (76). The variations of bone marrow diffusivity in children are based on patient's age, gender, the anatomical location and pre-existing primary or secondary bone marrow conditions (76,142). The relationship between these factors is not linear and exhibits vast variations in different body regions (76,142).

Developing a gender and age-based dataset for normal ADC values for paediatric skeleton, would be a significant milestone in standardisation of ADC values of reference paediatric bones.

The quantitative results of the ADC values in this study, reflect the complexity of paediatric bone marrow and demonstrate the relatively prominent variation of the mean ADC values in normal bone (76). The ADC values in the majority of MSK infections in this study were increased in comparison to the normal reference values and other bone marrow pathologies in keeping with the literature(76,142,143).The

mean ADC value was higher in the infectious lesions in comparison to non-infectious lesions and normal reference bone marrow, ADC normal bone marrow<ADC non-infection pathology<ADC infection (table 30 and figure 17). However the differences were not statistically significant between the average ADC values of the infection and non-infection pathologies as it was demonstrated in the ROC curve analyses and a threshold with satisfactory sensitivity and specificity could not be detected.

The ADC values of the focal malignant cases were not analysed as the number of bone (two cases) and soft tissue (one case) malignancies were below the detection level of ROC tests.

Acceptable ADC value thresholds could not be obtained from the study results for MSK infection, infarction or benign lesions, this was most likely due to a number of factors including, large variety of pathologies, low number of cases, inconstant and higher normal ADC values (increased perfusion, red marrow and water content), which are closer to moderately increased ADC values of benign pathologies and finally the changing nature of the pathology as the ADC values alter throughout an infectious process.

The ADC values vary during an infectious process, and increase initially in the acute phase followed by a possible decrease or plateau in the subacute phase and a further increase in the chronic phase, before the ADC values fall along the healing process(64,66,74,76,78).

4-6 Limitations:

There are several limitations in this study, which are as follows:

1- This is a single site design
2- The patient population is relatively small
3- The large age range of the participants and the consecutive large variation of bone marrow conversion

4- The relative inhomogeneity of the participants population regarding pre-existing chronic bone marrow abnormalities and altered ADC values of the normal bone marrow, which can potentially cause misinterpretations
5- The ADC map calculation was based on only 2 B values (B 0 and B 500) which may have influenced the accuracy of ADC values or neglected the perfusion or diffusion components of the signal
6- The relatively large number of pathologies
7- The small number of cases for some of the pathologies
8- The potential risk of selectivity of hand drawn ROIs.

Brownian motion or diffusion is a three dimensional process, however the ADC values in this study were measured in 2D (mm^2/s) as in the majority of recent publications. The 2 dimensional measurement is broadly accepted; however it is a limitation, which should be considered if the mean values are identical. 3D measurement softwares are now broadly available and should be considered for future studies.

All of the patients in this study were admitted with acute pain and suspected diagnosis of acute MSK infection; however the infection processes were possibly in different phases based on potential delays before admission. This could have influenced the ADC values based on cellularity, water and fat content in the region of interest.

4-7 Conclusion:

Diffusion weighted imaging is a novel bio-imaging tool with the potential to provide qualitative and quantitative information concerning musculoskeletal infections.

This study demonstrated that Diffusion weighted imaging is feasible in paediatric population and can detect and interpret infection related musculoskeletal lesions with good accuracy (76%-78.4% sensitivity, 90.3%-92% specificity). Diffusion weighted sequences based on EPI sequences are relatively fast, insensitive to motion

artefacts and can be used for whole body imaging; hence they are well suited for paediatric patients.

The ADC values are useful biomarkers that can further characterise tissue properties and potentially reveal different stages of an infectious process. This study however could not provide thresholds for ADC values, but revealed promising tendencies.

This study was the first prospective study to evaluate the utility of DWI in paediatric musculoskeletal infection with promising results. The study showed that the higher b-value images were useful for detection and interpretation of musculoskeletal infection, but the ADC values did not deliver what was proposed in the first hypothesis. The study's findings, limitations and inconclusive results, warrant further larger multicentre investigations, perhaps with better matched cohorts (regarding age, gender) and control groups, and normalised or otherwise modified ADC values (ratios) such as ADC pathology/ADC normal bone.

Chapter 5: Serial contrast enhanced imaging

5-1 Introduction:

Acute musculoskeletal infection in children continues to present a substantial clinical challenge with high morbidity and mortality(128).

Children with acute musculoskeletal infection are often significantly unwell, while the clinical symptoms and laboratory results are inconclusive.

Imaging has always played an important part in the diagnostic pathway for paediatric acute musculoskeletal pain(27). Many imaging modalities have been utilised in combination over the years for musculoskeletal infection to improve the diagnostic yield of imaging.

MRI has the advantage of excellent tissue characterization and differentiation with detailed resolution (26), which enables it to detect and distinguish different bone marrow compositions, bone marrow oedema and infiltration. Magnetic resonance imaging has therefore become the most advanced imaging tool for musculoskeletal diseases.

MRI can provide qualitative, semi-quantitative and quantitative information at a molecular level and reveal intercellular biodynamic changes within the examined tissue. Semi-quantitative and Quantitative magnetic resonance imaging techniques have been gaining more ground in recent years and continue to develop rapidly, with every new generation of scanners, sequences and software.

5-1-1 Permeability contrast enhanced imaging in paediatric musculoskeletal system:

Permeability contrast enhanced imaging including SCE and DCE has been sufficiently discussed in chapter 1, section 1-7-9 and it has been previously employed in paediatric oncology and rheumatology(104,113). There is however less experience or research in the utilisation of serial contrast enhanced MRI in paediatric musculoskeletal infection(10,20,26,51). The significant difference between paediatric and adult musculoskeletal vasculature is the main contributing factor as to why there are fewer publications about permeability contrast enhanced magnetic resonance imaging in children; however there are other limiting factors including the difficulty of performing contrast enhanced studies in children and carrying out cannulation in children.

5-1-2 Altered permeability in musculoskeletal infection in children:

There are fluent transformations in the musculoskeletal system during an infection at microscopic level, which profoundly alter the permeability of the affected tissue. The primary immune reactions trigger increased parenchymal perfusion and blood flow (hyperaemia), followed by increased trans-endothelial diffusion and permeability or leak (secondary reactions). The primary reactions followed by secondary reactions increase extracellular fluid and cells, replacement and destruction of fat cells and finally bony trabecular structure. These rapid changes modify not only the qualitative appearances of the hyper perfused tissue but also the quantitative parameters of the hyper permeable tissue in contrast enhanced examinations. The qualitative, semi-quantitative and quantitative parameters can aid detection and possibly differentiate musculoskeletal infection in children from other pathologies.

The data of the pilot study (section 3-1-3 chapter 3) are encouraging with statistically relevant results based on increased perfusion and permeability in the affected musculoskeletal system of the pilot cohort in qualitative and semi-quantitative assessments.

5-1-3 Challenges of pharmacokinetic modelling and quantitative assessment of contrast enhanced MRI:

Contrast enhanced MRI can provide qualitative, semi-quantitative and quantitative information, The qualitative aspects of the dynamic contrast enhanced MRI is slightly more elaborate but technically not significantly different from static contrast enhanced imaging, whilst the semi-quantitative and quantitative aspects of dynamic contrast enhanced MRI require complex mathematical MRI modelling and pharmacokinetic fitting. The complexity of the technical and operational requirements has been explained in section 1-7-9 (1-7-9-1 to 1-7-9-7). The accurate calculation or estimation of multiple essential parameters such as T_1 native, Arterial input function (AIF), flip angle, temporal resolution (temporal/spatial resolution balance) and the length of sequence or the length of sampling are as crucial as the consistency of Flip angle or magnetic field and the optimal choice of magnet, coils (receiver/transmitter), sequence, artefact reducing software/technique, scan planning, contrast agent and injection method, for the MRI and pharmacokinetic modelling. Dynamic contrast enhanced imaging (DCE) in acute paediatric clinical setting is challenging and time consuming, hence I decided to employ serial contrast enhanced imaging instead of dynamic contrast enhanced imaging in order to reduce the scanning time and improve the spatial resolution whilst scanning the entire field of view (the entire width of the patient), and not just a particular slice. The trade off produced by this strategy was the fact that although quantitative values could be calculated the values are not accurate, mainly due to inadequate sampling of the entire process (the number of pre and post contrast frames) which affects the pharmacokinetic fitting and fat saturation of SCE sequences. However the semi-quantitative parameters were unaffected as they don't require a pharmacokinetic modelling, thus the decision was made to utilise only the qualitative and semi-quantitative information derived from the SCE sequences and abandon the quantitative values.

5-2 Material and methods:

Contrast-enhanced imaging has been considered and repeatedly controversially discussed, as an option in magnetic resonance imaging of musculoskeletal infection in children. There have been publications in the past which have analysed the advantages and disadvantages of contrast-enhanced sequences to improve the diagnostic yield of MRI in paediatric infections (10,20,26,51).

This is the first prospective study to evaluate systemically the diagnostic value of serial contrast enhanced imaging with multiphase subtraction in paediatric MSK infection.

5-2-1 Objective:

The aim of this chapter of the study is to evaluate the feasibility and diagnostic accuracy of serial contrast enhanced imaging in the diagnosis of acute musculoskeletal infection in children and compare with DWI and structural sequences. Furthermore I will compare the subjective conspicuity and diagnostic confidence of the SCE sequences based on readers scoring with the other sequences of the study's protocol and finally I will evaluate the diagnostic performance of calculated semi-quantitative values (AUC and TME) in my study cohort and see if there are statistically significant thresholds for these values in the diagnosis of musculoskeletal infection in children.

5-2-2 Ethical approval:

Institutional, local and national ethic approval was sought (please see Appendix1).

5-2-3 Study structure:

The study structure has been described in chapter 3, section 3-2-1.

5-2-4 Study cohort and demographic:

99 patients were prospectively recruited over a period of two and half years. There were 44 girls and 55 boys included in this study. The age of the subjects ranged between 1 and 216 months (18 years) with a mean age of 101 months (8 years). Table 33 summarises the demographics of the children, please also see table 12 in

chapter 4, section 4-3-4 for more details about incidence of affected anatomical locations.

	Number of participants	Mean age in months	Most common anatomical location	Number of scans
Boys	55	95	40 (pelvis and lower limbs)	56
Girls	44	107	36 (pelvis and lower limbs)	47
Total	99	101	76	103

Table33. Demographics of study participants

5-2-5 Inclusion and exclusion criteria:

Inclusion and exclusion criteria have been presented in chapter 3 section 3-2-3

5-2-6 Information, consent and assent forms:

Information, consent and assent forms are described in chapter 3 section 3-2-5 and presented in appendix 2 and 3.

5-2-7 Recruitment:

The recruitment pathway has been described in chapter 3, section 3-2-4.

5-2-8 Magnetic resonance imaging, scanners and coils:

The scans were performed on three GE scanners, two of which were 1.5 T and one was 3 T scanners (see chapter 3, section 3-2-6-4). Varying field strength was not expected to create relevant alterations in semi-quantitative permeability analysis, as the employed analytic software (Olea sphere 2.2 software, Olea medical, Canon)

and the semi-quantitative analysis are independent from the scanner or even the modality(58,109). The software automatically did not analyse incompatible or deviating data.

The different coils have been described in chapter 3, section 3-2-6-4 and the patient preparation and immobilisation were discussed in chapter 3, section 3-2-6-3.

5-2-9 MRI protocol and SCE sequences:

The chosen contrast-enhanced sequence for the study protocol was Lava (Liver Acquisition with Volume Acquisition, GE health care), which is based on three-dimensional spoiled gradient echo sequence technique. The images are contrast enhanced and the fat suppression is uniform created by optimisation of the inversion pulse and an improved fat suppression technique called segmented special (150). The Lava sequences are very fast based on array spatial sensitivity encoding technique (ASSET) with partial data filling and shorter TR/TE, which enables the use of short breath holds or flat breathing for optimised serial contrast-enhanced imaging with multiple phases (150), even though the sequence was developed for liver imaging, it has proven (pilot data) to be excellent for musculoskeletal imaging.

The sequences were acquired in the coronal plane (eve. sagittal or axial) in order to optimise the slice thickness (slice thickness=1-4 mm), temporal resolution and scanning time, while maintaining best anatomical plane and large overview of contrast perfusion. The coronal plane is also helpful to combat the arterial inflow artefacts, as they are usually along the coronal axis, and the respiratory artefacts are in plane hence reduced in comparison to other planes(58). The subtraction maps were calculated as part of the post processing and displayed in coronal plane. All of the series including the raw data, the reconstructed and subtracted images were analysed. The details of LAVA sequences are presented in table 9 (chapter 3, section 3-2-6-5-3). The complete study protocol including the structural and diffusion sequences have been demonstrated in chapter 3, section 3-2-6-5-3.

5-2-10 Contrast agent:

The contrast agent employed in the study was ProHance (size: 559 Daltons) and the dose was 0.2 mg per kg.

5-2-11 Analytic software for detailed contrast agent distribution analysis:

The process of image analysis, creation of signal intensity and contrast intensity curves including MRI and pharmacokinetic modelling has already been discussed in chapter 1 (section 1-7-9-1 to 1-7-9-6).

The semi-quantitative analysis in this study was mostly performed automatically, utilising Olea sphere software (Olea sphere 2.2 software, Olea medical, Canon). The analytic model used in this study by the software is the extended Toft model, which is an extended version of the standard two compartmental model comprising plasma and extravascular extracellular space, known as Tofts model (107).

Olea MRI permeability plug-ins compute the main permeability maps from raw perfusion series (151). These plug-ins support irregular time sampling and different mathematical models with computation on every time point (151). MRI Permeability plug-ins provide optimized qualitative maps and semi-quantitative values (TME, AUC, Wash in, Wash out, Peak)(151). The quantitative maps and quantitative values (V_e, V_P, K_{ep}, K^{trans}) have been disregarded as the sampling of the pre and post contrast enhancement process was too short for accurate and meaningful quantitative results (please see section 1-7-9-6 and 5-1-3). Automatic arterial input function, venous output function, automatic background segmentation and instantaneous motion correction algorithm were embedded in the model used in this study (151).

5-2-12 Serial contrast enhanced image acquisition :

Image acquisition of the SCE sequences in this study was three dimensional (3D T1 weighted spoiled gradient-recalled echo sequences) in accordance with the published literature (92). 3D sequences are preferred as they offer more advanced FA homogeneity, which is important for MRI modelling, the estimation of arterial input function (AIF), balancing between contrast agent sensitivity and dynamic range (58) and higher SNR, however there is a trade off as the temporal resolution may be

lower for 3D sequences for the same amount of spatial coverage (92). 3D acquisition is also preferred for post processing and reconstruction. The utilised sequences in this study are 3D Lava sequences (GE health care) which have been described in section 5-2-9.

The ideal geometric plane for serial contrast enhanced sequences for the musculoskeletal system is the coronal or a modified coronal plane, which enables the main arteries to be sampled along their lengths and remove wash in artefacts. This is important for AIF calculation. The second advantage of the coronal plane is that the respiratory artefact is in plane and hence easier to eliminate (58).

The SCE (Lava) sequences in this study have been obtained predominantly in the coronal plane but occasionally sagittal or axial planes were added to the routine coronal plane to optimise the visibility of lesions.

Respiratory motion is less relevant in MRI of the appendicular skeleton, but it causes serious artefacts in axial skeleton, and thus needs to be addressed, in consideration of the age range (0-18) and the level of compliance (58). The following techniques have been employed in this study to improve the respiratory related artefacts: free breathing technique and minimising diaphragm movement by having one or both hands above the head, breath hold technique for short sequences, free breathing with respiratory monitoring and guided free breathing based on the level of compliance (58).

The 3D Lava sequences in this study have relatively thin slices (1-4 mm), high spatial resolution and SNR, and the number of dynamic frames is 4.

5-2-13 Semiquantitative image analysis:

The semi-quantitative tissue enhancement properties were analysed using Care stream Pacs workstation and Olea sphere (OLM 2.2, Olea medical) software.

The software automatically produced the signal intensity time curves and calculated semi-quantitative values. The mathematical fitting of the pharmacokinetic model values to the measured data was also processed automatically by the software and the quantitative parameters (K^{trans}, K_{ep}, V_e, V_p,..) were calculated, however the

quantitative measures were excluded from the study data as explained above (see 5-1-3 and 5-2-11).

The Image analysis was on a pixel by pixel basis. The semi-quantitative enhancement values of the lesions were obtained by drawing a region of interest in the main area of concern.

The manual ROI based enhancement measurements were conducted each time in one tissue compartment. The measurements were performed separately in different compartments in the case of multi-compartmental lesions. Multiple ROI measurements were performed in cases of multiple pathologies.

One set of semi-quantitative enhancement values including mean TME and AUC were documented for each lesion. The sizes of the ROIs were between 30 and 330 mm2.

Each permeability measurement was followed by a reference measurement in a similar location in healthy tissue. The measurements were conducted by an experienced paediatric radiologist with more than 10 years' experience in paediatric musculoskeletal imaging.

All measurements (in pathological and healthy reference tissues) in ten random cases were repeated one and half months later, in order to assess the intraobserver agreement or consistency of the measurement's process.

5-2-14 Qualitative image analysis:

The qualitative image analyses were conducted independently by two experienced musculoskeletal radiologists, using the study's multi parametric evaluation form.

5-2-14-1 Readers:

The specification of the readers has been explained in chapter 3, section 3-2-9.

5-2-14-2 Evaluation form:

The evaluation form has been described in chapter 3, section 3-2-10 and is attached to appendix 4.

5-2-14-3 Reading process and Gold standard:

The reading process and gold standard have been extensively explained in chapter 3, section 3-2-11and 3-2-8.

5-2-15 Data preparation:

The data preparation has been described in chapter 3, section 3-2-13.

5-2-16 Data analysis:

SPSS statistics program version 25 (IBM Company Chicago Illinois) was used in this study. The utilised statistical tests in this study were recommended by the biomedical statistics team of the Imperial College London. A p-value of less than 0.05 was considered to be statistically significant.

5-2-16-1 Inter and intraobserver agreement tests:

This section has been discussed in chapter 3, section 3-2-14-1.

5-2-16-2 Main data analysis:

The main data analysis including the chosen statistical tests has been extensively explored in chapter 3, section 3-2-14-2.

5-2-16-3 Statistical analysis of the semiquantitative permeability values

The numerical data produced by hand drawn ROI measurements including Area under the curve (AUC) and Time to maximum enhancement (TME) were analysed separately.

Initially two sets of permeability values of the same ten random scans (cases) were measured twice in pathologic and healthy reference tissues with an interval of one and a half months and the data was analysed using the two ways mixed interclass correlation coefficient statistic test to prove the intraobserver agreement of the hand drawn ROI measurement.

The contrast enhancement values of the main study's data were divided into four main tissue compartments including bone, cartilage, muscle & soft tissue and synovial membrane.

Receiver operating curve or ROC statistic tests were utilised to separately analyse the measured semiquantitative enhancement values of the four different musculoskeletal compartments with respect to the main four diagnoses (infection, infarction, benign and malignant processes) of the study. The ROC analyses were performed to reveal the correlation between the measured enhancement values and the clinical diagnosis of MSK infection and to filter a possible relevant diagnostic threshold based on the highest sensitivity and specificity to improve the diagnostic process (see also section 3-2-14-2-4).

5-3 Results:

5-3-1 Cohort:

Ninety nine children with acute musculoskeletal pain and suspected clinical diagnosis of musculoskeletal infection were prospectively recruited for this study.

One hundred and three MRI scans were performed, using the same novel MRI protocol, including permeability (SCE) and diffusion weighted sequences. Below is a consort table with the breakdown of the patients and scans.

Cohort	Number of cases
Approached candidates who have fulfilled the incl./excl. categories	99
Recruited patients	99
Scans performed(on 99 patients, including on multiple admissions)	103
Patients excluded due to incomplete scans (Hardware malfunction	4 (HM=2,

= HM or personal error of the operator = PE)	PE=2)
Semiquantitative permeability values (AUC & TME) excluded due to incomplete SCE sequences (see the previous point above) or incompatible pre & post contrast phases of the SCE sequences	6 (incomplete=4, incompatible=2)

Table34. Consort table with the number of excluded patients and scans for SCE sequences of the study.

5-3-2 Feasibility of serial contrast enhanced imaging:

All of the patients except those who had their scans under general anaesthetic tolerated the scanning protocol including the average 4-6 min for SCE sequence. Four cases had to be excluded for qualitative and semiquantitative analysis due to incomplete scans and in all four cases personal error or equipment malfunction was the reason for incomplete data acquisition and not the patient's cooperation. Hence the enrolment rate of the study was above the pre-set 90% and the feasibility was excellent. For more information please see section 3-2-14-2-1 in chapter 3.

Semiquantitative values (AUC & TME) of six cases were excluded from the semiquantitative assessment due to incomplete multiphase SCE sequences (4 cases) or incompatible scan parameters of the pre and post contrast serial sequences (2 cases). Personal error of the operator was the main reason for these exclusions from semiquantitative assessment.

5-3-3 Inter and intraobserver agreement tests:

The readers initially reviewed ten random cases independently from the pilot study with the same MRI protocol and a nearly identical evaluation form. The readers repeated the independent review of the same random ten cases one and a half months later.

The produced semi quantitative data from the scoring part of the evaluation form was analysed with a two- way mixed ICC test and the categorical data was analysed with Cohen's kappa test (Please see chapter 3, section 3-2-14-1).

Table 35 illustrates Interclass correlation coefficient results of inter and intraobserver agreement tests of the semi quantitative data (conspicuity scores).

There was an excellent correlation (according to Koo & Li) of the semi quantitative data (conspicuity scores) concerning the SCE sequences between the readers (Interobserver agreement) with a p-value of 0.001.

The Intraobserver agreement of semi quantitative data concerning the conspicuity scores of the SCE sequences, was moderate for the first reader (p-value=0.011), and excellent for the second reader (p value< 0.001).

	Interclass correlation average measures	%95 confidence interval lower - upper bound	Significance = p value
Intraobserver agreement test of reader 1	0.698	-0.070 – 0.860 -0.151 – 0.925	0.011
Intraobserver agreement test of reader 2	0.899	0.399 – 0.952 0.570 – 0.975	<0.001
Interobserver agreement test (between the readers)	0.899	0.443 – 0.950 0.614 – 0.975	0.001

Table35. Interclass correlation coefficient test for inter and intraobserver reliability for SCE sequences, p value is significant < 0.05.

The categorical data extracted from the evaluation forms of the ten random cases from the pilot study including the readers' diagnoses was analysed with Cohen's kappa test. The kappa measure of agreement between the readers was 0.756 and the p-value was 0.001 (sensitivity= %87.5 and specificity = %91), in keeping with good agreement.

The kappa values of the categorical data from the first and second reads of each reader (intra observer) were similar to the interobserver kappa value (good agreement) and the p-value for the first reader was 0.001 and the second reader <0.001.

The inter and intraobserver agreements are good-excellent, considering the categorical and numerical data from the evaluation form. The process of inter and intraobserver agreement tests is explained in details in chapter 3, section 3-2-14-1.

5-3-4 Intraobserver agreement for hand drawn ROI measurements of semiquantitative contrast enhancement values:

The hand drawn ROI measurement of the semiquantitative contrast enhancement values including AUC and TME was repeated in ten random cases one and a half months after the initial analysis. The measurement was repeated both in the main lesion and in the healthy reference tissue. The collected data was then analysed to assess the intraobserver agreement or consistency of the hand drawn ROI measurement. Two-way mixed ICC test was utilised and absolute agreement for semiquantitative parameters was calculated.

The following Table present the statistical results of the intraobserver agreement test for hand drawn ROI measurement of the area under the curve (AUC).

	Interclass correlation	95% Confidence interval lower-upper bound	Mean 1st – 2nd read	Std. deviation	p-Value
Consistency of pathological single measure[a]	0.987	0.917 - 0.998	132102 , 144957	131494 , 138533	<0.001
Consistency of pathological average measures[b]	0.993	0.957 - 0.999	132102 , 144957	131494 , 138533	<0.001
Consistency of reference	0.787	0.190 – 0.960	39604 , 34608	35706 , 28258	0.013

single measures[a]					
Consistency of reference average measures[b]	0.881	0.320 – 0.979	39604 , 34608	35706 , 28258	0.013

Table36. Interclass correlation coefficient test for Intraobserver agreement (consistency) of manual ROI measurement of AUC (semi-quantitative value), p value is significant < 0.05.
a. The estimator is the same, whether the interaction effect is present or not.
b. This estimate is computed assuming the interaction effect is absent, because it is not estimable otherwise.

The ICC test results are good or excellent in keeping with good intraobserver agreement, however the repetitive accurate manual measurements is a time consuming and tedious task, hence the ROI based measurements of the semiquantitative enhancement alteration values of the SCE sequences would benefit from automated and structured measurement to reduce time and effort required for measurements whilst reducing the risk of inaccuracy and inconsistency.

5-3-5 Diagnostic accuracy of the SCE sequences:

The categorical data concerning readers' diagnoses based on SCE sequences were compared with the clinical gold standard using a categorical agreement test (Cohen's kappa test) to determine the diagnostic accuracy of SCE sequences.

Cohen's kappa test was performed to compare the SCE diagnoses of the readers with the final clinical diagnoses. Cohen's kappa tests results are presented as demonstrated in SPSS statistic program with kappa value, significance level (p-value), sensitivity, specificity and 95% confidence interval lower-upper bound in the following tables. Table 37 includes the complete eight categories of diagnoses (see section 3-2-14-2-2, chapter 3) and table 38 includes only two diagnostic categories (infection versus not infection).

	Measure of agreement Kappa value	Sensitivity	Specificity	Sig. = p value
SCE Reader 1~ Clinical diag.	0.723	78.4%	95.1%	<0.001
SCE Reader 2~ Clinical diag.	0.816	91.9%	96.8%	<0.001

Table37. Level of agreement between SCE diagnoses and clinical diagnoses (8 diagnostic categories), the kappa value is the rate of agreement between SCE diagnoses and the clinical gold standard. The sensitivity and specificity relate to SCE as the diagnostic tool for MSK infection in comparison to the clinical gold standard, p value is significant < 0.05. The 95% confidence interval lower-upper bound was 0.000-0.029 for both readers.

	Measure of agreement Kappa value	Sensitivity	Specificity	Sig. = p value
SCE Reader 1~ Clinical diag.	0.755	78.4%	95.1%	<0.001
SCE Reader 2~ Clinical diag.	0.892	91.9%	96.8%	<0.001

Table38. Level of agreement between SCE diagnoses and clinical diagnoses (2 diagnostic categories), the kappa value is the rate of agreement between SCE diagnoses and the clinical gold standard. The sensitivity and specificity relate to SCE as the diagnostic tool for MSK infection in comparison to the clinical gold standard p value is significant < 0.05. The 95% confidence interval lower-upper bound was 0.000-0.029 for both readers.

The results of the Cohen's kappa tests for SCE sequences are very promising (good – excellent) and reflect the high diagnostic accuracy of the readers based on SCE sequences with excellent sensitivity and specificity.

The following tables demonstrate the level of agreement between the readers' diagnoses based on single sequences and the clinical gold standard except SCE sequences which are already presented above.

	Kappa value	Sensitivity	Specificity	p value
T1 diagnoses ~ clinical diagnosis	0.631	62.2%	96.8%	<0.001
T2 fat sat diagnoses ~ clinical diagnosis	0.732	75.7%	95.2%	<0.001
DWI diagnoses ~ clinical diagnosis	0.671	76%	90.3%	<0.001

Table39. Accuracy test of single sequences' diagnoses for the first reader (2 diagnoses). 95% confidence interval was 0.000-0.029 for all three sequences.

	Kappa value	Sensitivity	Specificity	p value
T1 diagnoses ~ clinical diagnosis	0.441	40.5%	98%	<0.001
T2 fat sat diagnoses ~ clinical diagnosis	0.760	81.1%	93.7%	<0.001
DWI diagnoses ~ clinical diagnosis	0.715	78.4%	92%	<0.001

Table40. Accuracy test for single sequences' diagnoses for the second reader (2 diagnoses). The 95% confidence interval was 0.000-0.029.

The highest kappa value of the single sequences was from SCE sequences, in keeping with good – excellent diagnostic accuracy and the lowest was from T1 sequences, in keeping with poor – moderate diagnostic accuracy (see section 3-2-14-2-2 for classification). The kappa values of DWI and T2 sequences were intermediate in keeping with moderate or good accuracy. Equally the highest

sensitivity was from SCE sequences and the lowest from T1 sequences whilst the sensitivity values of DWI and T2 fat sat sequences were intermediate. The specificity of all sequences was excellent and above 90%.

The serial contrasted-enhanced sequences have the highest level of accuracy, when compared with the gold standard between the study protocol's sequences.

5-3-6 Diagnostic value of the SCE sequences and their ranking:

The conspicuity and the diagnostic confidence scores (semiquantitative data) of the study's sequences were compared to determine significant differences between the sequences and a possible semiobjective ranking of the sequences and define the most valuable and practical sequence for the diagnosis of acute musculoskeletal infection in children based on readers scoring. The focus in this chapter is on SCE sequences and their position in the ranking.

5-3-6-1 Comparison based on Image conspicuity:

The methods and statistical tests used for this section have been extensively explained in chapter 3, section 3-2-14-2-3. Descriptive statistics, Friedman ANOVA and paired sample sign tests have been employed to explore the value of SCE sequences and their corresponding ranking. The descriptive statistics of the conspicuity scores of the readers are presented in table 19 and 20 in section 4-4-6-1 (chapter 4). Figure 8 in chapter 4, section 4-4-6-1 is a cluster column graph of the mean values of the conspicuity scores of the study's sequences, which visually simplifies the readers ranking concerning conspicuity.

Tables 19 and 20 in section 4-4-6-1 of chapter 4 summarise the descriptive statistics of the conspicuity scores of the study's sequences for both readers.

The descriptive statistic of the conspicuity scores demonstrates the readers' preferences, concerning detectability of the sequences.

Friedman ANOVA test was performed to determine any significant differences between the conspicuity scores of the SCE sequences and other study's sequences. The final results of the Friedman ANOVA multiple comparison tests for the

conspicuity scores of both readers are summarised in table 21 (chapter 4, section 4-4-6-1). The Friedman tests' results of the conspicuity scores were significant for both readers, thus post-hoc paired sample sign tests were performed between SCE sequences and other study sequences to determine which sequences demonstrate significant differences regarding their conspicuity scores. Bonferroni adjustment was required to control against type one error. The calculated p value after Bonferroni adjustment was 0.0167.

The results of the paired sample sign tests of the conspicuity scores which compare SCE sequence with other sequences are summarised in the following tables.

Sequence combination	Sig. Sign test (2-tailed) = p value	Z score	Frequencies of the scores excluding the ties
T1 fat sat SCE ~ T1	<0.001	-6.013	T1 fat sat serial contrast >T1 by 46 cases
T1 fat sat SCE ~ T2 fat sat	0.005	-2.833	T1 fat sat serial contrast >T2 fat sat by 18 cases
T1 fat sat SCE ~ DWI	0.243	-1.167	T1 fat sat serial contrast> DWI by 9 cases

Table41. Paired sample Sign test results of the conspicuity scores with p values and frequency differences after exclusion of ties for the first reader, which shows by how many cases one sequence was preferred to the other sequence after exclusion of ties (Z score is the calculated statistical Magnitude of this difference).

Sequence combination	Sig. Sign test (2-tailed) = p value	Z score	Frequencies of the scores excluding the ties
T1 fat sat SCE~ T1	<0.001	-6.625	T1 fat sat serial contrast >T1 by 54 cases
T1 fat sat SCE ~ T2 fat sat	0.004	-2.864	T1 fat sat serial contrast> T2 fat sat by 20 cases

T1 fat sat SCE ~ DWI	0.001	-3.283	T1 fat sat serial contrast> DWI by 26 cases

Table42. Paired sample Sign test results of the conspicuity scores with p values and frequency differences after exclusion of ties for the second reader, which shows by how many cases one sequence was preferred to the other sequence after exclusion of ties (Z score is the calculated statistical Magnitude of this difference).

The results of the sign test corroborate the tendency outcomes of the descriptive part of the statistics.

The first reader decided that T1 fat sat serial contrast-enhanced (SCE) sequence, provides the best lesion conspicuity and ranked T1 fat sat serial contrast enhanced sequence ahead of the other sequences (DWI, T2 fat sat and T1) based on conspicuity scores. The p-value was significant for all sequence combinations except for T1 fat sat serial contrast enhanced – DWI combination. The relationship between T1 fat sat serial contrast enhanced and DWI sequences was in the form of a tendency rather than a statistically significant difference.

The ranking of the second reader was statistically clearer, but the ranking was relatively similar to the first reader putting T1 fat sat serial contrast enhanced sequence ahead of the other sequences (T2 fat sat, DWI and T1).

The second reader also preferred SCE sequences as the sequence with the highest conspicuity. The ranking of the second reader was statistically significant for all tests with p-values < 0.0167.

The sign test results of the conspicuity scores reveal the superiority of the SCE sequences in comparison to the other protocol’s sequences and the preference of the readers concerning detectability.

5-3-6-2 Comparison based on diagnostic confidence:

The diagnostic confidence score was a new addition to the study's evaluation form based on experience with the evaluation form of the pilot study and the feedback of the readers. The diagnostic confidence scores of the study feature the second semiquantitative data set of the evaluation form.

The structure of the scoring system for diagnostic confidence characteristics adhered to the conspicuity scoring system. Equally the same methodology and statistical tests were used for this section which have been extensively explained in chapter 3, section 3-2-14-2-3. Descriptive statistic, Friedman ANOVA and paired sample sign tests have been employed to explore the value of SCE sequences and their corresponding ranking based on diagnostic confidence of the readers. The descriptive statistics of the diagnostic confidence scores of the readers are presented in table 24 and 25 in section 4-4-6-2 (chapter 4).

Tables 24 and 25 in section 4-4-6-2 of chapter 4 summarise the descriptive statistics of the confidence scores of the study's sequences for both readers.

There is an obvious tendency for the diagnostic confidence scores to be similar to conspicuity scores.

Figure 9 in chapter 4, section 4-4-6-2 illustrates the observed tendency in the mean values of the study sequences.

Similar to the conspicuity scores Friedman ANOVA test was initially performed to determine any significant differences between the diagnostic confidence scores of the SCE sequences and other study's sequences. The results of the Friedman ANOVA multiple comparison tests for the diagnostic confidence scores of both readers are summarised in table 26 (chapter 4, section 4-4-6-2). The Friedman tests' results of the diagnostic confidence scores were significant for both readers, as a consequence post-hoc paired sample sign tests were performed between SCE sequences and other study sequences to determine which sequences demonstrate significant differences based on the diagnostic confidence scores. Bonferroni

adjustment was applied similar to paired sample sign tests of the conspicuity scores. The calculated p value after Bonferroni adjustment was 0.0167.

The results of the paired sample sign tests of the diagnostic confidence scores for SCE sequences of the readers are summarised in the following tables.

Sequence combination	Sig. Sign test (2-tailed) = p value	Z score	Frequencies of the scores excluding the ties
T1 fat sat SCE ~ T1	<0.001	-6.281	T1 fat sat serial contrast > T1 by 48 cases
T1 fat sat SCE ~ T2 fat sat	0.002	-3.082	T1 fat sat serial contrast > T2 fat sat by 20 cases
T1 fat sat SCE ~ DWI	0.002	-3.031	T1 fat sat serial contrast > DWI by 22 cases

Table43. Paired sample Sign test results of the diagnostic confidence scores with p values and frequency differences after exclusion of ties for the first reader, which shows by how many cases one sequence was preferred to the other sequence after exclusion of ties (Z score is the calculated statistical Magnitude of this difference).

Sequence combination	Sig. Sign test (2-tailed) = p value	Z score	Frequencies of the scores excluding the ties
T1 fat sat SCE ~ T1	<0.001	-7.625	T1 fat sat serial contrast > T1 by 62 cases
T1 fat sat SCE ~ T2 fat sat	<0.001	-4.472	T1 fat sat serial contrast > T2 fat sat by 31 cases
T1 fat sat SCE ~ DWI	<0.001	-4.642	T1 fat sat serial contrast > DWI by 39 cases

Table44. Paired sample Sign test results of the diagnostic confidence scores with p values and frequency differences after exclusion of ties for the second reader, which shows by how many cases one sequence was preferred to the

other sequence after exclusion of ties (Z score is the calculated statistical Magnitude of this difference).

The sign tests of the diagnostic confidence scores were more conclusive than the conspicuity scores with p-values less than 0.0167.

The results of the sign test follow the trend of the descriptive part of the statistics.

The preferences of the readers were very similar, and their ranking highlighted the superiority of the T1 fat sat serial contrast enhanced sequence to the other sequences of the protocol based on diagnostic confidence scores.

However, when compared to the conspicuity scores the margins are different; this reflects how much one sequence is preferred over another.

The diagnostic confidence scores' sign tests not only exhibit the preferences of the readers, but also demonstrate the degree of reader's experience or level of confidence concerning the study sequences.

5-3-7 Time intensity curve (qualitative and semi-quantitative) analysis:

The time intensity curves are graphic illustrations of signal intensity changes per voxel over time (104). Time intensity curves do not provide quantitative measures, but their shape, magnitude, slope and other geometric characteristics reveal a vast amount of qualitative and semi-quantitative information, concerning tissue vascularisation, perfusion, vascular leak and extracellular interstitial space (92,104). Time intensity curve shapes have been previously analysed and categorised in other studies, and with a certain degree of success utilised in predominantly adult oncology, such as in breast cancer, and rheumatology but also in a few paediatric studies (103,104,152–154).

The time intensity curve shapes of paediatric musculoskeletal infection are relatively heterogeneous, and there are many non-infectious pathologies such as benign, malignant and inflammatory processes of MSK system which have overlapping time intensity curve shapes with MSK infection(104) however, based on this study's results, the magnitude and slope of the curves with their relevant semiquantitative

values are potentially instrumental biomarkers to reveal and possibly differentiate pathological perfusion and permeability in an infectious process(103,155).

5-3-8 Main data analysis of the contrast enhancement values:

One hundred and three MRI scans on ninety-nine children were performed. In total 6 cases were excluded for SCE analysis, from which 4 were excluded for qualitative and semiquantitative analysis and 2 were only excluded for semiquantitative value analysis. The reasons for exclusion are demonstrated in table 47.

Reasons of exclusion	Number of excluded cases	Percent of the cases excluded
Incomplete scans or No SCE sequences performed	4 (incomplete scan=3, No SCE=1)	3.9%
Analytic software inability to process the data due to incompatibility of pre and post contrast phases of the SCE sequences	2	1.9%

Table45. The reasons for exclusions of SCE studies for ROC curve analysis

Ninety seven SCE sets of sequences were analysed and multiple semiquantitative values were calculated per scan. Two semiquantitative values (AUC = area under the curve and TME = time to max. enhancement) were calculated for each pathology and reference healthy tissue per scan. AUC and TME are semi-quantitative values derived from qualitative signal intensity curves of the musculoskeletal lesions.

5-3-8-1 Receiver operating characteristic analysis of the semiquantitative contrast enhancement values:

Hand drawn ROI measurements were performed to assess the vascular leak parameters in pathological and healthy reference targets, and as in some cases the pathology involved different tissues or tissue compartments multiple measurements were performed in pathological and healthy tissue. 640 measurements in total have been performed.

The data, which included AUC and TME values of pathological and healthy reference targets, was subsequently divided into 4 groups based on main anatomical tissue compartments as follows:

1- Bones
2- Muscles, tendons and soft tissue
3- Synovial membrane
4- Cartilage (physeal, epiphyseal and articular)

There were 8 coded clinical diagnoses based on the gold standard categories, which are as follows:

1- Infection
2- Infarction
3- Benign tumour
4- Malignant tumour
5- Fracture
6- Inflammation
7- Normal
8- Muscular injury

Two of the coded clinical diagnoses including fracture and muscle injury have been dismissed following the semiquantitative measurements and prior to the statistical analysis as each represented only one or two cases. Receiver operating characteristic analysis, which is defined as a plot of test sensitivity as the y coordinate versus its 1-specificity or false positive rate as the x coordinate, was performed to evaluate the diagnostic performance of semiquantitative permeability values in diagnosis of acute MSK infection(156,157).

The measured semiquantitative values (TME and AUC) of the MSK lesions of the cohort were correlated with the clinical gold standard. Ten Receiver operating characteristic (ROC) analyses have been performed, from which eight of the ROC curves have been calculated for the clinical diagnoses of MSK infection in different tissue compartments (such as bone infection, synovial infection, muscle infection,…

see table 48 and 49) and the remaining two were for the clinical diagnosis of Bone infarction.

The intention was to determine the diagnostic value of TME and AUC values and detect possible thresholds for diagnosis of MSK infection. Two of the ROC analyses (TME and AUC ROC tests for cartilage infection) were not relevant as the number of non-infectious pathological cases were too low.

The descriptive statistics concerning the area under the curve of the ROC tests for measured AUC and TME values of suspected infectious lesions are presented in tables 48 and 49.

AUC	Area under the curve	Sig. p value	95% confidence interval lower-upper bound	Patients with infection	Patients without infection
Bone Infection	0.616	0.173	0.448-0.783	27	22
Muscle and soft tissue infection	0.721	0.179	0.471-0.970	17	4
Synovial infection	0.926	0.021	0.803-1.000	18	3
Cartilage infection	There are	not enough	Non-infectious	cases for ROC	analysis

Table46. Descriptive statistics of the ROC tests for AUC

TME	Area under the curve	Sig. p value	95% confidence interval lower-upper bound	Patients with infection	Patients without infection
Bone Infection	0.609	0.195	0.448-0.769	27	22
Muscle and soft tissue infection	0.792	0.074	0.608-0.976	17	4
Synovial infection	0.611	0.546	0.335-0.888	18	3

Cartilage infection	There are	not enough	Non-infectious	cases for ROC	analysis

Table47. Descriptive statistics of the ROC tests for TME

The most significant statistical outcome is from AUC values for synovial infection which was excellent. The results of AUC and TME of muscle infection are fair, but the p-values are not satisfactory (0.05<).

The ROC curves with fair-excellent results are demonstrated below.

The ROC analysis of the TME values for osseous pathologies demonstrates a poor-fair outcome with an area under the ROC curve of 0.609 and a suboptimal p-value of 0.195 (0.05<), hence the calculated threshold of <343 for osseous infections (sensitivity = 71%, specificity = 41%) is not relevant. Figure 18 illustrates the TME ROC curve of the osseous pathologies.

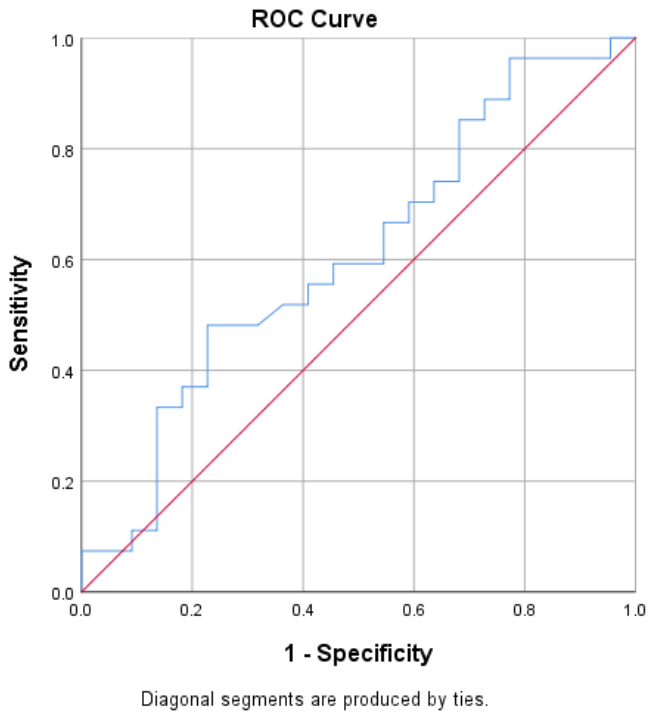

Fig. 18- TME ROC curve of hyperaemic osseous lesions

The ROC analysis of the TME values for muscle and soft tissue pathologies demonstrates a fair-good outcome which is encouraging with an area under the ROC curve of 0.792, but unfortunately the p-value was 0.074 (0.05<), hence the calculated threshold of <271.5 for muscle and soft tissue infections (sensitivity = 72%, specificity = 100%) cannot be considered. Figure 19 illustrates the TME ROC curve of muscle and soft tissue diseases.

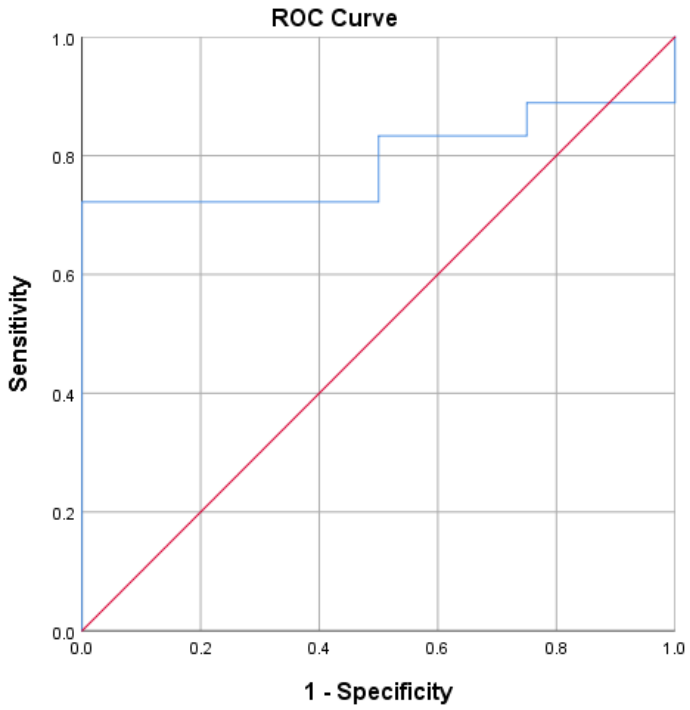

Fig. 19- TME ROC curve of hyperaemic muscle and soft tissue lesions (diagonal segments are produced by ties)

The ROC analysis of the AUC values from osseous lesions, reveals a poor-fair outcome with an area under the ROC curve of 0.616, a p-value of 0.173 (0.05<) and a threshold of 56485< for osseous infections (sensitivity = 71%, specificity = 62%). Figure 20 illustrates the AUC ROC curve of the osseous lesions, the curve is relatively flat and close to the diagonal line, which reflects the ties or chance effect and the p value is not satisfactory, hence the AUC values of bony pathologies cannot aid the diagnosis of infection in this cohort and is unable to offer a diagnostic threshold.

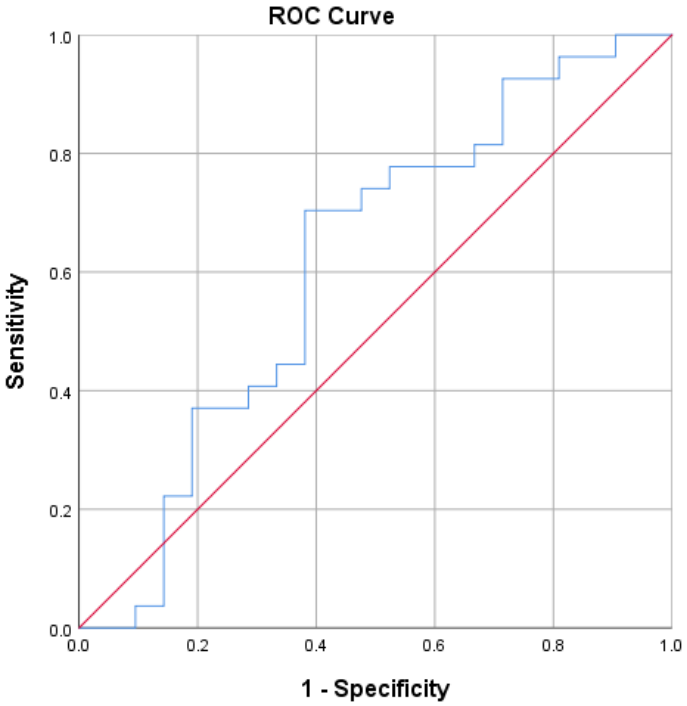

Fig. 20- AUC ROC curve of hyperaemic osseous lesions (diagonal segments are produced by ties)

Equally the ROC analysis of the AUC values for Muscle and soft tissue infections are not satisfactory, due to a suboptimal p-value of 0.179 (0.05<), although the results of the ROC analysis demonstrates a fair outcome with an area under the ROC curve of 0.721, hence the threshold of 34630< for muscle and soft tissue infection (sensitivity = 88%, specificity = 50%) is not good enough. Figure 21 illustrates the AUC ROC curve of Muscle and soft tissue infection. The ROC curve below is slightly better than the ROC curve for osseous infection (fig 20) however it is still relatively diagonal.

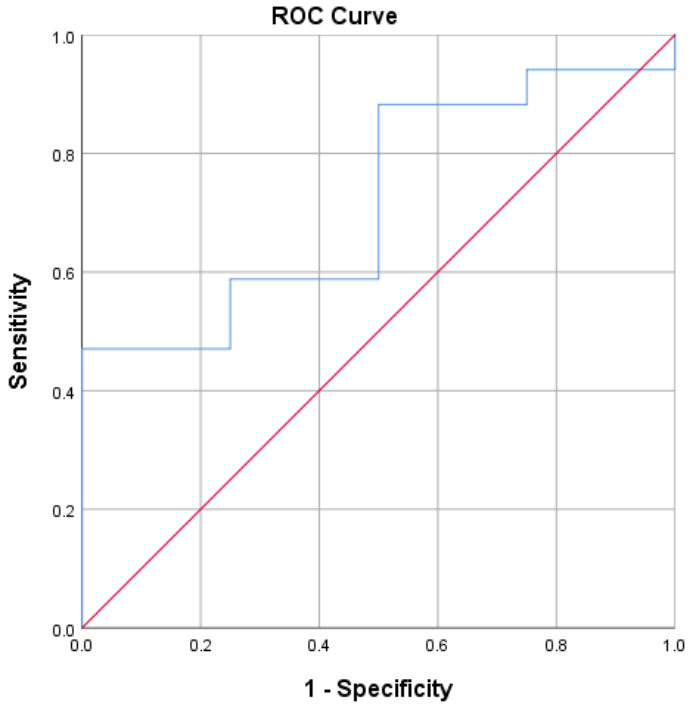

Fig. 21- AUC ROC curve of hyperaemic muscle/soft tissue lesions (diagonal segments are produced by ties)

The ROC analysis of the AUC values of the synovial pathologies shows an excellent result with an area under the ROC curve of 0.926, a p-value of 0.021 (<0.05) and a threshold of 57430< for synovial infections (sensitivity = 84%, specificity = 100%). Figure 22 illustrates the AUC ROC curve of the synovial diseases.

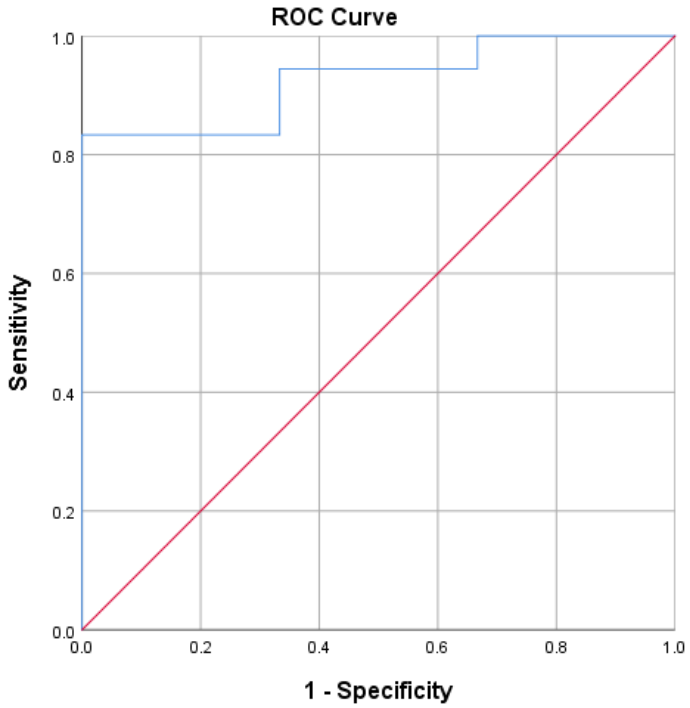

Fig. 22- AUC ROC curve of hyperaemic synovium

The ROC curve of the AUC values for the synovial pathologies is the only ROC analysis which delivers excellent outcomes based on the area under the ROC curve and a statistically significant p value. The number of non-infectious pathologies in synovial disease group was 1/6 of the total pathologies (infectious pathologies 5/6), the relatively disproportionate high number of infectious pathologies could have potentially influenced the outcomes of the ROC calculations, and hence the excellent results although very promising perhaps should be considered with caution.

There are few other parameters with fair-good ROC results, including AUC and TME of muscle and soft tissue infections as demonstrated above which show tendencies, however without statistically significant p-values.

A few of the other pathologies had poor- fair ROC results; the following curve illustrates the AUC ROC curve of bone infarction, which is the best non-infectious ROC curve with a poor-fair result.

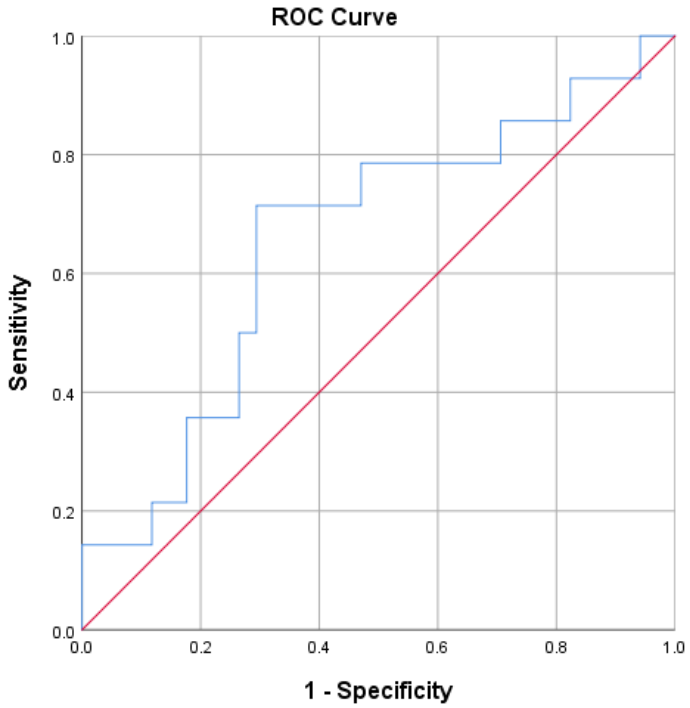

Fig. 23- AUC ROC curve of Bone infarction, with an area under the curve of 0.655 and a p-value of 0.093.

The remaining ROC analyses did not reveal any statistically relevant results. The few good-excellent ROC tests of the semiquantitative values (AUC & TME) are encouraging for future studies even though only one had a satisfactory p value.

The semi-quantitative parameters are generally good tendency predictors especially the AUC based on the results of few recent studies(104).

5-4 Discussion:

Characterisation of altered perfusion and permeability in pathological processes has been always challenging, but remains instrumental in the differentiation of varying pathologies.

Serial contrast enhanced magnetic resonance imaging which is based on trans-endothelial exchange of a tracer and depends on tissue perfusion, influx and efflux

phenomena through the endothelium is a sophisticated way to differentiate and characterise altered permeability (90,92).

The principles and relevance of contrast enhanced imaging including DCE and SCE imaging have been discussed in length in chapter 1, section 1-7-9 (1-7-9-1, 1-7-9-4 and 1-7-9-5).

Dynamic contrast enhanced imaging is the most commonly used technique for contrast enhanced magnetic resonance imaging outside the brain. Dynamic contrast enhanced magnetic resonance imaging is based on rapid and repetitive sequential acquisition of fast T1 weighted frames before, during and after intravenous administration of a low molecular weight contrast agent (92,101,102).

Quantification of the varying vascular leak pattern at an endothelial level represents a promising new approach to characterise and differentiate pathologies based on objective measurements, and has the potential to transform MRI from a qualitative and subjective diagnostic tool to an objective measuring devise(58), however the process of accurate vascular leak quantification is time consuming and requires advanced hardware, sophisticated software, fine tuning of the hardware to the specifications of the software and well trained staff.

The technical and operational challenges have been explained in chapter 1 (section 1-7-9-5, 1-7-9-6 and 1-7-9-7), chapter 3 (section 3-2-6-5-2) and chapter 5 (section 5-1-2 and 5-1-3). The technical and operational challenges for accurate vascular leak quantification, the length of sampling throughout the entire process, the low SNR and the lack of fat saturation of the DCE sequences with the consecutive necessity of additional fat saturated pre and post contrast high resolution T1 sequences in paediatric acute clinical setting were the main reasons this study utilised SCE sequences rather than DCE sequences.

Dynamic and serial contrast enhanced imaging has been previously utilised in oncology (90,107,114,158) including musculoskeletal tumours in children (113,159–161) and more recently in inflammatory, infectious and ischaemic diseases of the growing skeleton (103,104,125).

This is the first prospective study, which evaluates the utility of serial contrast enhanced magnetic resonance imaging in paediatric musculoskeletal infection .The aim of this chapter of the study was to analyse the feasibility, diagnostic accuracy and performance of SCE imaging with its qualitative and semi-quantitative properties in the diagnosis of musculoskeletal infection in children and comparison with DWI and structural sequences.

The model of the serial contrast-enhanced (SCE) sequence of the study was a combination of DCE and static high-resolution contrast enhanced models, both models have significant advantages, which can be complementary to one another; however, scanning acutely unwell paediatric patients comes with a strict time limitation. The idea of this study's SCE sequence was to extract the advantages of both techniques, while avoiding the complexity of performing quantitative DCE sequences and improving the diagnostic yield of static contrast enhanced sequences. The trade off was however to abandon the quantitative vascular leak parameters (K_{ep}, K^{trans}, V_e, V_p).

The evaluation form was specifically designed to cover all different aspects of the study protocol and its single sequences, while promoting quantification of non-parametric data (conspicuity and diagnostic confidence scores) in order to reduce reader's bias and produce additional semiobjective data to compare the sequences.

Inter and intraobserver agreements were statistically analysed as per independent reading protocol of the study with satisfactory results and p-values. The inter-observer agreement for the categorical and numerical (conspicuity and confidence scores) data was good with excellent p-value. The intra observer agreement of the categorical data was good with satisfactory p-values for both readers, while the intra observer agreement of the numerical data (conspicuity and confidence scores) was moderate for the first reader and excellent for the second reader.

All patients except those who had their scans under general anaesthesia tolerated the scanning protocol. 4 out of 103 scans (4%) were in total excluded and 6 semiquantitative values were excluded for semiquantitative analyses, resulting in a yield of 90% < feasibility (see consort table in section 5-3-1). The good feasibility

results of the study confirmed the results of other prospective studies (104,113) and proved that our MRI preparation protocol for children is sufficient.

There were no significant differences between the three MRI scanners (2 x 1.5 T and 1 x 3T). The reference AUC and TME measurements of the reference tissue did not vary significantly between different patients despite utilisation of different scanners and magnetic fields, in correlation with previous studies(104,113). The minor differences between different field strengths including slight varying signal to noise ratio (SNR), susceptibility artefacts and fat saturation levels, do not reveal any relevant differences according to the literature(104,113). Furthermore the semiquantitative values of SCE sequences are per definition (59,89,100) independent of the scanner and field strength and thus are not affected by employing three different scanners from the same manufacturer.

The intraobserver agreement for hand drawn ROI measurement of the semiquantitative values (AUC and TME) in this study was satisfactory-excellent, however automated ROI measurement methods are preferred as they offer better intraobserver consistency and are faster.

The diagnostic accuracy of the SCE sequences was assessed by comparing the readers' diagnoses based on qualitative information of SCE sequences, and the clinical gold standard using a categorical correlation test (Cohen's kappa test), which demonstrated good-excellent diagnostic accuracy with excellent sensitivity and specificity. The diagnostic accuracy of the SCE sequences have been compared with the other sequences of the study's protocol and SCE sequence has shown the highest diagnostic accuracy between the study's single sequences.

The semi-quantitative data of the conspicuity and diagnostic confidence scores were compared and analysed in this study using Friedman ANOVA and Paired sample sign tests to determine the readers' preference and to display a semi-objective prioritisation of the sequences based on conspicuity and diagnostic confidence scores. The results of the Friedman and Paired sample sign tests were significant for both readers and all sequence combinations except for one test (see table 42). The

ranking of the study's sequences based on paired sample sign test is nearly identical for conspicuity and confidence scores regarding SCE sequences.

SCE sequences are the preferred sequences of the readers concerning conspicuity and confidence scores. The paired sample sign test results of the confidence scores' reveal not only the preferences of the readers, but also unveil the degree of reader's experience concerning the study's sequences.

Multiphase subtraction is a post processing function based on subtraction of the pre-contrast phase of the SCE sequence from one of the post contrast phases, or subtraction of an early post contrast phase from a later post contrast phase (162,163). Multiphase subtraction was a significantly useful adjuvant source of information in this study which however was not separately evaluated but as part of the SCE sequences. Multiphase subtraction improves the detection of small lesions, especially in multifocal processes and improves the conspicuity of the lesions(107). Multiphase subtraction is also a useful tool to differentiate between diffuse physiological hyper-perfusion (inherent in paediatric skeleton) and pathological focal increased perfusion or vascular leak(103,162,163). Subtraction images are excellent road maps to guide surgical or radiological targeted interventions, such as drainage of abscesses or performing targeted biopsies of lesions. Multiphase subtraction should be evaluated separately in future studies in order to quantify statistically it's added value to the protocol.

The AUC and TME values are two of the most relevant semiquantitative serial contrast enhancement values, according to previous publications(104,152,153,155), which are derived from signal intensity curves. Two sets of semiquantitative permeability values including AUC and TME were calculated for each lesion representing the pathological and healthy reference tissue. Descriptive statistics and ROC curves were utilised to assess the diagnostic performance of the selected parameters to diagnose MSK infections and determine possible diagnostic thresholds.

The ROC curve of the AUC values of synovial infection was the only ROC curve from a total of ten ROC analyses which has demonstrated statistically significant

results with excellent outcome and a diagnostic, lower limit threshold (threshold = 57430<, sensitivity = 84%, specificity = 100%), however the number of non-infectious pathologies in the synovial pathology group is relatively low, thus the results should be considered with caution.

The results of AUC and TME of muscle infection are fair-good but the p-values are not satisfactory (0.5<). Equally the ROC curve's result of AUC values for bone infarction is fair without statistically significant p-values.

The remaining 6 ROC analyses were statistically irrelevant. AUC was the best predicting parameter for hyperaemia and infection, especially in synovial infection group. The superior results of the synovial infection in comparison to muscle, soft tissue and bone groups could be due to its rich vascular composition which consists of highly vascular and porous connective tissue.

Time intensity curves were not initially considered as possible sufficient imaging tools or complementary adjunct(104), and hence not provided to the readers at the time of reading. The complementary diagnostic potential however was noted and appreciated by the time of processing the semiquantitative aspect of SCE sequences and calculating the semiquantitative permeability values from signal intensity curves.

This potential of the time signal intensity curves was described and explained by Nusman et al. in their 2017 paper; Dynamic contrast-enhanced magnetic resonance imaging of the wrist in children with juvenile idiopathic arthritis(104), which has concluded that, although the time intensity curve shapes of paediatric musculoskeletal infection are heterogeneous and not able to differentiate between infection and other pathologies with altered permeability(104), the magnitude and slope of the curves in cases of abnormal endothelial permeability due to different pathologies are sufficient to visualise and detect altered tissue perfusion and vascular leak and perhaps can be utilised as a complementary tool to improve the diagnostic value of rapid pre and post contrast enhanced sequences, or for follow up scans to assess treatment success or prognosis. However this aspect was not evaluated systematically in this study and should be a subject for future studies. Fig

24 and 25 are time intensity curves from this study and are positive examples for the described findings above.

There were technical incompatibilities between scanned data and parametric requirements of the utilised software for MRI and pharmacokinetic modelling and calculation of the quantitative values at the onset of the study, which were the reason for exclusions of quantitative parameters and one of the reasons for replacement of DCE with SCE sequences. This was the main technical learning point from this section of the study that DCE sequences have to be chosen carefully and have to be absolutely compatible with the analysing software and the sequence and scanner parameters have to perfectly synchronise with the software in order to create valid quantitative data.

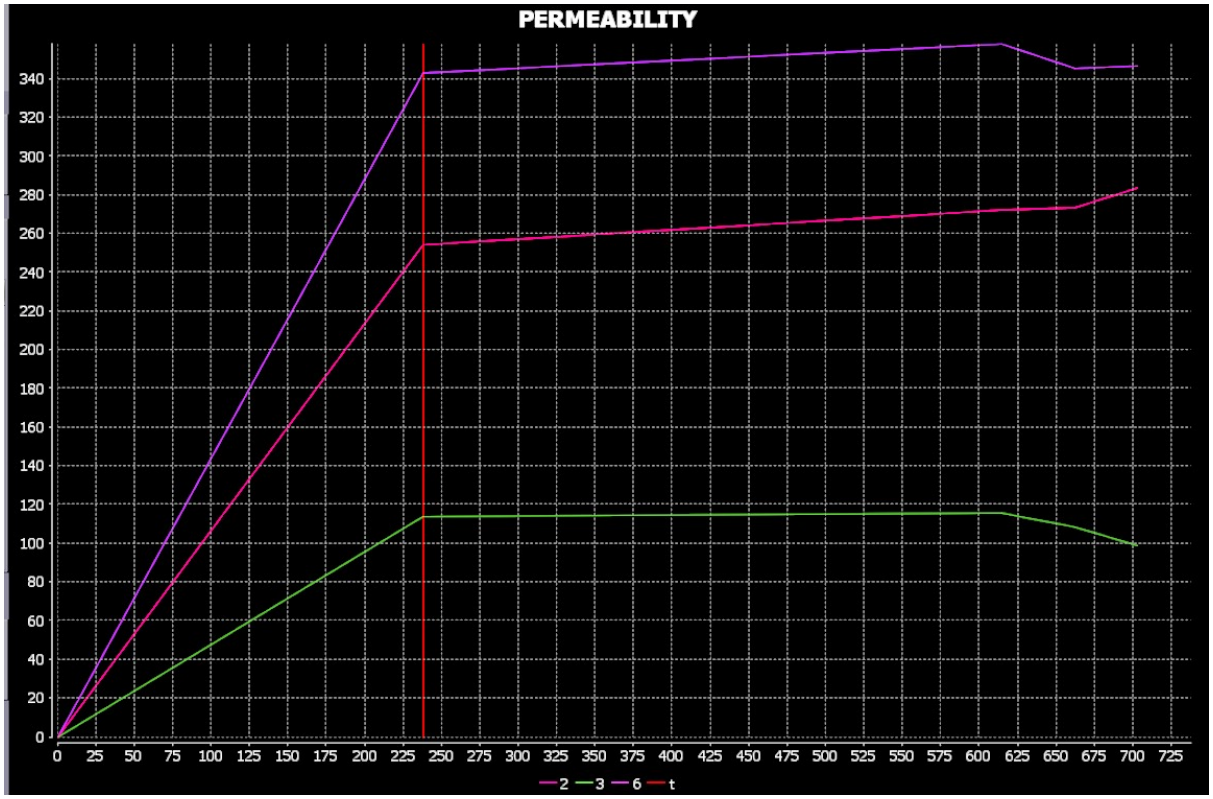

Fig. 24-The above purple curves (second and sixth ROIs) are from a significantly contrast enhancing poly articular juvenile arthritis and the green curve is representing the healthy reference tissue.

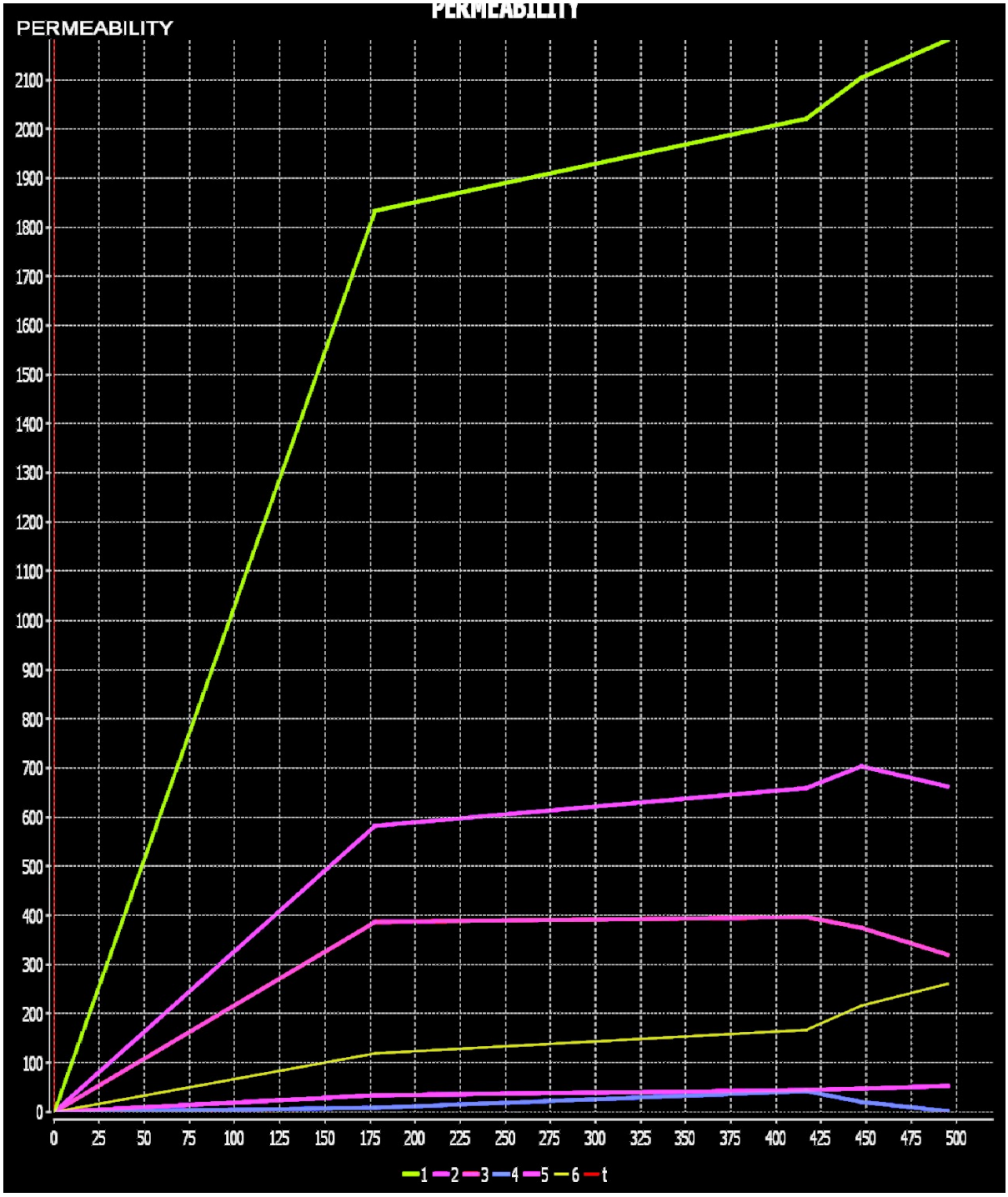

Fig. 25- The above green Curve (first ROI) is from a septic arthritis of the lower limb with significant contrast enhancement of the synovium and the remaining curves represent healthy reference tissue.

5-5 Limitation:

The limitations in this chapter of the study are divided into two main groups:

1-The study design related limitations

2-The quantification related limitations and the consecutive exclusion of the quantitative values and their replacement with semiquantitative contrast enhancement values.

The study design related limitations are as follows:

1- Single site study design
2- Relative small patient population
3- Large age range of the participants and the consecutive considerable variation of anatomy, bone marrow conversion and tissue physiology
4- High number of different pathologies (high level of inhomogeneity)
5- The small number of cases for some of the pathologies
6- Inhomogeneity of participants regarding pre-existing chronic bone marrow abnormalities and possibly altered quantitative values of normal bone marrow, which can potentially cause misinterpretations
7- Hand injection in a small group of patients was another limitation of this study due to an inherent lack of consistency in injections, the inaccuracy of the injection time (onset time of injection) and speed which is required for accurate AIF measurements, although only the very young patients had hand injection and the majority had automatic injections and accurate AIF is only necessary for calculation of quantitative values.
8- The ROI measurement of contrast enhancement values in this study was two dimensional (2D) and hand drawn, which is possibly prone to inconsistency and selectivity. 3D automated ROI measurement is a more resilient and independent approach for quantitative measurements.

The vascular leak quantification was actually not a limitation of the study as the default was noticed at the beginning of the study and was mitigated by excluding the

quantitative values and their analyses. It is however important to acknowledge that accurate quantification of trans-endothelial vascular leak is complex and multifaceted, hence I have added this section to the limitations as its magnitude was not initially envisaged.

The SCE sequences in this study are not capable of providing accurate quantitative values. There are very few prospectively designed DCE studies in children and the majority of these, have a small number of patients with very specific focus of interest and without inclusion of quantitative parameters (104).

There is limited experience in systematic paediatric DCE imaging and a general paucity of normal age-related quantitative values for children. There are many difficulties such as selecting the correct sequence, creating the right protocol, fine tuning of the parameters of the sequences and the calculating software, assessing the primary main (MRI and pharmacokinetic) parameters and the calculated final results (K^{trans}, K_{ep}...).

These issues are in addition to the usual limitations in paediatric population such as cannulation and immobilisation.

The use of commercial software programs for vascular leak parameter calculation is beneficial as these programs are standardised, validated and reliable and can be used in multicentre and international studies. However considering the complex nature of these parameters, pharmacokinetic modelling and its requirements, the structures of these software programs are very rigid and limiting. Appropriate knowledge of MRI and pharmacokinetic modelling, and if a commercial software is used, the detailed specification of the software is crucial in planning and performing quantitative MRI studies.

5-6 Conclusion:

This chapter of the study was a pragmatic attempt to use trans-endothelial contrast enhancement alterations and experiment with the most common serial contrast enhanced sequences in acute clinical setting to improve the diagnostic yield of paediatric musculoskeletal infection. The initial intension was to use DCE sequences, but with additional modification to adjust them optimally for the acute clinical paediatric setting which means shorter sequences, improved spatial resolution and higher conspicuity; however the trade off for this purely clinical and pragmatic approach was to sacrifice the accurate quantification and replace DCE sequence with SCE sequence. This study suggests that serial contrast enhanced imaging is a valuable tool in the diagnosis of acute musculoskeletal infection in children with the potential to detect, characterise and differentiate MSK infection in children.

The SCE sequences are feasible and demonstrate high diagnostic accuracy when compared with the gold standard. The overall performance of the SCE sequences in this study was scored by the readers superior to the structural, and by a narrow margin to the diffusion weighted sequences. SCE sequences have demonstrated the highest level of diagnostic confidence and diagnostic accuracy between the sequences of the study protocol.

The study's SCE sequence is an accurate qualitative imaging tool, which can produce qualitative curves and semiquantitative values. The semi-quantitative parameters in this study demonstrated multiple good-excellent results based on ROC curve analyses, however only one value, namely AUC of Synovium, could demonstrate statistical significance in the ROC analysis and deliver an acceptable threshold. Semiquantitative parameters derived from signal time intensity curves are relatively promising biomarkers, with potential to aid detection and characterisation of abnormal tissue biology and functional changes at the capillary level(104,113).

In summary serial contrast enhanced magnetic resonance imaging is a valuable functional bio imaging tool with enormous potential in detection and differential

diagnosis of paediatric musculoskeletal infection, however vascular leak quantification in children is still a work in progress and an on-going subject of research(104,113). Appropriate knowledge of MRI and pharmacokinetic modelling, and if a commercial software is used, the detailed specification of the software is crucial in planning and performing SCE or DCE studies. Future larger prospective studies with more sophisticated design, better adjusted and more resilient signal quantification software are required to extract the full potential of rapid contrast enhanced magnetic resonance imaging in children with MSK infections.

Chapter 6: Tailored magnetic resonance imaging protocol for musculoskeletal infection in children

6-1 Introduction:

The nature of bacterial infections in paediatric populations and their variants with more significant expression in paediatric musculoskeletal system have been discussed in chapter 1(1,2).

The diagnostic dilema of paediatric musculoskeletal infections is that they do not follow the same rules as for other organ systems(1,2). Musculoskeletal infections in children usually present with nonspecific signs and symptoms, and as a consequence often fail to be diagnosed early in the course of the disease with resultant delayed or suboptimal treatment.

Paediatric musculoskeletal infection as a result is often the cause of substantial morbidity and mortality in children with increasing frequency in recent decades (3,30).

6-1-1 Musculoskeletal infection in children:

Musculoskeletal infection in children has been discussed in section 1-2 to 1-7 in chapter 1 including the aetiological and the epidemiological changes in the recent decades.

6-1-2 Diagnosis of musculoskeletal infection in children:

The clinical presentation of musculoskeletal infection and the relevant diagnostic investigations such as laboratory and microbiology tests have been explained in sections 1-7-1 to 1-7-3 in chapter 1(10,30–32).

6-1-3 Imaging diagnosis of musculoskeletal infection in children:

Imaging has always been an integral part of the diagnosis and management of musculoskeletal infection in children, in particular when clinical symptoms, laboratory and microbiology results are nonspecific, confusing or even contradictory (for more details see section 1-7-4 in chapter 1).

The clinical manifestation and management of acute musculoskeletal infection in children has changed substantially over the past few decades (10). The imaging diagnosis of musculoskeletal infection in children must therefore adopt appropriately to address the emerging challenges.

A variety of imaging modalities are employed to diagnose acute musculoskeletal infection, these are: plain films, computed tomography, magnetic resonance imaging, ultrasound, bone scintigraphy, and positron emission tomography(43). These imaging modalities have been discussed in section 1-7-4 in chapter 1.

6-2 Material and methods:

The study structure has been explained in section 3-2-1 (chapter 3). This is the first prospective study to evaluate the diagnostic yield of advanced MRI techniques and a tailored protocol in the diagnosis of musculoskeletal infection in children.

6-2-1 Objective:

The aim of this chapter of the study is to assess the feasibility and the diagnostic accuracy of the study's tailored MRI protocol in the diagnosis of musculoskeletal infection in children. Furthermore I have evaluated the readers' preference regarding conspicuity and diagnostic confidence of the single sequences of the study protocol in comparison with each other and finally I will analyse the diagnostic merit of ADC TME and AUC values in differential diagnosis of paediatric musculoskeletal infection and their possible additive diagnostic value.

6-2-2 Ethic approval:

Institutional, local and national ethic approval was sought (please see Appendix 1).

6-2-3 Study population:

Ninety nine patients were prospectively recruited over a period of two and half years, between October 2014 and May 2017. The number of patients was estimated based on my retrospective pilot data (see section 3-1-3, chapter 3 for the pilot data).

There were 44 girls and 55 boys included in this study. The age of subjects ranged between 1 and 216 months (18 years) with a mean age of 101 months (8 years). Please see also sections 3-2-2 (in chapter 3) and 4-3-4 (in chapter 4).
The study was designed exclusively for children and the inclusion and exclusion criteria have been presented in section 3-2-3 in chapter 3.

The recruitment process is explained in section 3-2-4 and the structures of information, assent and consent forms are demonstrated in section 3-2-5 (chapter 3) and the forms are available in Appendix 2 and 3.

6-2-4 Magnetic resonance imaging:

This Section has been previously described in details in sections 3-2-6 (chapter 3), 4-3-5 (chapter4) and 5-2-8 in (chapter 5), including MRI imaging sites, radiography team, MRI scanners and coils, scanning method, patient preparation and immobilisation.

6-2-5 Magnetic resonance imaging protocol:

The intention of this study was to create an imaging tool based on magnetic resonance imaging that can capture the fluent phases of acute musculoskeletal infection early on in children. The plan was to create a protocol which enhances the known strength of conventional sequences and utilises the advanced approaches of diffusion and serial contrast enhanced sequences, in order to create an array of different signal detection techniques and expand the types of signals that can be

translated into informative images. The MRI protocol development, the single sequences, sequence optimisation and contrast agent selection are comprehensively detailed in sections 3-2-6-5 (chapter 3), 4-3-5 (chapter 4), and 5-2-9 (chapter 5).

The qualitative MRI analyses including the semiquantitative scoring of the study's sequences were conducted independently by two experienced musculoskeletal radiologists using a multi parametric evaluation form and are explained in sections 3-2-7 to 3-2-12 in chapter 3.

The quantitative MRI analyses are described in sections 3-2-12 (chapter 3), 4-3-7 (chapter 4) and 5-2-11 to 5-2-13 (chapter 5).

6-2-6 Readers:

The evaluation of the scans was conducted by two experienced musculoskeletal radiology consultants, for more details please see section 3-2-9 in chapter 3.

6-2-7 Evaluation form:

The combination of the study's sequences was designed to detect different physical signals and to provide more information about different aspects of an infection. The evaluation form should have the capability to capture the provided variation of information by the study sequences.

The study evaluation form is explained in section 3-2-10 in chapter 3 and is available in appendix 4.

6-2-8 Reading process:

The reading process has been described in section 3-2-11 and the relevant MRI criteria for Osteomyelitis and the Gold standard were presented in sections 3-2-7 and 3-2-8 in chapter 3 respectively.

6-2-9 Data preparation:

Data preparation has been presented in details in section 3-2-13.

6-2-10 Data analysis and statistics:

SPSS statistics program version 25 (IBM Company Chicago Illinois) was used to conduct statistical analysis in this study. A p value of less than 0.05 was considered to be statistically significant.

6-2-10-1 Inter and intraobserver agreement and data analysis:

Please see section 3-2-14-1 in chapter 3.

6-2-10-2 Main data analysis:

Please see section 3-2-14-2 in chapter 3 for comprehensive description of the main data analysis and for the specific statistical analysis of ADC values of DWI sequences and TME and AUC values of SCE sequences please referrer to sections 4-3-9-2, 5-2-17-2 and 5-2-17-3.

6-3 Results:

6-3-1 Cohort:

Ninety nine children with acute musculoskeletal pain and suspected clinical diagnosis of musculoskeletal infection were prospectively recruited for this study.

One hundred and three MRI scans were performed (between 1 and 3 scans per patient) on different admissions, using the same novel MRI protocol including diffusion weighted sequences with ADC maps and serial contrast enhanced sequences with multiphase subtractions. Three patients had more than 1 scan, two girls and one boy.

The most common pathology amongst the participants was infection; a total of 37 patients had musculoskeletal infection, while the second most common pathology was infarction, with 14 patients.

Table 48 illustrates the number of scans, patients, the pathologies and the gender related break downs.

Diagnostic categories	number of patients	Male	Female	MRI exams
Infection	37	23	14	37
Infarction	14	6	8	17
Inflammation	13	6	7	13
Malignant (solid) lesions	3	3	0	3
Benign lesions	8	5	3	8
Bony injuries	2	2	0	2
Muscular injuries (haematoma)	1	1	0	1
Normal	18	12	6	19
All categories	99	55	44	103

Table48. Number of scans and study participants for the diagnostic categories

The male participants are more represented in the infection group, this finding is not accounted for by the total male predominance of the participants.

Figure 26 demonstrates the numbers and the break down of the pathologies. Infection and inflamation count for more than 60% of the total number of the pathologies.

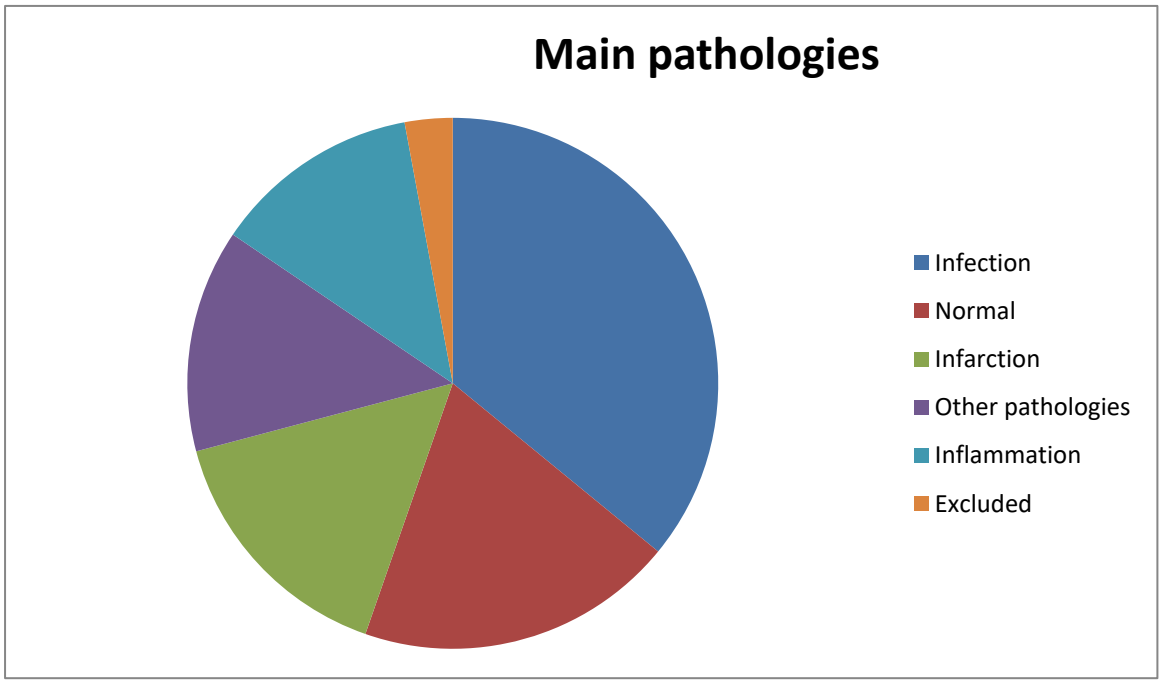

Fig. 26- Pathologies represented in the study

6-3-2 Feasibility of the MRI protocol:

All patients, except those who had their scans under general anaesthetic, tolerated the entire scanning protocol which took in average 43 min. The feasibility result satisfied the feasibility assumption (see section 3-2-14-2-1 in chapter 3) of more than 90% and was better than the result of the previous pilot study.

Three cases (~3%) had to be excluded, due to incomplete scans (see section 4-4-1). One additional case was excluded for qualitative SCE analysis as the post contrast sequence was not completed (see section 6-3-1).

The solely quantitative (Including ADC, AUC and TME values) exclusions were not included in the feasibility calculations as the scans were completed in these cases and the qualitative information of the sequences were evaluated and used for qualitative statistics, furthermore the reasons for exclusions were secondary to

analytic software incompatibilities and not related to patient cooperation or scan duration. If these cases however would have been included the feasibility would still be above 90% and hence satisfactory.

6-3-3 Inter and Intraobserver agreement tests:

The readers initially reviewed ten random cases independently from the pilot study with the same MRI protocol and a nearly identical evaluation form, to assess the inter-observer agreement. The readers repeated the independent review of the same cases 1.5 months later, in order to evaluate the intraobserver agreement.

The data produced, was a combination of categorical data which was extracted from the qualitative information (the diagnoses) and numerical data, based on semi-quantitative information (conspicuity scores of single sequences) of the evaluation form.

The numerical data was analysed with a two-tailed ICC test. A total of twelve interclass correlation coefficient tests were processed to address each sequence (4 sequences) of the protocol for both readers (2 x 4) and between the readers (1 x 4).

Table 49 illustrate the Interclass correlation coefficient results of inter and intraobserver agreement of the semi quantitative results (conspicuity scores).

	Average ICC T1, (p value)	Average ICC T2 fat sat, (p value)	Average ICC DWI, (p value)	Average ICC SCE, (p value)
Intraobserver agreement test of reader 1	0.816, (0.002)	0.703, (0.025)	0.895, (0.001)	0.698, (0.011)
Intraobserver agreement test of reader 2	0.883, (0.003)	0.903, (0.001)	0.723, (0.006)	0.899, (0.000)
Interobserver agreement test between the readers	0.832, (0.003)	0.681, (0.014)	0.883, (0.002)	0.899, (0.001)

Table49. Interclass correlation coefficient test for inter and intraobserver agreement, p value is significant < 0.05.

There was good to excellent agreement (according to Koo & Li) between the readers concerning the semi-quantitative data (conspicuity scores) of the protocol's sequences based on the ICC tests (p value= 0.001- 0.014). The Intraobserver agreement of both readers was good to excellent (according to Koo & Li) for all protocol's sequences, based on the ICC analysis.

The extracted data from the qualitative information (readers and final clinical diagnoses) of the evaluation form was categorical data, hence the correlation between the readers was analysed with Cohen's kappa test. Three Cohen's kappa tests were performed, 1 for inter-observer agreement and 2 for intraobserver agreement.

The kappa measure of agreement between the readers was 0.756 and the p value was 0.001 (sensitivity= %87.5 and specificity > %90 for MSK infection), in keeping with good agreement. The intraobserver agreement based on kappa value was good or excellent (0.756 – 1.000), with a p value less than 0.001.

6-3-4 ROI measurements' consistency analysis for ADC values:

The intraobserver agreement analysis of the manual ROI measurement of ADC values is discussed in section 4-4-4 and the results are presented in table 15.

6-3-5 ROI measurements' consistency analysis for Permeability values:

The intraobserver agreement analysis and the relevant results of the manual ROI measurement of TME and AUC values have been discussed in section 5-3-4 and the results are presented in table 36 of chapter 5.

6-3-6 Accuracy test of the study protocol and the single sequences:

The final clinical diagnoses (gold standard) were compared with the final diagnoses of the readers, based on the qualitative information of the entire protocol including all four sequences, by means of Cohen's kappa test to ascertain the level of accuracy

of the study protocol as an imaging tool. Separately the diagnoses based on the findings of single sequences were correlated with the final clinical diagnoses using equally Cohen's kappa test.

Ten Cohen's kappa tests were performed, 2 for the final readers' diagnoses and 4 x 2 for the single sequences of the two readers.

Table 50 demonstrates Cohen's kappa tests' results of the final clinical diagnoses (gold standard) in comparison to the readers' final diagnoses.

Whole MR protocol versus gold standard	Measure of agreement Kappa value	Sensitivity	Specificity	P value	95% confidence interval, lower-upper bound
First readers' diagnoses ~ Clinical diagnoses with 8 diagnostic categories	0.782	84%	95.2%	<0.001	0.000-0.029
First readers' diagnoses ~ Clinical diagnoses with 2 diagnostic categories	0.804	84%	95.2%	<0.001	0.000-0.029
Second readers' diagnoses ~ Clinical diagnoses with 8 diagnostic categories	0.778	92%	90.5%	<0.001	0.000-0.029
Second readers' diagnoses ~ Clinical diagnoses with 2 diagnostic categories	0.810	92%	90.5%	<0.001	0.000-0.029

Table50. Cohens Kappa agreement tests between final readers' diagnoses including all sequences and clinical gold standard, with 8 and 2 diagnostic categories. Kappa value is the rate of agreement. The sensitivity and specificity relate to the whole MRI protocol as the diagnostic tool for MSK infection in comparison with the clinical gold standard, p value is < 0.05.

There is good-excellent agreement between the readers and the clinical diagnoses based on the Kappa values in keeping with a high accuracy level.

The independent accuracy analysis of the single sequences including diffusion weighted and serial contrast enhanced sequences, based on Cohen's kappa test, have been presented in sections 4-4-5 and 5-3-5 of the previous chapters and evaluated in the discussions of chapters 4 and 5.

The following tables summarise the Cohen's kappa results of the single sequences based on 8 diagnostic categorise for comparison with the results of the whole protocol.

First readers' single sequences ~ clinical diagnosis	Kappa value	P value	Sensitivity	Specificity
T1 diagnoses ~ clinical diagnosis	0.617	<0.001	62.2%	96.8%
T2 fat sat diagnoses ~ clinical diagnosis	0.714	<0.001	75.7%	95.2%
DWI diagnoses ~ clinical diagnosis	0.647	<0.001	76%	90.3%
T1 fat sat serial contrast diagnoses ~ clinical diagnosis	0.723	<0.001	78.4%	95.1%

Table51. Accuracy test for single sequences' diagnoses with 8 diagnostic categorise for the first reader. The 95% confidence interval was 0.000-0.029 for all three sequences.

Second readers' single sequences ~ clinical diagnosis	Kappa value	P value	Sensitivity	Specificity
T1 diagnoses ~ clinical diagnosis	0.490	<0.001	40.5%	98%
T2 fat sat diagnoses ~ clinical diagnosis	0.717	<0.001	81.1%	93.7%
DWI diagnoses ~ clinical diagnosis	0.672	<0.001	78.4%	92%
T1 fat sat serial contrast diagnoses ~ clinical diagnosis	0.816	<0.001	91.9%	96.8%

Table52. Accuracy test for single sequences' diagnoses with 8 diagnostic categorise for the second reader. The 95% confidence interval Lower-upper bound = 0.000-0.029.

The Cohen's kappa tests indicate fair- excellent accuracy for the studies' sequences and good–excellent accuracy for the whole MRI protocol. The calculated results of the tables above are simplified in figure 27.

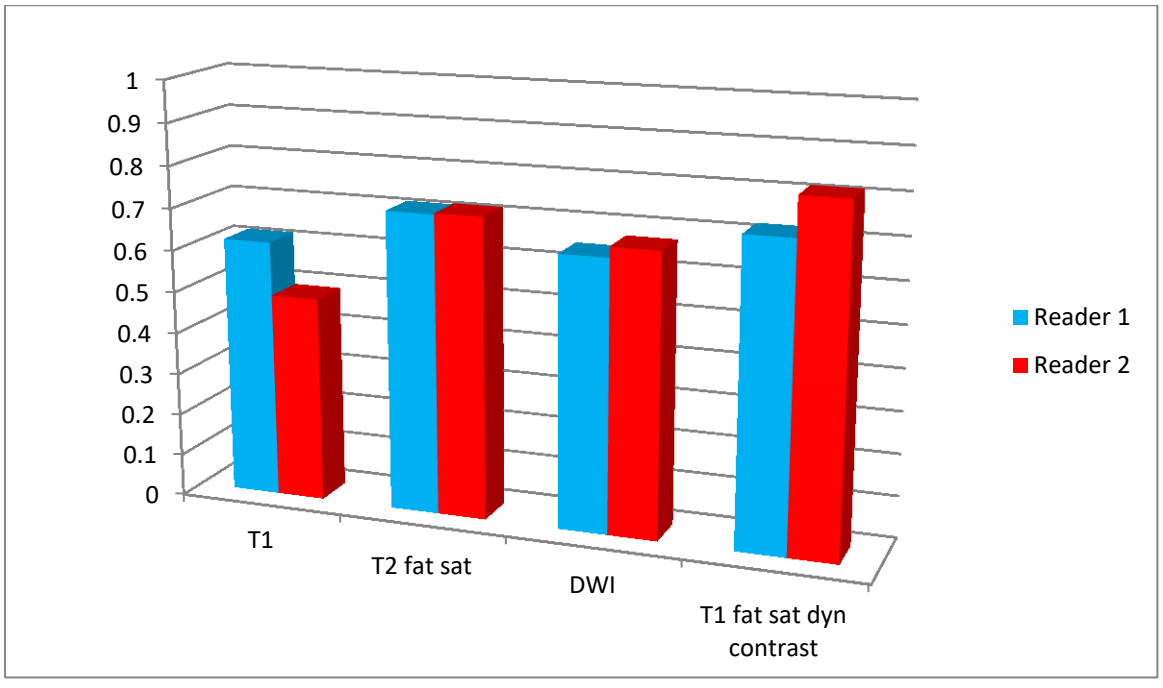

Fig. 27- Cohen's kappa values for the accuracy of single sequences of the readers

Figure 27 indicates indirectly the fine differences between the readers concerning their strengths or preferences. The preferences will be explored in the next section.

One additional Cohen's kappa test was performed to correlate the final diagnoses of the readers with each other. The correlation between the final diagnoses of the readers by means of Cohen's kappa test revealed similar results to the inter-observer agreement results in section 6-3-3 with a kappa value of 0.727 and a p value of 0.001 (sensitivity= %84 and specificity > %90 for MSK infection) in keeping with good correlation.

6-3-7 Diagnostic value of the study's sequences and their ranking:

The readers have evaluated subjectively the lesion conspicuity and the level of diagnostic confidence of the sequences of the study's protocol and were asked to score the conspicuity and the diagnostic confidence based on the qualitative information of the study's sequences (please see section 3-2-14-2-3 in chapter 3 for methodology). The scoring system was an attempt to produce numerical, semi-quantitative data, referring to subjective readers preferences. The conspicuity and the diagnostic confidence scores (semi quantitative data) of the study's sequences were compared to determine significant differences and a possible ranking for each scoring system and to define the most valuable sequence for the diagnosis of acute musculoskeletal infection in children based on the readers preference. The ADC, AUC and TME values and the related curves were not accessible to the readers, hence were not influential for the scoring and were separately analysed and described in the previous two chapters. The conspicuity and confidence scores of the DWI and SCE sequences with the relevant comparisons were already discussed in the previous two chapters in sections 4-4-6 and 5-3-6. In this chapter I will present the results of the conspicuity and diagnostic confidence scores of the remaining sequences including structural sequences and compare the results of the sequences with each other for each reader in order to create a comprehensive ranking for all sequences of the protocol.

6-3-7-1 Correlation based on Image conspicuity:

The conspicuity scores of the studies sequences were initially compared using a non-parametric multiple comparison test (Friedman ANOVA) for each reader, which demonstrated significant differences for both readers. Subsequently the conspicuity scores of the structural sequences were compared with each other and with the functional imaging sequences (DWI & SCE) for each reader using paired sample sign test, according to the methodology which was explained in section 3-2-14-2-3 in chapter 3, to find out where the significant differences lie. The functional imaging sequences related data has been already presented in the previous two chapters in sections 4-4-6-1 and 5-3-6-1.

The Friedman ANOVA tests results of the readers have been presented in table 21 (chapter 4, section 4-4-6-1).The descriptive statistics of the Friedman and paired sample sign analyses of the conspicuity scores are demonstrated in tables 19 and 20 and simplified in figure 8 in chapter 4. The descriptive statistic in tables 19 and 20 indicate the readers' preferences, concerning detectability of the sequences.

The results of the paired sample sign analyses of the structural sequences and a summary of their correlation with the functional sequences are presented in the following tables. The p value was 0.008 after Bonferroni adjustment, as there were 6 comparison groups for the four study sequences (see section 3-2-14-2-3 for methodology).

Paired groups	Sig. Sign test (2-tailed) = p value	Z score	Frequencies of the scores excluding the ties
T1 ~ DWI	<0.001	-4.002	DWI > T1 by 34 cases
T1 ~ T2 fat sat	<0.001	-3.506	T2 fat sat > T1 by 27 cases
T1 ~ T1 fat sat serial contrast	<0.001	-6.013	T1 fat sat serial contrast > T1 by 46 cases
T2 fat sat ~ DWI	0.480	-0.707	DWI > T2 fat sat by 6 cases
T2 fat sat ~ T1 fat sat serial contrast	0.005	-2.833	T1 fat sat serial contrast > T2 fat sat by 18 cases
DWI ~ T1 fat sat serial contrast	0.243	-1.167	T1 fat sat serial contrast > DWI by 9 cases

Table53. Paired sample Signe test results of the conspicuity scores with p values and frequency differences after exclusion of ties for the first reader, which shows by how many cases one sequence was preferred to the other sequence after exclusion of ties (Z score is the calculated statistical Magnitude of this difference).

	Sig. Sign test (2-tailed) = p value	Z score	Frequencies of the scores excluding the ties
T1 ~ DWI	0.008	-2.634	DWI > T1 by 25 cases
T1 ~ T2 fat sat	<0.001	-5.293	T2 fat sat > T1 by 42 cases
T1 ~ T1 fat sat serial contrast	<0.001	-6.625	T1 fat sat serial contrast > T1 by 54 cases
T2 fat sat ~ DWI	0.176	-1.354	T2 fat sat > DWI by 12 cases
T2 fat sat ~ T1 fat sat serial contrast	0.004	-2.864	T1 fat sat serial contrast > T2 fat sat by 20 cases
DWI ~ T1 fat sat serial contrast	0.001	-3.283	T1 fat sat serial contrast > DWI by 26 cases

Table54. Paired sample Signe test results of the conspicuity scores with p values and frequency differences after exclusion of ties for the second reader, which shows by how many cases one sequence was preferred to the other sequence after exclusion of ties (Z score is the calculated statistical Magnitude of this difference).

The results of the sign test corroborate the tendency outcomes of the descriptive part of the statistics (Tables 19 and 20).

The ranking of the first reader was as follows:

1- T1 fat sat serial contrast
2- DWI
3- T2 fat sat
4- T1

The p value was significant for all sequence combinations except for DWI - T2 fat sat and DWI – T1 fat sat serial contrast. The relationship between DWI and T2 fat sat sequences was similar to the relationship between DWI and T1 fat sat serial contrast enhanced sequences more in the form of a tendency, rather than a statistically significant difference.

The ranking of the second reader was statistically clearer, but the ranking was relatively similar to the first reader, which was the following:

1- T1 fat sat serial contrast
2- T2 fat sat
3- DWI
4- T1

The ranking of the second reader was statistically significant for all tests except for DWI – T2 fat sat combination with p values < 0.008. The difference between T2 fat sat and DWI sequences' scores are not significant and their relationship is more in the form of a tendency similar to the first reader.

The two readers' rankings can be summarised with reference to frequencies of the scores excluding the ties and the p values as follows:

1- T1 fat sat serial contrast
2- DWI and T2 fat sat (no significant statistical difference)
3- T1

The sign test results of the conspicuity scores reveal the preference of the readers concerning the detectability.

6-3-7-2 Correlation based on diagnostic confidence:

The diagnostic confidence score was not included in the pilot study's evaluation form and as a result the readers of the pilot study did not have the possibility to differentiate between lesion conspicuity or detectability and the differential diagnostic capability of the study's sequences. The diagnostic confidence scoring system was added to the main study's evaluation form as part of the modification of the study's

evaluation form prospectively. The diagnostic confidence score data is the second semi-quantitative data of the study's evaluation form and was analysed with Friedman ANOVA and paired sample sign tests to determine the relative diagnostic value of all study's sequences (reader's preference), following the methodology explained in section 3-2-14-2-3 in chapter 3.

The functional imaging sequences related data of the diagnostic confidence scores has already been presented in the previous two chapters in sections 4-4-6-2 and 5-3-6-2.

The Friedman test results are presented in table 26, chapter 4. The descriptive statistics of the diagnostic confidence Friedman and paired sample sign analyses are demonstrated in tables 24 and 25 and simplified in figure 9 in chapter 4.The descriptive statistics of the diagnostic confidence scores show a clear tendency, similar to conspicuity scores.

The results of the paired sample sign analyses of the structural sequences, including a summary of their correlation with the functional sequences are presented in the following tables. The p value was 0.008 (after Bonferroni adjustment).

	Sig. Sign test (2-tailed) = p value	Z score	Frequencies of the scores excluding the ties
T1 ~ DWI	0.001	-3.323	DWI > T1 by 28 cases
T1 ~ T2 fat sat	<0.001	-3.714	T2 fat sat > T1 by 27 cases
T1 ~ T1 fat sat serial contrast	<0.001	-6.281	T1 fat sat serial contrast > T1 by 48 cases
T2 fat sat ~ DWI	0.779	-0.280	T2 > DWI fat sat by 3 cases
T2 fat sat ~ T1 fat sat serial contrast	0.002	-3.082	T1 fat sat serial contrast > T2 fat sat by 20 cases
DWI ~ T1 fat sat serial contrast	0.002	-3.031	T1 fat sat serial contrast > DWI by 22 cases

Table55. Paired sample Sign test results of the diagnostic confidence scores with p values and frequency differences after exclusion of ties for the first

reader, which shows by how many cases one sequence was preferred to the other sequence after exclusion of ties (Z score is the calculated statistical Magnitude of this difference).

	Sig. Sign test (2-tailed) = p value	Z score	Frequencies of the scores excluding the ties
T1 ~ DWI	0.007	-2.700	DWI > T1 by 25 cases
T1 ~ T2 fat sat	<0.001	-4.609	T2 fat sat > T1 by 37 cases
T1 ~ T1 fat sat serial contrast	<0.001	-7.625	T1 fat sat serial contrast > T1 by 62 cases
T2 fat sat ~ DWI	0.160	-1.404	T2 fat sat > DWI by 13 cases
T2 fat sat ~ T1 fat sat serial contrast	<0.001	-4.472	T1 fat sat serial contrast > T2 fat sat by 31 cases
DWI ~ T1 fat sat serial contrast	<0.001	-4.642	T1 fat sat serial contrast > DWI by 39 cases

Table56. Paired sample Sign test results of the diagnostic confidence scores with p values and frequency differences after exclusion of ties for the second reader, which shows by how many cases one sequence was preferred to the other sequence after exclusion of ties (Z score is the calculated statistical Magnitude of this difference).

The results of the sign test follow the trend of the descriptive part of the statistics (Tables 24 & 25).

The sign tests of the diagnostic confidence scores were more conclusive than the conspicuity scores, with p values less than 0.008 except in one test. The ranking of both readers was similar and as follows:

1- T1 fat sat serial contrast
2- T2 fat sat

3- DWI
4- T1

However, the margins are different, this means, by how much one sequence is preferred to the other. The p values were all significant, except for the DWI-T2 fat sat paired sample sign test. The DWI and T2 fat sat sequences are very close, with very similar results and without statistically significant differences; hence the ranking could be modified as follows:

1- T1 fat sat serial contrast
2- DWI and T2 fat sat
3- T1

This ranking is identical to conspicuity score rankings.

The diagnostic confidence scores' sign tests not only exhibit the preferences of the readers, but also unveil the degree of reader's experience (level of confidence) concerning the study sequences.

6-3-8 Quantitative statistic and quantitative diagnostic thresholds:

One hundred and three MRI scans on ninety-nine children were performed. In total, eight cases were excluded for diffusion analysis and ninety-five DWI sequences, including multiple ADC measurements per scan were analysed. The main data ADC value analyses are presented and explained in details in chapter 4, section 4-4-7-1. In total 6 cases were excluded for serial contrast-enhanced analysis and ninety seven SCE sets of sequences, including multiple permeability measurements per scan, were analysed. The permeability values measurements, detailed analyses and related curves are presented in chapter 5, section 5-3-8-1.

6-3-8-1 Main data ADC value analysis:

Please refer to section 4-4-7 and 4-4-7-1.

6-3-8-2 Main data permeability value analysis:

Please refer to section 5-3-8 and 5-3-8-1.

6-4 Discussion:

Musculoskeletal infections continue to be responsible for substantial morbidity and mortality amongst children (3). New organisms with progressive virulence on the one hand and increasing antibiotic resistance, on the other hand, complicate the advances in diagnostic and treatment methods seen in recent years.

Sir Alexander Fleming predicted the current scenario in his Nobel prize lecture in December 1945, in that misuse (or widespread use) of antibiotics would educate the pathogens how to resist the toxic effects of antibiotics (164,165). While new treatment strategies are required to tackle increasing and changing infections; early diagnosis remains crucial to limit the damage, shorten the treatment and improve the prognosis.

Imaging has always been an important pillar of the diagnosis of musculoskeletal infection in children, and MRI has emerged as the imaging tool of choice for diagnostic and surgical guidance of paediatric MSK infection in recent decades (166,167). There have been many retrospective but few prospective studies evaluating aspects of magnetic resonance imaging for the diagnosis of MSK infection in children, however most of the studies have been limited by low patient numbers and are retrospective or not exclusively paediatric. There is lack of consensus amongst radiologists regarding a comprehensive standard MRI protocol for MSK infection in children.

This study is the first prospective and exclusively paediatric study evaluating the utility of conventional and functional MRI sequences, including DWI and SCE in musculoskeletal infection in children.

The clinical potential of magnetic resonance imaging in paediatric populations with suspected MSK infection, is to visualise the pathology, detect multifocal lesions and characterise biological specifications of the investigated tissue (76,84).

The descriptive statistics of the study cohort revealed the higher proportion of male patients in the MSK infection and the traumatic injury groups. The male dominance in these two groups was beyond the total male proportion in the study cohort. The dominance of male paediatric population in the traumatic injury group has been discussed in the past in the literature (19,chapter 170 & 172), and preceding injury has been suggested as a risk factor for MSK infections in many publications (4,17) in keeping with the study results. Infection was by far the most common pathology and nearly 46% of the total pathologies after deduction of normal cases.

The excellent feasibility results of this study confirm the outcomes of the few prospective studies performed in children(76,78,104,113).

The study's feasibility result is contrary to what has been postulated in some publications in the past which is that MRI examinations are not well tolerated by children and are less suitable for paediatric populations. In our experience initial assessment by a clinician and a play-specialist, strict assignment of children into different preparation pathways (see section 3-2-6-3) and intensive prospective preparation of the children age 5 and older, significantly improves patients' compliance and delivers similar feasibility results to adult studies.

The results of inter and intraobserver agreement tests were good or excellent (see 6-3-3). The experience of the radiologists was very important, to achieve good or excellent results based on the experience from the current study. The correlation between the readers' final diagnoses from the main study demonstrated similar results to inter and intraobserver agreement tests as highlighted in section 6-3-6.

The ROI's placed in this study for contrast enhancement and ADC measurements were hand drawn and the methodologies were explained in sections 3-2-12-1 and 3-2-12-2. The intraobserver agreement analyses of the manual ROI measurement for AUC, TME and ADC values were excellent. It has been postulated that hand drawn ROIs might be a source of potential error (80) due to inconsistency and hence automatic or semiautomatic ROI measurements should be preferred. Our consistency (intraobserver agreement) test results of the study's permeability and ADC measurements did not support such concerns, however the risk of

inconsistency definitely remains, especially if there are multiple operators (see also section 6-5, limitations).

The reference measurements of contrast enhancement and ADC values are not significantly different between scanners with varying magnetic fields, according to many previous studies (64,77,80,104,113,134,145,146), this finding correlates with my observation of the reference AUC, TME and ADC values between the study participants.

The information produced by the studies' sequences was classified into the three following groups:

1- Subjective, qualitative information
2- Objective, quantitative or semiquantitative measurements (ADC and permeability values)
3- Semi-quantitative, semi-objective information (conspicuity and confidence scores)

This classification was employed to create different types of data (categorical and numerical) and to use different statistical tests, in order to improve informational value and to clarify statistical test results.

The final clinical diagnoses (gold standard) were compared with the final diagnoses of the readers and the diagnoses based on the findings of single sequences by means of Cohen's kappa test to ascertain the level of accuracy of the study protocol and separately the single sequences.

There was good or excellent correlation between the readers' final diagnoses and the clinical gold-standard in keeping with high accuracy of the MRI protocol as an imaging tool. The correlation between the diagnoses of the single sequences and the final clinical gold standard was fair- excellent with a relative ranking between the sequences based on the extended results of the accuracy tests (Cohen's kappa) including sensitivity, specificity, significant level (p value) and 95% interval lower-upper bound. While diagnoses based on qualitative data of serial contrast-enhanced sequences provided the highest level of accuracy (excellent), the diagnoses based

on T1 sequences had the lowest (fair). The qualitative information derived from DWI and T2 fat sat sequences had displayed similarly good correlation with the gold-standard in keeping with relatively high accuracy.

T2 fat sat sequences are the most commonly used sequences for the diagnosis of musculoskeletal lesions in general, based on the water sensitivity and increased contrast through fat saturation, which can reveal fluid collection, oedema and tumour inhomogeneity and hence their position in the ranking.

DWI sequences in this study are diffusion sensitised T2 fat sat sequences. DWI sequences have lower resolution and signal to noise ratio (SNR) and higher level of susceptibility in comparison to T2 fat sat sequences. These characteristics are not beneficial, however the significantly higher contrast between pathological and normal tissue, due to diffusion properties equalise the above described shortcomings and the added information from ADC maps and the ADC values can probably underpin the potential predominance of the diffusion weighted sequences in comparison to conventional sequences.

The ADC maps are significantly helpful in differentiating malignant lesions from benign lesions and conditions including inflammation and infection; however the very low number of benign and malignant cases in this study has undermined this advantage of DWI sequences. The literature(75,76,142,143) suggests that ADC values in musculoskeletal infections are increased in comparison to normal or malignant tissue, which was seen in this studies ADC values. The accuracy tests in this study were based on only qualitative information of the DWI sequences; and the ADC values were not presented to the readers. The additive value of the quantitative information of the DWI sequences to the qualitative information would have probably improved the accuracy results of DWI sequences, this has been discussed in section 4-5 in chapter 4 and should be investigated in future studies.

The application and evaluation of DWI sequences are dependent on the experience of the reader and the frequency of clinical implementation as these sequences require a completely different type of signal evaluation and interpretation, hence the more experience the higher the accuracy and level of confidence.

T1 sequences are the only non-fat saturated sequences in the protocol and the signal characteristic is not water sensitive based on TE parameter of signals, but based on TR parameter. T1 sequences can detect and characterise pathologic signals which are not covered clearly by fat saturated or contrast enhanced sequences. The T1 sequences are most important for the study's protocol to detect bone marrow changes including infiltration, iron overloading, conversion or reconversion but also subtle fractures; however the low number of the above listed conditions in this study and the inherent limited or poor T1 contrast between normal and pathological tissue in musculoskeletal infections are the main reasons for suboptimal ranking of T1 sequences and their lower accuracy in comparison to other sequences.

T1 fat sat serial contrast-enhanced sequences displayed the highest level of accuracy (good-excellent) owing to their high spatial resolution, contrast enhancement of pathologies with the relevant surrounding oedema, depiction of abscesses and infarction. The serial contrast enhancement, the multiphase subtraction and the AUC and TME values derived from qualitative permeability maps have the potential to further improve the leading position of the SCE sequences and should be evaluated separately in future studies in order to quantify statistically the added value to the protocol.

In summary, the study's MRI protocol is a highly accurate tool and benefits from the positive complimentary effect of the single sequences, and while the different sequences are all necessary, DWI and SCE sequences with their qualitative and quantitative information resources are the most promising and versatile sequences.

It was important for this project to compare the different sequences of the study's protocol and evaluate the diagnostic value of the single sequences. The role of the scoring systems (conspicuity and diagnostic confidence) in the evaluation form was to deliver semiquantitative data based on subjective preferences of the readers to compare the diagnostic value of the qualitative information of the studies sequences for the readers.

Firstly, the conspicuity of lesions was scored for each sequence in order to assess the value of each sequence in detecting the lesions. The ratings of the readers concerning conspicuity of the lesions were similar, but with slightly different statistical significance (p value).

The results of the sign test that compared the conspicuity scores of the study's sequences revealed that the conspicuity of DWI sequences is statistically superior to T1 sequences. The conspicuity scores of the DWI and T2 fat saturated sequences were nearly equal without any statistical relevant differences (p value> 0.008). The conspicuity scores of T1 fat sat serial contrast enhanced sequences were higher than the other sequences, although the mean conspicuity score difference between DWI and T1 fat sat serial contrast enhanced sequences was statistically significant only by the second reader.

The possibly better conspicuity of DWI sequences in comparison to structural sequences was postulated in some previous studies to be due to lower resolution of the background bone marrow and surrounding tissue (64,76) and to a degree due to additional diffusion properties. This phenomenon was observed in multiple cases in this study, where DWI conspicuity was advanced in comparison to T2 fat sat, as scored by the first reader, and even in few cases in comparison to serial contrast enhanced sequences, however without statistical significance.

The sign test results of the conspicuity scores reveal the preference of the readers regarding detectability value of the sequences.

The diagnostic confidence score was the second type of scoring system used in the evaluation form, which was designed to evaluate the confidence of the readers based on the qualitative information of the sequences.

The sign tests of the diagnostic confidence scores were more conclusive than the conspicuity scores, however the margins are different meaning by how much one sequence is preferred to the other sequence. The p-values of the diagnostic confidence scores were all significant except the DWI-T2 fat sat paired sample sign test. The DWI and T2 fat sat sequences were very close with very similar results and without statistically significant differences.

The paired sign tests' results of the diagnostic confidence scores based on readers' preferences, when evaluating the qualitative information of the study's sequences have established the superiority of SCE sequences in comparison to the other sequences and equally the inferiority of T1 sequences. The DWI and T2 fat sat sequences were ranked in the middle with very similar results. The ranking of the confidence scores is identical to conspicuity score ranking.

The order of the sequences based on the sign tests' results of the conspicuity and confidence scores (see section 6-3-7-1 and 6-3-7-2) is also similar to the relative order of the sequences based on accuracy test results. The results of the accuracy tests of the readers are in a way confirming the readers' preferences regarding lesion conspicuity and diagnostic confidence.

The diagnostic confidence scores' sign tests not only exhibit the preferences of the readers, but also unveil the degree of reader's experience concerning the study sequences.

Differentiating between conspicuity and diagnostic confidence scores was not always straightforward for the readers, for example one of the reasons for high T2 fat sat rating in diagnostic confidence score ranking, in some cases, was their outstanding performance in detecting lesions (conspicuity) rather their contribution to final differential diagnoses. This was highlighted in the final interview with the readers.

Quantification of MRI signal changes with relevant translation in imaging diagnosis started decades ago(58,59,100,102) and the current move to try to use artificial intelligence in imaging diagnosis has highlighted its importance.

The distribution of the ADC values in this study is encouraging, as it confirms the findings of several previous publications(75,76,142,143), which have demonstrated that ADC values are increased in MSK infection in comparison to most other pathologies and normal bone, however statistically significant ADC thresholds for MSK infection could not be delivered based on ROC curve analysis. The distribution of the ADC values, which have been discussed in section 4-5 (please also see table 28 and fig. 17), are more in keeping with a trend rather statistically significant distinctive thresholds. There are a number of possible explanations which have been

presented in section 4-5 and 4-6, including the limited total number of patients and particularly the significantly low number of benign and malignant lesions (below the detection level of the ROC analysis). The main strength of ADC maps and ADC values is to differentiate between malignant and benign conditions, hence future studies with larger population and a more balanced number of different pathologies would most likely better demonstrate the merit of ADC values and maps beyond the qualitative information of DWI sequences.

The qualitative information of the SCE sequences was sufficient enough to promote serial contrast enhanced sequences to the first place in accuracy and subjective preference analyses (see results in chapter 5). There was however further diagnostic information derived from SCE sequences which have not been assessed separately or systematically in this study or the information was not available to the readers and was separately evaluated. Multiphase subtraction has enriched the variety of information delivered by SCE sequences and improved diagnostic differentiation of hyperaemic lesion's and conspicuity in small or multifocal processes in line with the literature(103,107,162,163). There are other advantages of multiphase subtractions which were not separately evaluated but as part of the SCE sequences, and have been discussed in more details in section 5-4 of chapter 5.

The semiquantitative parameters of the signal intensity curves of the SCE sequences were analysed via ROC curves and whilst it is promising that one of the tests (synovial infection ROC test) revealed statistically significant results, the remaining tests concerning MSK infections did not show relevant statistical results, hence the results should be considered with caution (for more details see section 5-4). The signal intensity curves were not included in the initial systematic analysis of the study but were found useful during the measurement process of the AUC and TME parameters, in line with some previous publications(104,155). These additional sources of information of SCE sequences should be evaluated separately in future studies in order to quantify statistically their added value to the protocol.

There remain important learning points for clinical radiologists, in order to use the full capacity of DWI and SCE sequences, even for experienced radiologists.

6-5 Limitations:

There are several limitations in this study which are the following:

1- Single site study design
2- Small patient population, which effects the significance of test statistics
3- Large age range of the participants and the consecutive considerable variation of bone marrow conversion, which affects the signal characteristics of the studies sequences
4- Inhomogeneity of participants regarding pre-existing chronic bone marrow abnormalities and altered ADC and possibly contrast enhancement values of normal bone marrow, which can potentially cause misinterpretations
5- ADC map calculations were based on only two ADC values, which may have influenced the accuracy of ADC values or neglected the perfusion or diffusion components of the signal
6- High number of pathologies
7- Low number of cases in some of the pathologies such as trauma and malignant cases
8- The risk of selectivity of hand-drawn ROIs.

All study's patients were admitted with acute pain and a suspected diagnosis of acute MSK infection; however the infection processes were in slightly different phases based on potential delays before admission.

This could have influenced the ADC, AUC and TME values based on cellularity, water and fat content in the region of interest.

6-6 Conclusion:

The diagnosis of musculoskeletal infection in children remains a clinical challenge and while the common pathogens, their frequency and virulence are changing, the current imaging strategies and pathways have not matched these changes. A more comprehensive imaging approach is required to tackle these challenges in a more sophisticated manner.

The current study has revealed that a comprehensive MRI protocol with advanced MRI techniques and inclusion of qualitative and quantitative tools can provide a feasible and accurate tool for the diagnosis of musculoskeletal infection in children. The study has equally demonstrated the defaults, limitations and difficulties in the acute clinical setting to pursue clinical research and to introduce different ways of imaging.

This was the first prospective and exclusively paediatric study to assess the utility of tailored conventional MRI sequences in conjunction with molecular and bio-imaging techniques including DWI and SCE in paediatric musculoskeletal infection and the results have proven to be promising and encouraging for future studies.

The study's MRI protocol is a feasible and accurate tool which has the potential to detect and differentiate musculoskeletal infections with sufficient accuracy.

Chapter 7: What has been learned and future development

The initial idea for this study was to design a feasible and accurate imaging diagnostic tool for musculoskeletal infection in children, and the driving motivation was to address the ongoing struggle with existing imaging tools and suboptimal outcomes.

The main learning points of the study are summarised below in this concluding short chapter.

The evolution of the study has exposed a few study design limitations which were listed in section 6-5 of the previous chapter. These limitations have highlighted the importance of a comprehensive prospective study design.

The design of the statistical tests of the study was prospective and sufficient to cover the main calculations, but this had to be amended during the study to accommodate the finer details, which were not considered initially, and had significantly prolonged the process of the statistical calculations. A well thought through prospective statistical design is crucial for outcomes and significantly saves time.

The initial evaluation form was amended after the pilot study and based on the interviews with the readers and whilst the outcome was a more comprehensive form addressing different aspects of the study protocol in more details, it increased significantly the volume of the produced data. The volume of varying type of data prolonged the process of statistical calculation, and complicated the concluding aspect of the thesis write up.

The technical challenges presented during the course of the study, specifically those concerning the study's sequences and the processing of advanced software, have revealed the importance of deep technical knowledge about; the chosen sequences; the specifications of the scanners; and the capability and compatibility of the processing softwares.

These challenges have prolonged the course of the data processing phase and resulted in forced exclusion of aspects of the data concerning functional imaging sequences. These aspects have already been discussed in chapters 5 and 6.

This study has however demonstrated that a balanced combination of complementary MR sequences can improve the diagnostic yield of the single components and create a feasible and accurate imaging diagnostic tool for the diagnosis of Paediatric MSK infection.

The study's findings and limitations warrant further more multicentre studies, perhaps with a larger sample size, enhanced statistical power, fine-tuned techniques and software for the quantitative aspect of the protocol to improve the performance of the study's sequence combination.

Bibliography

1. Mccarthy JJ, Dormans JP, Kozin SH, Pizzutillo PD. Musculoskeletal Infections in Children BASIC TREATMENT PRINCIPLES AND RECENT ADVANCEMENTS [Internet]. Vol. 86. [cited 2019 Feb 16]. Available from: https://teleducacion.medicinaudea.co/pluginfile.php/50328/mod_resource/content/2/Infecciones ME en niños.pdf

2. Nelson JD. Skeletal infections in children. Adv Pediatr Infect Dis [Internet]. 1991 [cited 2019 Feb 16];6:59–78. Available from: http://www.ncbi.nlm.nih.gov/pubmed/2054120

3. Guillerman RP. Osteomyelitis and beyond. Pediatr Radiol [Internet]. 2013 Mar 12 [cited 2019 Feb 16];43(S1):193–203. Available from: http://link.springer.com/10.1007/s00247-012-2594-9

4. Offiah AC. Acute osteomyelitis, septic arthritis and discitis: Differences between neonates and older children. Eur J Radiol [Internet]. 2006 [cited 2019 Feb 16];60:221–32. Available from: https://pdfs.semanticscholar.org/497b/5973e5bf722dd9bf21568b92e518288ddedd.pdf

5. Faust SN, Clark J, Pallett A, Clarke NMP. Managing bone and joint infection in children. Arch Dis Child [Internet]. 2012 Jun [cited 2019 Feb 16];97(6):545–53. Available from: http://www.ncbi.nlm.nih.gov/pubmed/22440930

6. van Schuppen J, van Doorn MMAC, van Rijn RR. Childhood osteomyelitis: imaging characteristics. Insights Imaging [Internet]. 2012 Oct [cited 2019 Feb 16];3(5):519–33. Available from: http://www.ncbi.nlm.nih.gov/pubmed/22875760

7. Peltola H, Pääkkönen M. Acute Osteomyelitis in Children. N Engl J Med [Internet]. 2014 Jan 23 [cited 2019 Mar 31];370(4):352–60. Available from: http://www.nejm.org/doi/10.1056/NEJMra1213956

8. Dodwell ER. Osteomyelitis and septic arthritis in children. Curr Opin Pediatr [Internet]. 2013 Feb [cited 2019 Mar 31];25(1):58–63. Available from: http://www.ncbi.nlm.nih.gov/pubmed/23283291

9. Arnold JC, Bradley JS. Osteoarticular Infections in Children. Infect Dis Clin North Am [Internet]. 2015 Sep [cited 2019 Mar 31];29(3):557–74. Available from: http://www.ncbi.nlm.nih.gov/pubmed/26311358

10. Jaramillo D, Dormans JP, Delgado J, Laor T, St Geme JW. Hematogenous Osteomyelitis in Infants and Children: Imaging of a Changing Disease. Radiology [Internet]. 2017 Jun [cited 2019 Mar 31];283(3):629–43. Available from: http://www.ncbi.nlm.nih.gov/pubmed/28514223

11. Frank G, Mahoney HM, Eppes SC. Musculoskeletal Infections in Children. Pediatr Clin North Am [Internet]. 2005 Aug [cited 2019 Mar 31];52(4):1083–106. Available from:

https://linkinghub.elsevier.com/retrieve/pii/S0031395505000751

12. Kao H-C, Huang Y-C, Chiu C-H, Chang L-Y, Lee Z-L, Chung P-W, et al. Acute hematogenous osteomyelitis and septic arthritis in children. J Microbiol Immunol Infect [Internet]. 2003 Dec [cited 2019 Feb 16];36(4):260–5. Available from: http://www.ncbi.nlm.nih.gov/pubmed/14723255

13. Pineda C, Vargas A, Rodríguez AV. Imaging of Osteomyelitis: Current Concepts. Infect Dis Clin North Am [Internet]. 2006 Dec [cited 2019 Feb 16];20(4):789–825. Available from: http://www.ncbi.nlm.nih.gov/pubmed/17118291

14. Dahl LB, Høyland AL, Dramsdahl H, Kaaresen PI. Acute osteomyelitis in children: a population-based retrospective study 1965 to 1994. Scand J Infect Dis [Internet]. 1998 [cited 2019 Feb 16];30(6):573–7. Available from: http://www.ncbi.nlm.nih.gov/pubmed/10225385

15. Riise ØR, Kirkhus E, Handeland KS, Flatø B, Reiseter T, Cvancarova M, et al. Childhood osteomyelitis-incidence and differentiation from other acute onset musculoskeletal features in a population-based study. BMC Pediatr [Internet]. 2008 Oct 20 [cited 2019 Feb 16];8(1):45. Available from: https://bmcpediatr.biomedcentral.com/articles/10.1186/1471-2431-8-45

16. Gafur OA, Copley LAB, Hollmig ST, Browne RH, Thornton LA, Crawford SE. The Impact of the Current Epidemiology of Pediatric Musculoskeletal Infection on Evaluation and Treatment Guidelines. J Pediatr Orthop [Internet]. 2008 Oct [cited 2019 Mar 31];28(7):777–85. Available from: http://www.ncbi.nlm.nih.gov/pubmed/18812907

17. Cunnington A, Brick T, Cooper M, Danin J, Hunt D, Jeanes A, et al. Severe invasive Panton-Valentine Leucocidin positive Staphylococcus aureus infections in children in London, UK. J Infect [Internet]. 2009 Jul 1 [cited 2019 Feb 14];59(1):28–36. Available from: https://www.sciencedirect.com/science/article/abs/pii/S0163445309001522

18. Peltola H, Pääkkönen M, Kallio P, Kallio MJT, Osteomyelitis-Septic Arthritis Study Group. Short- Versus Long-term Antimicrobial Treatment for Acute Hematogenous Osteomyelitis of Childhood. Pediatr Infect Dis J [Internet]. 2010 Dec [cited 2019 Feb 16];29(12):1123–8. Available from: http://www.ncbi.nlm.nih.gov/pubmed/20842069

19. Thomas L. Slovis. Caffey's Pediatric Diagnostic Imaging, 11th ed. 2-Vol. Set. Am J Neuroradiol [Internet]. 2008 Aug 1 [cited 2019 Feb 16];29(7):e63–e63. Available from: http://www.ajnr.org/lookup/doi/10.3174/ajnr.A1024

20. Connolly SA, Connolly LP, Drubach LA, Zurakowski D, Jaramillo D. MRI for Detection of Abscess in Acute Osteomyelitis of the Pelvis in Children. Am J Roentgenol [Internet]. 2007 Oct 23 [cited 2019 Feb 16];189(4):867–72. Available from: http://www.ajronline.org/doi/10.2214/AJR.07.2416

21. Castellazzi L, Mantero M, Esposito S. Update on the Management of Pediatric

Acute Osteomyelitis and Septic Arthritis. Int J Mol Sci [Internet]. 2016 Jun 1 [cited 2019 Mar 31];17(6). Available from: http://www.ncbi.nlm.nih.gov/pubmed/27258258

22. Haney Carr J, Hageman J. Guidance on the diagnosis and management of PVL-associated Staphylococcus aureus infections (PVL-SA) in England, 2 nd Edition [Internet]. [cited 2019 Feb 17]. Available from: https://assets.publishing.service.gov.uk/government/uploads/system/uploads/attachment_data/file/322857/Guidance_on_the_diagnosis_and_management_of_PVL_associated_SA_infections_in_England_2_Ed.pdf

23. Gillet Y, Issartel B, Vanhems P, Fournet J-C, Lina G, Bes M, et al. Association between Staphylococcus aureus strains carrying gene for Panton-Valentine leukocidin and highly lethal necrotising pneumonia in young immunocompetent patients. Lancet (London, England) [Internet]. 2002 Mar 2 [cited 2019 Feb 17];359(9308):753–9. Available from: http://www.ncbi.nlm.nih.gov/pubmed/11888586

24. Bhattacharya D, Carleton H, Tsai CJ, Baron EJ, Perdreau-Remington F. Differences in clinical and molecular characteristics of skin and soft tissue methicillin-resistant Staphylococcus aureus isolates between two hospitals in Northern California. J Clin Microbiol [Internet]. 2007 Jun [cited 2019 Feb 17];45(6):1798–803. Available from: http://www.ncbi.nlm.nih.gov/pubmed/17409211

25. Helgason KO, Jones ME, Edwards G. Panton-valentine leukocidin-positive Staphylococcus aureus and foreign travel. J Clin Microbiol [Internet]. 2008 Feb [cited 2019 Feb 17];46(2):832–3. Available from: http://www.ncbi.nlm.nih.gov/pubmed/18077637

26. Averill LW, Hernandez A, Gonzalez L, Peña AH, Jaramillo D. Diagnosis of Osteomyelitis in Children: Utility of Fat-Suppressed Contrast-Enhanced MRI. Am J Roentgenol [Internet]. 2009 May 23 [cited 2019 Feb 17];192(5):1232–8. Available from: http://www.ajronline.org/doi/10.2214/AJR.07.3400

27. Frush DP, Heyneman LE, Ware RE, Bissett GS. MR features of soft-tissue abnormalities due to acute marrow infarction in five children with sickle cell disease. AJR Am J Roentgenol [Internet]. 1999 Oct 19 [cited 2019 Feb 14];173(4):989–93. Available from: http://www.ncbi.nlm.nih.gov/pubmed/10511164

28. Moumile K, Merckx J, Glorion C, Pouliquen J, Berche P, Ferroni A. Bacterial aetiology of acute osteoarticular infections in children. Acta Paediatr [Internet]. 2007 Jan 2 [cited 2019 Feb 17];94(4):419–22. Available from: http://doi.wiley.com/10.1111/j.1651-2227.2005.tb01911.x

29. Goergens E, McEvoy A, Watson M, Barrett I. Acute osteomyelitis and septic arthritis in children. J Paediatr Child Health [Internet]. 2005 Jan 1 [cited 2019 Feb 17];41(1–2):59–62. Available from: http://doi.wiley.com/10.1111/j.1440-1754.2005.00538.x

30. Pugmire BS, Shailam R, Gee MS. Role of MRI in the diagnosis and treatment of osteomyelitis in pediatric patients. World J Radiol [Internet]. 2014 [cited 2019 Mar 31];6(8):530. Available from: http://www.wjgnet.com/1949-8470/full/v6/i8/530.htm

31. Lee YJ, Sadigh S, Mankad K, Kapse N, Rajeswaran G. The imaging of osteomyelitis. Quant Imaging Med Surg [Internet]. 2016 Apr [cited 2019 Mar 31];6(2):184–98. Available from: http://www.ncbi.nlm.nih.gov/pubmed/27190771

32. Harris JC, Caesar DH, Davison C, Phibbs R, Than MP. Review article: How useful are laboratory investigations in the Emergency Department evaluation of possible osteomyelitis? Emerg Med Australas [Internet]. 2011 Jun [cited 2019 Mar 31];23(3):317–30. Available from: http://www.ncbi.nlm.nih.gov/pubmed/21668719

33. Kallio MJ, Unkila-Kallio L, Aalto K, Peltola H. Serum C-reactive protein, erythrocyte sedimentation rate and white blood cell count in septic arthritis of children. Pediatr Infect Dis J [Internet]. 1997 Apr [cited 2019 Feb 17];16(4):411–3. Available from: http://www.ncbi.nlm.nih.gov/pubmed/9109146

34. de Graaf H, Sukhtankar P, Arch B, Ahmad N, Lees A, Bennett A, et al. Duration of intravenous antibiotic therapy for children with acute osteomyelitis or septic arthritis: a feasibility study. Health Technol Assess (Rockv) [Internet]. 2017 Sep [cited 2019 Feb 17];21(48):1–164. Available from: https://www.journalslibrary.nihr.ac.uk/hta/hta21480

35. Verdier I, Gayet-Ageron A, Ploton C, Taylor P, Benito Y, Freydiere A-M, et al. Contribution of a Broad Range Polymerase Chain Reaction to the Diagnosis of Osteoarticular Infections Caused by Kingella kingae. Pediatr Infect Dis J [Internet]. 2005 Aug [cited 2019 Feb 17];24(8):692–6. Available from: https://insights.ovid.com/crossref?an=00006454-200508000-00007

36. Rosey A-L, Abachin E, Quesnes G, Cadilhac C, Pejin Z, Glorion C, et al. Development of a broad-range 16S rDNA real-time PCR for the diagnosis of septic arthritis in children. J Microbiol Methods [Internet]. 2007 Jan 1 [cited 2019 Feb 17];68(1):88–93. Available from: https://www.sciencedirect.com/science/article/pii/S0167701206001965

37. Connolly LP, Connolly SA, Drubach LA, Jaramillo D, Treves ST. Acute Hematogenous Osteomyelitis of Children: Assessment of Skeletal Scintigraphy-Based Diagnosis in the Era of MRI [Internet]. [cited 2019 Feb 18]. Available from: http://jnm.snmjournals.org/content/43/10/1310.full.pdf

38. Laor T, Jaramillo D. MR Imaging Insights into Skeletal Maturation: What Is Normal? Radiology [Internet]. 2009 Jan 1 [cited 2019 Feb 19];250(1):28–38. Available from: http://pubs.rsna.org/doi/10.1148/radiol.2501071322

39. Lew DP, Waldvogel FA. Osteomyelitis. Lancet (London, England) [Internet]. 2004 Jul 24 [cited 2019 Apr 1];364(9431):369–79. Available from: http://www.ncbi.nlm.nih.gov/pubmed/15276398

40. Capitanio MA, Kirkpatrick JA. EARLY ROENTGEN OBSERVATIONS IN ACUTE OSTEOMYELITIS* [Internet]. [cited 2020 Jan 26]. Available from: www.ajronline.org

41. Jaramillo D. Infection: Musculoskeletal. Vol. 41, Pediatric Radiology. Springer; 2011. p. 127–34.

42. Steer AC, Carapetis JR. Acute hematogenous osteomyelitis in children: Recognition and management [Internet]. Vol. 6, Pediatric Drugs. 2004 [cited 2020 Apr 28]. p. 333–46. Available from: https://reference.medscape.com/medline/abstract/15612835

43. Smith BJ, Buchanan GS, Shuler FD. A comparison of imaging modalities for the diagnosis of osteomyelitis. Marshall J Med [Internet]. 2016 [cited 2019 Apr 1];2(3):10. Available from: http://mds.marshall.edu/mjmDOI:http://dx.doi.org/10.18590/mjm.2016.vol2.iss3.10Availableat:http://mds.marshall.edu/mjm/vol2/iss3/10

44. Pineda C, Espinosa R, Pena A. Radiographic Imaging in Osteomyelitis: The Role of Plain Radiography, Computed Tomography, Ultrasonography, Magnetic Resonance Imaging, and Scintigraphy. Semin Plast Surg. 2009 May;23(02):080–9.

45. Harcke HT, Grissom LE, Finkelstein MS. Evaluation of the musculoskeletal system with sonography. AJR Am J Roentgenol [Internet]. 1988 Jun 23 [cited 2019 Feb 19];150(6):1253–61. Available from: http://www.ncbi.nlm.nih.gov/pubmed/3285648

46. Malcius D, Jonkus M, Kuprionis G, Maleckas A, Monastyreckienė E, Uktveris R, et al. The accuracy of different imaging techniques in diagnosis of acute hematogenous osteomyelitis. Medicina (B Aires). 2009 Aug 9;45(8):624.

47. Karmazyn B, Kim JY, Jaramillo D. Imaging of hematogenous osteomyelitis and septic arthritis in children. In: Evidence-Based Imaging in Pediatrics: Optimizing Imaging in Pediatric Patient Care. Springer New York; 2010. p. 245–58.

48. Mettler FA, Guiberteau MJ. Essentials of nuclear medicine imaging [Internet]. Elsevier/Saunders; 2012 [cited 2019 Apr 2]. 607 p. Available from: https://www.sciencedirect.com/book/9781455701049/essentials-of-nuclear-medicine-imaging

49. Termaat MF, Raijmakers PGHM, Scholten HJ, Bakker FC, Patka P, Haarman HJTM. The Accuracy of Diagnostic Imaging for the Assessment of Chronic Osteomyelitis: A Systematic Review and Meta-Analysis. J Bone Jt Surg [Internet]. 2005 Nov 1 [cited 2019 Apr 2];87(11):2464. Available from: http://www.ncbi.nlm.nih.gov/pubmed/16264122

50. Kan JH, Young RS, Yu C, Hernanz-Schulman M. Clinical impact of gadolinium in the MRI diagnosis of musculoskeletal infection in children. Pediatr Radiol [Internet]. 2010 Jul 24 [cited 2019 Apr 2];40(7):1197–205. Available from:

http://www.ncbi.nlm.nih.gov/pubmed/20180105

51. Browne LP, Guillerman RP, Orth RC, Patel J, Mason EO, Kaplan SL. Community-acquired staphylococcal musculoskeletal infection in infants and young children: Necessity of contrast-enhanced MRI for the diagnosis of growth cartilage involvement. Am J Roentgenol. 2012 Jan;198(1):194–9.

52. Karmazyn B. Imaging approach to acute hematogenous osteomyelitis in children: An update. Semin Ultrasound, CT MRI. 2010 Apr;31(2):100–6.

53. Harik NS, Smeltzer MS. Management of acute hematogenous osteomyelitis in children [Internet]. Vol. 8, Expert Review of Anti-Infective Therapy. Expert Reviews Ltd.; 2010 [cited 2020 Aug 16]. p. 175–81. Available from: /pmc/articles/PMC2836799/?report=abstract

54. Beltran J, Noto AM, McGhee RB, Freedy RM, McCalla MS. Infections of the musculoskeletal system: high-field-strength MR imaging. Radiology [Internet]. 1987 Aug 1 [cited 2019 Apr 3];164(2):449–54. Available from: http://www.ncbi.nlm.nih.gov/pubmed/3602386

55. Weishaupt D, Köchli VD, Marincek B. How does MRI work? : an introduction to the physics and function of magnetic resonance imaging [Internet]. Springer; 2003 [cited 2019 Mar 11]. 138 p. Available from: https://books.google.co.uk/books/about/How_does_MRI_work.html?id=-Dbxa-prLvIC

56. K.Subhawong, Michael A Jacobs LMF. Diffusion-weighted MR Imaging for Characterizing Musculoskeletal Lesions 1. RadioGraphics [Internet]. 2014 [cited 2019 Mar 10]; Available from: www.rsna.org/rsnarights.

57. Khoo MMY, Tyler PA, Saifuddin A, Padhani AR. Diffusion-weighted imaging (DWI) in musculoskeletal MRI: a critical review. Skeletal Radiol [Internet]. 2011 Jun 12 [cited 2019 Mar 10];40(6):665–81. Available from: http://link.springer.com/10.1007/s00256-011-1106-6

58. Paul S. Tofts. T1-weighted DCE Imaging Concepts: Modelling, Acquisition and Analysis [Internet]. Brighton; 2010 [cited 2019 Apr 23]. Available from: www.siemens.com/magnetom-world

59. Tofts PS. Modeling tracer kinetics in dynamic Gd-DTPA MR imaging. J Magn Reson Imaging [Internet]. [cited 2019 May 8];7(1):91–101. Available from: http://www.ncbi.nlm.nih.gov/pubmed/9039598

60. Kwee TC, Takahara T, Ochiai R, Nievelstein RAJ, Luijten PR. MAGNETIC RESONANCE Diffusion-weighted whole-body imaging with background body signal suppression (DWIBS): features and potential applications in oncology. Eur Radiol. 2008;18:1937–52.

61. Paul Flowers KT& RL. 2.1: Brownian Motion - Evidence for Atoms - Chemistry LibreTexts [Internet]. General Chemistry at OpenStax CNX. 2018 [cited 2019 Mar 10]. Available from:

https://chem.libretexts.org/Bookshelves/General_Chemistry/Map%3A_A_Molecular_Approach_(Tro)/02%3A_Atoms_and_Elements/2.1%3A_Brownian_Motion_-_Evidence_for_Atoms

62. Einstein A, Cowper AD. INVESTIGATIONS O N THE THEORY .OF ,THE BROWNIAN MOVEMENT R. F ü R T H TRANSLATED BY [Internet]. [cited 2019 Mar 10]. Available from: http://users.physik.fu-berlin.de/~kleinert/files/eins_brownian.pdf

63. Dietrich O, Biffar A, Reiser MF, Baur-Melnyk A. Diffusion-weighted imaging of bone marrow. Semin Musculoskelet Radiol [Internet]. 2009 [cited 2019 Mar 10];13(2):134–44. Available from: http://dx.doi.org/10.1055/s-0029-1220884

64. Neubauer H, Evangelista L, Morbach H, Girschick H, Prelog M, Köstler H, et al. Diffusion-weighted MRI of bone marrow oedema, soft tissue oedema and synovitis in paediatric patients: feasibility and initial experience. Pediatr Rheumatol Online J [Internet]. 2012 Jul 31 [cited 2019 Mar 10];10(1):20. Available from: http://www.ncbi.nlm.nih.gov/pubmed/22849717

65. Le Bihan D. Molecular diffusion, tissue microdynamics and microstructure. NMR Biomed [Internet]. [cited 2019 Mar 10];8(7–8):375–86. Available from: http://www.ncbi.nlm.nih.gov/pubmed/8739274

66. Dallaudière B, Lecouvet F, Berg B Vande, Omoumi P, Perlepe V, Cerny M, et al. Diffusion-weighted MR imaging in musculoskeletal diseases: Current concepts. Diagn Interv Imaging [Internet]. 2015 [cited 2019 Mar 10];96:327–40. Available from: http://dx.doi.org/10.1016/j.diii.2014.10.008

67. Bloch ' F, Hahn ; E L. Spin Echoes*t [Internet]. Vol. 70, Phys. Rev. 1946 [cited 2019 Mar 10]. Available from: https://www.physics.rutgers.edu/grad/506/Hahn_PR80.pdf

68. Stejskal EO, Tanner JE. Spin Diffusion Measurements: Spin Echoes in the Presence of a Time Dependent Field Gradient. Cit J Chem Phys [Internet]. 1965 [cited 2019 Mar 10];42:288. Available from: http://mriquestions.com/uploads/3/4/5/7/34572113/stejskal_and_tanner1965.pdf

69. Klaus-Dietmarmerboldt, Jensfrahm. Self-Diffusion NMR Imaging Using Stimulated Echoes [Internet]. Vol. 64, JOURNAL OF MAGNETIC RESONANCE. 1985 [cited 2019 Mar 12]. Available from: https://bayes.wustl.edu/Manual/SelfDiffusion.pdf

70. Taylor DG, Bushell MC. The spatial mapping of translational diffusion coefficients by the NMR imaging technique. Phys Med Biol [Internet]. 1985 Apr 1 [cited 2019 Mar 12];30(4):345–9. Available from: http://stacks.iop.org/0031-9155/30/i=4/a=009?key=crossref.1149643d9bb1ec0159f28e3beda85a39

71. Le Bihan D, Breton E. MR Imaging of Intravoxel Incoherent Motions: Application to Diffusion and Perfusion in Neurologic Disorders' [Internet]. [cited 2019 Mar 12]. Available from:

https://mriquestions.com/uploads/3/4/5/7/34572113/dlbihanradiology1986.pdf

72. Gyngell ML. The application of steady-state free precession in rapid 2DFT NMR imaging: FAST and CE-FAST sequences. Magn Reson Imaging. 1988 Jul 1;6(4):415–9.

73. Bruder H, Fischer H, Graumann R, Deimling M. A new steady-state imaging sequence for simultaneous acquisition of two MR images with clearly different contrasts. Magn Reson Med [Internet]. 1988 May 1 [cited 2020 May 9];7(1):35–42. Available from: http://doi.wiley.com/10.1002/mrm.1910070105

74. MacKenzie JD, Gonzalez L, Hernandez A, Ruppert K, Jaramillo D. Diffusion-weighted and diffusion tensor imaging for pediatric musculoskeletal disorders. Pediatr Radiol [Internet]. 2007 Jul 9 [cited 2019 Feb 24];37(8):781–8. Available from: http://link.springer.com/10.1007/s00247-007-0517-y

75. Nonomura Y, Yasumoto M, Yoshimura R, Haraguchi K, Ito S, Akashi T, et al. Relationship between bone marrow cellularity and apparent diffusion coefficient. J Magn Reson Imaging [Internet]. 2001 May [cited 2019 Mar 26];13(5):757–60. Available from: http://www.ncbi.nlm.nih.gov/pubmed/11329198

76. Leclair N, Thörmer G, Sorge I, Ritter L, Schuster V, Hirsch FW. Whole-Body Diffusion-Weighted Imaging in Chronic Recurrent Multifocal Osteomyelitis in Children. PLoS One [Internet]. 2016 [cited 2019 Mar 13];11(1):e0147523. Available from: http://www.ncbi.nlm.nih.gov/pubmed/26799970

77. Neubauer H. World Journal of Pediatrics. World J Pediatr [Internet]. 2012 [cited 2019 Mar 13];8(4). Available from: www.wjpch.com

78. Barendregt AM, Charlotte Van Gulik E, Lavini C, Nusman CM, Merlijn Van Den Berg & J, Schonenberg-Meinema D, et al. Diffusion-weighted imaging for assessment of synovial inflammation in juvenile idiopathic arthritis: a promising imaging biomarker as an alternative to gadolinium-based contrast agents. [cited 2019 Mar 13]; Available from: https://link.springer.com/content/pdf/10.1007%2Fs00330-017-4876-y.pdf

79. Mulkern R V, Schwartz RB. In re: characterization of benign and metastatic vertebral compression fractures with quantitative diffusion MR imaging. AJNR Am J Neuroradiol [Internet]. 2003 Aug 1 [cited 2019 Mar 13];24(7):1489–90; author reply 1490-1. Available from: http://www.ncbi.nlm.nih.gov/pubmed/12917152

80. MacKenzie JD, Hernandez A, Pena A, Ruppert K, Khrichenko D, Gonzalez L, et al. Magnetic resonance imaging in children with sickle cell disease—detecting alterations in the apparent diffusion coefficient in hips with avascular necrosis. Pediatr Radiol [Internet]. 2012 Jun 27 [cited 2019 Mar 13];42(6):706–13. Available from: http://link.springer.com/10.1007/s00247-011-2327-5

81. Yoo WJ, Kim Y-J, Menezes NM, Cheon J-E, Jaramillo D. Diffusion-weighted MRI reveals epiphyseal and metaphyseal abnormalities in Legg-Calvé-Perthes

disease: a pilot study. Clin Orthop Relat Res [Internet]. 2011 Oct [cited 2019 Mar 13];469(10):2881–8. Available from: http://www.ncbi.nlm.nih.gov/pubmed/21660596

82. Bley TA, Wieben O, Uhl M. Diffusion-Weighted MR Imaging in Musculoskeletal Radiology: Applications in Trauma, Tumors, and Inflammation. Magn Reson Imaging Clin N Am [Internet]. 2009 May 1 [cited 2019 Mar 13];17(2):263–75. Available from: https://www.sciencedirect.com/science/article/pii/S1064968909000063

83. Bhojwani N, Szpakowski P, Partovi S, Maurer MH, Grosse U, von Tengg-Kobligk H, et al. Diffusion-weighted imaging in musculoskeletal radiology-clinical applications and future directions. Quant Imaging Med Surg [Internet]. 2015 Oct [cited 2019 Feb 24];5(5):740–53. Available from: http://www.ncbi.nlm.nih.gov/pubmed/26682143

84. Biffar A, Sourbron S, Dietrich O, Schmidt G, Ingrisch M, Reiser MF, et al. Combined diffusion-weighted and dynamic contrast-enhanced imaging of patients with acute osteoporotic vertebral fractures. Eur J Radiol [Internet]. 2010 Dec 1 [cited 2019 Mar 26];76(3):298–303. Available from: http://www.ncbi.nlm.nih.gov/pubmed/20580503

85. Raya JG, Dietrich O, Reiser MF, Baur-Melnyk A. Methods and applications of diffusion imaging of vertebral bone marrow. J Magn Reson Imaging [Internet]. 2006 Dec 1 [cited 2020 May 10];24(6):1207–20. Available from: http://doi.wiley.com/10.1002/jmri.20748

86. Pui MH, Mitha A, Rae WID, Corr P. Diffusion-weighted magnetic resonance imaging of spinal infection and malignancy. J Neuroimaging. 2005 Apr;15(2):164–70.

87. Harada Y, Tokuda O, Matsunaga N. Magnetic resonance imaging characteristics of tuberculous spondylitis vs. pyogenic spondylitis. Clin Imaging. 2008 Jul;32(4):303–9.

88. Jackson A, Buckley D (David), Parker GJM (Geoffrey JM. Dynamic contrast-enhanced magnetic resonance imaging in oncology. Springer; 2005. 311 p.

89. Paul S. Tofts. Quantitative MRI of the Brain [Internet]. Tofts P, editor. Chichester, UK: John Wiley & Sons, Ltd; 2003 [cited 2019 May 5]. Available from: http://doi.wiley.com/10.1002/0470869526

90. Nielsen T, Wittenborn T, Horsman MR. Dynamic Contrast-Enhanced Magnetic Resonance Imaging (DCE-MRI) in Preclinical Studies of Antivascular Treatments. Pharmaceutics [Internet]. 2012 Nov 7 [cited 2019 May 6];4(4):563–89. Available from: http://www.ncbi.nlm.nih.gov/pubmed/24300371

91. Villringer A, Rosen BR, Belliveau JW, Ackerman JL, Lauffer RB, Buxton RB, et al. Dynamic imaging with lanthanide chelates in normal brain: contrast due to magnetic susceptibility effects. Magn Reson Med [Internet]. 1988 Feb [cited 2019 May 6];6(2):164–74. Available from:

http://www.ncbi.nlm.nih.gov/pubmed/3367774

92. Essig M, Shiroishi MS, Nguyen TB, Saake M, Provenzale JM, Enterline D, et al. Perfusion MRI: The Five Most Frequently Asked Technical Questions. Am J Roentgenol [Internet]. 2013 Jan [cited 2019 May 6];200(1):24–34. Available from: http://www.ncbi.nlm.nih.gov/pubmed/23255738

93. Robinson SP, Rijken PFJW, Howe FA, McSheehy PMJ, van der Sanden BPJ, Heerschap A, et al. Tumor vascular architecture and function evaluated by non-invasive susceptibility MRI methods and immunohistochemistry. J Magn Reson Imaging [Internet]. 2003 Apr [cited 2019 May 6];17(4):445–54. Available from: http://www.ncbi.nlm.nih.gov/pubmed/12655584

94. Petersen ET, Zimine I, Ho Y-CL, Golay X. Non-invasive measurement of perfusion: a critical review of arterial spin labelling techniques. Br J Radiol [Internet]. 2006 Aug [cited 2019 May 6];79(944):688–701. Available from: http://www.ncbi.nlm.nih.gov/pubmed/16861326

95. Järnum H, Steffensen EG, Knutsson L, Fründ E-T, Simonsen CW, Lundbye-Christensen S, et al. Perfusion MRI of brain tumours: a comparative study of pseudo-continuous arterial spin labelling and dynamic susceptibility contrast imaging. Neuroradiology [Internet]. 2010 Apr 20 [cited 2019 May 6];52(4):307–17. Available from: http://www.ncbi.nlm.nih.gov/pubmed/19841916

96. van Westen D, Petersen ET, Wirestam R, Siemund R, Bloch KM, Ståhlberg F, et al. Correlation between arterial blood volume obtained by arterial spin labelling and cerebral blood volume in intracranial tumours. Magn Reson Mater Physics, Biol Med [Internet]. 2011 Aug 19 [cited 2019 May 6];24(4):211–23. Available from: http://www.ncbi.nlm.nih.gov/pubmed/21594585

97. Ostergaard L, Weisskoff RM, Chesler DA, Gyldensted C, Rosen BR. High resolution measurement of cerebral blood flow using intravascular tracer bolus passages. Part I: Mathematical approach and statistical analysis. Magn Reson Med [Internet]. 1996 Nov [cited 2019 May 6];36(5):715–25. Available from: http://www.ncbi.nlm.nih.gov/pubmed/8916022

98. Ostergaard L, Sorensen AG, Kwong KK, Weisskoff RM, Gyldensted C, Rosen BR. High resolution measurement of cerebral blood flow using intravascular tracer bolus passages. Part II: Experimental comparison and preliminary results. Magn Reson Med [Internet]. 1996 Nov [cited 2019 May 6];36(5):726–36. Available from: http://www.ncbi.nlm.nih.gov/pubmed/8916023

99. Kiselev VG, Strecker R, Ziyeh S, Speck O, Hennig J. Vessel size imaging in humans. Magn Reson Med [Internet]. 2005 Mar [cited 2019 May 6];53(3):553–63. Available from: http://www.ncbi.nlm.nih.gov/pubmed/15723391

100. Tofts PS, Brix G, Buckley DL, Evelhoch JL, Henderson E, Knopp M V., et al. Estimating kinetic parameters from dynamic contrast-enhanced t1-weighted MRI of a diffusable tracer: Standardized quantities and symbols. J Magn Reson Imaging [Internet]. 1999 Sep 1 [cited 2019 Apr 23];10(3):223–32. Available from: http://doi.wiley.com/10.1002/%28SICI%291522-

2586%28199909%2910%3A3%3C223%3A%3AAID-JMRI2%3E3.0.CO%3B2-S

101. Brix G, Semmler W, Port R, Schad LR, Layer G, Lorenz WJ. Pharmacokinetic parameters in CNS Gd-DTPA enhanced MR imaging. J Comput Assist Tomogr [Internet]. [cited 2019 May 6];15(4):621–8. Available from: http://www.ncbi.nlm.nih.gov/pubmed/2061479

102. Tofts PS, Kermode AG. Measurement of the blood-brain barrier permeability and leakage space using dynamic MR imaging. 1. Fundamental concepts. Magn Reson Med [Internet]. 1991 Feb [cited 2019 May 6];17(2):357–67. Available from: http://www.ncbi.nlm.nih.gov/pubmed/2062210

103. Kim EY, Kwack K-S, Cho JH, Lee D-H, Yoon S-H. Usefulness of Dynamic Contrast-Enhanced MRI in Differentiating Between Septic Arthritis and Transient Synovitis in the Hip Joint. Am J Roentgenol [Internet]. 2012 Feb 23 [cited 2019 Jun 15];198(2):428–33. Available from: http://www.ajronline.org/doi/10.2214/AJR.11.6937

104. Nusman CM, Lavini C, Hemke R, Caan MWA, Schonenberg-Meinema D, Dolman KM, et al. Dynamic contrast-enhanced magnetic resonance imaging of the wrist in children with juvenile idiopathic arthritis. Pediatr Radiol [Internet]. 2017 Feb 12 [cited 2019 May 25];47(2):205–13. Available from: http://link.springer.com/10.1007/s00247-016-3736-2

105. Dijkhoff RAP, Maas M, Martens MH, Papanikolaou N, Lambregts DMJ, Beets GL, et al. Correlation between quantitative and semiquantitative parameters in DCE-MRI with a blood pool agent in rectal cancer: can semiquantitative parameters be used as a surrogate for quantitative parameters? Abdom Radiol [Internet]. 2017 May 1 [cited 2020 Sep 17];42(5):1342–9. Available from: https://pubmed.ncbi.nlm.nih.gov/28050622/

106. Larsson HB, Stubgaard M, Frederiksen JL, Jensen M, Henriksen O, Paulson OB. Quantitation of blood-brain barrier defect by magnetic resonance imaging and gadolinium-DTPA in patients with multiple sclerosis and brain tumors. Magn Reson Med [Internet]. 1990 Oct [cited 2019 May 8];16(1):117–31. Available from: http://www.ncbi.nlm.nih.gov/pubmed/2255233

107. Amarnath J, Sangeeta T, Mehta SB. Role of quantitative pharmacokinetic parameter (transfer constant: K(trans)) in the characterization of breast lesions on MRI. Indian J Radiol Imaging [Internet]. 2013 Jan [cited 2019 Apr 23];23(1):19–25. Available from: http://www.ncbi.nlm.nih.gov/pubmed/23986614

108. Lawrence KS St., Lee T-Y. An Adiabatic Approximation to the Tissue Homogeneity Model for Water Exchange in the Brain: I. Theoretical Derivation. J Cereb Blood Flow Metab [Internet]. 1998 Dec 31 [cited 2019 May 8];18(12):1365–77. Available from: http://www.ncbi.nlm.nih.gov/pubmed/9850149

109. Donaldson SB, West CML, Davidson SE, Carrington BM, Hutchison G, Jones

AP, et al. A comparison of tracer kinetic models for T_1 -weighted dynamic contrast-enhanced MRI: Application in carcinoma of the cervix. Magn Reson Med [Internet]. 2010 Mar [cited 2019 May 8];63(3):691–700. Available from: http://www.ncbi.nlm.nih.gov/pubmed/20187179

110. Gordon Y, Partovi S, Müller-Eschner M, Amarteifio E, Bäuerle T, Weber M-A, et al. Dynamic contrast-enhanced magnetic resonance imaging: fundamentals and application to the evaluation of the peripheral perfusion. Cardiovasc Diagn Ther. 2014;4(2):147–14764.

111. Grossman RI, Gonzalez-Scarano F, Atlas SW, Galetta S, Silberberg DH. Multiple sclerosis: gadolinium enhancement in MR imaging. Radiology [Internet]. 1986 Dec 1 [cited 2019 May 13];161(3):721–5. Available from: http://www.ncbi.nlm.nih.gov/pubmed/3786722

112. MILLER DH, RUDGE P, JOHNSON G, KENDALL BE, MACMANUS DG, MOSELEY IF, et al. SERIAL GADOLINIUM ENHANCED MAGNETIC RESONANCE IMAGING IN MULTIPLE SCLEROSIS. Brain [Internet]. 1988 Aug 1 [cited 2019 May 13];111(4):927–39. Available from: http://www.ncbi.nlm.nih.gov/pubmed/3401689

113. Guo J, Reddick WE, Glass JO, Ji Q, Billups CA, Wu J, et al. Dynamic contrast-enhanced magnetic resonance imaging as a prognostic factor in predicting event-free and overall survival in pediatric patients with osteosarcoma. Cancer [Internet]. 2012 Aug 1 [cited 2019 May 25];118(15):3776–85. Available from: http://doi.wiley.com/10.1002/cncr.26701

114. Li L, Wang K, Sun X, Wang K, Sun Y, Zhang G, et al. Parameters of dynamic contrast-enhanced MRI as imaging markers for angiogenesis and proliferation in human breast cancer. Med Sci Monit [Internet]. 2015 Feb 1 [cited 2019 May 25];21:376–82. Available from: http://www.ncbi.nlm.nih.gov/pubmed/25640082

115. 0stergaard M, Hansen M, Stoltenberg M, Lorenzen I. QUANTITATIVE ASSESSMENT OF THE SYNOVIAL MEMBRANE IN THE RHEUMATOID WRIST: AN EASILY OBTAINED MRI SCORE REFLECTS THE SYNOVIAL VOLUME [Internet]. Vol. 35, British Journal of Rheumatology. 1996 [cited 2019 May 25]. Available from: https://academic.oup.com/rheumatology/article-abstract/35/10/965/1782493

116. Huang J, Stewart N, Crabbe J, Robinson E, McLean L, Yeoman S, et al. A 1-year follow-up study of dynamic magnetic resonance imaging in early rheumatoid arthritis reveals synovitis to be increased in shared epitope-positive patients and predictive of erosions at 1 year. Rheumatology [Internet]. 2000 Apr 1 [cited 2019 May 25];39(4):407–16. Available from: https://academic.oup.com/rheumatology/article-lookup/doi/10.1093/rheumatology/39.4.407

117. Axelsen M, Ejbjerg B, Hetland M, Skjødt H, Majgaard O, Lauridsen U, et al. Differentiation between early rheumatoid arthritis patients and healthy persons by conventional and dynamic contrast-enhanced magnetic resonance imaging.

Scand J Rheumatol [Internet]. 2014 Mar 6 [cited 2019 May 25];43(2):109–18. Available from: http://www.tandfonline.com/doi/full/10.3109/03009742.2013.824022

118. Miyazaki K, Jerome NP, Collins DJ, Orton MR, d'Arcy JA, Wallace T, et al. Demonstration of the reproducibility of free-breathing diffusion-weighted MRI and dynamic contrast enhanced MRI in children with solid tumours: a pilot study. Eur Radiol [Internet]. 2015 Sep 15 [cited 2019 Apr 28];25(9):2641–50. Available from: http://link.springer.com/10.1007/s00330-015-3666-7

119. Fletcher BD, Hanna SL, Fairclough DL, Gronemeyer SA. Pediatric musculoskeletal tumors: use of dynamic, contrast-enhanced MR imaging to monitor response to chemotherapy. Radiology [Internet]. 1992 Jul 1 [cited 2019 May 25];184(1):243–8. Available from: http://www.ncbi.nlm.nih.gov/pubmed/1319075

120. Mukundan S, Fuchs H, Alexander MJ, Grant GA. Dynamic contrast-enhanced magnetic resonance angiography of vascular malformations in pediatric patients. J Neurosurg Pediatr [Internet]. 2007 Sep 1 [cited 2019 May 25];107(3):228–31. Available from: http://thejns.org/doi/abs/10.3171/PED-07/09/228

121. McDaniel BB, Jones RA, Scherz H, Kirsch AJ, Little SB, Grattan-Smith JD. Dynamic Contrast-Enhanced MR Urography in the Evaluation of Pediatric Hydronephrosis: Part 2, Anatomic and Functional Assessment of Uteropelvic Junction Obstruction. Am J Roentgenol [Internet]. 2005 Dec 23 [cited 2019 May 25];185(6):1608–14. Available from: http://www.ajronline.org/doi/10.2214/AJR.04.1574

122. Sanavi C, Dacher J-N, Caudron J, Dolores M, Liard A, Vivier P-H. Supranormal differential renal function in unilateral hydronephrotic kidney: insights from functional MR urography. J Magn Reson Imaging [Internet]. 2014 Sep [cited 2019 May 25];40(3):577–82. Available from: http://doi.wiley.com/10.1002/jmri.24440

123. Vivier P-H, Dolores M, Taylor M, Dacher J-N. MR urography in children. Part 2: how to use ImageJ MR urography processing software. Pediatr Radiol [Internet]. 2010 May 25 [cited 2019 May 25];40(5):739–46. Available from: http://link.springer.com/10.1007/s00247-009-1536-7

124. Vivier P-H, Dolores M, Taylor M, Elbaz F, Liard A, Dacher J-N. MR urography in children. Part 1: how we do the F0 technique. Pediatr Radiol [Internet]. 2010 May 25 [cited 2019 May 25];40(5):732–8. Available from: http://link.springer.com/10.1007/s00247-009-1538-5

125. Magni-Manzoni S, Malattia C, Lanni S, Ravelli A. Advances and challenges in imaging in juvenile idiopathic arthritis. Nat Rev Rheumatol [Internet]. 2012 Jun 27 [cited 2019 May 25];8(6):329–36. Available from: http://www.nature.com/articles/nrrheum.2012.30

126. Colebatch-Bourn AN, Edwards CJ, Collado P, Agostino M-AD'. EULAR-PReS

points to consider for the use of imaging in the diagnosis and management of juvenile idiopathic arthritis in clinical practice. [cited 2019 May 25];9:10. Available from: http://dx.doi.org/10.1136/annrheumdis-2015-207892

127. Barendregt AM, Nusman CM, Hemke R, Lavini C, Amiras D, Kuijpers TW, et al. Feasibility of diffusion-weighted magnetic resonance imaging in patients with juvenile idiopathic arthritis on 1.0-T open-bore MRI. Skeletal Radiol [Internet]. 2015 Dec [cited 2019 Mar 26];44(12):1805–11. Available from: http://www.ncbi.nlm.nih.gov/pubmed/26205760

128. Funk SS, Copley LAB. Acute Hematogenous Osteomyelitis in Children: Pathogenesis, Diagnosis, and Treatment. Orthop Clin North Am [Internet]. 2017 Apr 1 [cited 2019 May 4];48(2):199–208. Available from: http://www.ncbi.nlm.nih.gov/pubmed/28336042

129. Singhal R, Perry DC, Khan FN, Cohen D, Stevenson HL, James LA, et al. The use of CRP within a clinical prediction algorithm for the differentiation of septic arthritis and transient synovitis in children. J Bone Joint Surg Br [Internet]. 2011 Nov [cited 2020 Jan 21];93-B(11):1556–61. Available from: https://online.boneandjoint.org.uk/doi/10.1302/0301-620X.93B11.26857

130. Pääkkönen M, Peltola H. Management of a child with suspected acute septic arthritis. Vol. 97, Archives of Disease in Childhood. 2012. p. 287–92.

131. Yeo A, Ramachandran M. Acute haematogenous osteomyelitis in children. BMJ [Internet]. 2014 Jan 20 [cited 2019 Mar 31];348:g66. Available from: http://www.ncbi.nlm.nih.gov/pubmed/24446020

132. Cameron AR, Baldock FC. A new probability formula for surveys to substantiate freedom from disease. Vol. 34, Preventive Veterinary Medicine. 1998.

133. Manaster BJ, Petersilge CA, Roberts CC, Hanrahan CJ, Moore S. Diagnostic Imaging: Musculoskeletal-Non-Traumatic Disease. 2012 [cited 2019 Feb 17]; Available from: http://jnm.snmjournals.org/site/misc/permission.xhtml

134. Neubauer, Henning, isabel platzerVerena Rabea Mueller, Thomas Meyer, Johannes Liese, Herbert Koestler, Dietbert Hahn MB. Diffusion-weighted MRI of abscess formations in children and young adult. World J Pediatr [Internet]. 2012 [cited 2020 Jul 7];8(3). Available from: www.wjpch.com

135. Tamada T, Huang C, Ream JM, Taffel M, Taneja SS, Rosenkrantz AB. Apparent Diffusion Coefficient Values of Prostate Cancer: Comparison of 2D and 3D ROIs. Am J Roentgenol [Internet]. 2018 Jan 1 [cited 2020 Jul 11];210(1):113–7. Available from: https://www.ajronline.org/doi/10.2214/AJR.17.18495

136. Fouladi DF, Zarghampour M, Pandey P, Pandey A, Varzaneh FN, Ghasabeh MA, et al. Baseline 3D-ADC outperforms 2D-ADC in predicting response to treatment in patients with colorectal liver metastases. Eur Radiol [Internet]. 2020 Jan 1 [cited 2020 Jul 11];30(1):291–300. Available from:

https://link.springer.com/article/10.1007/s00330-019-06289-3

137. Bickel H, Pinker K, Polanec S, Magometschnigg H, Wengert G, Spick C, et al. Diffusion-weighted imaging of breast lesions: Region-of-interest placement and different ADC parameters influence apparent diffusion coefficient values. Eur Radiol [Internet]. 2017 May 1 [cited 2020 Jul 11];27(5):1883–92. Available from: https://link.springer.com/article/10.1007/s00330-016-4564-3

138. Cicchetti D V. Guidelines, criteria, and rules of thumb for evaluating normed and standardized assessment instruments in psychology. Psychol Assess [Internet]. 1994 [cited 2019 Apr 23];6(4):284–90. Available from: http://doi.apa.org/getdoi.cfm?doi=10.1037/1040-3590.6.4.284

139. Koo TK, Li MY. A Guideline of Selecting and Reporting Intraclass Correlation Coefficients for Reliability Research. J Chiropr Med [Internet]. 2016 Jun [cited 2019 Apr 23];15(2):155–63. Available from: http://www.ncbi.nlm.nih.gov/pubmed/27330520

140. Kennet E. Freedland. THE “NUTS AND BOLTS” OF BEHAVIORAL INTERVENTION DEVELOPMENT: STUDY DESIGNS, METHODS AND FUNDING OPPORTUNITIES. Ann Behav Med. 2017 Mar 22;51(S1):1–2867.

141. Frassica FJ, Khanna JA, McCarthy EF. The role of MR imaging in soft tissue tumor evaluation: perspective of the orthopedic oncologist and musculoskeletal pathologist. Magn Reson Imaging Clin N Am [Internet]. 2000 Nov [cited 2019 Mar 10];8(4):915–27. Available from: http://www.ncbi.nlm.nih.gov/pubmed/11149686

142. Padhani AR, Gogbashian A. Bony metastases: assessing response to therapy with whole-body diffusion MRI. Cancer Imaging [Internet]. 2011 Oct 3 [cited 2019 Mar 26];11 Spec No(1A):S129-45. Available from: http://www.ncbi.nlm.nih.gov/pubmed/22185786

143. Blackledge MD, Collins DJ, Tunariu N, Orton MR, Padhani AR, Leach MO, et al. Assessment of treatment response by total tumor volume and global apparent diffusion coefficient using diffusion-weighted MRI in patients with metastatic bone disease: a feasibility study. PLoS One [Internet]. 2014 [cited 2019 Mar 27];9(4):e91779. Available from: http://www.ncbi.nlm.nih.gov/pubmed/24710083

144. Goo HW. Regional and whole-body imaging in pediatric oncology. [cited 2019 Mar 26]; Available from: https://link.springer.com/content/pdf/10.1007%2Fs00247-011-2050-2.pdf

145. Rosenkrantz AB, Oei M, Babb JS, Niver BE, Taouli B. Diffusion-weighted imaging of the abdomen at 3.0 Tesla: Image quality and apparent diffusion coefficient reproducibility compared with 1.5 Tesla. J Magn Reson Imaging [Internet]. 2011 Jan [cited 2019 Mar 26];33(1):128–35. Available from: http://www.ncbi.nlm.nih.gov/pubmed/21182130

146. Gawande RS, Gonzalez G, Messing S, Khurana A, Daldrup-Link HE. Role of

diffusion-weighted imaging in differentiating benign and malignant pediatric abdominal tumors. Pediatr Radiol [Internet]. 2013 Jul 12 [cited 2019 Mar 26];43(7):836–45. Available from: http://link.springer.com/10.1007/s00247-013-2626-0

147. Unal O, Koparan HI, Avcu S, Kalender AM, Kisli E. The diagnostic value of diffusion-weighted magnetic resonance imaging in soft tissue abscesses. Eur J Radiol [Internet]. 2011 Mar [cited 2019 Mar 26];77(3):490–4. Available from: http://www.ncbi.nlm.nih.gov/pubmed/19748752

148. Herneth AM, Ringl H, Memarsadeghi M, Fueger B, Friedrich KM, Krestan C, et al. Diffusion Weighted Imaging in Osteoradiology. Top Magn Reson Imaging [Internet]. 2007 Jun [cited 2019 Mar 26];18(3):203–12. Available from: https://insights.ovid.com/crossref?an=00002142-200706000-00006

149. Hillengass J, Bäuerle T, Bartl R, Andrulis M, McClanahan F, Laun FB, et al. Diffusion-weighted imaging for non-invasive and quantitative monitoring of bone marrow infiltration in patients with monoclonal plasma cell disease: a comparative study with histology. Br J Haematol [Internet]. 2011 Jun 1 [cited 2019 Mar 26];153(6):721–8. Available from: http://doi.wiley.com/10.1111/j.1365-2141.2011.08658.x

150. Magnetic resonance - technology information portal. LAVA SEQUENCE MRI - MR-TIP: Database [Internet]. [cited 2019 May 26]. Available from: https://www.mr-tip.com/serv1.php?type=db1&dbs=LAVA SEQUENCE MRI

151. Olea medical C medical system. Olea medical perfusion software [Internet]. 2019 [cited 2019 Jul 16]. Available from: https://www.olea-medical.com/en/about/

152. Lavini C, de Jonge MC, van de Sande MGH, Tak PP, Nederveen AJ, Maas M. Pixel-by-pixel analysis of DCE MRI curve patterns and an illustration of its application to the imaging of the musculoskeletal system. Magn Reson Imaging [Internet]. 2007 Jun [cited 2019 Jun 15];25(5):604–12. Available from: http://www.ncbi.nlm.nih.gov/pubmed/17540271

153. Lavini C, Buiter MS, Maas M. Reports in Medical Imaging Use of dynamic contrast enhanced time intensity curve shape analysis in MRI: theory and practice. Reports Med Imaging [Internet]. 2013 [cited 2019 Jun 15];6–71. Available from: http://dx.doi.org/10.2147/RMI.S35088

154. CIMMINO MA, BARBIERI F, BOESEN M, PAPARO F, PARODI M, KUBASSOVA O, et al. Dynamic Contrast-enhanced Magnetic Resonance Imaging of Articular and Extraarticular Synovial Structures of the Hands in Patients with Psoriatic Arthritis. J Rheumatol Suppl [Internet]. 2012 Jul 1 [cited 2019 Jun 15];89(0):44–8. Available from: http://www.ncbi.nlm.nih.gov/pubmed/22751591

155. Hemke R, Lavini C, Nusman CM, Van Den Berg JM, Dolman KM, Schonenberg-Meinema D, et al. Pixel-by-pixel analysis of DCE-MRI curve shape patterns in knees of active and inactive juvenile idiopathic arthritis

patients. Eur Radiol [Internet]. 2014 Apr 26 [cited 2020 Sep 30];24(7):1686–93. Available from: https://link.springer.com/article/10.1007/s00330-014-3168-z

156. Fawcett T. doi:10.1016/j.patrec.2005.10.010. 2005 [cited 2020 Sep 24]; Available from: www.elsevier.com/locate/patrec

157. Park SH, Goo JM, Jo CH. Receiver operating characteristic (ROC) curve: Practical review for radiologists [Internet]. Vol. 5, Korean Journal of Radiology. Korean Radiological Society; 2004 [cited 2020 Sep 24]. p. 11–8. Available from: /pmc/articles/PMC2698108/?report=abstract

158. Erlemann R, Reiser MF, Peters PE, Vasallo P, Nommensen B, Kusnierz-Glaz CR, et al. Musculoskeletal neoplasms: static and dynamic Gd-DTPA--enhanced MR imaging. Radiology [Internet]. 1989 Jun 1 [cited 2019 Jun 15];171(3):767–73. Available from: http://www.ncbi.nlm.nih.gov/pubmed/2717749

159. Verstraete KL, Woude H-J Van der, Hogendoorn PCW, De Deene Y, Kunnen M, Bloem JL. Dynamic contrast-enhanced MR imaging of musculoskeletal tumors: Basic principles and clinical applications. J Magn Reson Imaging [Internet]. 1996 Mar 1 [cited 2019 Jun 15];6(2):311–21. Available from: http://doi.wiley.com/10.1002/jmri.1880060210

160. van der Woude HJ, Verstraete KL, Hogendoorn PC, Taminiau AH, Hermans J, Bloem JL. Musculoskeletal tumors: does fast dynamic contrast-enhanced subtraction MR imaging contribute to the characterization? Radiology [Internet]. 1998 Sep 1 [cited 2019 Jun 15];208(3):821–8. Available from: http://www.ncbi.nlm.nih.gov/pubmed/9722866

161. Sugawara Y, Murase K, Kikuchi K, Sakayama K, Miyazaki T, Kajihara M, et al. Measurement of Tumor Blood Flow Using Dynamic Contrast-enhanced Magnetic Resonance Imaging and Deconvolution Analysis. J Comput Assist Tomogr [Internet]. 2006 Nov [cited 2019 Jun 15];30(6):983–90. Available from: https://insights.ovid.com/crossref?an=00004728-200611000-00021

162. Lamer S, Dorgeret S, Khairouni A, Mazda K, Brillet P-Y, Bacheville E, et al. Femoral head vascularisation in Legg-Calvé-Perthes disease: comparison of dynamic gadolinium-enhanced subtraction MRI with bone scintigraphy. Pediatr Radiol [Internet]. 2002 Aug 14 [cited 2019 Jul 7];32(8):580–5. Available from: http://www.ncbi.nlm.nih.gov/pubmed/12136349

163. Sebag G, Ducou Le Pointe H, Klein I, Maiza D, Mazda K, Bensahel H, et al. Dynamic gadolinium-enhanced subtraction MR imaging - a simple technique for the early diagnosis of Legg-Calvé-Perthes disease: preliminary results. Pediatr Radiol [Internet]. 1997 Mar 19 [cited 2019 Jul 7];27(3):216–20. Available from: http://www.ncbi.nlm.nih.gov/pubmed/9126573

164. Alexander Fleming. AL E X A N D E R F L E M I N G Penicillin [Internet]. [cited 2019 Apr 19]. Available from: https://www.nobelprize.org/uploads/2018/06/fleming-lecture.pdf

165. Godley DR. Managing musculoskeletal infections in children in the era of increasing bacterial resistance. J Am Acad Physician Assist [Internet]. 2015 Apr [cited 2019 Apr 19];28(4):24–9. Available from: https://insights.ovid.com/crossref?an=01720610-201504000-00004

166. Monsalve J, Kan JH, Schallert EK, Bisset GS, Zhang W, Rosenfeld SB. Septic Arthritis in Children: Frequency of Coexisting Unsuspected Osteomyelitis and Implications on Imaging Work-Up and Management. Am J Roentgenol [Internet]. 2015 Jun [cited 2019 Apr 19];204(6):1289–95. Available from: http://www.ajronline.org/doi/10.2214/AJR.14.12891

167. K. Schallert E, Herman Kan J, Monsalve J, Zhang W, Bisset GS, Rosenfeld S. M1. K. Schallert E, Herman Kan J, Monsalve J, Zhang W, Bisset GS, Rosenfeld S. Metaphyseal osteomyelitis in children: how often does MRI-documented joint effusion or epiphyseal extension of edema indicate coexisting septic arthritis? Pediatr Radiol [Inter. Pediatr Radiol [Internet]. 2015 Aug 20 [cited 2019 Apr 19];45(8):1174–81. Available from: http://link.springer.com/10.1007/s00247-015-3293-0

Appendix

Appendix 1- Ethic approval

Research Ethics Committee established by the Health Research Authority

NRES Committee South West - Frenchay

Level 3, Block B
Whitefriars
Lewins Mead,
Bristol BS1 2NT
nrescommittee.southwest-frenchay@nhs.net

21 May 2014

Dr Afshin Alavi
Imperial college NHS trust, St Marys hospital
radiology department, QEQM building
praed street
london, uk
W2 1NY

Dear dr alavi **Study title:**

	Tailored MRI protocols are the ultimate imaging tools in the diagnostic and differential diagnostic of musculoskeletal infection in children
REC reference:	**14/SW/0086**
IRAS project ID:	**139300**

Thank you for your letter of 14 May 2014, responding to the Proportionate Review Sub-Committee's request for changes to the documentation for the above study.

The revised documentation has been reviewed and approved by the sub-committee.
We plan to publish your research summary wording for the above study on the NRES website, together with your contact details, unless you expressly withhold permission to do so. Publication will be no earlier than three months from the date of this favourable opinion letter. Should you wish to provide a substitute contact point, require further information, or wish to withhold permission to publish, please contact the REC Manager Miss Stephanie Macpherson, .

Confirmation of ethical opinion

On behalf of the Committee, I am pleased to confirm a favourable ethical opinion for the above research on the basis described in the application form, protocol and supporting documentation as revised.

Conditions of the favourable opinion

The favourable opinion is subject to the following conditions being met prior to the start of the study. **You should notify the REC in writing once all conditions have been met (except for site approvals from host organisations) and provide copies of any revised documentation with updated version numbers. The REC will acknowledge receipt and provide a final list of the approved documentation for the study, which can be made available to host organisations to facilitate their permission for the study. Failure to provide the final versions to the REC may cause delay in obtaining permissions**

Management permission or approval must be obtained from each host organisation prior to the start of the study at the site concerned.

Management permission ("R&D approval") should be sought from all NHS organisations involved in the study in accordance with NHS research governance arrangements.

Guidance on applying for NHS permission for research is available in the Integrated Research Application System or at http://www.rdforum.nhs.uk.

Where a NHS organisation's role in the study is limited to identifying and referring potential participants to research sites ("participant identification centre"), guidance should be sought from the R&D office on the information it requires to give permission for this activity.

For non-NHS sites, site management permission should be obtained in accordance with the procedures of the relevant host organisation.

Sponsors are not required to notify the Committee of approvals from host organisations.

Registration of Clinical Trials

All clinical trials (defined as the first four categories on the IRAS filter page) must be registered on a publically accessible database within 6 weeks of recruitment of the first participant (for medical device studies, within the timeline determined by the current registration and publication trees).

There is no requirement to separately notify the REC but you should do so at the earliest opportunity e.g. when submitting an amendment. We will audit the registration details as part of the annual progress reporting process.

To ensure transparency in research, we strongly recommend that all research is registered but for non-clinical trials this is not currently mandatory.
The favourable opinion applies to all NHS sites taking part in the study, subject to management permission being obtained from the NHS/HSC R&D office prior to the start of the study (see “Conditions of the favourable opinion” above)If a sponsor wishes to contest the need for registration they should contact Catherine Blewett (catherineblewett@nhs.net), the HRA does not, however, expect exceptions to be made. Guidance on where to register is provided within IRAS. It is the responsibility of the sponsor to ensure that all the conditions are complied with before the start of the study or its initiation at a particular site (as applicable).

Ethical review of the research sites.

Approved documents

The documents reviewed and approved by the Committee are: *Document*	*Version*	*Date*
Participant consent form [Parents/Guardians]	1.0	01 December 2013
Participant consent form [16-18 YR]	2.	01 May 2014
Participant consent form [16 Year Olds]	1.0	01 December 2013
Participant consent form [Children Under 16 Years Old]	1.0	01 December 2013
Participant information sheet (PIS) [16-18YR]	2.	01 May 2014
Participant information sheet (PIS) [16 Year Olds]	1.0	01 December 2013
Participant information sheet (PIS) (UNDER 10YR)	2.	01 May 2014
Participant information sheet (PIS) [Parents/Guardians]	1.0	01 December 2013
Participant information sheet (PIS) [11-15 Year Olds]	1.0	01 December 2013
REC Application Form	1	18 March 2014
Referee's report or other scientific critique report		
Research protocol or project proposal	1.0	01 December 2013
Response to Request for Further Information	EMAIL	14 May 2014
Summary CV for Chief Investigator (CI) /Student) Dr Afshin Alavi		
Summary CV for Chief Investigator (CI) Academic Supervisor Prof Michael Levin		

Statement of compliance

The Committee is constituted in accordance with the Governance Arrangements for Research Ethics Committees and complies fully with the Standard Operating Procedures for Research Ethics Committees in the UK.

After ethical review

Reporting requirements

The attached document “After ethical review – guidance for researchers” gives detailed guidance on reporting requirements for studies with a favourable opinion, including:

Notifying substantial amendments
Adding new sites and investigators
Notification of serious breaches of the protocol
Progress and safety reports
Notifying the end of the study

The HRA website also provides guidance on these topics, which is updated in the light of changes in reporting requirements or procedures.

Feedback

You are invited to give your view of the service that you have received from the National Research Ethics Service and the application procedure. If you wish to make your views known please use the feedback form available on the HRA website:
http://www.hra.nhs.uk/about-the-hra/governance/quality-assurance

We are pleased to welcome researchers and R & D staff at our NRES committee members' training days – see details at http://www.hra.nhs.uk/hra-training/

14/SW/0086 Please quote this number on all correspondence

With the Committee's best wishes for the success of this project.

Yours sincerely
Mr Peter Jones
Chair

Email: nrescommittee.southwest-frenchay@nhs.net

Enclosures: *"After ethical review – guidance for researchers"* Copy to: *Mrs Christine Buicke, Imperial College Healthcare NHS trust*

Appendix 2- Patient information sheet

Tailored MRI protocols are the ultimate imaging tools in the diagnostic a
And Differential diagnostic of musculoskeletal infection in children

Participant Information Sheet – under 10 years old
Principal investigator: Dr. Afshin Alavi

Introduction:
We would like to tell you about our research project and how you could help us.

What is research? Why this project is being done?
Research is a way we try to find out answers to questions. We want to find better ways to workout what illness children have if they come to hospital with limbs pain. When we know the exact type of illness, we can sometimes make children better much faster and easier.
Why have you been asked?
All children who had an MRI of their skeleton as part of their clinical care during their hospital stay with signs of infection are eligible for this project.

Do I have to help you?
No it is up to you. It is OK if you want to help us or if you don't want to. Whatever you decide, you can change your mind at anytime and nobody will be upset.

What will happen if I agree and are there any additional examinations?
We are going to compare the results of the MRI examinations which were done over a period of two years with the relevant final results and see how good MRI really is. The MRI examination is part of your routine clinical care and therefore you don't need to do anything for this research study. There will be no additional examinations.

Will this project help me?

We cannot promise you that our project will help you, but in the future, we hope we will learn how to get better at treating children with infection. In this way if you have a similar illness in the future we could help you better and faster.

Is there anything to worry about?

No there is not. The MRI examination will be done anyway as part of your routine care and there are no additional examinations.

Will anyone else know I am doing this?

No. We will only tell your doctors at the hospital who need to know to help you.

What will happen to the results of the research study?

If we find out anything about you that is important, we will tell your doctors about it. However in most cases it is not necessary.

Who to contact for future information?

You can contact the chief investigator under the following contact details:

Dr. Afshin Alavi
St Marys Hospital, QEQM building
3rd floor Radiology department
Praed Street W2 1NY

Thank You for your Time

Patient information sheet version 1.0 Under 10 years old 01 December 2013

Tailored MRI protocols are the ultimate imaging tools in the diagnostic And Differential diagnostic of musculoskeletal infection in children

Participant Information Sheet – 11-15 years old

Principal investigator: Dr. Afshin Alavi

Introduction:

You are being invited to take part in a research study. We are asking you if you are happy for us to include the anonymised results of your MRI examination which has been performed as part of your acute clinical care and the final clinical results in to our study to see how useful they are.

What is the purpose of the study?

Muscles and bones infections are relatively common amongst children. Unfortunately it is not always easy to tell if there is an infection and where is the infection. We would like to improve our knowledge and ability to detect infections in children muscles and bones. That way we can make sure we are treating the children appropriately. MRI is one of the best ways to find infections and we think it should be done relatively soon if an infection is suspected in a child. In order to prove the value of MRI we need to compare many MRI examinations with the infection results to see how good MRI really is. In this way we hope we can make the detection of muscles and bone infections in children faster and easier.

Why have I been asked?

All children who had an MRI as part of their acute clinical care during their hospital stay with signs of muscles or bone infection are eligible for this study.

Do I have to take part?

It is totally up to you whether or not you want us to include your anonymised MRI results in our study. If you agree you will be given this information sheet to keep and you will be asked to sign a consent form. Your decision wouldn’t change anything in your routine care and treatment.

What will happen if I agree and are there any additional examinations?

The study is planned for two years. Over this period of time we will compare the anonymised results of your MRI examination with the clinical results and evaluate the value of MRI. The MRI examination is part of your acute clinical care and therefore you don’t need to do anything for this research study. There will be no additional examinations.

What are the benefits of this study?

Through the information that we can gather from this study we would be able to show the value of MRI in the diagnostic of acute infection in muscles and bones and we hope to find an effective way to find these infections, which could be used for future guidelines (missing at the moment). This is beneficial for you in case you have another infection or other similar conditions in the future but also for all other children who will suffer from infections of their muscles and bones.

Are there any disadvantages?

No there are no disadvantages or risks. The MRI examination will be performed anyway as part of the acute clinical care and there are no additional examinations.

Will anyone else know I am doing this?

We will remove your details including your name and address from your MRI examination before entering our study. The only people who have access to your details are your doctors, who have anyway access to your records. We will not tell anybody that your MRI examination has been used in this study.

What will happen to the results of the research study?

If our MRI results reveal information that might be important for your future care, we will feed this back to you and your doctor. However, in most cases, we would not expect to contact you with any results. Results of this research may be published but will not contain any of your personal information

Who is organising the research?

The study is sponsored by Imperial College NHS Trust and run by the Radiology and Paediatric departments at Imperial College.

Who to contact for future information?

You can contact the chief investigator under the following contact details:

Dr. Afshin Alavi
St Marys Hospital, QEQM building
3rd floor Radiology department
Praed Street W2 1NY

Thank You for your Time

Patient information sheet version 1.0 11-15 years old 01 December 2013

Tailored MRI protocols are the ultimate imaging tools in the diagnostic And Differential diagnostic of musculoskeletal infection in children

Participant Information Sheet – 16 years old and above
Principal investigator: Dr. Afshin Alavi

Introduction:
This is a research study as part of a higher educational degree. We are asking you for your permission to include the anonymised results of your MRI examination which has been performed as part of your acute clinical care and the relevant clinical details in to our study to elaborate the value of MRI.

What is the purpose of the study?
Musculoskeletal infections are relatively common amongst children, it is the most common reason for acute musculoskeletal pain after trauma. Unfortunately the diagnostic pathway for children is not streamlined yet and there are no guidelines for the diagnostic. The role of imaging and different imaging modalities are not prospectively (sufficiently?) explored. It is vital for the future development and improvement of the diagnostic path to elaborate the role of MRI as the most sophisticated imaging tool for the musculoskeletal system. We are planning to create a unified path for the imaging diagnostic of the musculoskeletal infection in children.

Why have I been asked?
All children who had an MRI as part of their acute clinical care with signs and symptoms of MSK infection are eligible for this study.

Do I have to take part?
It is totally up to you whether or not you want us to include your anonymised MRI results in our data (study?). If you agree you will be given this information sheet to keep and you will

be asked to sign a consent form. Your decision wouldn't change anything in your routine diagnostic and treatment.

What will happen if I agree and are there any additional examinations?

The study is planned for two years. Over this period of time we will compare the anonymised results of the acute MRI examinations with the final clinical diagnosis and evaluate the diagnostic value of MRI and its different sequences. The MRI examination is part of your acute clinical care and therefore you don't need to do anything for this research study. There will be no additional examinations.

What are the benefits of this study?

Through the information that we can gather (extract?) from this study we would be able to show the value of MRI in the diagnostic of acute musculoskeletal infection and infarction and we hope to establish a sufficient diagnostic pathway, which could be used for future guidelines (missing at the moment). This is beneficial for you in case of recurrence or other similar musculoskeletal conditions in the future but also for all other children who will suffer from musculoskeletal infections or infarction.

Are there any disadvantages?

No there are no disadvantages or risks. The MRI examination will be performed anyway as part of the acute clinical care and there are no additional examinations for the study.

Will the information be kept confidential?

The chief investigator and his team are all members of the acute clinical care involved in your diagnostic and treatment. All of the MRI examinations will be anonymised before entering the study. All of the MRI examinations and the clinical information will be kept confidential. The chief investigator is the only person who has access to all radiological and clinical data and he will make sure that the confidentiality is warranted. The anonymised data wouldn't leave the hospital. If we publish our data it won't contain information that could lead to the identification of participants.

What will happen to the results of the research study?

If our MRI results reveal information that might be important for your future care, we will feed this back to you and your medical team. However, in most cases, we would not expect to

contact you with any results. Results of this research may be published in scientific journals but will not contain information that could lead to the identification of participants.

Who is organising and funding the research?

The study is sponsored by Imperial College NHS Trust and run by the Radiology and Paediatric departments at imperial college. There are no external funding sources and none of the investigators are paid for this study.

The study was approved by NRES committee South West – Frenchay and was given a favourable opinion.

Who to contact for future information?

You can contact the chief investigator under the following contact details:

Dr. Afshin Alavi

St Marys Hospital, QEQM building

3rd floor Radiology department

Praed Street W2 1NY

Thank You for your Time

Patient information sheet version 1.0 16 years old and above 01 December 2013

Tailored MRI protocols are the ultimate imaging tools in the diagnostic a
And Differential diagnostic of musculoskeletal infection in children

Participant Information Sheet – Parents or Guardians
Principal investigator: Dr. Afshin Alavi

Introduction:

Dear Parents this is a research study as part of a higher educational degree. We are asking you for your permission to include the anonymised results of your Childs MRI examination

which has been performed as part of the acute clinical care and the relevant clinical details in to our study to elaborate the value of MRI.

What is the purpose of the study?

Musculoskeletal infections are relatively common amongst children, it is the most common reason for acute musculoskeletal pain after trauma. Unfortunately the diagnostic pathway for children is not streamlined yet and there are no guidelines for the diagnostic. The role of imaging and different imaging modalities are not prospectively (sufficiently?) explored. It is vital for the future development and improvement of the diagnostic path to elaborate the role of MRI as the most sophisticated imaging tool for the musculoskeletal system. We are planning to create a unified path for the imaging diagnostic of the musculoskeletal infection in children.

Why have I been asked?

All children who had an MRI as part of their acute clinical care with signs and symptoms of MSK infection are eligible for this study and their parents will be asked to give us the permission to evaluate the anonymised MRI exams.

Does my child have to take part?

It is totally up to you whether or not you want us to include the anonymised MRI results of your child in our data (study?). If you agree you will be given this information sheet to keep and you will be asked to sign a consent form. Your decision wouldn't change anything in the routine diagnostic and treatment of your child.

What will happen if I agree and are there any additional examinations?

The study is planned for two years. Over this period of time we will compare the anonymised results of the acute MRI examinations with the final clinical diagnosis and evaluate the diagnostic value of MRI and its different sequences. The MRI examination is part of the routine clinical care and therefore your child doesn't need to do anything for this research study. There will be no additional examinations.

What are the benefits of this study?

Through the information that we can gather (extract?) from this study we would be able to show the value of MRI in the diagnostic of acute musculoskeletal infection and infarction and we hope to establish a sufficient diagnostic pathway, which could be used for future

guidelines (missing at the moment). This is beneficial for your child/ children in case of recurrence or other similar musculoskeletal conditions in the future but also for all other children who will suffer from musculoskeletal infections or infarction.

Are there any disadvantages?

No there are no disadvantages or risks. The routine MRI examination will be performed anyway as part of the acute clinical care and there are no additional examinations for the study.

Will the information be kept confidential?

The chief investigator and his team are all members of the acute clinical care involved in the diagnostic and treatment of your child. All of the MRI examinations and the clinical information will be kept confidential. All of the MRI examinations will be anonymised before entering the study. The chief investigator is the only person who has access to all radiological and clinical data and he will make sure that the confidentiality is warranted. The anonymised data wouldn't leave the hospital. If we publish our data it won't contain information that could lead to the identification of participants.

What will happen to the results of the research study?

If our MRI results reveal information that might be important for your child's future care, we will feed this back to you and your child's medical team. However, in most cases, we would not expect to contact you with any results. Results of this research may be published in scientific journals but will not contain information that could lead to the identification of participants.

Who is organising and funding the research?

The study is sponsored by Imperial College NHS Trust and run by the Radiology and Paediatric departments at Imperial College. There are no external funding sources and none of the investigators are paid for this study.

The study was reviewed by the NRES committee South West – Frenchay and was given a favourable opinion.

Who to contact for future information?

You can contact the chief investigator under the following contact details:

Dr. Afshin Alavi
St Marys Hospital, QEQM building
3rd floor Radiology department
Praed Street W2 1NY

Thank You for your Time

Patient information sheet version 1.0 Parents or Guardians 01 December 2013

Appendix 3- Consent and Assent forms

Use patient label

Patient name:

ASSENT FORM
- Children under 16

London

Department of

Imperial College

St Mary's Campus
St Mary's Hospital
Praed Street
London W2 1NY

Tailored MRI protocols are the ultimate imaging tools in the diagnostic

And differential diagnostic of musculoskeletal infection in children

Principal investigator: Dr. Afshin Alavi

Child (or if unable, parent on their behalf)/ young person to circle all they agree with:

Have you read (or had read to you) about this project? YES / NO

Has somebody else explained this project to you? YES / NO

Do you understand what this project is about? YES / NO

Have you asked all the questions you want? YES / NO

Have you had your questions answered in a way you understand? YES / NO

Are you happy to take part? YES / NO

If you want to take part, you can write your name below:

…….. ……. ……

Name of Participant Date Signature

The doctor or nurse who explained this project to you needs to sign too:

……. ……. ……

Name of Researcher Date Signature

Use patient label

Patient name:

CONSENT FORM – 16-18 years old.

Department of

Imperial College

St Mary's Campus
St Mary's Hospital
Praed Street
London W2 1NY

Tailored MRI protocols are the ultimate imaging tools in the diagnostic

and differential diagnostic of musculoskeletal infection in children

Principal investigator: Dr. Afshin Alavi

Please tick

1. I confirm that I have read and understand the subject information sheet dated 01 of July 2013 for the above study and been given a copy to keep. I have had the opportunity to ask questions and have had these answered satisfactorily ☐

2. I understand that participation is voluntary, and that I am free to withdraw consent at any time, without giving any reason, without my medical care or legal rights being affected. ☐

3. I understand that sections of any of the medical notes and data collected during the study may be looked at by responsible individuals from Imperial College, Imperial College Healthcare NHS Trust or from regulatory authorities, where it is relevant to my taking part in this research. I give permission for these individuals to access my records. ☐

4 I agree to the use of my anonymised MRI scans in this research project, as described on the patient information sheet. ☐

5. I agree to the use of my anonymised MRI scans in any future ethically-approved studies. ☐

6. I agree to take part in this research project. ☐

_____	_____	_____
Name of Subject	Signature (if able)	Date

_____	_____	_____
Name of Parent/Guardian/Legal representative	Signature	Date

_____	_____	_____
Name of Person taking consent	Signature	Date

_____	_____	_____
Principal Investigator	Signature	Date

Use patient label

Patient name:

CONSENT FORM – parents or guardians

Department of

Imperial College

London

St Mary's Campus
St Mary's Hospital
Praed Street
London W2 1NY

Tailored MRI protocols are the ultimate imaging tools in the diagnostic

And differential diagnostic of musculoskeletal infection in children

Principal investigator: Dr. Afshin Alavi

		Please tick
1.	I confirm that I have read and understand the subject information sheet dated 01 of December 2013 for the above study and been given a copy to keep. I have had the opportunity to ask questions and have had these answered satisfactorily	☐
2.	I understand that participation is voluntary, and that I am free to withdraw consent at any time, without giving any reason and without my child's medical care or legal rights being affected.	☐
3.	I understand that sections of any of my child's hospital notes and data collected during the study may be looked at by responsible individuals from Imperial College, Imperial College Healthcare NHS Trust or from regulatory authorities, where it is relevant to my taking part in this research. I give permission for these individuals to access my child's records.	☐
4	I agree to the use of my child's anonymised MRI scan in this research project, as described on the patient information sheet.	☐
5.	I agree to the use of my child's anonymised MRI scan in any future ethically-approved studies.	☐
6.	I agree for my child to take part in this research project.	☐

_____	_____	_____
Name of Subject	Signature (if able)	Date

_____	_____	_____
Name of Parent/Guardian/Legal representative	Signature	Date
_____	_____	_____
Name of Person taking consent	Signature	Date
_____	_____	_____
Principal Investigator	Signature	Date

Appendix 4- Evaluation form

Patient's number: Scan number: Age:

1-Any Abnormality in DWI: YES NO

Conspicuity score of the DWI (1-5):

MRI findings (diagnosis) in DWI:

Diagnostic confidence score of DWI (1-5):

Was the ADC Value helpful?

2-Any Abnormality in T2 fat sat: YES NO

Conspicuity score of the T2 fat sat (1-5):

MRI findings (diagnosis) in T2 fat sat:

Diagnostic confidence score of T2 fat sat (1-5):

3-Any Abnormality in T1: YES NO

Conspicuity score of the T1 (1-5):

MRI findings (diagnosis) in T1:

Diagnostic confidence score of T1 (1-5):

4-Any Abnormality in T1fat sat dynamic contrast: YES NO

Conspicuity score of the T1 fat sat post contrast (1-5)

MRI findings (diagnosis) in T1 fat sat post contrast:

Diagnostic confidence score of T1 fat sat post contrast(1-5):

Was final diagnosis/ differential diagnosis possible on the basis of:

DWI:

T2 fat sat:

T1:

T1 fat sat post contrast:

Whole protocol: